



**Universidade de Brasília  
Instituto de Geociências**

**GEOLOGIA, PETROLOGIA E GEOCRONOLOGIA DO COMPLEXO  
ACAMADADO LAGO GRANDE: EVIDÊNCIA PARA UMA SUÍTE  
MAGMÁTICA MINERALIZADA A EGP NA PROVÍNCIA MINERAL DE  
CARAJÁS, BRASIL.**

**Dissertação de Mestrado nº 315**

**Antônio Sales Teixeira**

**BRASÍLIA – JULHO/2013**



**Universidade de Brasília  
Instituto de Geociências**

**GEOLOGIA, PETROLOGIA E GEOCRONOLOGIA DO COMPLEXO  
ACAMADADO LAGO GRANDE: EVIDÊNCIA PARA UMA SUÍTE  
MAGMÁTICA MINERALIZADA A PGE NA PROVÍNCIA MINERAL DE  
CARAJÁS, BRASIL.**

Antônio Sales Teixeira

Orientador: Prof. Dr. César Fonseca Ferreira Filho (IG - UnB)

Co-orientadora: Prof<sup>a</sup>. Dra Maria Emília S. Della Giustina (IG - UnB)

Examinadores:

Prof. Dr Raimundo Netuno Nobre Villas – (IG - UFPA)

Prof<sup>a</sup>. Dra Catarina Labouré Bemfica Toledo - (IG - UnB)

Local e data da defesa: Brasília, 26 de julho de 2013

## **AGRADECIMENTOS**

Esta dissertação de mestrado somente pôde ser realizada com o apoio da VALE, por intermédio dos geólogos Fernando Martins Vieira Matos e Dênisson Pacine Leal de Oliveira, pela liberação do acervo técnico referente à etapa de pesquisa realizada no Complexo Lago Grande e pela disponibilização de sua infraestrutura em Carajás.

Agradecimentos ao CNPq pelo apoio financeiro ao projeto “Desenvolvimento de parâmetros comparativos da fertilidade do magmatismo máfico-ultramáfico de Carajás para mineralizações magmáticas (Ni, Cu, EGP, Cr, Ti-V) com base em estudos geocronológicos, petrológicos e do seu posicionamento tectônico-estratigráfico”, aprovado no Edital MCT/CTMineral/VALE/CNPq 12/2009, com recursos liberados em 08/2010.

Ao Instituto de Geociências da Universidade de Brasília pelo suporte aos trabalhos em todas as etapas.

À empresa Furnas Centrais Elétricas S.A., através da Gerência de Tecnologia de Empreendimentos – GST.E pela liberação do uso de seus laboratórios para análises de petrografia e MEV.

Agradecimento especial aos orientadores Prof. César Ferreira Filho e Prof<sup>a</sup>. Maria Emília Schutesk Della Giustina pela paciência, dedicação e ensinamentos ao longo destes anos e à Prof<sup>a</sup>. Sylvia Maria Araújo pela contribuição quanto ao conteúdo do estudo.

Agradecimentos aos geólogos Enio e Ricardo pelo suporte nos trabalhos de microsonda. Aos colegas Marco Antonio Paixão – do IFG Goiânia pela ajuda nas descrições petrográficas. À geóloga Caroline Gomide quanto à complementação das análises dos PGEs por MEV no Labmic da UFG.

Agradecimentos ao Tecnólogo em Geoprocessamento Igor Dias Fonseca Luz pelo apoio para a realização dos mapas e integração de dados.

Meu especial agradecimento à Geóloga Heloisa Helena – minha querida esposa e companheira de todas as horas, pela valiosa ajuda e irrestrito incentivo para a concretização deste trabalho e pelo apoio para a caracterização dos platinóides. Por fim, agradeço aos meus filhos e noras pela compreensão por minha ausência necessária para elaboração deste estudo.

## INDICE

Agradecimentos	i
Índice	ii
Índice de figuras	iii
Índice de tabelas	vii
Resumo	viii
Introdução	1
Conclusões	73

## **GEOLOGY, PETROLOGY AND GEOCHRONOLOGY OF THE LAGO GRANDE LAYERED COMPLEX: EVIDENCE FOR A PGE-MINERALIZED MAGMATIC SUITE IN THE CARAJÁS MINERAL PROVINCE, BRAZIL.**

<b>Abstract</b>	<b>4</b>
<b>Introduction</b>	<b>7</b>
<b>Regional Setting</b>	<b>8</b>
The Carajás Mineral Province	8
The Serra Leste Magmatic Suite	11
<b>Analytical Procedures</b>	<b>14</b>
Microprobe analyses	14
Bulk rock analyses (ICP-MS)	14
Sm-Nd isotopic analyses	14
LA-ICPMS (U-Pb zircon analyses)	15
PGE and PGM analyses	16
<b>The Lago Grande Layered Mafic-Ultramafic Complex</b>	<b>17</b>
Geology	17
The Ultramafic Zone	21
The Mafic Zone	25
Mineral Chemistry	26
Bulk Rock Geochemistry	30
Major and Minor Elements	30
Trace Elements	33
Sm-Nd Systematics	38
U-Pb geochronology	39



Platinum Group Mineral	42
<b>Discussion</b>	<b>48</b>
Magmatic structure	48
Constraints for the composition of parental magma and fractionation	49
Metamorphism and hydrothermal alteration of magmatic rocks	52
The petro-tectonic setting of the Lago Grande Complex and associated layered intrusions of the Serra Leste region	55
Origin of Platinum Group Minerals and implication for exploration	57
<b>Conclusions</b>	<b>61</b>
<b>Acknowledgments</b>	<b>63</b>
<b>References</b>	<b>64</b>
<b>ANEXOS</b>	
Anexo I – Fluxgramas	76
Anexo II – Análise de Química Mineral	79
Anexo III – Petrografia	117
Anexo IV – Microscopia Eletrônica de Varredura – MEV	173
Anexo V – Geocronologia	202
Anexo VI – Litogeoquímica	204

## ÍNDICE DE FIGURAS

Figure 1 - A) Location of the Carajás Mineral Province. B) Geology of the northern domain of the CMP. Modified from Vasquez et al., (2008).	09
Figure 2 - Geology of the Serra Leste region. Partially modified from VALE's internal reports.	13
Figure 3 - Geological map of the Lago Grande Complex (partially modified from unpublished report of VALE). Location of the map in Fig. 4 is indicated by dashed rectangle.	18

Figure 4 - Geological map of the central portion of the Lago Grande Complex (partially modified from unpublished report of VALE). 19

Figure 5 - Geological section (partially modified from unpublished report of VALE). See Fig. 4 for captions and location of drill holes. Dashed line indicates the limit of the weathering profile (saprolite or partially weathered rocks). 20

Figure 6 - A) Boulders of ultramafic rocks of the Lago Grande Complex. B) Harzburgite. Large Opx oikocrysts within domains of medium-grained Opx+Cpx (whitish color). See sample 04 in Fig. 4 for location. C) Detail of the medium-grained domains of the previous photo. D) Harzburgite. Detail of Opx oikocrysts (with inclusion of anhedral Ol) and euhedral (black color due to serpentinization) Ol. E) Harzburgite. Photomicrograph of large Opx oikocryst enclosing several olivine (Ol) anhedral crystals and chromite (opaque) euhedral crystals. F) Orthopyroxenite. Photomicrograph of an aggregate of Opx crystals with minor associated white to paleo green amphibole crystals. G) Medium-grained gabbroic rock consisting of anhedral pyroxene (black) and tabular plagioclase (whitish color). See sample 08 in Fig. 4 for location. H) Pegmatoid gabbroic pod from the same outcrop of the previous photo. 23

Figure 7 - Ni content for Drill Hole FD26. See Fig. 4 for captions and location of drill hole. 24

Figure 8 - Compositional variation of olivine and orthopyroxene for Drill Hole FD26. See Fig. 4 for captions and location of drill hole. 29

Figure 9 - Plot of MgO versus major element contents for rocks of the Lago Grande Complex. Data from Table 4 recalculated to anhydrous compositions. Compositions of plotted Ol, Opx and Pl correspond to microprobe analyses reported in this study. Ol and Opx crystals were analyzed in harzburgite, whereas Pl crystals were analyzed in gabbroic rocks. \* Corresponds to sample LUSL19 (metabasalt the Rio Novo Group). 31

Figure 10 - Plot of MgO versus minor element contents for rocks of the Lago Grande Complex. Data from Table 4 recalculated to anhydrous compositions. \* Corresponds to sample LUSL19 (metabasalt of the Rio Novo Group). 32

Figure 11 - Al<sub>2</sub>O<sub>3</sub>-CaO plot for rocks of the Lago Grande Complex. Data from Table 4 recalculated to anhydrous compositions. Compositions of plotted Opx and Pl correspond to microprobe analyses reported in this study, whereas plotted Cpx corresponds to expected composition of Cpx in gabbroic rocks. \* Corresponds to sample LUSL19 (metabasalt of the Rio Novo Group). 33

Figure 12 - Primitive mantle-normalized REE profiles for samples of the Lago Grande Complex. A) Samples of gabbroic rocks from outcrops of the Mafic Zone. Sample LUSL19 is a mafic rock from the Rio Novo Group. B) Samples of gabbroic rocks from drill core FD26, located at the lower most part of the Mafic Zone. C) Samples of orthopyroxenite from drill core FD26. D) Samples of harzburgite from drill core FD26. Data from Table 4. Primitive mantle normalization values are from Sun and McDonough (1989). 37

Figure 13 - Primitive mantle-normalized alteration-resistant profiles for samples of gabbroic rocks of the Lago Grande Complex. Sample LUSL19 is a mafic rock from the Rio Novo Group. Data from Table 4. Primitive mantle normalization values are from Sun and McDonough (1989). 38

Figure 14 - True color CL images of selected zircon grains from sample LUSL-20, showing low luminescent cores surrounded by irregular, bright rim. Also shown is the location of U-Pb spot analyses. 40

Figure 15 - LA-MC-ICPMS U-Pb plots for sample LUSL-20B. 40

Figure 16 - Plot of Pd, Pt, and Rh versus sulfur (S) for borehole FD-02. Data from mine drilling assay database (VALE, unpublished internal report). 45

Figure 17 - Plot of Pd versus Pt for borehole FD-02. Data from mine drilling

assay database (VALE, unpublished internal report).

46

Figure 18 - PGE03. Primitive mantle-normalized PGE profiles for chromitite samples from the Lago Grande (data from tabela 08) and Luanga Complex (data from Diella et al., 1995) Primitive mantle normalization values are from Sun and McDonough (1989).

47

Figure 19 - Primitive mantle-normalized alteration-resistant profiles for samples of gabbroic rocks of the Lago Grande Complex, average composition of the upper and lower crust (Wedepohl 1995), and average composition of the B1 rocks of the Bushveld Complex (Barnes et al. 2010). Primitive mantle normalization values are from Sun and McDonough (1989).

51

## ÍNDICE DE TABELAS

Table 1 – Representative Analyses of Olivine from drill hole FD26 - Lago Grande Complex	27
Table 2 – Representative Analyses of Orthopyroxene from drill hole FD26 - Lago Grande Complex	28
Table 3 – Representative Analyses of Plagioclase from drill hole FD 26 - Lago Grande Complex.	28
Table 4 – Whole rock analyses for Lago Grande	34
Table 5 – Sm-Nd isotopic data for the Lago Grande Complex.	41
Table 6 – U-Pb LA-MC-ICPMS data for sample LU	41
Table 7 – PGE analyses of representative samples of Lago Grande Complex.	46
Table 8 – PGM analyses of sulfide-poor chromitite and sulfide-bearing harzburgite.	47

## RESUMO

O **Complexo Máfico-Ultramáfico Acamadado Lago Grande** contém mineralização de EGP associada a níveis centimétricos de cromititos e sulfetos. Pertence à Suíte Máfica-Ultramáfica Serra Leste (Ferreira Filho et al., 2007) – região leste da Província Mineral Carajás, cujo principal representante é o Complexo Luanga também mineralizado a EGP. A Suíte Serra Leste situa-se nas imediações de Serra Pelada, importante depósito epigenético de Au-PGE (Grainger et al., 2002). Trata-se de um corpo intrusivo posicionado entre o Complexo Xingu e o Grupo Rio Novo, com estratigrafia magmática composta por estrato ultramáfico harzburgítico na base, seguido de pacote piroxenítico e espessa unidade de gabro no topo. O pacote ultramáfico apresenta textura primária cumulática produzida pela olivina e pelo ortopiroxênio, enquanto que no pacote gabróico a textura cumulática é dada pelo plagioclásio. Resultados de química mineral revelam magma relativamente primitivo - olivina ( $Fo_{82,5}$  a  $Fo_{85,7}$ ); piroxênio ( $En_{82,6}$  a  $En_{85,3}$ ); plagioclásio ( $An_{67,9}$  a  $An_{45,7}$ ). Ocorre cromita sob a forma disseminada e de delgado estrato de cromitito situado no topo do pacote de rochas ultramáficas. O empilhamento estratigráfico revela “trend” de diferenciação normal da base para o topo do Complexo e os dados estruturais sugerem que a câmara magmática esteja invertida. A mineralogia primária das rochas está praticamente toda transformada hidrotermalmente, restando relictos da mineralogia primária. Olivina, opx, cpx e plagioclásio estão transformados em serpentina, hornblenda, Mg-cumingtonita, tremolita, actinolita, talco, saussurita, carbonato, epidoto, clorita e quartzo. Estas condições metamórficas são condizentes com fácies xisto verde a anfíbolito. O conteúdo em elementos maiores e menores, bem como elementos traço reflete a percentagem de cumulados de olivina–opx-pl-cromita nas rochas indicando o fracionamento do magma da base para o topo da câmara magmática. Os teores de ETR nas rochas do Complexo Lago Grande apresentam inclinação positiva, sendo suave para as rochas ultramáficas e mais forte para a unidade gabróica, denotando enriquecimento em ETRL e forte anomalia de Eu para as rochas do Complexo Lago Grande. Dosagens em cristais de zircão extraídos de leucogabros pegmatóides retornaram idade por Sm/Nd de 2,72 Ga, com  $\epsilon_{Nd} (T=2.72 Ga)$  valores (-0.32 a -4.25), indicando contaminação das rochas por elementos das encaixantes. Datações U/Pb indicaram idade de  $2.722 \pm 53$  Ma para cristalização das rochas do Complexo Lago Grande e intersecção com a concórdia em  $2.553 \pm 61$  Ma, sugerindo atuação do processo metassomático hidrotermal IOCG sobre as rochas deste complexo. Há ainda outra intersecção com a concórdia em 600 Ma representado influência do evento Brasileiro sobre estas rochas. Os estudos focando a caracterização de EGP demonstram que nos cromititos predomina alta relação Pt-Pd-Rh e sulfo-arsenietos de Pt e Pd, enquanto que nos

níveis sulfetados predomina baixa relação Pt-Pd e bismutetos de Pd e cloretos de Bi, contendo Te, Tc e ligas de Ni, Zn, Cu, Sn e Au.

Palavras chave: EGP, intrusão acamadada, geocronologia, litogeoquímica, Carajás

## 1. INTRODUÇÃO

Esta dissertação de mestrado faz parte do Projeto Integrado de Pesquisa denominado “**Desenvolvimento de parâmetros comparativos da fertilidade do magmatismo máfico-ultramáfico de Carajás para mineralizações magmáticas (Ni, Cu, EGP, Cr, Ti-V) com base em estudos geocronológicos, petrológicos e do seu posicionamento tectônico-estratigráfico**”, aprovado no Edital MCT/CTMineral/VALE/CNPq 12/2009.

A metodologia para desenvolvimento deste estudo constou de petrografia, microsonda eletrônica, litogeoquímica, microscopia eletrônica de varredura e análises isotópicas para a geração de dados primários sobre as rochas do Complexo Lago Grande, os quais permitiram uma melhor compreensão dos processos geológicos que atuaram em sua evolução no contexto do magmatismo máfico-ultramáfico de Carajás.

O Complexo Máfico-Ultramáfico Acamadado Lago Grande faz parte da suíte de intrusões acamadadas localizadas na porção leste da Província Mineral Carajás, denominada de **Suíte Máfica-Ultramáfica Serra Leste** (Ferreira Filho et al., 2007).

Esta dissertação pretende contribuir para a compreensão da evolução do conhecimento geológico da porção leste da Província Mineral Carajás, onde ocorrem importantes mineralizações de Au-EGP, como Serra Pelada (Grainger et al., 2002) e intrusões máficos-ultramáficas acamadadas contendo cromititos com EGP, tendo o Complexo de Luanga como principal representante (Medeiros Filho e Meireles, 1985; Suita, 1988; Diella et al., 1995; Ferreira Filho et al., 2007).

As informações utilizadas para a realização deste trabalho foram gentilmente cedidas pela VALE, as quais foram integradas com as informações versando sobre a geologia regional e a tipologia desta modalidade de depósito.



## 2. METODOLOGIA DE TRABALHO

A metodologia de trabalho adotada para a realização da pesquisa está sintetizada no Anexo 01 - Fluxograma de Trabalho. A sistemática de trabalho compreendeu a integração das informações bibliográficas e do acervo técnico da VALE sobre o Complexo Lago Grande e a geologia regional no primeiro momento. Posteriormente, realizou-se uma etapa de campo no local de ocorrência do Complexo Lago Grande para estudo de sua geologia e para coleta de amostras de rocha dos principais tipos litológicos existentes destinadas aos estudos de petrografia, litogeoquímica, geocronologia, química mineral e microscopia eletrônica de varredura. As amostras coletadas foram de afloramentos e de testemunhos de sondagem.

As amostras destinadas à geocronologia foram coletadas nas porções pegmatóides da unidade gabróica e em um dique de diabásio existente na porção central do Complexo. As amostras, com massa em torno 10 kg cada, foram britadas, moídas e concentradas em bateia e separador eletromagnético tipo Frantz, com objetivo de concentrar os minerais pesados. Posteriormente o concentrado foi levado à lupa binocular para separação de cristais de zircão. Estes por sua vez foram submetidos a procedimentos de preparação e análise conforme detalhado no item 3 do artigo.

As amostras destinadas à laminação serviram para os estudos petrográficos, em luz refletida e luz transmitida, química mineral e microscopia eletrônica de varredura - MEV. A caracterização da composição primária dos minerais foi realizada por intermédio da seleção de núcleos preservados dos minerais primários, como olivinas, opx, plagioclásio e cpx. O estudo no MEV teve como foco a identificação dos minerais do grupo da platina e suas relações com os minerais metálicos (sulfetos e cromita) e silicatos presentes.

As amostras destinadas a litogeoquímica foram enviadas ao Laboratório ALS do Canadá para análise por XRF, ICP-MS, ICP-AES, IR07, IR08 para dosagem dos elementos e compostos discriminados no fluxograma de trabalho do Anexo 01.

**Submitted to Ore Geology Reviews – Manuscript number: ORGEO-D-13-00209**

**GEOLOGY, PETROLOGY AND GEOCHRONOLOGY OF THE LAGO GRANDE LAYERED COMPLEX: EVIDENCE FOR A PGE-MINERALIZED MAGMATIC SUITE IN THE CARAJÁS MINERAL PROVINCE, BRAZIL.**

Antonio Sales Teixeira\*; Cesar Fonseca Ferreira Filho\*; Maria Emília Schutesky Della Giustina\*; Sylvia Maria Araújo\*; Heloisa Helena Azevedo Barbosa da Silva\*\*

\* Instituto de Geociências, Universidade de Brasília, Brasília-DF, 70910-900, Brazil;

\*\* Furnas Centrais Elétricas S.A, Aparecida de Goiânia-GO, 74923-650, Brazil

## Abstract

The Lago Grande and Luanga mafic-ultramafic complexes are part of a cluster of PGE-mineralized layered intrusions located in the eastern part of the Carajás Mineral Province (CMP). The CMP occurs in the southeastern portion of the Amazonian Craton and is divided in the Rio Maria Domain to the south, where typical NeoArchean granite-greenstone terrains occur, and the Itacaiúnas Domain to the north. The latter includes the Archean (ca 2.75 Ga) metabasalt sequence of the Grão Pará Group, footwall to the jaspilite-hosted, giant iron deposits of Carajás. The PGE-mineralized intrusions occur in the Itacaiúnas Domain, which is also known for hosting several Cu-Au, Au-PGE and Ni world-class deposits.

The Lago Grande Complex is a NE-trending medium-size (12-km-long and average 1.7-km-wide) layered intrusion consisting mainly of mafic cumulate rocks and minor ultramafic cumulates. The stratigraphy of the intrusion is overturned and, to the south, overlain by highly foliated metamorphic rocks of the Xingu Complex. The layered sequence consists of an Ultramafic Zone to the southeast, and a Mafic Zone to the northwest. Geological sections defined by drilling indicate that igneous layers have moderate dip to the SE, such that the Ultramafic Zone overlie the Mafic Zone. The Ultramafic Zone, about 4 km long and 500 meter wide, comprises an up to 250 meter-thick sequence of interlayered harzburgite and pyroxenite at the base and pyroxenite at the top. The lower contact of the Ultramafic Zone with the Xingu Complex is poorly exposed, whereas the contact with the overlying Mafic Zone is gradational and characterized by interlayered pyroxenite and gabbroic rocks. The Mafic Zone consists of a monotonous sequence of gabbroic rocks with an estimated thickness of up to 1,000 meters in the central part.

Primary igneous minerals of the Lago Grande Complex are partially replaced by metamorphic assemblages that indicate temperatures up to the amphibolite facies of regional metamorphism. This metamorphic alteration is heterogeneous and characterized by an extensive hydration that largely preserves primary textures and bulk chemical composition. The penetrative fabric when present is restricted to narrow domains of up to few meters, and igneous textures are identified in adjacent non-deformed domains. Metamorphic assemblages consist of variable proportions of Mg-cummingtonite, serpentine, talc and magnetite in ultramafic rocks, and hornblende and/or actinolite-tremolite, clinozoizite, chlorite, micas, albite and minor quartz in mafic rocks.

The compositional range of cumulus olivine ( $Fo_{82.5-85.7}$ ) is consistent with a moderately primitive composition for the parental magma of the Lago Grande Complex. Cryptic variation of olivine in the Ultramafic Zone suggests the existence of one major compositional reversal interpreted as resulting of open-system crystallization involving replenishment by new primitive magma pulses. The sequence of crystallization in the Lago Grande Complex, consisting of

olivine + chromite, orthopyroxene + chromite, orthopyroxene, orthopyroxene + plagioclase and orthopyroxene + plagioclase + clinopyroxene, suggests that the parental magma was silica saturated. Mantle-normalized alteration-resistant trace element profiles of gabbroic rocks of the Lago Grande Complex are fractionated, as indicated by relative enrichment in LREE and Th, with pronounced negative Nb and Ta anomalies. Nd isotopic data obtained for both mafic and ultramafic lithotypes render Nd model ages between 2.94 and 3.56 Ga, with variably negative  $\epsilon_{\text{Nd}} (T=2.72 \text{ Ga})$  values (-0.32 to -4.25). The crystallization sequence of the intrusion and the composition of cumulus minerals, together with lithogeochemical and Nd isotopic results, are consistent with an original mantle melt contaminated with older continental crust.

Different styles of PGE mineralization occur in the Lago Grande Complex, as indicated by PGE mineralization associated with sulfide-poor chromitite, sulfide-bearing harzburgite and venulated sulfide-bearing altered rocks. The latter is considered to result from hydrothermal remobilization of the chromitite-hosted and/or sulfide-bearing magmatic mineralization. In sulfide-poor chromitite of the Lago Grande Complex the PPGE are highly enriched and show a negative slope in mantle-normalized profile for PGE contents, whereas IPGE are moderately enriched and show a positive slope. Normalized profile of the chromitite sample from the Lago Grande Complex is generally similar to profiles from Middle Group (MG) and Upper Group (UG) chromitites from the Bushveld Complex, and very close to profiles and overall contents of the MG-4 chromitites. Platinum group minerals (PGM) occur mainly at the edge of chromite crystals in the Lago Grande chromitite, consisting mainly of arsenites and sulfo-arsenites. Sulfide-bearing harzburgite samples with well preserved igneous mineralogy of the Lago Grande complex have low Pt/Pd (0.2 to 0.3) and high Pd/Ir (116.7 to 170.0) ratios. These ratios are very distinct from those obtained in the chromitite sample, thus suggesting that PGE contents in sulfide-bearing harzburgites and chromitites result from different magmatic concentration processes. Altered and venulated sulfide-bearing harzburgite samples from the Lago Grande complex have highly variable PGE contents. This variation is indicated by Pt/Pd ratio (< 0.02 to 8.0) and Pd/Ir ratio (5.0 to 810.0), suggesting that PGE were mobile and fractionated during hydrothermal alteration. Preliminary studies of PGM in venulated samples from the Lago Grande complex identified several minerals with variable contents of Cl and Bi. Mineralogical results in venulated and altered sulfide-bearing rocks suggest that Cl-bearing saline hydrothermal fluids, similar to those considered to be associated with the origin of both NeoArchean IOCG deposits and smaller Paleoproterozoic Cu-Au-W-Bi deposits in the Carajás Mineral Province, may be involved in the PGE remobilization by hydrothermal fluids.

The  $2722 \pm 53$  Ma U-Pb zircon age determined in this study for the Lago Grande Complex overlaps with the crystallization age of the Luanga Complex. This result supports the interpretation that layered intrusions in the eastern portion of the Carajás region result from coeval magmatic events. Similar styles of magmatic PGE mineralization, including PGE associated with sulfide-poor chromitites and PGE associated with disseminated sulfides in

ultramafic cumulates, occur in the coeval Luanga and Lago Grande complexes. PGE profiles for chromitites of the Lago Grande and Luanga complexes are remarkably similar suggesting that the same parental magma and/or magmatic concentration process were involved. The distribution of different styles of magmatic PGE mineralization in these two complexes, as well as in other intrusions located in the eastern portion of the Carajás Mineral Province, support the concept that they belong to a PGE-enriched mafic-ultramafic magma type, designated the Serra Leste Magmatic Suite. These layered complexes crystallized from siliceous high magnesian basaltic magmas, similar to the parental liquids to the world's principal PGE-sulfide deposits, such as those hosted by the Bushveld and Stillwater complexes.

*Keywords:* Carajás, PGE, layered intrusion, geochronology, lithogeochemistry

## 1. Introduction

The PGE-mineralized Lago Grande and Luanga complexes are part of a cluster of layered mafic-ultramafic intrusions located in the eastern part of the Carajás Mineral Province (CMP). This cluster of mafic-ultramafic intrusions, denominated Serra Leste Magmatic Suite (Ferreira Filho et al., 2007), is characterized by frequent PGE mineralizations of different styles. Magmatic PGE mineralizations are located close to the epigenetic Serra Pelada Au-PGE deposit (Grainger et al., 2002). This led to the suggestion that a fertile magmatism for PGE mineralization intruded the eastern part of the CMP (Ferreira Filho et al., 2007). Even though these layered intrusions were target for mineral exploration since the 80', published data is limited and so far restricted to the Luanga Complex. Therefore the geological, petrological and metallogenetic characteristics of the Serra Leste Magmatic Suite are loosely defined and mainly based on unpublished mineral exploration results.

This study consists of a geological, geochemical and geochronological characterization of the Lago Grande Complex and associated PGE mineralization. Results for the Lago Grande Complex obtained in this study are compared to published data for the Luanga Complex and provide key features supporting that PGE-mineralized layered intrusions in the Serra Leste region are linked to a specific magmatic suite. These closely associated PGE-mineralized intrusions suggest the existence of relatively PGE-enriched mafic-ultramafic magmatism in eastern portion of the Carajás Mineral Province. Because mafic-ultramafic magmas with abnormally enriched PGE content are uncommon, the slightly enriched Pt content in some marginal rocks of the Bushveld Complex (Barnes et al., 2010) and the small Permian Jinbaoshan ultramafic sill in China (Wang et al., 2010) are rare examples, the tectonic setting and mantle process involved in the origin of the Serra Leste Magmatic Suite are discussed in this study.

## **2. Regional Setting**

### *2.1 The Carajás Mineral Province*

The Carajás Mineral Province (CMP), located in the southeastern portion of the Amazonian Craton (Fig. 1A), is divided in two distinct domains: Rio Maria Domain to the south and Itacaiúnas Domain to the north (Araújo et al., 1988; Huhn et al., 1988). The Itacaiúnas Domain (Fig. 1B) is best known for hosting several world-class deposits (Docegeo, 1988), including the largest iron ore deposit in the world, as well as several Cu-Au and Ni world-class deposits. The CMP is bordered to the east by the Neoproterozoic Araguaia Belt and to the west by overlying Paleoproterozoic sequences of the Uatumã Supergroup (Docegeo, 1988; Araújo and Maia, 1991). Geological limits to the south, where typical granite-greenstone terrains occur of the Rio Maria Domain occur, and to the north, where Paleoproterozoic gneiss-migmatite-granulite terrains predominate, are not precisely defined.

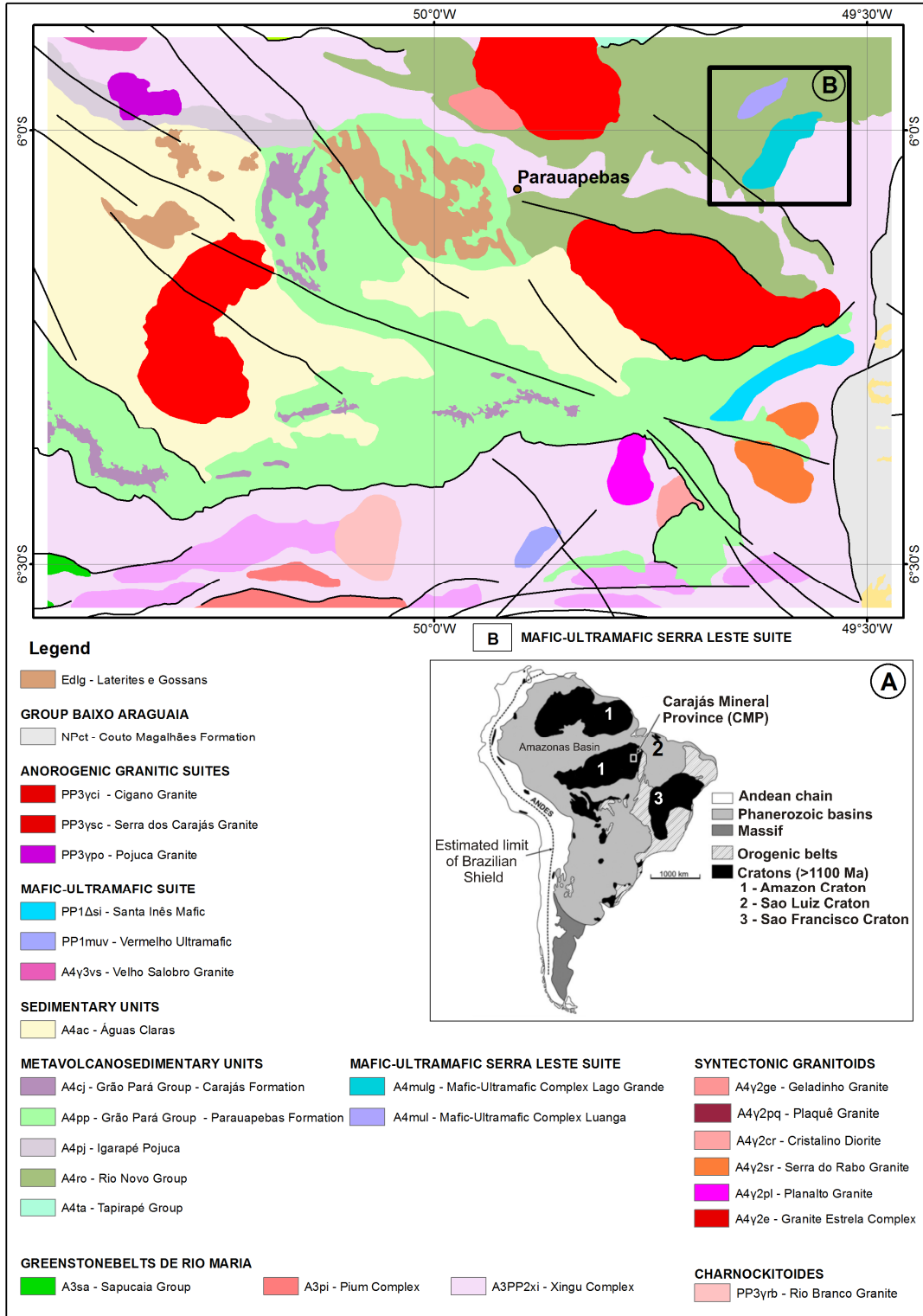


Fig. 1. A) Location of the Carajás Mineral Province. B) Geology of the northern domain of the CMP. Modified from Vasquez et al. (2008).



Archean basement of the CMP consists mainly of gneiss, migmatite and minor granulite, generally related to the Xingu Complex (Docegeo, 1988). U-Pb zircon dating of high-grade metamorphic rocks yielded Archean ages,  $2859 \pm 9$  Ma for edembergites of the Pium Complex (Pidgeon et al., 2000) and  $2859 \pm 2$  Ma for migmatites of the Xingu Complex (Machado et al., 1991). These are interpreted to represent ages of metamorphic recrystallization.

The Itacaiúnas Supergroup includes several Archean (ca. 2.75 Ga; Machado et al., 1991; Trendall et al., 1998) volcano-sedimentary sequences (Docegeo, 1988). These include the large sequence of metabasalts of the Grão Pará Group, footwall to the jaspilite-hosted, giant iron deposits of Carajás (Docegeo, 1988). This extensive basaltic volcanism is usually considered to result of intra-plate rifting of older continental crust (Gibbs et al., 1986; Olszewski et al., 1989; Villas and Santos, 2001) but subduction-related environments have also been proposed (Dardenne et al., 1988; Teixeira and Egger, 1994).

The Rio Fresco Group (Docegeo, 1988) or Águas Claras Formation (Araújo et al., 1988; Soares et al., 1994) is a low-grade metamorphic sedimentary sequence. This sequence of clastic sedimentary rocks, comprising mainly sandstone and siltstone formed in shallow marine to fluvial environment (Nogueira et al., 1994; 2000), covers different sequences of the Itacaiúnas Supergroup. The U-Pb zircon age of  $2645 \pm 12$  Ma for gabbroic dikes cross cutting the Águas Claras Formation provides a minimum age for this sedimentary sequence (Dias et al., 1996).

The CMP was intruded by granitic magmas of distinct ages and compositions. These intrusions are mainly correlated to three distinct periods. Archean (ca. 2.74-2.76 Ga) intrusions include the Plaquê Suite, as well as the Planalto, Estrela and Serra do Rabo granites (Avelar et al., 1999; Dall'Agnol et al., 1997; Barros et al., 2001). Younger (ca. 2.56 Ga) intrusions include granites like the Old Salobo (Machado et al., 1991) and Itacaiúnas intrusions (Souza et al., 1996). Paleoproterozoic (ca. 1.88 Ga) intrusions include several anorogenic granitic plutons (Machado et al., 1991; Dall'Agnol et al., 1997) that belong to an

extensive A-type Proterozoic province of the Amazon Craton (e.g., Santos et al., 2001).

Several mafic-ultramafic complexes intrude the Xingu Complex or the Itacaiúnas Supergroup (Docegeo, 1988). These intrusions include large Ni-mineralized layered intrusions of the Cateté Suite and the PGE-mineralized Luanga Complex (Ferreira Filho et al., 2007). The latter crystallized at  $2763 \pm 6$  Ma (Machado et al., 1991) and is coeval with the extensive mafic magmatism of the Itacaiúnas Supergroup.

The structural evolution of the CMP is attributed to the development of regional E-W trending, steeply dipping fault zones, reactivated in several episodes in the Archean and Paleoproterozoic (Holdsworth and Pinheiro, 2000).

The Paleoproterozoic (ca. 1.87-1.88 Ga) extension event of the Amazonian Craton is indicated by dyke swarms in the CMP (Rivalenti et al., 1998).

## *2.2 The Serra Leste Magmatic Suite*

The Serra Leste Magmatic Suite (Ferreira Filho et al., 2007) consists of a cluster of small- to medium-size layered mafic-ultramafic intrusions located in the eastern part of the CMP (Fig. 2). Mafic-ultramafic complexes are intrusive into gneiss and migmatite of the Xingu Complex and/or volcanic-sedimentary rocks of the Itacaiúnas Supergroup (known as Rio Novo Group in the region; see Fig. 2). The regional distribution of intrusions considered to be part of the Serra Leste Magmatic Suite is loosely constrained. They were grouped based on the presence of PGE mineralization or PGE anomalies, disregarding any geological, stratigraphic or petrological consideration. During early exploration for PGE deposits nearby the Luanga Complex, these intrusions have been interpreted as tectonically dismembered segments of a single large intrusion. However, the different stratigraphic sequences of three PGE-mineralized medium-size layered complexes (e.g. Luanga, Formiga and Lago Grande) in the Serra Leste region (Fig. 2) indicate that they are separate intrusions (Ferreira Filho et al., 2007).

The PGE-mineralized Luanga Complex is the only intrusion of the Serra Leste Magmatic Suite with published data (Medeiros Filho and Meireles, 1985; Suita, 1988; Diella et al., 1995; Ferreira Filho et al., 2007). The Luanga Complex is a medium-size ( $\sim 18 \text{ km}^2$ ) mafic-ultramafic intrusion hosting stratabound PGE-Ni mineralization (Ferreira Filho et al., 2007; 2010). Based on U-Pb zircon age of gabbroic rocks ( $2763 \pm 6 \text{ Ma}$ ; Machado et al., 1991) the Luanga Complex is considered to be coeval with the extensive bimodal volcanism of the Grão Pará Group (ca. 2.75 Ga; Machado et al., 1991; Trendall et al., 1998). The PGE-Ni mineralization is hosted in orthopyroxenite and harzburgite located in the transition from a lower ultramafic zone to an upper zone of interlayered ultramafic and mafic cumulates. PGE-Ni mineralization occurs in a continuous ( $\sim 5 \text{ km}$ ) and thick (10-50 meter-thick) layer of disseminated (1-3 vol. %) base metal sulfides. Anomalous PGE content also occurs in massive chromitites of the Luanga Complex (Diella et al., 1995).

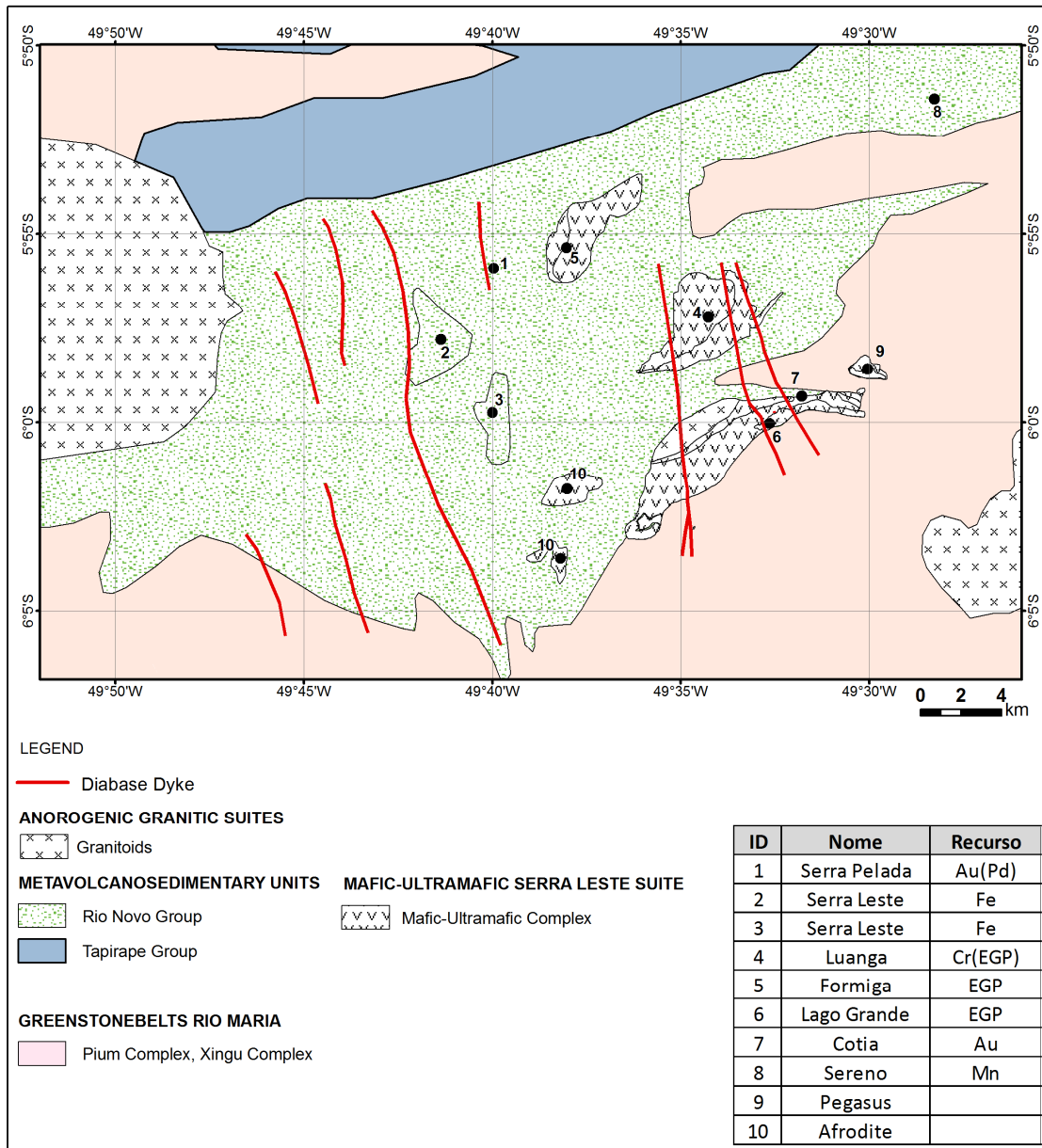


Fig. 2. Geology of the Serra Leste region. Partially modified from VALE's internal reports.

### **3. Analytical Procedures**

#### *3.1 Microprobe analyses*

Mineral analyses were performed on polished thin section using a 5-spectrometer JEOL JXA-8230 SuperProbe at the Electron Microprobe Laboratory of the University of Brasília (Brazil). The wavelength dispersive (WDS) analyses were performed at an accelerating voltage of 15 kV and a beam current of 10 nA. Both synthetic and natural mineral standards were used for the analyses and the same standards and procedure were retained throughout. Fe<sup>3+</sup> contents were estimated using site and charge balance calculations on cation-normalised analyses. Routine analyses (EDS) of several minerals were also used to support petrographic studies. Systematic WDS analyses were obtained for olivine, orthopyroxene, clinopyroxene, and plagioclase. Tables 01 and 03 show representative analyses of olivine, orthopyroxene and plagioclase.

#### *3.2 Bulk rock analyses*

Sample preparation and litho-geochemistry analyses were performed at the ALS Chemex (Canada). A total of 16 representative samples from outcrops and from one diamond borehole were analysed using three different procedures. These include the whole rock package plus LOI (ALS Chemex codes: ME-XRF12st and OA-GRA05x), total S plus total C (ALS Chemex codes: S-IR08 and C-IR07) and 38 elements fusion ICP-MS package (ALS Chemex code: ME-MS81). A complete description of analytical methods is available in the ALS Chemex Home Page ([www.alsglobal.com](http://www.alsglobal.com)). Results for these 16 samples are shown in Table 04.

#### *3.3 Sm-Nd isotopic analyses*

Sm-Nd isotopic analyses followed the method described by Gioia and Pimentel (2000) and were carried out at the Geochronology Laboratory of the University of Brasília. Whole rock powders (ca. 3000 mg) were mixed with

<sup>149</sup>Sm-<sup>150</sup>Nd spike solution and dissolved in Savillex bombs. Sm and Nd extraction of whole-rock samples followed conventional cation exchange techniques. Sm and Nd samples were loaded on Re evaporation filaments of double filament assemblies and the isotopic measurements were carried out on a multi-collector Finnigan MAT 262 mass spectrometer in static mode. Uncertainties for Sm/Nd and <sup>143</sup>Nd/<sup>144</sup>Nd ratios are better than ±0.5% (2 σ) and ±0.005% (2 σ), respectively, based on repeated analyses of international rock standards BHVO-1 and BCR-1. The <sup>143</sup>Nd/<sup>144</sup>Nd ratios were normalized to <sup>146</sup>Nd/<sup>144</sup>Nd of 0.7219 and the decay constant used was 6.54 × 10<sup>-12</sup> a<sup>-1</sup>. The TDM values were calculated using the model of DePaolo (1981). Nd procedure blanks were better than 100 pg. Sm-Nd results for 12 samples are shown in Table 5.

### *3.4 LA-ICPMS U-Pb zircon analyses*

Zircon concentrates were extracted from ca. 10 kg rock samples using conventional gravimetric and magnetic techniques at the Geochronology Laboratory of the University of Brasília. Mineral fractions were handpicked under a binocular microscope to obtain fractions of similar size, shape and color. For in situ U-Pb analyses, hand-picked zircon grains were mounted in epoxy blocks and polished to obtain a smooth surface. Before every micro-analytical procedure, mounts were cleaned with dilute (ca. 2%) HNO<sub>3</sub>. Backscattered electron and cathodoluminescence images were obtained using a FEI-QUANTA 450 SEM working at 15 kV at the University of Brasília.

For U-Pb isotopic LA-ICPMS analyses, the sample was mounted in an especially adapted laser cell and loaded into a New Wave UP213 Nd:YAG laser (λ = 213 nm), linked to a Thermo Finnigan Neptune Multi-collector ICPMS. Helium was used as the carrier gas and mixed with argon before entering the ICP. The laser was run at a frequency of 10 Hz and energy of ~100 mJ/cm<sup>2</sup> with a spot diameter of 30 μm for U-Pb systematics. The U-Pb LA-ICPMS analyses followed the analytical procedure described by Buhn et al. (2009) and were carried out at the Geochronology Laboratory of the University of Brasília.

Two international zircon standards were used. A fragment of zircon standard GJ-1 (Jackson et al., 2004) was used as the primary reference material in a standard-sample bracketing method, accounting for mass bias and drift correction. The resulting correction factor for each sample analysis considers the relative position of each analysis within the sequence of 4 samples bracketed by two standard and two blank analyses each (Albarède et al., 2004). An internal standard was run at the start and at the end of each analytical session, yielding accuracy around 2% and a precision in the range of 1% ( $1\sigma$ ). Uncertainties in sample analyses were propagated by quadratic addition of the external uncertainty observed for the standards to the reproducibility and within-run precision of each unknown analysis. Zircon grains with  $^{206}\text{Pb}/^{204}\text{Pb}$  lower than 1000 were rejected. Plotting of U–Pb data was performed using ISOPLOT v.3 (Ludwig, 2003) and errors for isotopic ratios are presented at the  $1\sigma$  level. U-Pb results for sample LU-SI-20B are shown in Table 6.

### *3.5 PGE and PGM analyses*

Sample preparation and PGE analyses were performed at the ALS Chemex (Canada). A total of 05 samples from boreholes were selected based on Pt-Pd exploration data, for PGE+Au analyses. These were performed using pre-concentration and neutron activation analyses (ALS-CHEMEX code PGM-NAA26). A complete description of analytical methods is available in the ALS Chemex Home Page ([www.alsglobal.com](http://www.alsglobal.com)). Results for these 05 samples are shown in Table 07.

Description and analyses of PGM by Scanning Electron Microscopy (SEM) were developed in FURNAS Laboratory (LEICA SEM model S440i with and Oxford EDS) and in the LabMic Laboratory of the Universidade Federal de Goiás (JEOL SEM model JSM 6610). PGM results are shown in Table 8.

## 4. The Lago Grande Layered Mafic-Ultramafic Complex

### 4.1 Geology

This study provides the first published geological-stratigraphic description of the Lago Grande layered complex. Geological maps (Figs 3 and 4) and section (Fig. 5) are mainly based on extensive mapping and drilling data developed by VALE for exploration programs in the region. The Lago Grande Complex consists of a 12-km-long and average 1.7-km-wide NE trending sequence of layered mafic-ultramafic rocks (Fig. 3). This layered sequence is truncated by the EW trending Cotia shear zone in the northeastern portion. Host rocks of the Lago Grande Complex consist of highly foliated gneiss, migmatite and amphibolite of the Xingu Complex in the south. To the north the complex is limited by metavolcanic rocks of the Rio Novo Group and a metadiorite body interpreted as a granitoid of the Estrela Suite. Host rocks are poorly exposed in the contact zone, and geological contacts are partially based on soil geochemistry and geophysical surveys.

Poorly exposed magnetite-bearing rocks occur close to the upper (northwestern) contact of the Mafic Zone (Fig. 3). This sequence of magnetite-bearing mafic rocks is well defined by ground magnetometric surveys, and consists mainly of fine to medium-grained plagioclase, actinolite/hornblende and magnetite crystals. Rocks with distinct foliation and nematoblastic texture (amphibolite) occur associated with massive rocks with intergranular to subophitic texture. They were previously (e.g. VALE's internal reports) interpreted to represent an upper and more fractionated portion of the Mafic Zone. They are however re-interpreted in this paper as part of the Vila Nova volcanic sequence.

Several NNW diabase dykes cross cut the Lago Grande Complex and host rocks (Fig. 3). These dykes are up to several meters-wide and belong to a regional swarm of magnetic mafic dykes. These dykes have an aphanitic chilled margin, usually few millimeter-wide, with fine to medium grained intergranular to ophitic texture in the central portions. They consist mainly of clinopyroxene,



olivine and plagioclase, with accessory Ti-magnetite. Primary igneous minerals are largely preserved, with minor alteration of clinopyroxene to chlorite and Ti-magnetite to titanite. Thin dykes with intersected texture consist of microphenocrysts of olivine, clinopyroxene and plagioclase within an aphanitic matrix. Olivine microphenocrysts consist of corroded euhedral crystals altered to a reddish fine-grained aggregate (iddingsite).

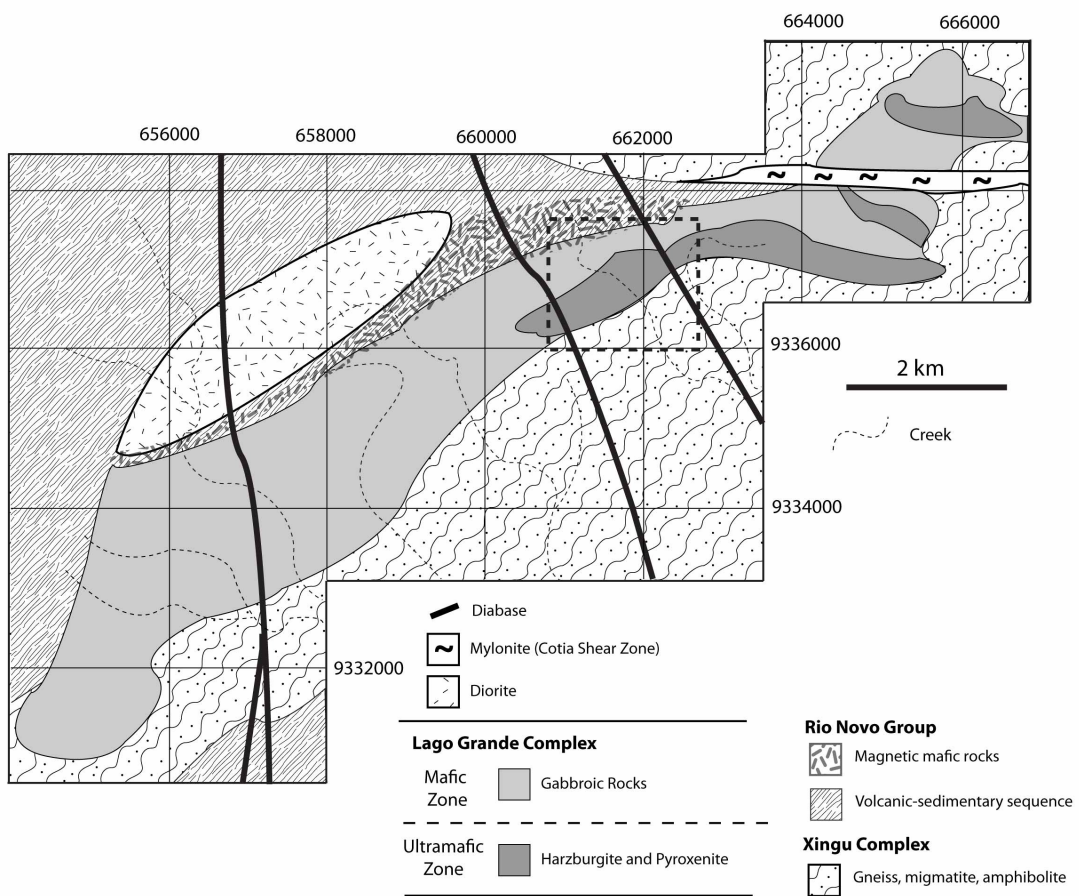


Fig. 3. Geological map of the Lago Grande Complex (partially modified from unpublished report of VALE). Location of the map in Fig. 4 is indicated by dashed rectangle.

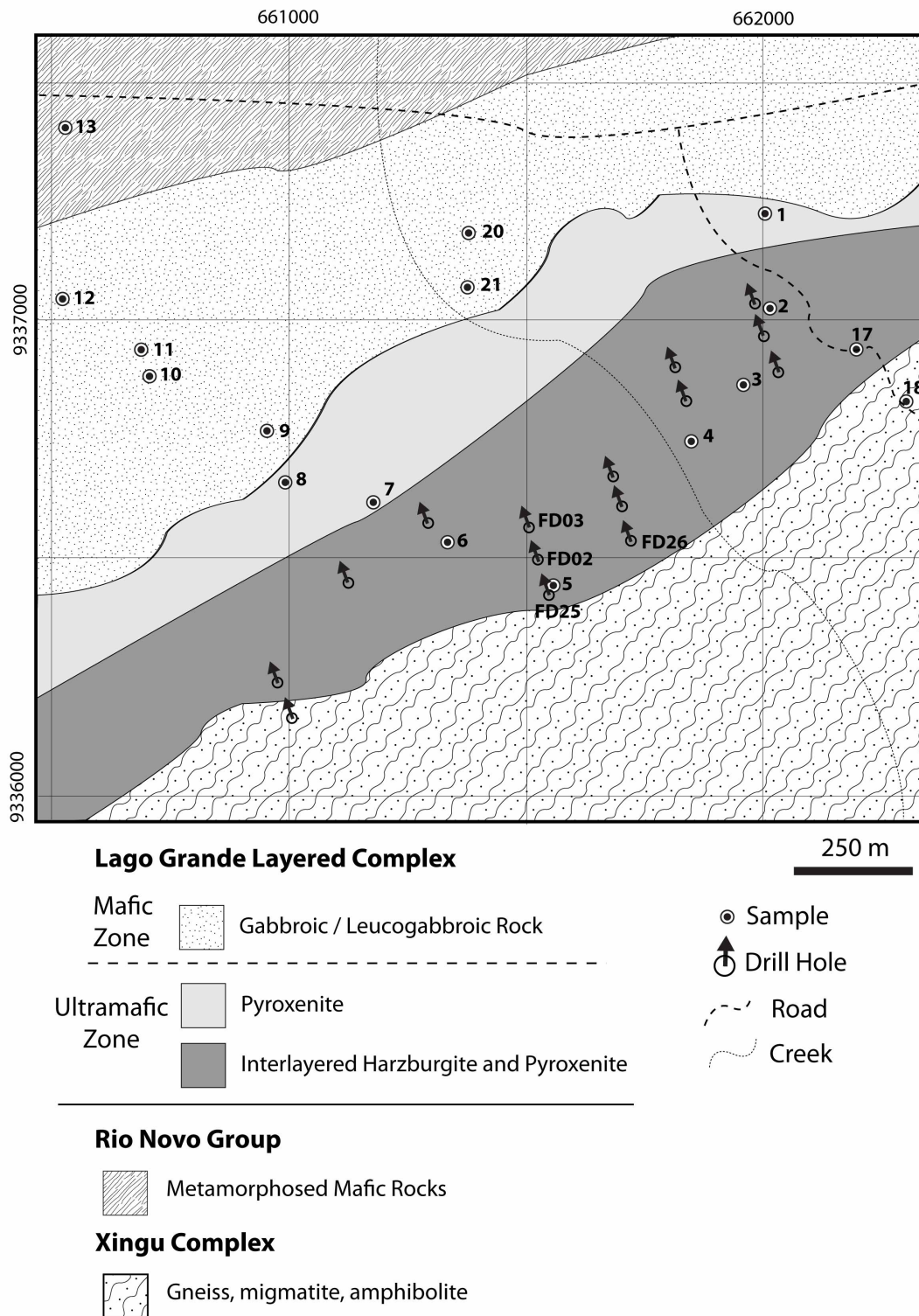


Fig. 4. Geological map of the central portion of the Lago Grande Complex (partially modified from unpublished report of VALE).

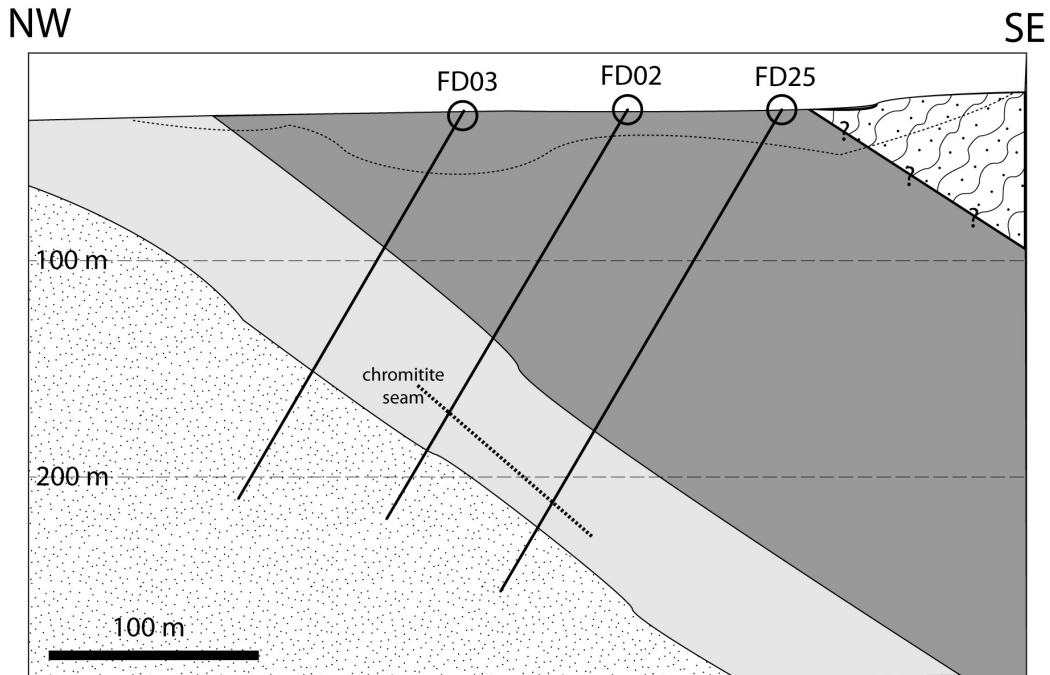


Fig. 5. Geological section (partially modified from unpublished report of VALE). See Fig. 4 for captions and location of drill holes. Dashed line indicates the limit of the weathering profile (saprolite or partially weathered rocks).

Outcrops of mafic-ultramafic rocks of the Lago Grande Complex consist mainly of massive blocks and boulders scattered in a flat lying area of cattle ranches (Fig. 6A). Mafic cumulates predominate and ultramafic cumulates are restricted to a 5-km-long zone in the eastern portion of the Lago Grande Complex (Fig. 3). Primary igneous textures are largely preserved but primary igneous minerals are partially to extensively altered to metamorphic minerals. Extensive drilling in the central portion of the complex exposed complete sections of the layered sequence (Figs. 4 and 5). In this portion of the Lago Grande Complex, the layered sequence consists of an Ultramafic Zone to the southeast, and a Mafic Zone to the northwest. Geological sections defined by drilling (Fig. 7) indicate that igneous layers have moderate dip to the SE, such that the Ultramafic Zone overly the Mafic Zone. Geological sections based on drilling together with petrological data (to be discussed in following sections) suggest that the layered sequence is overturned. Even though tectonic

processes leading to this overturned sequence layered rocks are not discussed in this paper, and robust structural data of regional structures in this region are not available, the layered sequence is described as overturned in the following descriptions. An overturned layered sequence was also described for the Luanga Complex (Ferreira Filho et al., 2007), suggesting the existence of regional scale structures leading to large overturned blocks in the Serra Leste region, a subject to be further addressed in the discussion of this paper.

#### *4.1.1 The Ultramafic Zone*

The Ultramafic Zone, about 4 km long and 500 meter wide, is restricted to the NE portion of the complex. It comprises an up to 250 meter-thick sequence of interlayered harzburgite and pyroxenite at the base (e.g. considering an overturned sequence) and pyroxenite at the top. The southeastern contact (lower contact) of the Ultramafic Zone with the Xingu Complex is poorly exposed. The contact with the overlying Mafic Zone is also poorly exposed in the field, but is well exposed in several drilling sections. This contact is gradational and characterized by a dozen of meters thick sequence of interlayered pyroxenite and mafic rocks.

Olivine-bearing rocks are mainly harzburgite consisting of olivine (Ol), orthopyroxene (Opx), minor clinopyroxene (Cpx) and accessory chromite. The relative amount of Ol and Opx is variable, from dunite (Ol + Chr cumulate) to Ol orthopyroxenite (Ol + Opx + Chr cumulate). Different lithotypes (dunite, harzburgite, Ol orthopyroxenite) occur interlayered in scales that vary from few centimeters to several meters. Primary igneous textures vary accordingly, from adcumulate in dunite to meso or orthocumulate in harzburgite. The latter is usually characterized by highly absorbed anhedral Ol crystals enclosed in larger poikilitic Opx crystals. Coarse-grained (up to several centimeters) anhedral Opx crystals with irregular distribution in medium-grained harzburgite (Fig. 6B and 6C) form breccia-like structures in outcrops. These structures are likely to represent zones with abundant trapped intercumulus liquid, possibly partially remobilized from the cumulate pile. Most harzburgites consist of larger anhedral Opx crystals, frequently enclosing partially absorbed anhedral Ol, surrounded

by aggregates of medium-grained euhedral Ol crystals (Fig. 6D). Chromite is a ubiquitous accessory mineral (about 2-3 vol. %) in harzburgite and Ol orthopyroxenite, suggesting cotectic crystallization.

Orthopyroxenite are medium- to coarse-grained rocks with adcumulate to mesocumulate texture, the latter characterized by interstitial plagioclase (Pl) and/or minor Cpx. Chromite occurs frequently, but not always, as an accessory mineral (< 2 vol. %). This indicates the upward transition from Opx + Chr cumulates to Opx cumulates in the Ultramafic Zone.

Primary igneous minerals are partially to extensively replaced by metamorphic assemblages. Metamorphic alteration is heterogeneous and extensively replaced rocks are closely associated with rocks with primary igneous minerals. Rocks with extensively replaced igneous minerals usually preserve primary textures, frequently as pseudomorphs of Ol replaced by Mg-cummingtonite, serpentine and magnetite and pseudomorphs of Opx replaced by Mg-cummingtonite, talc and serpentine. Metamorphic assemblage replacing orthopyroxenite with interstitial plagioclase are characterized by the presence of chlorite, usually forming aureoles around larger pseudomorphs of Opx replaced by Mg-cummingtonite, talc and serpentine. Metamorphic assemblages of ultramafic rocks indicate physical conditions that reached temperatures equivalent of the amphibolite facies of regional metamorphism. Exploration assays of core samples (sampled at 1 meter-long interval) provide the chemostratigraphy of the Ultramafic Zone. This is illustrated in Figure 7 by the variation of Ni content throughout the stratigraphy in Drill Hole FD26. Ni contents in the Ultramafic Zone are positively correlated to the amount of olivine or olivine pseudomorphs. Harzburgite has Ni contents above 1,000 ppm (up to 2,500 ppm in thin dunite layers intercepted in few drill holes), whereas orthopyroxenite has Ni contents below 500 ppm. Interlayered harzburgite and pyroxenite at the base of the Ultramafic Zone is characterized by overall higher Ni contents and sharp variation in Ni contents (Fig. 7). Pyroxenite at the top of the Ultramafic Zone has lower Ni contents and is characterized by a gradational transition to gabbroic rocks of the Mafic Zone (Fig. 7).



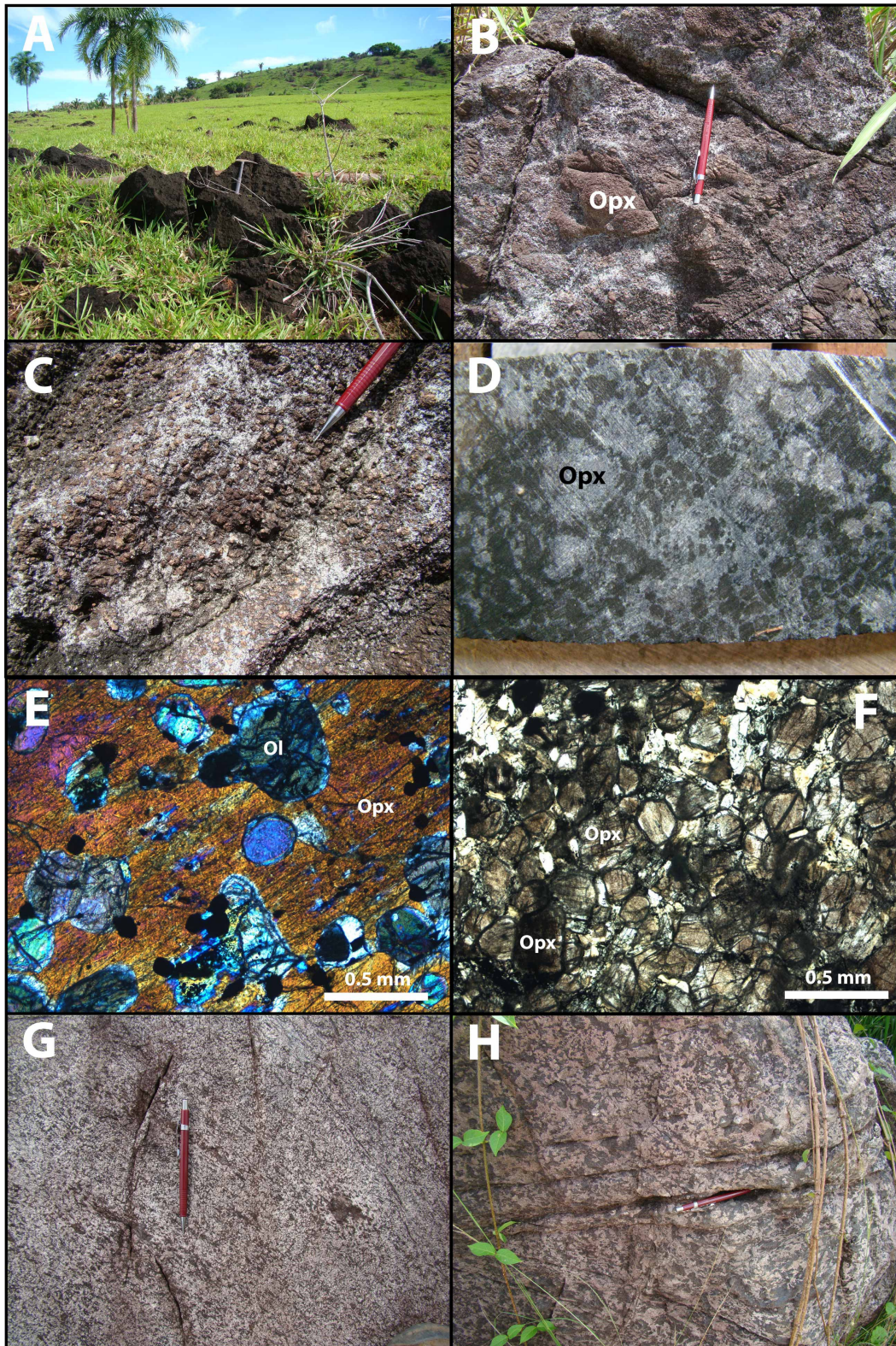


Fig. 6. A) Boulders of ultramafic rocks of the Lago Grande Complex. B) Harzburgite. Large Opx oikocrysts within domains of medium-grained Opx+Cpx



(whitish color). See sample 04 in Fig. 4 for location. C) Detail of the medium-grained domains of the previous photo. D) Harzburgite. Detail of Opx oikocrysts (with inclusion of anhedral Ol) and euhedral (black color due to serpentinization) Ol. E) Harzburgite. Photomicrograph of large Opx oikocryst enclosing several olivine (Ol) anhedral crystals and chromite (opaque) euhedral crystals. F) Orthopyroxenite. Photomicrograph of an aggregate of Opx crystals with minor associated white to pale green amphibole crystals. G) Medium-grained gabbroic rock consisting of anhedral pyroxene (black) and tabular plagioclase (whitish color). See sample 08 in Fig. 4 for location. H) Pegmatoid gabbroic pod from the same outcrop of the previous photo.

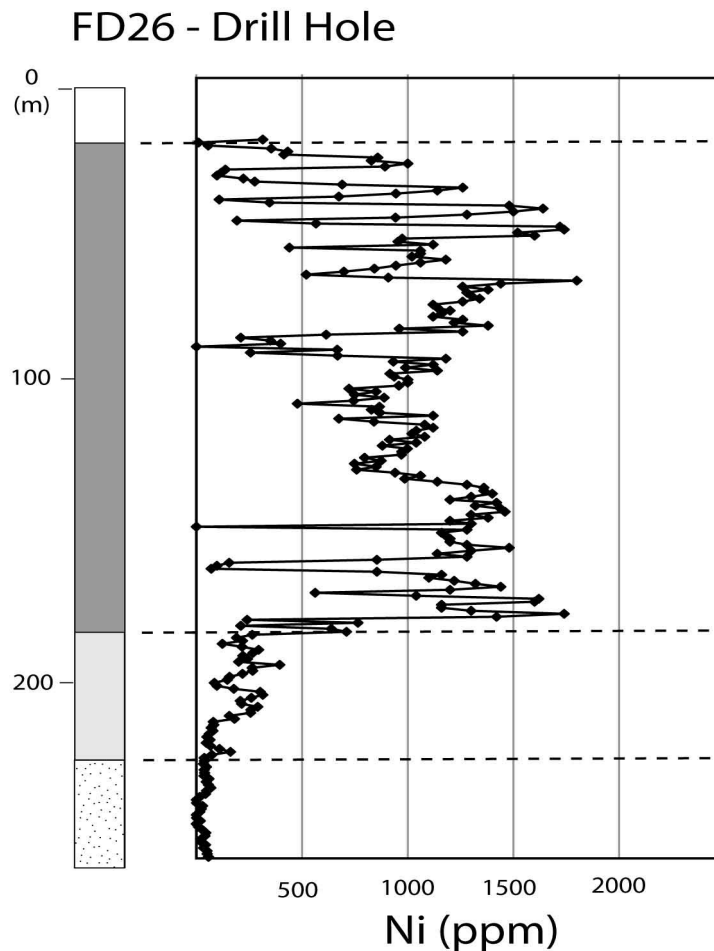


Fig. 7. Ni content for Drill Hole FD26. See Fig. 4 for captions and location of drill hole.

#### 4.1.2 *The Mafic Zone*

The Mafic Zone comprises most of the Lago Grande Complex. It consists of a monotonous sequence of gabbroic rocks with an estimated thickness of up to 1,000 meters in the central part. Most of the sequence consists of massive medium-grained gabbroic rocks (Fig. 6G), consisting of anhedral pyroxene pseudomorphs and variably altered tabular plagioclase. Because pyroxene crystals are pervasively altered in the studied gabbroic rocks, optical and chemical (see mineral chemistry section in this study) identification (i.e., Opx and/or Cpx) are not possible. These rocks are therefore described as PI and pyroxene cumulates and discussions on the composition of pyroxenes will be addressed together with chemical data.

Elongated pods or irregular dykes of pegmatoid gabbroic rocks, up to several meters wide, occur associated with medium-grained gabbroic rocks (Fig. 6H). These pegmatoidal rocks consist of coarse-grained plagioclase and pyroxene crystals associated with accessory fine-grained apatite and quartz, as well as minor zircon. Pegmatoidal pods are interpreted as resulting of later crystallization of trapped intercumulus liquid. Ductile shear zones eventually truncate massive gabbroic rocks. Within these sheared zones, which are up to several meters wide, gabbroic rock developed a distinct foliation, frequently defined by elongated plagioclase and pyroxene crystals.

Primary igneous minerals are partially to extensively replaced by metamorphic assemblages in the Mafic Zone. Igneous plagioclase is extensively altered to a fine-grained aggregate of clinozoizite, micas, albite and minor quartz. Relicts of igneous plagioclase are just eventually preserved, usually in small portions of large crystals. Igneous pyroxene is pervasively altered to a fine-grained aggregate of amphiboles (hornblende and/or actinolite-tremolite) and chlorite. Metamorphic assemblages of gabbroic rocks indicate physical conditions that reached temperatures equivalent to the amphibolite facies of regional metamorphism.



## 4.2 Mineral Chemistry

Systematic studies of mineral composition of cumulus minerals of the Lago Grande Complex are limited due to extensive alteration of the igneous assemblage. Olivine and Opx were analyzed on samples of harzburgite throughout drill hole FD26. Plagioclase crystals were analyzed on 3 samples of gabbroic rocks from outcrops and 1 sample from drill hole FD26. Limited quantitative analyses of amphiboles and qualitative (EDS) analyses of several minerals were performed to support petrographic descriptions. Representative analyses of olivine, orthopyroxene and plagioclase are reported in Tables 1-2-3.

Detailed sampling (20 drill core samples) and petrographic studies of drill hole FD26 provided for chemical analyses 7 samples with igneous Ol and 4 samples with igneous Opx. Compositional variation of Ol and Opx with stratigraphic height (Fig. 8) in drill hole FD26 is limited to samples of harzburgite located in the central portion of the Ultramafic Zone. In these samples Ol compositions range from  $Fo_{86.7}$  to  $Fo_{80.4}$  indicating moderately primitive compositions. Compositional variation of olivine with stratigraphic height (considering an overturned stratigraphy) indicates a more fractionated composition for the lowermost analyzed harzburgite ( $Fo_{82.5}$  to  $Fo_{80.4}$ ), followed by an interval where Ol compositions have very limited compositional variation ( $Fo_{83.0}$  to  $Fo_{85.7}$ ). In the latter the compositional variation of olivine shows a general upward fractionation trend (e.g. decrease in Fo content). Ni contents in olivine range from 1900-3700 ppm and are positively correlated with Fo content. Opx compositions in harzburgite, limited to 4 samples, do not match perfectly the fractionation trend defined by olivine compositions. Compositional variation of Opx with stratigraphic height indicates a more fractionated composition for the lowermost analyzed harzburgite ( $En_{82.0}$ ), followed by three samples where Opx compositions have very limited compositional variation ( $En_{82.6}$  to  $En_{85.3}$ ). These features are consistent with olivine composition for this stratigraphic interval, except for the fact that Opx compositions do not show a general upward fractionation trend. Distinct compositional trends for Ol and Opx compositions in these three samples are likely to result from samples where Opx is an intercumulus mineral. Opx crystals have ubiquitous exsolution

lamellae or irregular blebs of Cpx, resulting in highly variable CaO contents for individual samples. To reduce scattering of the data, analyses with CaO content higher than 2.0 wt. % were disregarded during the interpretation of compositional variation with stratigraphic height. Opx crystals have  $Al_2O_3$  contents < 2.6 wt.%, and highly scattered contents of  $TiO_2$  (< 0.25 wt.%),  $Na_2O$  (< 0.14 wt.%) and Ni (< 900 ppm).

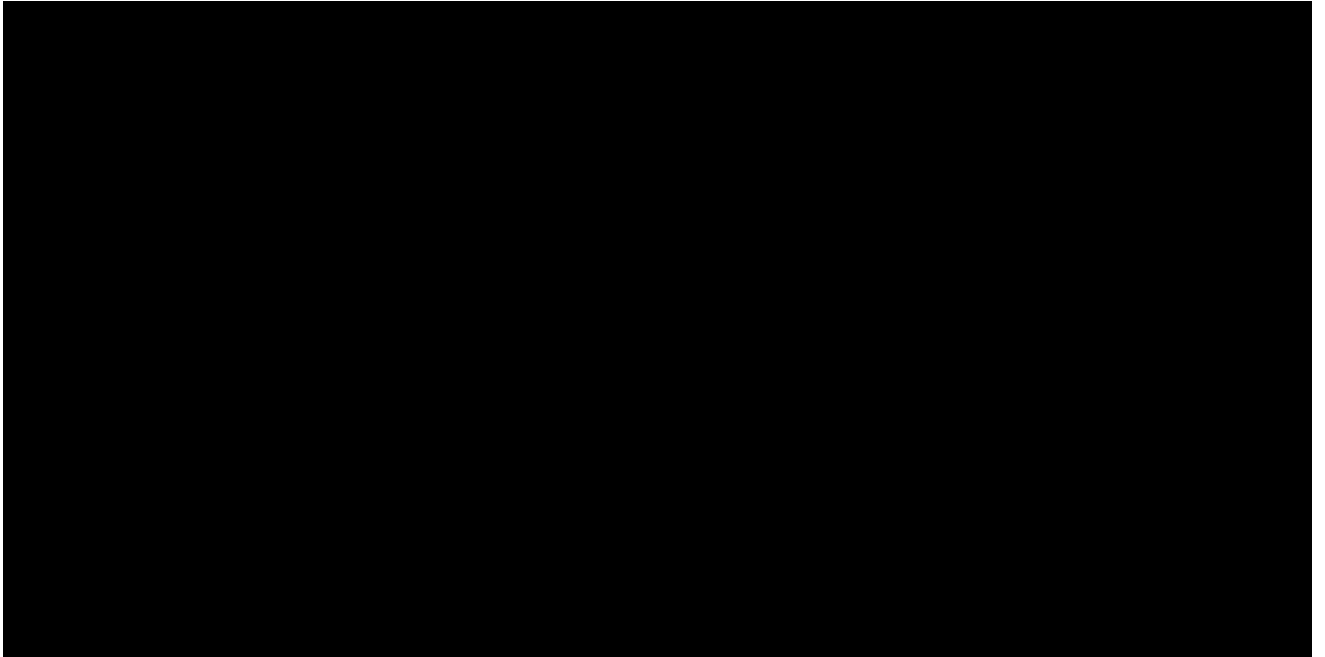


Table 01 – Representative analyses of olivine. Harzb = harzburgite.

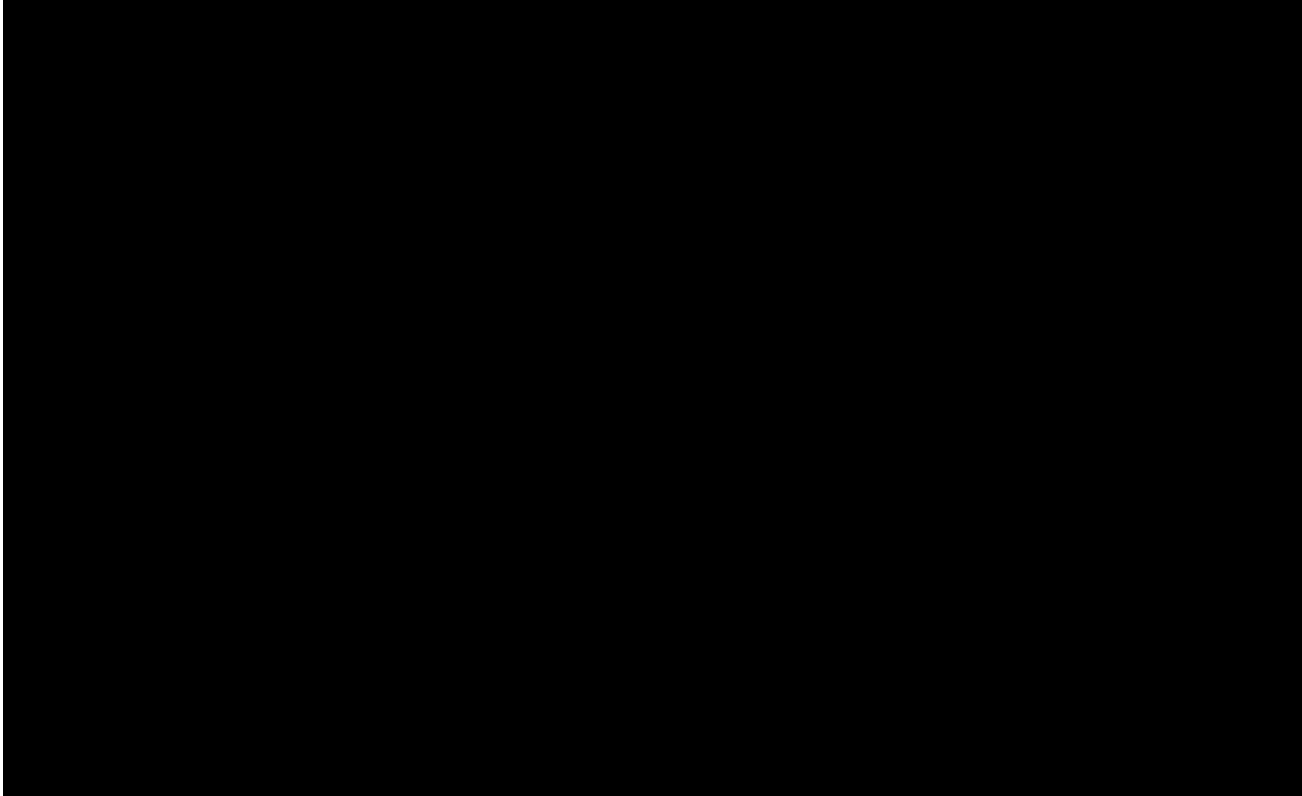
A large black rectangular redaction box covering the content of Table 02.

Table 02 – Representative analyses of orthopyroxene. Harzb = harzburgite.

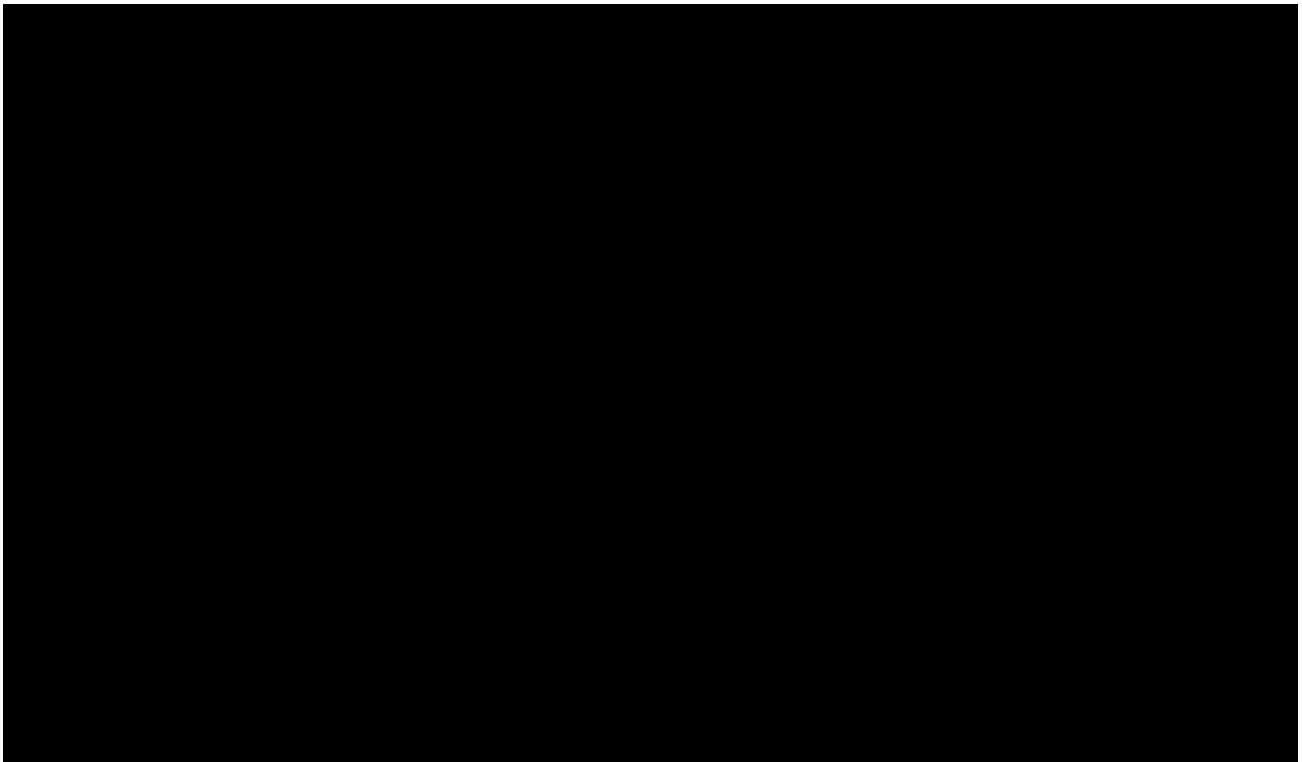
A large black rectangular redaction box covering the content of Table 03.

Table 03 – Representative analyses of plagioclase.

Due to extensive alteration compositions of igneous plagioclase were obtained just for 4 samples. These samples, located in different stratigraphic positions of the Mafic Zone, show a wide compositional range from  $An_{67.9}$  to  $An_{45.7}$ . Plagioclase crystals with the most primitive compositions ( $An_{67.9}$  to  $An_{63.1}$ ) were analyzed in a gabbroic sample (drill core FD26 - 260.5 meter) from the lower part of the Mafic Zone, located about 50 meters above the contact with the Ultramafic Zone. Plagioclase crystals with the most fractionated compositions ( $An_{48.8}$  to  $An_{45.7}$ ) were analyzed in a gabbroic sample (Sample 12 in Fig. 04) from the upper portion of the Mafic Zone. The latter corresponds to the sample with preserved igneous plagioclase located in the uppermost stratigraphic position within the Mafic Zone of the Lago Grande Complex.

Plagioclase compositions throughout the Mafic Zone suggest fractionation from moderately primitive compositions at the base (SE in Fig. 04) to more fractionated compositions toward the upper part (NW in Fig 04).

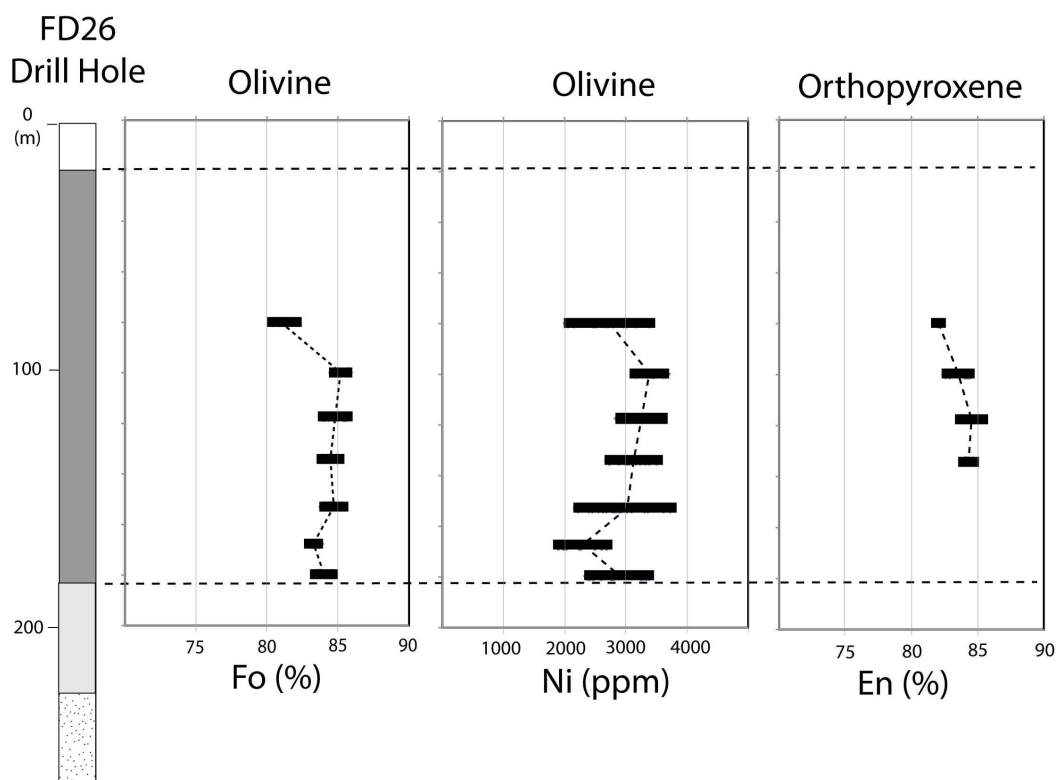


Fig. 8. Compositional variation of olivine and orthopyroxene for Drill Hole FD26. See Fig. 4 for captions and location of drill hole.

### 4.3 Bulk Rock Geochemistry

#### 4.3.1 Major and Minor Elements

Whole-rock chemical compositions of the Lago Grande Complex samples are listed in Table 4. Variable amounts of loss on ignition reflect the degree of alteration. Hence, the presented data are recalculated to anhydrous compositions for major and minor elements. Because the Lago Grande Complex consists of cumulate rocks, their major and minor element compositions are dominantly controlled by the type of cumulus minerals. The plot of major element oxides against MgO indicates the predominance of olivine, pyroxene and plagioclase cumulates (Fig. 9).

Olivine-bearing rocks have MgO contents (anhydrous base) bracket between 34.6 and 37.3 wt. %, consistent with the predominance of harzburgite. A comparison with the compositions of major constituent silicate minerals reveals that the contents of SiO<sub>2</sub>, CaO, Al<sub>2</sub>O<sub>3</sub>, Na<sub>2</sub>O and K<sub>2</sub>O in harzburgites are not controlled just by the proportions of olivine and orthopyroxene in the rocks (Fig. 9). Contents of Al<sub>2</sub>O<sub>3</sub>, CaO and K<sub>2</sub>O above the Ol-Opx tie lines, and SiO<sub>2</sub> below the Ol-Opx tie lines, result from the presence of minor intercumulus Cpx and phlogopite. The contents of Ni and Cr in harzburgites are controlled by olivine and accessory chromite, respectively (Fig. 10). Cr<sub>2</sub>O<sub>3</sub> contents (between 0.19 and 0.52 wt. %) are consistent with the occurrence of cumulus chromite in harzburgites.

Two samples of orthopyroxenites have MgO contents (anhydrous base) of 19.0 and 23.3 wt. %. These samples are partially to highly transformed Opx cumulates with minor intercumulus Pl. A comparison with the compositions of major constituent silicate minerals in orthopyroxenites (Fig. 9) is hampered by the fact that Opx crystals were analyzed just in harzburgite samples, which are expected to be more primitive (e.g. higher En content) than Opx crystals in orthopyroxenite. Cr<sub>2</sub>O<sub>3</sub> contents (up to 0.29 wt. %) are consistent with the occurrence of cumulus chromite in orthopyroxenite samples (Opx + Chr cumulate).

Gabbroic rocks are characterized by low MgO contents (< 10 wt. % in anhydrous base). A comparison with the compositions of major constituent silicate minerals in gabbroic rocks (Fig. 9) is also hampered by the fact that Opx were analyzed just in harzburgite. Nevertheless, contents of  $Al_2O_3$  and  $Na_2O$  below the PI- crystals were Opx tie lines, and  $K_2O$  well above the PI-Opx tie lines, suggest the common presence of minor K-feldspar and phlogopite (Fig. 9). Just the latter was eventually identified in partially to extensively altered gabbroic rocks. High  $TiO_2$  content in two samples of gabbroic rocks (up to 1.1 wt. %) is consistent with the occurrence of accessory Fe-Ti oxides in few samples (Fig. 10).

$CaO-Al_2O_3$  plot suggests that gabbroic rocks consist of PI+Opx or PI+Opx+Cpx (Fig. 11). This is consistent with a crystallization sequence characterized by Opx cumulates (orthopyroxenite) in the base, and Opx+Cpx+PI cumulates in the top.

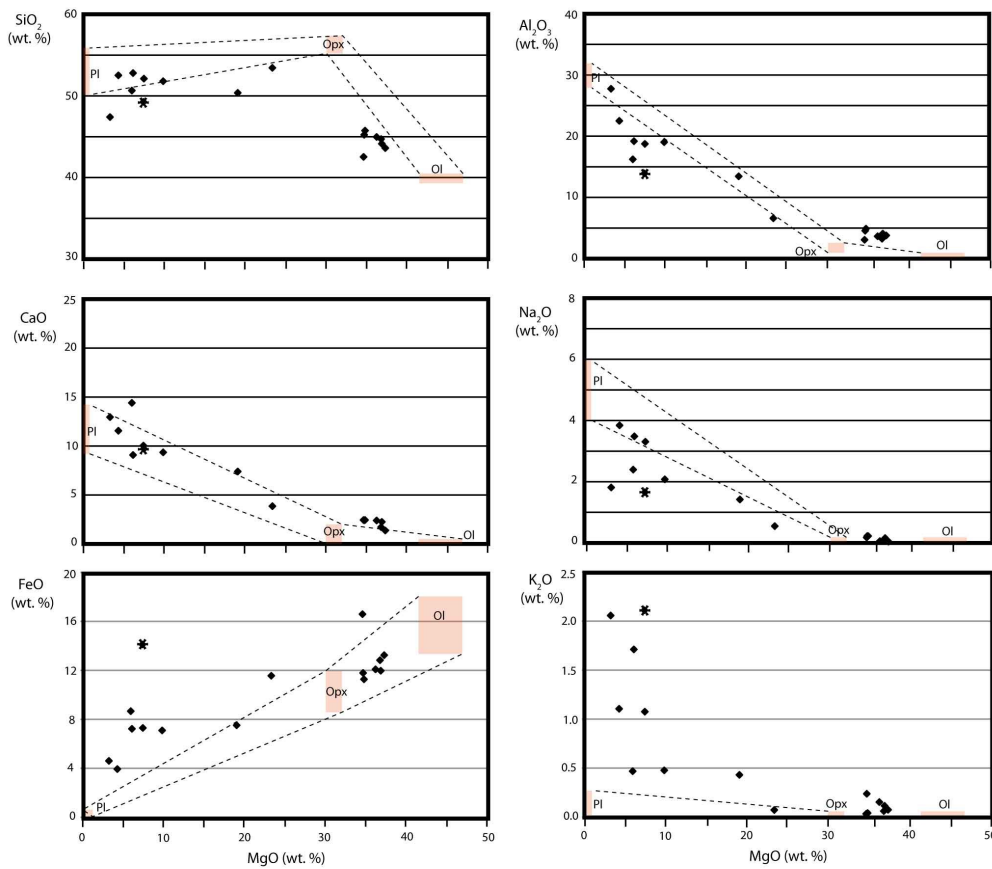


Fig. 9. Plot of MgO versus major element contents for rocks of the Lago Grande Complex. Data from Table 4 recalculated to anhydrous compositions.

Compositions of plotted Ol, Opx and Pl correspond to microprobe analyses reported in this study. Ol and Opx crystals were analyzed in harzburgite, whereas Pl crystals were analyzed in gabbroic rocks. \* Corresponds to sample LUSL19 (mafic rock from the Rio Novo Group).

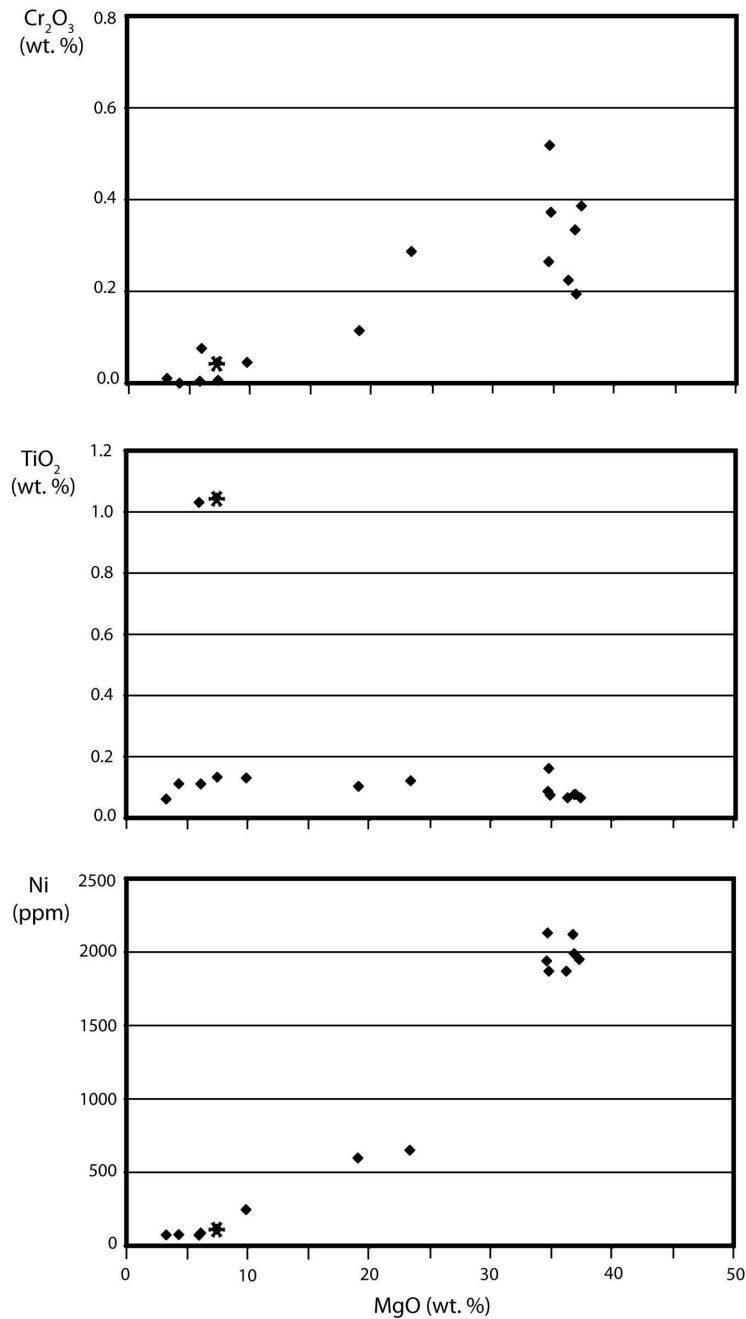


Fig. 10. Plot of MgO versus minor element contents for rocks of the Lago Grande Complex. Data from Table 4 recalculated to anhydrous compositions. \* Corresponds to sample LUSL19 (mafic rock from the Rio Novo Group).

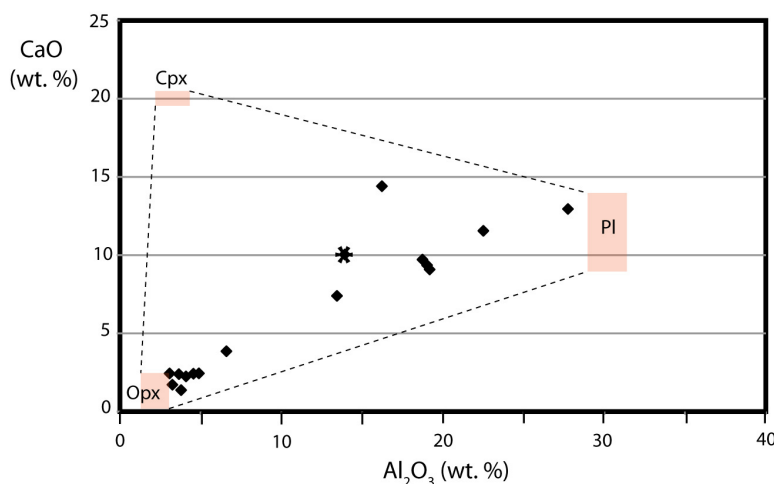


Fig. 11. Al<sub>2</sub>O<sub>3</sub>-CaO plot for rocks of the Lago Grande Complex. Data from Table 4 recalculated to anhydrous compositions. Compositions of plotted Opx and Pl correspond to microprobe analyses reported in this study, whereas plotted Cpx corresponds to expected composition of Cpx in gabbroic rocks. \* Corresponds to sample LUSL19 (mafic rock from the Rio Novo Group).

As a reconnaissance exercise, the composition of one mafic sample from the Rio Novo Group (LUSL19) was considered in this study. This sample has subophitic texture and is interpreted as a mafic sill or internal portion of a thick volcanic flow. Major and minor element contents indicate a composition of fractionated sub-alkaline basalt, characterized by low MgO/(MgO+Fe<sub>2</sub>O<sub>3</sub> total) ratio (0.34), moderate Ni (114 ppm) and Cr (350 ppm) contents, and high TiO<sub>2</sub> content (1.04 wt. %). The latter is consistent with accessory magnetite with abundant exsolution lamellae of ilmenite in sample LUSL19.

#### 4.3.2 Trace Elements

Mafic-ultramafic rocks of the Lago Grande Complex have relatively low contents of incompatible trace elements (Table 4), which are expected for olivine, pyroxene and plagioclase cumulates. Variations in contents of incompatible trace elements in mafic-ultramafic cumulates in layered complexes result from the combined effect of variable assemblages of cumulate minerals,



fractionation of the parental magma and variable amounts of trapped intercumulus liquid (Barnes, 1986; Ferreira Filho et al., 1998).

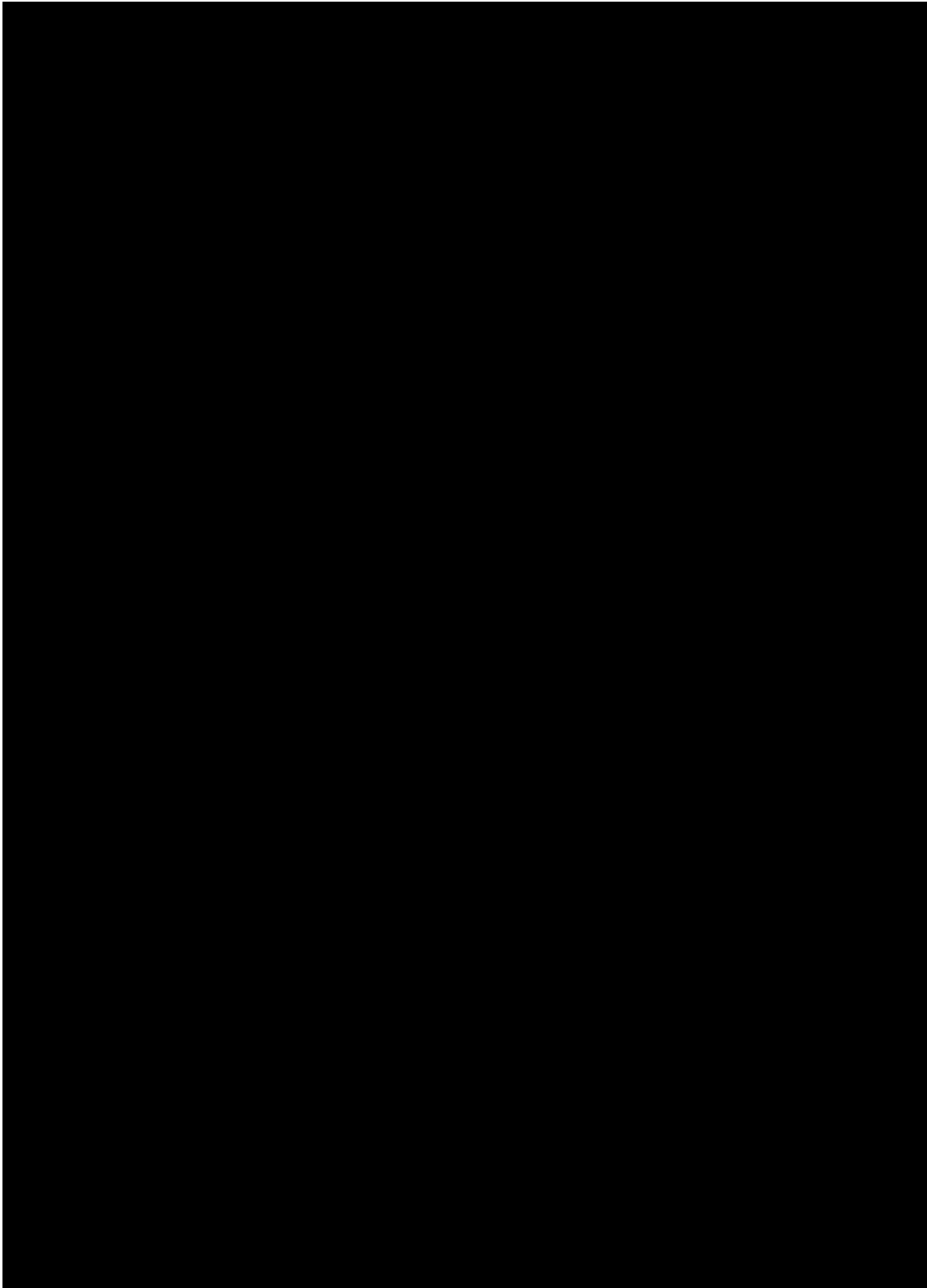


Table 04 – Whole rock analyses of representative samples from the Lago Grande Complex. Gbr = gabbroic rock; Opxt = orthopyroxenite; Hzb = harzburgite. Sample LUSL19 is a mafic rock from the Rio Novo Group.

Distinct mantle-normalized rare earth element (REE) profiles characterize different cumulate rocks of the Lago Grande Complex (Fig. 12). REE profiles for gabbroic rocks (PI + pyroxene cumulates) have distinctively positive slopes for LREE (e.g. progressive enrichment toward lighter REE), flat to slightly positive slope for HREE, and distinct Eu anomalies (Fig. 12A and 12B). These features are illustrated by samples of gabbroic rocks collected in a short interval (~ 20 meters apart) in drill hole FD26 (Fig. 12B). Sample LUSL26-240.50, a leucocratic gabbroic rock characterized by abundant cumulus PI, has very steep positive slope for LREE elements, the highest Eu anomaly, and overall low REE contents. Distinct REE element content and REE profile for sample LUSL26-240.50, compared to other gabbroic rocks, are likely to result from the combined effect of greater amount of cumulus plagioclase and lesser amounts of trapped intercumulus liquid in this sample. REE profiles for samples of orthopyroxenite (Fig. 12C) and harzburgite (Fig. 12D) have positive slope for LREE and flat distribution of HREE. REE profiles have distinct Eu anomalies for orthopyroxenite (Fig. 12C) and for few harzburgite samples (Fig. 12D). REE profiles of harzburgite, orthopyroxenite and gabbroic rocks indicate a progressive increase in REE contents and positive LREE slopes. Whereas the difference in LREE slopes result from the abundance of cumulus plagioclase in gabbroic rocks, the overall increase in REE elements with stratigraphic height are likely to result from the upward fractionation of the parental magma.

Contents for several highly incompatible high field strength cations, including Ta, Nb, Th and Hf, in cumulate rocks of the Lago Grande Complex are below detection limits for most samples (Table 4). In addition, contents for several LILE (large ion lithophile element) are variable due to heterogeneous effect of metamorphic/hydrothermal alteration in different samples. Mantle-normalized lithophile trace element profiles of the Lago Grande Complex are limited alteration-resistant trace elements and restricted to two samples of gabbroic rocks with higher contents of incompatible trace elements (Fig. 13). The profiles of gabbroic rocks very similar, except for Ti, Hf and Zr. Different contents for these elements are explained by the occurrence of accessory ilmeno-magnetita, which increase the Ti content, and traces of zircon, which increases contents of Zr and Hf, in one gabbroic sample. Mantle-normalized

alteration-resistant trace element profiles of gabbroic rocks are fractionated, as indicated by relative enrichment in LREE and Th, with pronounced negative Nb and Ta anomalies (Fig. 13). Both features are consistent with the presence of a component from the continental crust; possibly due to assimilation during ascend of the mafic-ultramafic magma, an issue to be addressed in the discussion of this study.

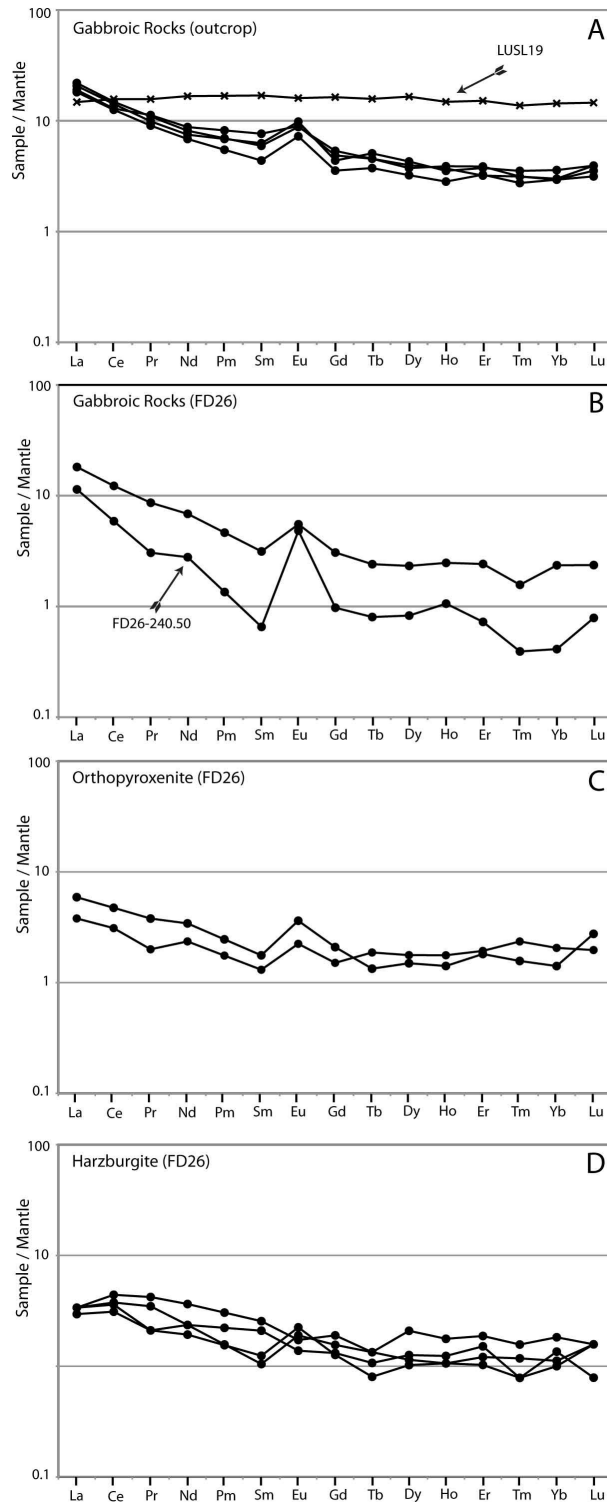


Fig. 12. Primitive mantle-normalized REE profiles for samples of the Lago Grande Complex. A) Samples of gabbroic rocks from outcrops of the Mafic Zone. Sample LUSL19 is a mafic rock from the Rio Novo Group. B) Samples of gabbroic rocks from drill core FD26, located at the lowermost part of the Mafic Zone. C) Samples of orthopyroxenite from drill core FD26. D) Samples of

harzburgite from drill core FD26. Data from Table 4. Primitive mantle normalization values are from Sun and McDonough (1989).

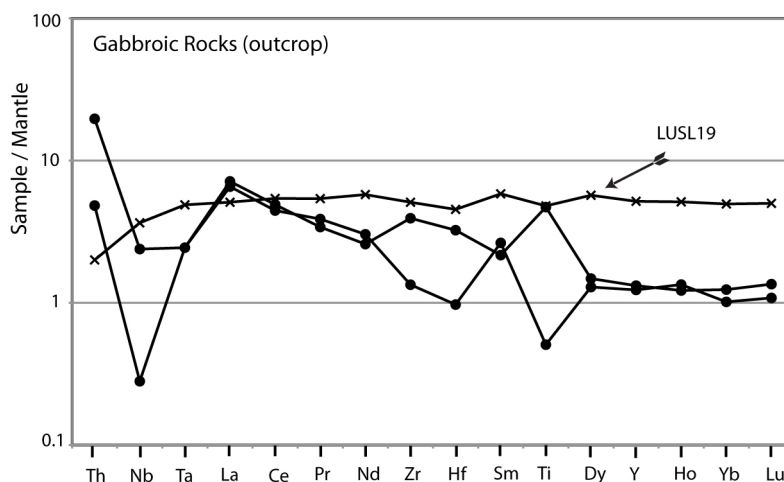


Fig. 13. Primitive mantle-normalized alteration-resistant profiles for samples of gabbroic rocks of the Lago Grande Complex. Sample LUSL19 is a mafic rock from the Rio Novo Group. Data from Table 4. Primitive mantle normalization values are from Sun and McDonough (1989).

Sample LUSL19, a mafic sill or internal portion of a thick volcanic flow of the Rio Novo Group, has distinctively different content of trace elements compared to mafic-ultramafic cumulates of the Lago Grande Complex (Fig. 12 and 13). This sample represents a composition of a mafic liquid, as indicated by higher contents for most incompatible elements compared to mafic cumulates. Mantle-normalized REE profile for sample LUSL19 is flat ( $La/Sm_N = 1.03$ ), whereas mantle-normalized alteration-resistant trace element profile is flat except for distinctively lower contents of Nb and Th. Lithogeochemical characteristics of sample LUSL19 will be compared with those from mafic-ultramafic rocks of the Lago Grande Complex, as well as metavolcanic rocks of the Rio Novo Group, in the discussions of this study.

#### 4.4 Sm-Nd Systematics

The Sm-Nd isotopic data of the Lago Grande layered intrusion as listed in Table 05. Nd isotopic data obtained for both mafic and ultramafic lithotypes render Nd model ages between 2.94 and 3.56 Ga, with variably negative  $\epsilon_{\text{Nd}}$  ( $T=2.72$  Ga) values (-0.32 to -4.25). Plotted against the stratigraphy, the Sm–Nd data do not correlate with the layering sequence and, therefore the observed small scale variation observed in  $\epsilon_{\text{Nd}}$  values may be related merely to different degrees of assimilation during the emplacement into an older continental crust. Sample LUSL19, a mafic sill or internal portion of a thick volcanic flow of the Rio Novo Group has positive  $\epsilon_{\text{Nd}}$  ( $T=2.72$  Ga) value (1.69).

#### *4.5 U-Pb geochronology*

Sample LUSL 20B was selected for U-Pb zircon dating and the analytical results are presented in Table 6. This sample corresponds to a pegmatoid leucogabbro, interpreted as representative of the most evolved rocks of the Mafic Zone. Zircon grains are colorless and show a stubby prismatic habit with subhedral shape and irregular surfaces. The crystals vary in size from 100  $\mu\text{m}$  to 300  $\mu\text{m}$ . Fractures and inclusions are common. BSE and CL imaging reveals extremely complex internal zircon textures, with a dark, low luminescent cores, surrounded by a bright outer part, which corresponds to relatively lower Th/U ratios (Figure 14). However, these domains do not correlate with distinct U-Pb ages.

U-Pb isotopic analyses render highly discordant U-Pb dates (Table 6; Figure 15). Nevertheless, nineteen spot analyses define a Discordia line with an upper intercept age of  $2722\pm 53$  Ma (MSWD=17; Figure 15). The lower intercept points toward Neoproterozoic dates ( $\sim 600$  Ma), a feature also observed by Grainger et al. (2008) in the Formiga granite-hosted Au-Cu mineralization, which is explained by the spatial proximity of the Araguaia Fold Belt, outcropping a few kilometers to the east of the Lago Grande Complex. Other remarkable feature is the cluster of concordant to slightly discordant dates at ca. 2.55 Ga (tentative Discordia upper intercept =  $2553\pm 61$  Ma, MSWD=13; Figure 15) which, in the Carajás Province, corresponds to the large-scale IOCG

mineralizing event (Tallarico et al., 2005), characterized by extensive metasomatism.

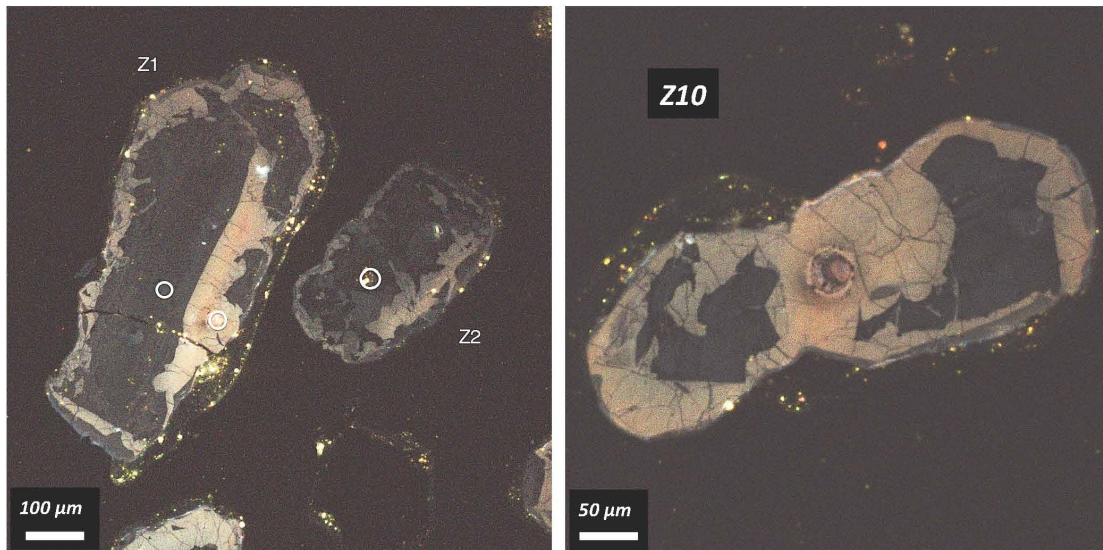


Fig. 14. True color CL images of selected zircon grains from sample LUSL-20, showing low luminescent cores surrounded by irregular, bright rim. The location of U-Pb spot analyses is also shown.

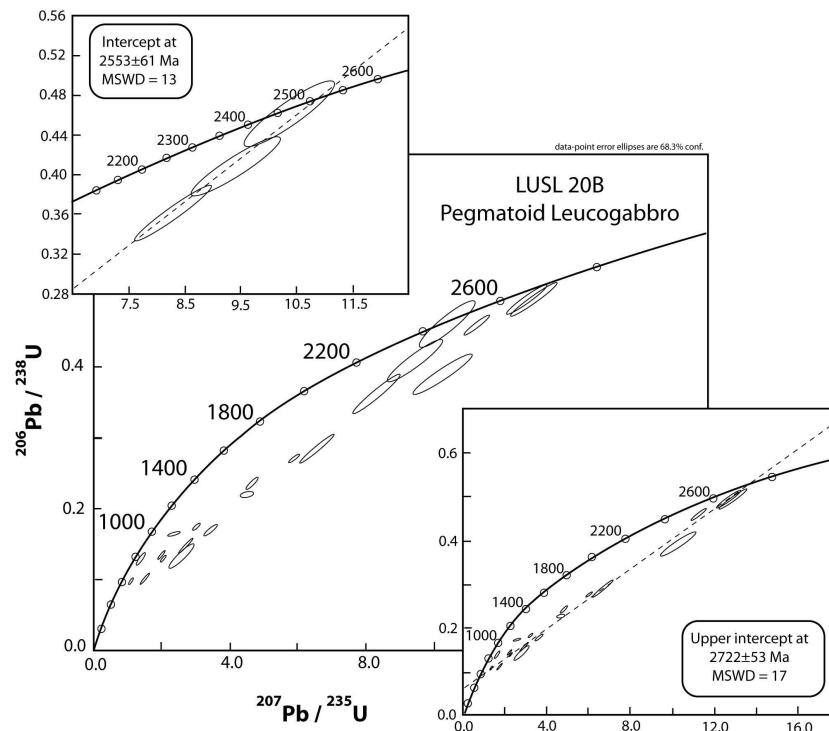


Fig. 15. LA-MC-ICPMS U-Pb plots for sample LUSL-20B. See text for explanation.

Sample	Sm(ppm)	Nd(ppm)	<sup>147</sup> Sm/ <sup>144</sup> Nd	<sup>143</sup> Nd/ <sup>144</sup> Nd	( <sup>143</sup> Nd/ <sup>144</sup> Nd) <sub>i</sub>	ε <sub>(0)</sub>	ε <sub>(T)</sub>	T <sub>DM</sub> (Ga)
LUSL 19	2.386	7.239	0.1992	0.512769+/-24	0.508997	2.56	1.68	
LUSL 20B	0.793	3.548	0.1351	0.511458+/-20	0.509141	-23.02	-1.14	3.10
LUSL 79.85	0.128	0.409	0.1899	0.512697+/-17	0.509256			
LUSL 99.85	0.425	1.936	0.1327	0.511427+/-12	0.509010	-23.62	-0.89	3.06
LUSL 117.45	0.233	1.040	0.1353	0.511470+/-13	0.509006	-22.78	-0.98	3.08
LUSL 134.05	0.184	0.759	0.1467	0.511609+/-21	0.508937	-20.07	-2.32	3.31
LUSL 152.90	0.275	1.230	0.1351	0.511467+/-52	0.509006	-22.84	-0.96	3.08
LUSL 179.60	0.230	0.844	0.1649	0.511936+/-18	0.508932	-13.69	-2.41	3.56
LUSL 205.00	0.336	1.670	0.1215	0.511272+/-10	0.509059	-26.65	0.07	2.94
LUSL 220.00	0.301	1.163	0.1566	0.511852+/-10	0.509000	-33.45	-3.81	3.23
LUSL 240.55	0.265	1.413	0.1132	0.510923+/-6	0.508861	-15.33	-1.09	3.23
LUSL 260.50	0.636	3.356	0.1146	0.511049+/-18	0.508962	-31.00	-1.84	3.08

Table 05 - Sm–Nd isotopic data for the Lago Grande Complex. Sample LUSL19

is a mafic rock from the Rio Novo Group.

Sample	f(206) %	Th/U	Apparent ages												Rho	Conc (%)	
			6/4 ratio	7/6 ratio	1s (%)	7/5 ratio	1s (%)	6/8 ratio	1s (%)	7/6 age	2σ	7/5 age	2σ	6/8 age			2σ
Z1-N	2.18	0.42	648	0.14362	3.0	4.6834	2.2	0.23650	2.0	2271.4	51.2	1764.3	18.6	1368.5	24.9	0.93	60
Z1-R	0.34	0.38	5076	0.14042	11.7	2.5951	8.6	0.13404	7.9	2232.4	188.9	1299.3	61.1	810.9	59.8	0.92	36
Z3	3.21	0.12	551	0.10725	8.7	1.5040	6.3	0.10170	5.8	1753.3	150.7	932.0	37.7	624.4	35.3	0.96	36
Z2	0.32	0.82	4962	0.16662	6.9	6.5555	4.9	0.28535	4.8	2524.0	111.4	2053.4	42.5	1618.2	68.8	0.98	64
Z4	42.32	0.65	38	0.10329	4.7	2.3643	4.3	0.16601	1.1	1684.1	85.0	1231.9	30.6	990.1	17.3	0.81	59
Z6	7.42	0.62	234	0.07796	8.4	1.3911	6.5	0.12941	4.9	1145.9	158.1	885.2	37.7	784.5	39.1	0.89	68
Z7-N	3.17	0.45	521	0.14828	3.2	4.5020	2.9	0.22020	1.2	2326.2	53.4	1731.3	24.1	1283.0	13.9	0.51	55
Z7-R	0.07	0.06	20330	0.18919	0.8	12.9187	3.3	0.49525	3.2	2735.1	13.1	2673.7	30.7	2593.4	67.5	0.97	95
Z8-N	1.32	0.79	914	0.11457	2.9	2.0583	2.1	0.13029	1.9	1873.2	50.8	1135.0	14.6	789.5	14.1	0.91	42
Z8-R	7.31	0.62	231	0.14584	4.7	3.4268	3.6	0.17041	2.8	2297.7	79.0	1510.6	27.8	1014.4	28.8	0.91	44
Z9	3.43	0.35	425	0.16694	7.3	9.4095	5.4	0.40879	4.8	2527.2	118.0	2378.8	48.6	2209.4	91.4	0.92	87
Z10-N	5.19	0.72	326	0.12492	2.4	3.0061	1.9	0.17453	1.4	2027.6	41.1	1409.2	14.2	1037.0	13.6	0.83	51
Z10-R	2.66	0.20	202	0.16591	7.7	8.2816	5.6	0.36202	5.2	2516.8	124.2	2262.3	49.2	1991.7	91.1	0.97	79
Z11	8.25	0.16	177	0.18999	7.5	10.2111	5.5	0.38980	4.7	2742.1	118.3	2454.1	49.7	2121.9	91.4	0.96	77
Z12	5.10	0.57	337	0.13216	6.2	2.7029	4.4	0.14833	4.1	2126.9	105.0	1329.3	32.4	891.6	36.0	0.99	42
Z13	0.20	0.59	17289	0.17697	0.7	11.2355	2.1	0.46047	2.0	2624.7	11.2	2542.9	19.8	2441.6	40.9	0.96	93
Z14	0.76	0.66	2120	0.15785	1.9	5.8959	1.4	0.27089	1.3	2432.8	31.6	1960.6	12.1	1545.3	17.3	0.93	64
Z15	0.17	0.83	10338	0.10643	3.6	1.9896	2.6	0.13558	2.5	1739.2	64.3	1112.0	17.3	819.6	19.1	0.95	47
Z16-R	0.11	-0.02	12737	0.16275	2.1	10.3671	5.2	0.46198	4.8	2484.5	35.1	2468.1	48.1	2448.3	97.0	0.92	99
Z17	0.04	1.08	47771	0.08163	3.7	1.1049	2.6	0.09817	2.5	1236.6	70.0	755.7	13.9	603.7	14.6	0.96	49
Z18	0.50	0.16	2800	0.18601	4.0	12.6866	2.9	0.49465	2.8	2707.2	64.5	2656.7	26.8	2590.8	58.8	0.97	96

Table 06 – U-Pb LA-MC-ICPMS data for sample LUSL-20B (N - nucleus; R – rim).



#### *4.6 Platinum Group Elements and Minerals*

PGE mineralization was discovered in ultramafic rocks of the Lago Grande Complex by VALE in 2002 during exploration for PGE-Ni deposits in the Serra Leste region. Resources and contents of PGE mineralization in the Lago Grande Complex are not available for publication at this moment. The following description, based upon representative unweathered samples, characterizes two different styles of PGE mineralization intercepted by diamond drilling in the Lago Grande Complex. PGE mineralization occurs associated with disseminated base metal sulfides in harzburgite and within small (< 10 cm thick) seams of chromitite. Pt-Pd-Rh-S analyses taken from exploration data from one borehole (FD02) illustrate the main differences between chromitite-hosted and sulfide-bearing PGE mineralization. Sulfide-bearing harzburgite samples are characterized by lower Pt/Pd ratios and variable contents of sulfur, while the chromitite sample is characterized by high Pt/Pd ratio, high Pt-Pd-Rh contents and low sulfur contents (Fig. 16 and 17).

Five samples were selected for PGE analyses (Table 07). Samples FD02-44.50m and FD02-44.00m are sulfide-bearing harzburgite with well-preserved igneous mineralogy and texture, while samples FD02-110.00m and FD02-110.75m are partially transformed sulfide-bearing harzburgites. The same type of sulfide minerals occur in altered and preserved harzburgites. They consist mainly of pentlandite with minor amounts of chalcopyrite and pyrrhotite. Sulfide occurs as interstitial aggregates in harzburgite where primary igneous minerals and textures are preserved, whereas sulfide minerals are concentrated in thin (< few millimeter) veins in highly transformed harzburgite. Sample FD02-163.25 is a thin (few centimeters thick) chromitite hosted in a transformed pyroxenite. The host rock is a fine- to medium-grained chlorite amphibolite (~ 80 vol. % pale amphibole) with diablastic texture. Chromite (up to 60 vol. %) is fine-grained with frequent atoll texture.

Sulfide-poor chromitite (sample FD02-163.25) has the highest PGE content (6PGE ~ 10ppm) and is characterized by high Pt/Pd ratio (4.3) and low Pd/Ir ratio (13.9). Mantle-normalized profile for PGE contents of sample FD02-

163.25 (Fig. 18) indicates distinct distribution for PPGE (Rh, Pt, Pd) and IPGE (Os, Ir, Rh). PPGE are highly enriched and show a negative slope, whereas IPGE are moderately enriched and show a positive slope. Chromitite samples from Lago Grande (this study) and Luanga Complex (Diella et al., 1995) have similar mantle-normalized PGE plots (Fig. 18).

Sulfide-bearing harzburgite samples have Os and Ru values below detection limit (Table 07) and mantle-normalized profiles for PGE contents are poorly constrained. Sulfide-bearing harzburgite samples with well preserved igneous mineralogy (samples 44.00 and 44.50) have low Pt/Pd ratio (0.2 to 0.3), a feature consistent with Pt/Pd ratio observed in samples of sulfide-bearing harzburgite from the exploration database (Fig. 17). Low Pt/Pd ratio and high Pd/Ir ratio (116.7 to 170.0) for samples 44.00 and 44.50 are very distinct from those ratios in the chromitite sample, suggesting that PGE contents in sulfide-bearing harzburgites and chromitites result from different concentration processes. Such distinct PGE contents in chromitite samples and sulfide-bearing samples were also described in the Luanga Complex (Ferreira Filho et al., 2007). Altered and venulated sulfide-bearing harzburgite (samples 110.75 and 110.00) have highly variable PGE contents. This variation is indicated by Pt/Pd ratio (< 0.02 to 8.0) and Pd/Ir ratio (5.0 to 810.0), suggesting that PGE were mobile during hydrothermal alteration.

A preliminary study of the Platinum Group Minerals (PGM) for the selected samples was developed by MEV (Table 08). The assemblage of PGM identified in these samples is consistent with PGE analyses, and a relatively large number of PGM were just identified in the PGE-rich and sulfide-poor chromitite (Table 7; sample FD02-163.25). In this sample PGM (up to several  $\mu\text{m}$  long) occur mainly at the edge of chromite crystals and subordinately as inclusions in amphibole and chlorite. PGM associated with chromitite have variable compositions but consist mainly of arsenides and sulfo-arsenides, with hollingworthite and sperrylite as the most frequent and abundant minerals (i.e., abundance estimated based on the size of identified crystals). Rh arsenide and a Pt-Ru-Rh-Os sulfo-arsenide occur as frequent PGM in sample FD02-163.25. The assemblage of PGM identified in this sulfide-poor chromitite is consistent

with high Pt and Rh contents, as well as the high Pt/Pd ratio, of this sample (Table 07 and Fig. 18).

PGM in sulfide-rich harzburgite (samples FD02-44.00 and FD02-44.50) are very fine-grained (< 1  $\mu\text{m}$  long), thus hampering their identification. Relatively abundant PGM are mainly restricted to pentlandite- or serpentine-hosted Pd-Te-Bi minerals (Table 8). Rare Pd-bearing sulfo-arsenides and arsenides were also identified.

Minerals consisting mainly of Bi and Cl occur in sample FD02-100.00, a highly transformed sulfide-bearing harzburgite, and sample FD02-44.00, a partially preserved sulfide-bearing harzburgite. These minerals have variable contents of Cl and Bi, from 13.95-14.98 wt. % Bi and 76.81-77.14 wt. % Cl in crystals identified in sample FD02-44.00. Analyses in two distinct very fine-grained grains (nor necessarily a single crystal) in sample FD02-44.00 yielded one result of 77.50 wt. % Bi and 14.00 wt. % Cl, and another of 89.52 wt. % Bi and 10.48 wt. % Cl. The presence of frequent chlorite-bearing minerals in these samples suggests the effect of hydrothermal fluids, an issue to be evaluated in the discussions of this paper.

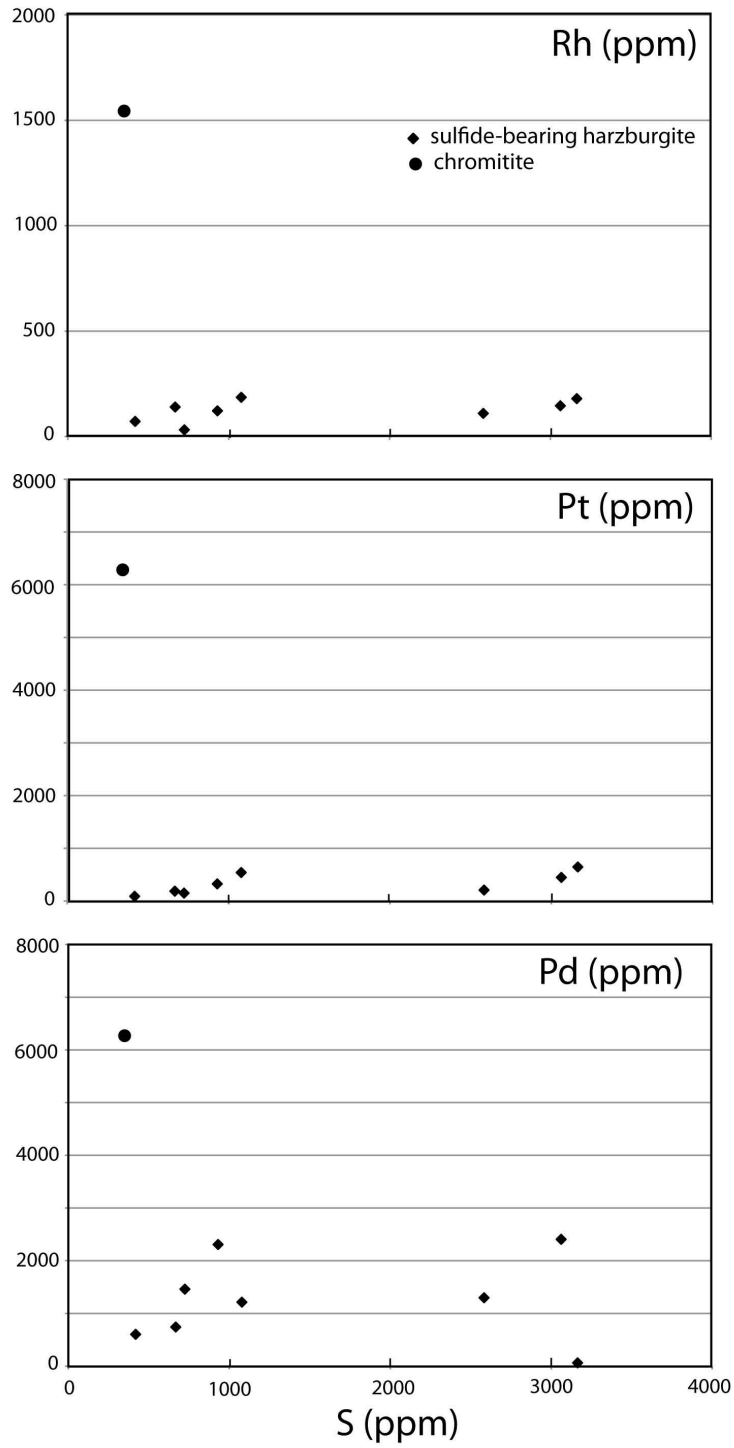


Fig. 16. Plot of Pd, Pt, and Rh versus sulfur (S) for borehole FD02. Data from mine drilling assay database (VALE, unpublished internal report).

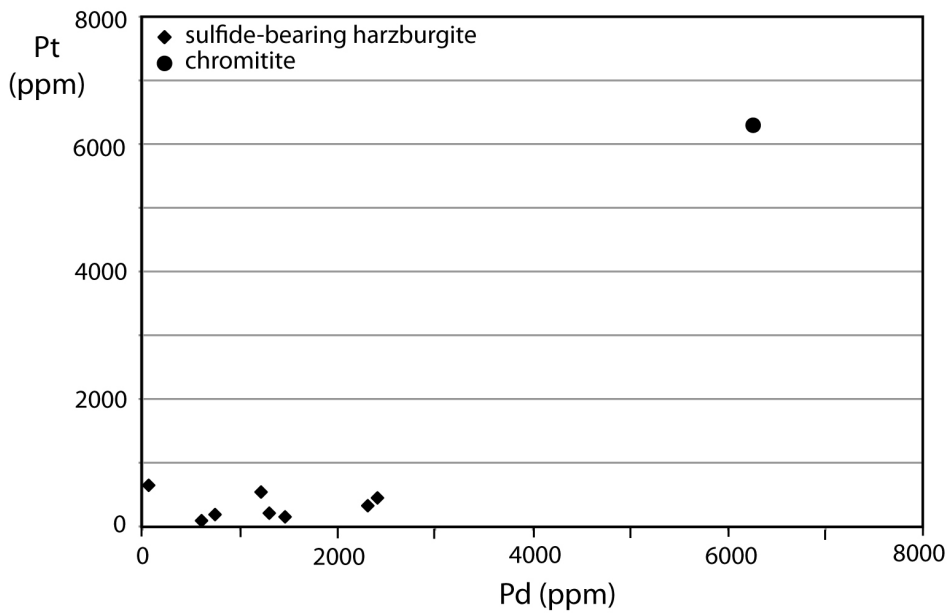


Fig. 17. Plot of Pd versus Pt for borehole FD02. Data from mine drilling assay database (VALE, unpublished internal report).

Sample	Unit	163.25	110.00	110.75	44.00	44.50
Rock		Chromitite	Harzburgite	Harzburgite	Harzburgite	Harzburgite
Pt	ppb	6,810.00	<20	160.00	200.00	80.00
Pd	ppb	1,600.00	810.00	20.00	700.00	510.00
Au	ppb	23.00	21.00	5.00	20.00	10.00
Os	ppb	60.00	<10	<10	<10	<10
Ru	ppb	250.00	<50	<50	<50	<50
Ir	ppb	115.00	1.00	4.00	6.00	3.00
Rh	ppb	1,260.00	<5	31.00	48.00	30.00
Pt/Pd		4.26	<0.02	8.00	0.29	0.16
Pd/Ir		13.91	810.00	5.00	116.67	170.00

Table 7 - PGE analyses of representative samples of Lago Grande Complex.

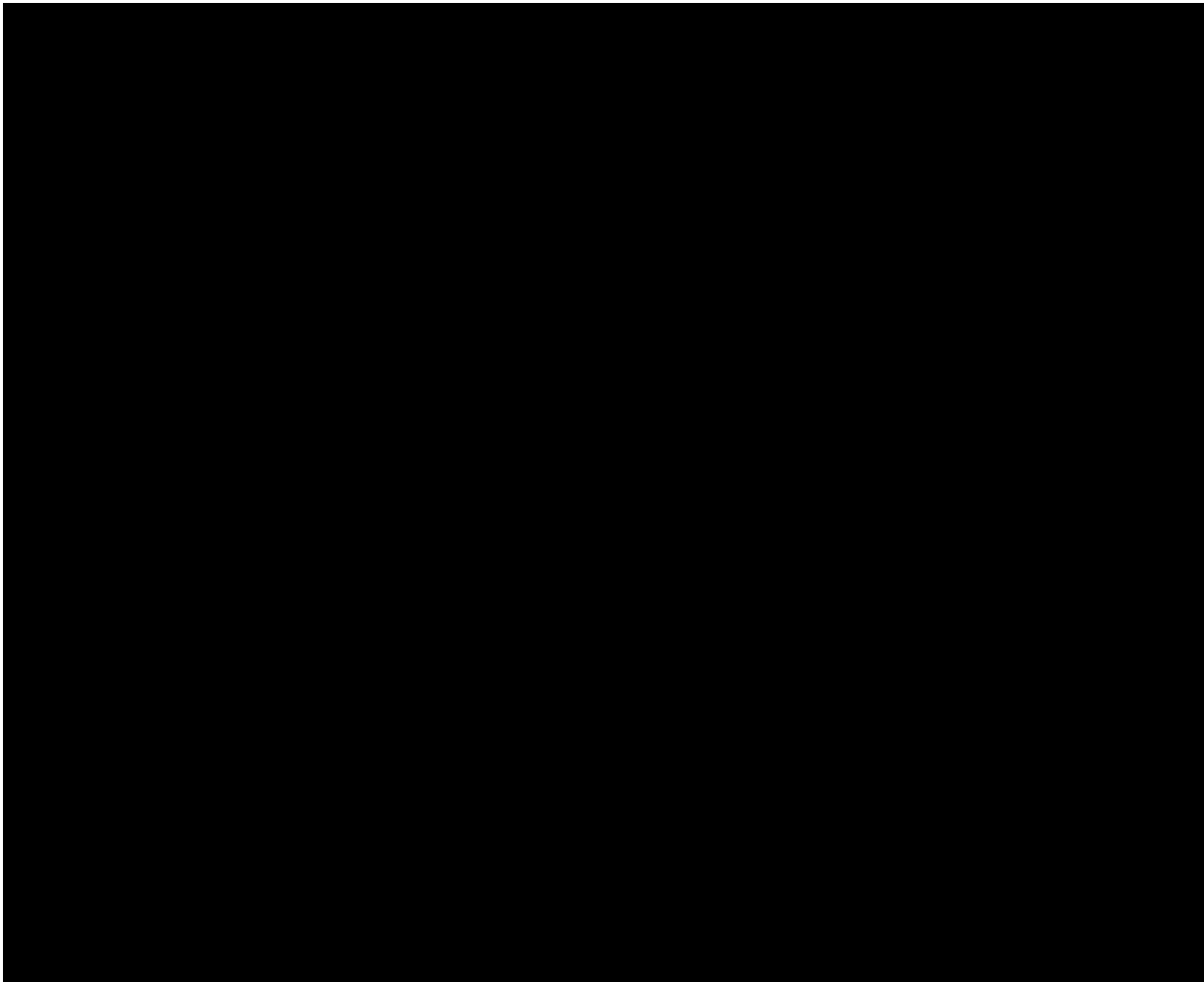


Table 8 - Analyses of PGM for sulfide-poor chromitite and sulfide-bearing harzburgite. Relative abundance of PGM for these samples is indicated as: A = abundant (several minerals identified); F = frequent (few minerals identified); R = rare (very few minerals identified).

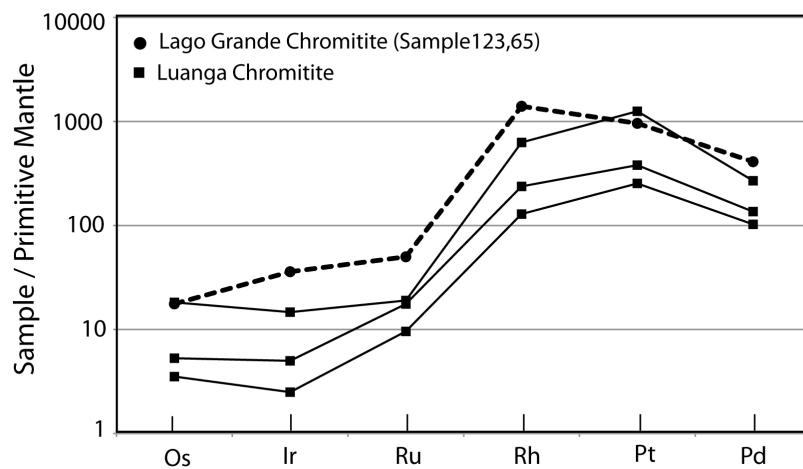


Fig. 18 - Primitive mantle-normalized PGE profiles for chromitite samples from the Lago Grande (data from Table 08) and Luanga Complex (data from Diella et

al., 1995). Primitive mantle normalization values are from Sun and McDonough (1989).

## **5. Discussion**

### *5.1 Magmatic structure*

The layered sequence of the Lago Grande Complex is interpreted in this study as overturned. This interpretation carries significant implications for the understanding of the primary structure and fractionation of the sequence of the layered rocks. This is therefore the first subject to be discussed in our study. The actual architecture of the intrusion, characterized by moderate dip to the southeast, shows an extensive sequence of mafic rocks underlying a sequence of ultramafic rocks, which is followed upwards by highly foliated rocks of the Xingu Complex in the south (Fig. 4 and 5). An overturned layered sequence is consistent with the stratigraphic sequence of layered rocks as well as mineralogical and geochemical evidences presented in this study. Considering that normal fractionation processes have taken place in the Lago Grande Complex, both the crystallization sequence and cryptic variation of cumulus minerals (Fig. 8) support an overturned sequence.

The architecture of the intrusion, the crystallization sequence and cryptic variations described in the Luanga Complex, located a few km to the north of the Lago Grande Complex, also indicate an overturned layered sequence (Ferreira Filho et al., 2007). Physical markers that provide facing criteria in the Lago Grande and Luanga complexes consist of repeated characteristic sequences of cumulate rocks, which correspond to cyclic units described in several layered complexes (Eales and Cawthorn, 1996). Facing criteria is abundant in the PGE mineralized and extensively drilled Luanga Complex, especially in the transition from the Ultramafic Zone to Mafic Zone, as indicated by several few meter thick cyclic units ranging from ultramafic to mafic cumulates (Ferreira Filho et al., 2007).

The identification of two closely associated overturned medium-size layered intrusions suggests that regional scale structures leading to large overturned crustal blocks were developed in the Serra Leste region in Carajás. The tectonic processes leading to the overturned sequence of layered rocks in the Lago Grande and Luanga Complexes have so far not been addressed in published papers. Because robust structural data of regional structures in this region are not available, these processes are unconstrained at this point in time. The timing of the tectonic processes leading to crustal overturning in the Serra Leste is also poorly constrained, bracket between the crystallization age of the layered intrusions ( $2722\pm 53$  Ma; this paper) and the age of later cross cutting mafic dykes ( $1515\pm 8$  Ma; Teixeira 2013, unpublished M.Sc. thesis). Discussion of tectonic processes leading to overturned blocks, as well as regional implications associated with the existence of overturned blocks in the Serra Leste region, is beyond the scope of this study. It is however important to indicate that processes of this type may induce the transport of hydrothermal fluids, a subject to be addressed when the origin and remobilization of PGE is considered in this study.

### *5.2 Constraints for the composition of parental magma and fractionation*

The Lago Grande Complex is a layered intrusion consisting mainly of mafic cumulate rocks and minor ultramafic cumulates. The stratigraphy of the intrusion is overturned and truncated in the northern portion by the Cotia EW shear zone (Fig. 3). The tectonic disruption of the primary stratigraphy together with poor outcropping and limited drilling, the latter mainly restricted to the Ultramafic Zone, pose restrictions for the understanding of the bulk composition of the intrusion. The composition of the parental magma of the Lago Grande Complex cannot be constrained by common approaches used to define their composition in well-exposed and unaltered intrusions (e.g., chilled margin, bulk composition, extrusive equivalents, related dykes, and melt inclusions). Whenever a direct composition of the parental magma is not possible in layered intrusions, the nature of the parental magmas has been inferred from the crystallization sequences of the intrusions and cumulates geochemistry. The compositional range of cumulus olivine ( $Fo_{82.5-85.7}$ ) is consistent with a



moderately primitive (or moderately MgO rich) composition for the parental magma of the Lago Grande Complex. The composition of the most primitive cumulus olivine in the Lago Grande Complex is comparable with those reported for the central zone of the Jinchuan intrusion ( $Fo_{83-86}$ ) (Li et al., 2004) and Luanga Complex ( $Fo_{80.0-84.7}$ ) (Ferreira Filho et al., 2007). Even though limited to a few samples due to extensive alteration of the magmatic minerals, the cryptic variation of olivine in the Ultramafic Zone suggests the existence of one major compositional reversal (Fig. 8). This reversal within a restricted compositional range of olivine compositions in the Ultramafic Zone suggests open-system crystallization involving replenishment by new primitive magma pulses. Cumulus minerals in the layered rocks suggest that the sequence of crystallization in the Lago Grande Complex consists of olivine + chromite, orthopyroxene + chromite, orthopyroxene, orthopyroxene + plagioclase and orthopyroxene + plagioclase + clinopyroxene. The crystallization sequence of the Lago Grande Complex is similar to those of the major PGE-bearing intrusions in which orthopyroxene precedes clinopyroxene (Eales and Cawthorn, 1996). The early crystallization of orthopyroxene relative to clinopyroxene indicates that the primary magma was silica saturated. Several studies suggest that, since orthopyroxene was an early-crystallizing mineral in many layered intrusions worldwide, the assimilation of continental crust may have induced enrichment in silica in these magmas (Campbell, 1985).

Evidence for assimilation of continental crust during the ascent and/or emplacement of the mafic-ultramafic magma of the Lago Grande Complex is also provided by geochemistry and isotopic data. Mantle-normalized alteration-resistant trace element profiles of gabbroic rocks are fractionated, as indicated by relative enrichment in LREE and Th, with pronounced negative Nb and Ta anomalies (Fig. 13). These alteration-resistant element profiles were compared with average compositions of the upper and lower crust (Wedepohl, 1995) and with average composition of the B1 rocks of the Bushveld Complex (Barnes et al., 2010) in Figure 19. B1 rocks of the Bushveld Complex are chilled margins interpreted as representative of the composition of the parental magma of the cumulate rocks of the Lower Zone of the Bushveld Complex. The B1 magma is interpreted as the product of a mixture of a primitive mantle melt mixed with

continental crust, and has been successfully modelled as the parental magma of the cumulate rocks of Lower and Lower Critical Zone of the Bushveld Complex (Barnes et al., 2010; Godel et al., 2011). The distribution of alteration-resistant elements in the Lago Grande Complex is therefore consistent with a mixture of a moderately primitive mantle melt of poorly constrained composition with continental crust. Additional evidence for crustal contamination of the parental magma of the Lago Grande Complex is provided by Sm-Nd isotopic data (Table 05). Nd isotopic data obtained for both mafic and ultramafic lithotypes render Nd model ages between 2.94 and 3.56 Ga, with variably negative  $\epsilon_{Nd}(T=2.72 \text{ Ga})$  values (-0.32 to -4.25). These results are consistent with an original mantle melt contaminated with older continental crust, which is compatible with intrusive relationship with gneiss and migmatites of the ca. 3.0 Ga Xingu Complex.

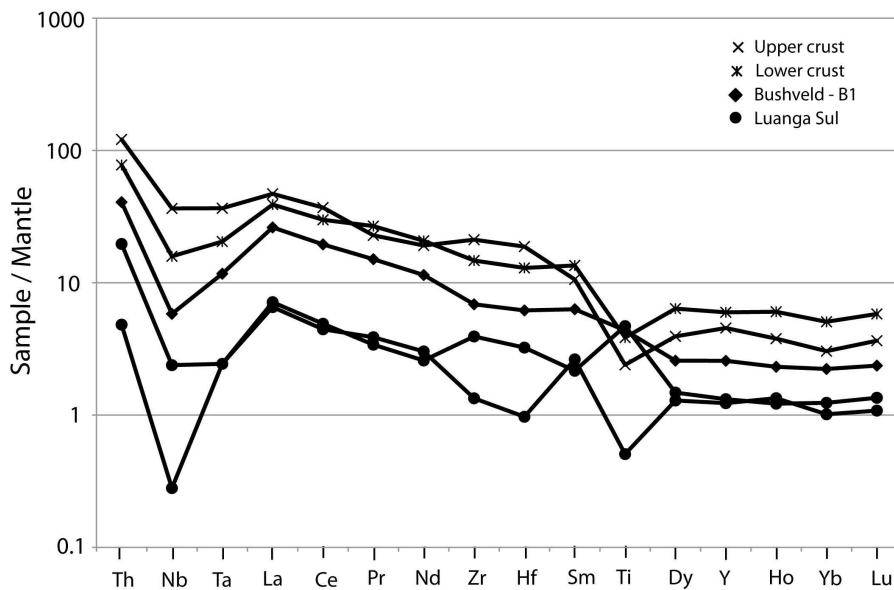


Fig. 19. Primitive mantle-normalized alteration-resistant profiles for samples of gabbroic rocks of the Lago Grande Complex, average composition of the upper and lower crust (Wedepohl, 1995), and average composition of the B1 rocks of the Bushveld Complex (Barnes et al., 2010). Primitive mantle normalization values are from Sun and McDonough (1989).

### *5.3 Metamorphism and hydrothermal alteration of magmatic rocks*

Metamorphic assemblages that indicate temperatures up to the amphibolite facies of regional metamorphism largely replace primary igneous minerals of the Lago Grande Complex. This metamorphic alteration is heterogeneous and characterized by an extensive hydration that largely preserves primary textures and bulk chemical composition, as well as the compositional domains of igneous minerals. The penetrative fabric when present is restricted to narrow domains of up to few meters, and igneous textures are identified in adjacent non-deformed domains.

The metamorphic assemblages and preserved primary textures of the Lago Grande Complex rock's contrast with the highly tectonized and higher grade rocks of the Xingu Complex in the south. The latter consists of highly foliated rock, including quartz-feldspathic gneiss with migmatite pods and bands. U-Pb zircon dating of high-grade metamorphic rocks yielded Archean ages,  $2859\pm 9$  Ma for edembergites of the Pium Complex (Pidgeon et al., 2000) and  $2859\pm 2$  Ma for migmatites of the Xingu Complex (Machado et al., 1991). These geological and isotopic data are consistent with regional interpretation of the Xingu Complex as older crustal rocks where the Lago Grande Complex intruded.

Mafic metavolcanics located to the north of the Lago Grande Complex are variably foliated and have amphibolite facies assemblages, consisting mainly of amphibolite and garnet amphibolite. Because no age dating of metamorphic minerals is available, the timing of the metamorphic recrystallization of the cumulate rocks of the Lago Grande Complex and associated metavolcanics is poorly constrained. The crystallization age of the layered intrusions ( $2722\pm 53$  Ma; this paper) provides an upper limit for the metamorphic event, while the age of cross cutting mafic dykes ( $1515\pm 8$  Ma; Teixeira, 2013) provides a lower limit. The latter are pristine mafic dykes that truncate the metamorphosed rocks of the Lago Grande Complex and host metavolcanics. Metamorphic features described in the Luanga Complex and host metavolcanics (Suita, 1988; Ferreira Filho et al., 2007) are similar to those described in this study. These features suggest that the same metamorphic

event affected mafic-ultramafic complexes and volcanic-sedimentary rocks in the Serra Leste region. Robust geochronological data of metamorphic minerals are also not available for metamorphosed cumulate rocks of the Luanga Complex and associated metavolcanics.

The type of metamorphism in the metavolcanic rocks of CMP, including the Serra Leste region and different mafic metavolcanic sequences of the Itacaiúnas Supergroup, is a debatable issue. This metamorphic recrystallization has been interpreted either as a typical regional metamorphic event (Docegeo, 1988) or as the result of widespread hydrothermal metamorphism (Dardenne et al., 1988). Several Cu-Au deposits of the Carajás region are now considered to belong to the IOCG class of deposits (Tallarico et al., 2005; Grainger et al., 2002) and formed as part of a major hydrothermal system. This hydrothermal-metassomatic event, described in several Cu-Au deposits in the CMP (e.g. Bahia-Alemão, Salobo, Sossego, Cristalino), is characterized by: 1) intense Fe metasomatism resulting in the formation of abundant Fe-bearing silicates (garnet, grunerite, fayalite) and/or Fe oxides (magnetite and/or hematite); 2) associated K-Na alteration (frequently indicated by abundant biotite and/or scapolite); 3) sulfur-poor ore paragenesis; 4) enrichment in LREE and U. Precise dating of hydrothermal minerals in the Bahia deposit ( $2575 \pm 12$  Ma; Tallarico et al., 2005) and Salobo ( $2576 \pm 9$  Ma, Requia et al., 2003) suggests a NeoArchean ages for the regional scale hydrothermal system and associated Cu-Au deposits. Even though these hydrothermal-metassomatic processes were considered as part of the regional metamorphic event in the past (as illustrated by the original descriptions of the Salobo deposit), their characteristics are now well defined and they were mapped as complex zones consisting of variable hydrothermal rocks associated with Cu-Au mineralization (Tallarico et al., 2005; Grainger et al., 2008). Precise identification of the hydrothermal-metassomatic processes in the CMP is facilitated when the primary rocks are clearly known. Metamorphic alteration observed in the Lago Grande and Luanga complexes is characterized by extensive addition of H<sub>2</sub>O in a process that largely preserves the primary bulk chemical composition, such that variably transformed mafic-ultramafic rocks (e.g. metaharzburgite, metaorthopyroxenite, etc) may be unequivocally identified by their recalculated

anhydrous composition. Hydrothermal-metassomatic alteration characteristic of IOCG-type deposits were not identified in the studied portion of the Lago Grande Complex, but it is developed in the Cotia shear zone (Fig. 3) as well as in few narrow discrete zones observed in the Luanga Complex (e.g. indicated by few meter-thick magnetite-garnet-grunerite bearing rocks cross cutting orthopyroxenite; personal observation by Cesar Ferreira Filho). Considering that the Serra Leste region are affected by major fault zones known to be regionally associated with IOCG type deposits (Fig. 1 and 2), the presence of discrete hydrothermal-metassomatic zones is expected. U-Pb isotope analyses of zircon crystals from a pegmatoid gabbro from the Lago Grande Complex show a cluster of concordant to slightly discordant dates at  $2553\pm 61$  Ma (Fig. 16). These dates overlap with zircon dates from hydrothermal minerals in the Bahia and Salobo Cu-Au deposits in Carajás, and are likely to correspond to a significant disturbance of the U-Pb system during the regional scale hydrothermal event associated with the origin of IOCG type deposits. Zircon grains also show evidences of an extensive recrystallization, as revealed by complex internal textures with an irregular, curved-inward shape with well-defined boundaries along distinct CL domains (Fig. 15). Several authors have attributed these features to a fluid-induced dissolution-precipitation process (Geisler et al., 2007; Putnis, 2009; among others). Throughout this sub-solidus mechanism, a fluid/melt phase facilitates the removal of non-formula elements from zircon structure, such as REE, U and Pb, thus causing a chemical and isotopic re-equilibration in the crystal (Geisler et al., 2007). In some cases, this process can almost completely reset the U-Pb isotopic information, leading to dates without a geological significance, which has been already described in other mafic-ultramafic complexes elsewhere (Giustina et al., 2011a, b). However, in the Lago Grande Complex, U-Pb isotope analyses obtained on bright luminescent rims with typical recrystallization features reveal a cluster of concordant to slightly discordant dates pointing at  $2553\pm 61$  Ma (Fig. 16). These younger dates overlap with zircon ages from hydrothermal minerals in the Bahia and Salobo Cu-Au deposits in Carajás and, therefore, are likely to correspond to a significant disturbance of the U-Pb system during the regional scale hydrothermal event associated with the origin of IOCG type deposits

#### *5.4 The petro-tectonic setting of the Lago Grande Complex and associated layered intrusions of the Serra Leste region*

Discussion of the petro-tectonic setting of the layered intrusions of the Serra Leste region may be linked to the setting of coeval basaltic volcanism of the Itacaiúnas Supergroup, and specially the bimodal volcanism of the Grão Pará Group. The accumulation of this extensive and thick pile (up to 4-6 km, Gibbs, 1986) of basaltic rocks was determined by various authors at ca. 2.75 Ga. Precise U-Pb zircon ages ( $2759\pm 2$  Ma, Machado et al., 1991;  $2760\pm 11$  Ma, Trendall et al., 1998) of the bimodal volcanism of the Grão Pará Group overlap with available U-Pb zircon ages for the Luanga ( $2763\pm 6$  Ma, Machado et al., 1991) and Lago Grande ( $2722\pm 53$  Ma, this study) complexes, thus supporting the interpretation that mafic volcanics and mafic-ultramafic layered intrusions resulted from coeval magmatic events (Machado et al., 1991; Ferreira Filho et al., 2007).

The tectonic setting of the volcanic-sedimentary sequences of Carajás is highly debated. This extensive basaltic volcanism is usually considered to result of intra-plate rifting of older continental crust (Gibbs et al., 1986; Olszewski et al., 1989; Villas and Santos, 2001) but subduction-related environments have also been proposed (Dardenne et al., 1988; Teixeira and Egger, 1994; Zucchetti, 2007). An extensive discussion of the tectonic setting of the Archean sequences of the Carajás region is beyond the scope of this paper. The following reasoning, focused on the mafic-ultramafic intrusions of the Serra Leste region, aims to provide additional constraints for this on-going discussion.

The assimilation of older continental crust during the ascent and/or emplacement of the mafic-ultramafic magma of the Lago Grande Complex is consistent with field, petrological and isotopic results discussed in this paper. Similar field and petrological results reported for the Luanga Complex (Ferreira Filho et al., 2007) also suggest the assimilation of older continental crust. Regardless of the specific conditions of magma generation, these results are consistent with large volume of primitive magma being transferred through continental crust in the Carajás region. One step ahead from the indication that

mafic-ultramafic intrusions and extensive basaltic volcanism are coeval, and therefore associated to the same regional tectonic setting, is the identification of specific parts of the basaltic stratigraphy that are comagmatic with these contaminated intrusions.

Extensive petrological studies developed in the Triassic Siberian traps and associated Ni-Cu-PGE mineralized intrusions of the Noril'sk-Talnakh provide evidence for comagmatic origin of intrusions and specific stratigraphic sequence of volcanics (e.g., Lightfoot et al., 1990; Arndt et al., 2003, and references herein for a review). These studies suggest that the Noril'sk-Talnakh intrusions are fossil conduits that originally linked deeper magma chambers to the volcanic pile at the surface. Even though the petrological models connecting volcanics and intrusions in Noril'sk-Talnakh are controversial, they concur on the importance of these intrusions as dynamic systems where magma passed through the crust before reaching the surface (Lightfoot and Keays, 2005, and references herein for a review). These studies also agree that magmatic plumbing system plays a crucial role in the formation of Ni-Cu-PGE deposits in the Noril'sk-Talnakh region, a principle applied for the origin of different styles of magmatic sulfides worldwide (e.g., Barnes and Lightfoot, 2005, and references herein for a review).

Systematic lithostratigraphic studies of volcanic rocks of the Grão Pará Group are not available, and the composition of layered intrusions of the Serra Leste region cannot be compared to specific stratigraphic portions of the volcanic pile. An added complexity is that basaltic volcanic rocks of the Serra Leste region are frequently altered by hydrothermal processes (Dardenne et al., 1988; Teixeira and Eggler, 1994; Zucchetti, 2007). Extensively altered volcanic rocks of the Grão Pará Group, especially when associated with IOCG-type alteration, have distinct chemical and isotopic compositions when compared with less transformed samples (Lindenmayer et al., 2001). Lithochemical and Nd isotope results for best-preserved basaltic rocks of the Grão Pará Group are consistent with variable contamination of parental magmas with older continental crust (Olszewski et al., 1989). These are indicated by variable patterns of REE elements (from flat or slightly LREE depleted to LREE enriched) and variable  $\epsilon_{Nd(T)}$  values (from -0.7 to + 4.6). Because most of the

$\epsilon_{\text{Nd}}(T)$  values of mafic volcanics cluster around positive values typical for depleted mantle at 2.76 Ga, Olszewski et al. (1989) suggested that mafic magmas derived from a depleted mantle source. Lithogeochemical results obtained for one sample of basaltic rock of the Rio Novo Group in this study (sample LUSL19, Fig. 12 and 13) is comparable to those provided for the Grão Pará Group (Olszewski et al., 1989). Mantle-normalized REE profile for sample LUSL19 is flat, whereas mantle-normalized alteration-resistant trace element profile lacks the pronounced negative Nb and Ta anomalies, consistent with an origin from an uncontaminated magma derived from a depleted mantle source. Both lithogeochemical results and positive  $\epsilon_{\text{Nd}}(T)$  value (+ 1.69, Table 5) for sample LUSL19 are distinct from those obtained for cumulate rocks of the Lago Grande Complex, those suggesting a distinct parental magma. Mafic and ultramafic cumulates of the Lago Grande Complex are characterized by distinctively negative  $\epsilon_{\text{Nd}}(T)$  values (from -0.32 to -4.25, Table 5). These results are consistent with an original mantle melt contaminated with older continental crust for the parental magma of the Lago Grande Complex. Contrasting  $\epsilon_{\text{Nd}}(T)$  values for mafic-ultramafic cumulates of the Lago Grande Complex compared with most volcanic rocks of the Grão Pará Group, as well as sample LUSL19 of the Rio Novo Group, suggest that the parental magma of the Lago Grande Complex is not comagmatic with typical volcanic rocks of the Carajás region. Future systematic lithostratigraphic studies of volcanic rocks of the Grão Pará Group should provide evidence for continuous changes in basalt chemistry through the stratigraphy, such that processes that took place in layered intrusions may eventually be connected with specific sections of the volcanic pile.

### *5.5 Origin of Platinum Group Minerals and implication for exploration*

Our results indicate that different styles of PGE mineralization occur in the Lago Grande Complex. These results also suggest that PGE mineralization associated with both sulfide-poor chromitite and sulfide-bearing harzburgite represent primary magmatic concentration of PGE, whereas hydrothermal processes are significant in altered and venulated sulfide-bearing harzburgite.



The origin of chromitites in layered intrusions is controversial and subject of a number of conflicting ideas in the literature (e.g. Mondal and Mathez, 2007; Ferreira Filho and Araújo, 2009; Naldrett et al., 2012; and references herein for a review). The origin of PGE mineralized chromitites is no less controversial, as illustrated by recent papers dealing with the origin of chromitites and associated PGE mineralizations in the Bushveld Complex (Naldrett et al., 2012; Maier et al., 2013). The PGE mineralization associated with chromitites in the Lago Grande Complex share several features with PGE-mineralized chromitites described in layered intrusions, as illustrated by those of the Bushveld Complex. These similar features should reflect, independently of favoured models, that similar geological processes were involved in their origin. In sulfide-poor chromitite of the Lago Grande Complex the PPGE are highly enriched and show a negative slope in mantle-normalized profile for PGE contents, whereas IPGE are moderately enriched and show a positive slope (Fig. 19). Normalized profile of the chromitite sample from the Lago Grande Complex is generally similar to profiles from Middle Group (MG) and Upper Group (UG) chromitites from the Bushveld Complex, and very close to profiles and overall contents of the MG-4 chromitites (Naldrett et al. 2012). Platinum group minerals (PGM) occur mainly at the edge of chromite crystals in the Lago Grande chromitite, consisting mainly of arsenites and sulfo-arsenites. PGM frequently occur closely associated, mainly as inclusions within chromite in PGE-mineralized chromitites (Talkington and Lipin, 1986; Markle, 1992; Zaccarini et al., 2002). This close association of PGM and chromite has been interpreted in different ways (e.g. Naldrett et al., 2012, for a review), that tend to concur that PGM inclusions in chromite were encapsulated within enlarging chromite crystals. Experimental studies developed by Finnigan et al. (2008) indicate that a localised reduction front developed around chromite crystals during their crystallization from natural basaltic liquids induced, due to lower PGE solubility in this front, the crystallization of PGE alloys. An important conclusion derived from this experimental study is that the association of chromite and PGM, as observed in most of the Bushveld chromitites and in our study of the Lago Grande chromitite should be restricted to natural magmatic systems close to PGE saturation. This assumption allows distinguishing magmatic systems close to PGE saturation, and therefore prone to produce PGE-mineralized chromitites, from those

systems that chromite crystallization does not induce PGM crystallization due to PGE contents far from their saturation level. When applied to the layered complexes of the Serra Leste Suite, this assumption suggest that they crystallized from magmas close to PGE saturation, as indicated by PGE-rich chromitites in the Lago Grande (this study) and Luanga (Diella et al., 1995; Ferreira Filho et al., 2007) complexes.

PGE mineralization associated with base metal sulfides are usually considered to form as a result of segregation of an immiscible sulfide liquid from mafic or ultramafic magma (Naldrett, 2004). Sulfide-bearing harzburgite samples with well preserved igneous mineralogy of the Lago Grande complex have low Pt/Pd (0.2 to 0.3) and high Pd/Ir (116.7 to 170.0) ratios. These ratios are very distinct from those obtained in the chromitite sample, thus suggesting that PGE contents in sulfide-bearing harzburgites and chromitites result from different concentration processes. Geochemical features, together with their close association with interstitial base metal sulfides, suggest that this PGE mineralization resulted from segregation of sulfide liquids.

Altered and venulated sulfide-bearing harzburgite samples from the Lago Grande complex have highly variable PGE contents. This variation is indicated by Pt/Pd ratio (< 0.02 to 8.0) and Pd/Ir ratio (5.0 to 810.0), suggesting that PGE were mobile during hydrothermal alteration. PGE mineralization produced by hydrothermal processes appears to be the result of Cl-rich aqueous fluids concentrating PGE, or just remobilizing previously concentrated PGE, in layered intrusions (Mungall and Naldrett, 2008). Preliminary studies of PGM in venulated samples from the Lago Grande complex identified several minerals with variable contents of Cl and Bi. The importance of Cl-bearing saline hydrothermal fluids in the origin of both NeoArchean IOCG deposits and smaller Paleoproterozoic Cu-Au-W-Bi deposits in the Carajás Mineral Province is indicated in several studies (Grainger et al., 2008, Xavier et al., 2009). The epigenetic Serra Pelada Au-PGE deposit was also considered to result from hydrothermal fluids that possibly leached adjacent mafic-ultramafic complexes, including the PGE-mineralized Luanga Complex, located in the eastern portion of the Carajás Mineral Province (Grainger et al., 2002, 2008). The chlorite-

bearing minerals identified in highly transformed PGE-mineralized ultramafic rocks of the Lago Grande Complex in this study, provide an evidence for the suggested PGE remobilization by hydrothermal fluids. This remobilization may lead to economic concentrations like Serra Pelada Au-PGE deposit.

Different styles of magmatic PGE mineralization, including PGE associated with sulfide-poor chromitites and PGE associated with disseminated sulfides in ultramafic cumulates, occur in the coeval Luanga and Lago Grande complexes. PGE profiles for chromitites of the Lago Grande and Luanga complexes are remarkably similar (Fig. 19B) suggesting that their PGE content originated from the same parental magma and/or magmatic concentration process. The distribution of different styles of magmatic PGE mineralization in these complexes, as well as in other intrusions located in the eastern portion of the Carajás Mineral Province, support the concept that they belong to a PGE-enriched mafic-ultramafic magma type, designated the Serra Leste Magmatic Suite by Ferreira Filho et al., (2007). Combined results obtained for the Lago Grande Complex (this study) and the Luanga Complex (Ferreira Filho et al., 2007) indicate that layered complexes associated with Serra Leste Magmatic Suite crystallized from moderately primitive parental magmas (olivine compositions are up to  $Fo_{85.7}$  and  $Fo_{84.7}$  for the Lago Grande and Luanga Complexes, respectively), which promote abundant crystallization of opx in the ultramafic cumulates and were characterized by significant contamination by older crustal rocks. These features are consistent with the ultramafic cumulates of the intrusions being formed from siliceous high magnesian basaltic magmas, similar to the parental liquids to the world's principal PGE-sulfide deposits, such as those hosted by the Bushveld and Stillwater complexes (Harmer and Sharpe 1985, Naldrett, 1994, Keays et al., 2012). The origin of siliceous high magnesian basaltic magmas, including the origin of the parental magma of the Bushveld Complex, is controversial but tends to converge into two distinct possibilities. They are either considered to be highly contaminated komatiite (Barnes, 1989; Eales and Costin, 2012) or they may be boninite (Hamlyn et al., 1985; Sun et al., 1989). Given the current state of knowledge of this subject, as well as the debatable tectonic setting of the mafic magmatism of the Carajás Mineral Province, tectonic-petrogenetic discussions on the origin of parental magmas of

the Serra Leste Suite are unresolved in the present context.

Apart from specific petrogenetic discussions, the characteristics of the layered intrusions of the Serra Leste Suite provide a framework to identify promising layered intrusions for PGE mineralization in the Carajás Mineral Province. The available data suggest that crustal contaminated and moderately primitive intrusions, characterized by abundant crystallization of opx in the ultramafic cumulates, provide favourable targets for exploration for PGE deposits. Considering that the Serra Leste Magmatic Suite was originally defined by a region where PGE-mineralized mafic-ultramafic intrusions occur, and that this region also coincides with the location of the hydrothermal Serra Pelada Au-PGE deposit, the presence of covered PGE-mineralized layered intrusions in the eastern portion of the Carajás Mineral Province should not be overlooked. Exploration for unconventional hydrothermal PGE deposits, likely to be associated with major faults, should also be considered.

## 6. Conclusions

The principal conclusions of this study are as follows:

- a) The Lago Grande Complex is a NE-trending medium-size (12-km-long and average 1.7-km-wide) layered intrusion consisting mainly of mafic cumulate rocks and minor ultramafic cumulates. The stratigraphy of the intrusion is overturned and, to the south, overlain by highly foliated metamorphic rocks of the Xingu Complex.
  
- b) The compositional range of cumulus olivine ( $Fo_{82.5-85.7}$ ) is consistent with a moderately primitive (or moderately MgO rich) composition for the parental magma of the Lago Grande Complex. Cryptic variation of olivine in the Ultramafic Zone suggests the existence of one major compositional reversal, suggesting open-system crystallization involving replenishment by new primitive magma pulses. Cumulus minerals in the layered rocks suggest that the sequence of crystallization in the Lago Grande Complex consists of olivine + chromite, orthopyroxene + chromite, orthopyroxene, orthopyroxene + plagioclase and orthopyroxene + plagioclase + clinopyroxene.

c) Mantle-normalized alteration-resistant trace element profiles of gabbroic rocks are fractionated, as indicated by relative enrichment in LREE and Th, with pronounced negative Nb and Ta anomalies. Nd isotopic data obtained for both mafic and ultramafic lithotypes render Nd model ages between 2.94 and 3.56 Ga, with variably negative  $\epsilon_{\text{Nd}}(T=2.72 \text{ Ga})$  values (-0.32 to -4.25). These results are consistent with an original mantle melt contaminated with older continental crust, which is compatible with intrusive relationship with gneiss and migmatites of the ca. 3.0 Ga Xingu Complex.

d) U-Pb zircon age for the Lago Grande Complex was determined in this study at  $2722 \pm 53$  Ma. This age overlaps with the crystallization age of the Luanga Complex ( $2763 \pm 6$  Ma, Machado et al., 1991) thus providing the first analytical result supporting the interpretation that layered intrusions in the eastern portion of the Carajás region resulted from coeval magmatic events (Machado et al., 1991; Ferreira Filho et al., 2007).

e) U-Pb isotope analyses of zircon crystals from a pegmatoid gabbro from the Lago Grande Complex show a cluster of concordant to slightly discordant dates at  $2553 \pm 61$  Ma. These dates overlap with zircon dates from hydrothermal minerals in the Bahia and Salobo Cu-Au deposits in Carajás, and are likely to correspond to a significant disturbance of the U-Pb system during the regional scale hydrothermal event associated with the origin of IOCG type deposits.

f) Different styles of PGE mineralization occur in the Lago Grande Complex. These include primary magmatic PGE mineralization associated with sulfide-poor chromitite and sulfide-bearing harzburgite, as well as hydrothermal PGE mineralization associated with altered and venulated sulfide-bearing harzburgite.

g) The distribution of different styles of PGE mineralization in the Lago Grande and Luanga complexes, as well as in other intrusions located in the eastern portion of the Carajás Mineral Province, support the concept that they belong to a PGE-enriched mafic-ultramafic magma type, designated the Serra Leste

Magmatic Suite by Ferreira Filho et al., (2007). Petrological results indicate that the Serra Leste Magmatic Suite originated from siliceous high magnesian basaltic magmas, similar to the parental liquids to the world's principal PGE-sulfide deposits.

h) Exploration for covered PGE-mineralized layered intrusions and/or hydrothermal PGE deposits in the eastern portion of the Carajás Mineral Province should not be overlooked.

### **Acknowledgments**

This study was supported by CNPq (Conselho Nacional de Desenvolvimento Científico e Tecnológico and VALE S.A. (Projeto 550398/2010-4). Analytical facilities of the Instituto de Geociências (UnB), Furnas Centrais Elétricas and the LabMic Laboratory of the Universidade Federal de Goiás (UFG) provided additional support for this research. The authors are glad to Fernando Martins Matos and Denisson Oliveira from VALE for their support during fieldwork and interpretation of exploration data, as well as stimulating discussions on the geology of the Carajás Mineral Province. Cesar F. Ferreira Filho is a Research Fellow of CNPq since 1996, and acknowledge the continuous support through research grants and scholarships for the "Metalogenênese de Depósitos Associados ao Magmatismo Máfico-Ultramáfico" Research Group. This study is part of the first author's (Antonio Sales Teixeira) M.Sc dissertation developed as a research paper in the Instituto de Geociências (UnB).

## References

- Albarède F., Télouk P., Blichert-Toft J., Boyet M., Agranier A., Nelson B., 2004. Precise and accurate isotopic measurements using multiple-collector ICPMS. *Geochim. Cosmochim. Acta* 68, 2725-2744.
- Araújo, O.J.B., Maia, R.G.N., João, X.S.J., Costa, J.B.S., 1988. A megaestruturação arqueana da Folha Serra dos Carajás: *in* Congresso Latino Americano de Geologia, Anais, Belém-Brazil, pp. 324-338.
- Araújo, O.J.B., Maia, R.G.N., 1991. Projeto especial mapas de recursos minerais, de solos e de vegetação para a área do Programa Grande Carajás; Subprojeto Recursos Minerais; Folha SB.22-Z-A Serra dos Carajás - Estado do Pará: DNPM/CPRM.
- Arndt, N. T., Czamanske, G., Walker, R. J., Chauvel, C., and Fedorenko, V., 2003. Geochemistry and origin of the intrusive hosts of the Noril'sk-Talnakh Cu-Ni-PGE sulfide deposits: *Econ. Geol.* 98, 495-515.
- Avelar, V.G., Lafon, J.M., Correia Jr., F.C., Macambira, B.E.M., 1999. O magmatismo arqueano da região de Tucumã-Província Mineral de Carajás: Novos dados geocronológicos. *Rev. Bras. Geoc.* 29, 453-460.
- Barnes, S.J., 1986. The Effect of Trapped Liquid Crystallization on Cumulus Mineral Compositions in Layered Intrusions. *Contrib. Mineral. Petrol.* 93, 524–531.
- Barnes, S.J., 1989. Are Bushveld U-type parent magmas boninites or contaminated komatiites?: *Contrib. Mineral. Petrol.* 101, 447–457.
- Barnes, S.-J., Lightfoot, P.C., 2005. Formation of magmatic nickel-sulfide ore deposits and processes affecting their copper and platinum-group element contents. *Econ. Geol.*, 100th Anniversary Volume, pp. 179-213.
- Barnes, S.-J., Maier, W.D., Curl, E.A., 2010. Composition of the Marginal Rocks and Sills of the Rustenburg Layered Suite, Bushveld Complex, South Africa: Implications for the Formation of the Platinum-Group Element Deposits. *Econ. Geol.* 105, 1491–1511.

- Barros, C.E.M., Sardinha, A.S., Barbosa, J.P.O., Krimski, R., Macambira, M.J.B., 2001. Pb–Pb and U–Pb zircon ages of Archean syntectonic granites of the Carajás metallogenic province, northern Brazil. In: South American Symposium on Isotopic Geology. Extended Abstract Volume, Pucón, Chile, vol. 3, pp. 94–97.
- Campbell, I.H. 1985. The difference between oceanic and continental tholeiites: A fluid dynamic explanation. *Contrib. Mineral. Petrol.* 91, 37–43.
- Dall’Agnol, R., Souza, Z.S., Althoff, F.J., Barros, C.E.M., Leite, A.A.S., João, X.S.J., 1997. General aspects of the granitogenesis of the Carajás metallogenic province. In: Proceedings of the International Symposium on Granites and Associated Mineralizations, Salvador, Excursion Guide, pp. 135-161.
- Dardenne, M.A., Ferreira Filho, C.F., Meirelles, M.R., 1988. The role of shoshonitic and calc-alkaline suites in the tectonic evolution of the Carajás District, Brazil. *J. South Am. Earth Sci.* 1, 363–372.
- DePaolo, D.J., 1981. Neodymium isotopes in the Colorado Front Range and implications for crust formation and mantle evolution in the Proterozoic. *Nature* 291, 193-197.
- Dias, G.S., Macambira, M.J.B., Dall’Agnol, R., Soares, A.D.V., Barros, C.E.M., 1996. Datação de zircões de sill de metagabro: Comprovação da idade arqueana da Formação Águas Claras, Carajás, Pará. In: SBG-NNO (Eds.), V Simpósio de Geologia da Amazônia, Belém, Boletim Resumo, vol. 5, pp. 376–379.
- Diella, V., Ferrario, A., Girardi, V.A.V., 1995. PGE and PGM in the Luanga mafic-ultramafic intrusion in Serra dos Carajás (Pará State, Brazil). *Ore Geol. Rev.* 9, 445-453.
- Docegeo - Rio Doce Geologia e Mineração, 1988. Revisão Litoestratigráfica da Província Mineral de Carajás. In: SBG-NNO (Eds.), 35<sup>o</sup> Congresso Brasileiro Geologia, Belém, Anais, pp. 11-59.
- Eales, H.V., Cawthorn, R.G., 1996. The Bushveld Complex. In: Cawthorn, R.G. (Ed.), *Layered Intrusions*. Amsterdam, pp.181–229.



- Eales, H.V., Costin G., 2012. Crustally contaminated komatiite: Primary source of the chromitites and Marginal, Lower, and Critical Zone magmas in a staging chamber beneath the Bushveld Complex. *Econ. Geol.* 107, 645-665.
- Ferreira Filho, C.F., 2010. Geological and Petrological Constraints on the Origin of Brazilian Ni-Cu Sulfide and PGE Deposits. 11th International Platinum Symposium, Sudbury, Ontario Geological Survey, Miscellaneous Release–Data, pp. 1-4.
- Ferreira Filho, C.F., Araujo, S.M., 2009. Review of Brazilian chromite deposits associated with layered intrusions: geological and petrological constraints for the origin of stratiform chromitites: *Appl. Earth Sci. (Trans. Inst. Min. Metall. B)* 118, 86-100.
- Ferreira Filho, C.F., Caçado, F., Correa, C., Macambira, E.M.B., Siepierski, L., Brod, T.C.J., 2007. Mineralizações estratiformes de EGP-Ni associadas a complexos acamadados em Carajás: os exemplos de Luanga e Serra da Onça. In: Publitec Gráfica & Editora, *Contribuições à Geologia da Amazônia*, vol. 5, pp. 01-14.
- Ferreira Filho, C.F., Naldrett, A.J., Gorton, M.P., 1998. REE and pyroxene compositional variation across the Niquelândia layered intrusion, Brazil: petrological and metallogenetic implications. *Appl. Earth Sci. (Trans. Inst. Min. Metall. B)* 107, 1-22.
- Finnigan C.S., Brenan J.M., Mungall J.E., McDonough W.F., 2008. Experiments and models bearing on the role of chromite as a collector of platinum group minerals by local reduction. *J. Petrol* 49, 1647–1665.
- Geisler, T., Schaltegger, U., Tomaschek, F., 2007. Re-equilibration of Zircon in Aqueous Fluids and Melts. *Elements*, 3, 43-50.
- Gibbs, A.K., Wirth, K.R., Hirata, W.K., Olszewski Jr, W.J., 1986. Age and composition of the Grão Pará Group volcanics, Serra dos Carajás. *Rev. Bras. Geoc.* 16, 201-211.
- Gioia, S.M.C.L., Pimentel, M.M., 2000. The Sm-Nd isotopic method in the geochronology laboratory of University of Brasilia. *Anais da Academia Brasileira de Ciências* 72, 219-245.

- Giustina, M.E.S.D., Pimentel, M.M., Ferreira Filho, C.F., Hollanda, M.H.B.M. 2011a. Dating coeval mafic magmatism and ultrahigh temperature metamorphism in the Anápolis–Itaçu Complex, Central Brazil. *Lithos*, 124: 82-102
- Giustina, M.E.S.D., Pimentel, M.M., Ferreira Filho, C.F., Fuck, R. A., Andrade, S. 2011b. U–Pb–Hf-trace element systematics and geochronology of zircon from a granulite-facies metamorphosed mafic–ultramafic layered complex in Central Brazil. *Precambrian Research*, 189: 176-192.
- Godel, B., Barnes, S-J., Maier, W. D., 2011. Parental magma composition inferred from trace element in cumulus and intercumulus silicate minerals: An example from the Lower and Lower Critical Zones of the Bushveld Complex, South-Africa. *Lithos* 125, 537–552.
- Grainger C.J., Groves D.I., Costa C.H.C., 2002. The epigenetic sediment hosted Serra Pelada Au–PGE deposit and its potential genetic association with Fe-oxide Cu–Au mineralisation within the Carajás Mineral Province, Amazon Craton, Brazil. *Soc. Econ. Geol. Spec. Publ*, pp. 47–64.
- Grainger, C.J., Groves, D.I., Tallarico, F.H.B., Fletcher, I.R., 2008. Metallogensis of the Carajás Mineral Province, Southern Amazon Craton, Brazil: Varying styles of Archean through Paleoproterozoic to Neoproterozoic base and precious-metal mineralization. *Ore Geol. Rev.* 33, 451-489.
- Hamlyn P.R., Keays R.R., Cameron W.E., Crawford A.J., Waldron H.M., 1985. Precious metals in magnesian low-Ti lavas: Implications for metallogensis and sulfur saturation in primary magmas. *Geochim. Cosmochim. Acta* 49, 1797–1811.
- Harmer, R.E., Sharpe M.R., 1985. Field relations and strontium isotope systematics of the Marginal rocks of the Eastern Bushveld Complex. *Econ. Geol.* 80, 813-837.
- Holdsworth, R.E., Pinheiro, R.V.L., 2000. The anatomy of shallow-crustal transpressional structures: insights from the Archean Carajás fault zone, Amazon, Brazil. *J. Struct. Geol.* 22, 1105–1123.

- Huhn, S.R.B., Santos, A.B.S., 1988. O terreno granito-greenstone da região de Rio Maria-Sul do Pará. In: Amaral, A.F., Ledsham, E.J., Gouveia, J.L., Martins, F. (Eds.), SBG-NNO, 35° Congresso Brasileiro de Geologia. Belém, Anais, v. 35, pp. 1438–1452.
- Jackson, S.E., Pearson, N.J., Griffin, W.L., Belousova, E.A., 2004. The application of laser ablation inductively coupled plasma mass spectrometry to in situ U-Pb zircon geochronology. *Chem. Geol.* 211, 47-69.
- Keays, R.R., Lightfoot, P. C., Hamlyn. P.R., 2012. Sulfide saturation history of the Stillwater Complex, Montana: chemostratigraphic variation in platinum group elements. *Miner. Deposita* 47, 151–173.
- Li, C., Xu Z., Waal, A., Ripley, E.M., Maier, W.D., 2004. Compositional variations of olivine from the Jinchuan Ni–Cu sulfide deposit, western China: implications for ore genesis. *Miner. Deposita* 39, 159–172.
- Lightfoot, P.C., Keays, R.R., 2005. Siderophile and chalcophile metal variations in flood basalts from the Siberian trap, Noril'sk region: Implications for the origin of the Ni-Cu-PGE sulfide ores. *Econ. Geol.* 100, 246-261.
- Lightfoot, P.C., Naldrett, A.J., Gorbachev, N.S., Doherty, W, Fedorenko, V.A., 1990. Geochemistry of the Siberian trap of the Noril'sk area, USSR, with implications for the relative contributions of crust and mantle to flood basalt magmatism. *Contrib. Mineral. Petrol.* 104, 631–644.
- Lindenmayer, Z.G., Sial A.N., Pimentel M.M., Ronchi L.H., Althoff F.J., Laux J.H., Araújo J.C., Fleck A., Becker C.A., Carvalho D.B., Nowatzki A.C., 2001. Geologia do Depósito de Cu-Au de Gameleira, Serra dos Carajás, Pará. In: Jost H., Brod J.A., Queiroz E.T. de. (Eds.), *Caracterização de Depósitos Auríferos Brasileiros*, Brasília, DNPM - ADIMB, pp.79-139.
- Ludwig, K.R., 2003. User's manual for Isoplot 3.00: a geochronological toolkit for Microsoft Excel. Berkeley Geochronology Center Special Publication, pp. 1–70.
- Machado, W., Lindenmayer, Z.G., Krogh, T.E., Lindenmayer, D., 1991. U-Pb geochronology of Archean magmatism and basement reactivation in the Carajás area, Amazon shield, Brazil. *Precam. Res.* 49, 329-354.

- Maier, W.D., Barnes, S.-J., Groves, D.I., 2013. The Bushveld Complex, South Africa: formation of platinum–palladium, chrome- and vanadium-rich layers via hydrodynamic sorting of a mobilized cumulate slurry in a large, relatively slowly cooling, subsiding magma chamber. *Miner. Deposita* 48, 1–56.
- Merkle R.K.W., 1992. Platinum-group element minerals in the Middle Group of chromitite layers, Western Bushveld Complex: indications for collection mechanisms and postmagmatic modification. *Can. J. Earth Sci.* 29, 209-221.
- Medeiros Filho, C.A., Meireles, E.M., 1985. Dados preliminares sobre a ocorrência de cromita na área de Luanga. In: SBG-NNO (Eds.), *Simpósio de Geologia da Amazônia Anais*, Belém, vol. 3, pp. 90-96.
- Mondal S.K., Mathez E.A., 2007. Origin of the UG2 chromitite layer, Bushveld Complex. *J. Petrol.* 48, 495–510.
- Mungall, J.E., Naldrett, A.J., 2008. Ore deposits of the platinum-group elements. *Elements* 4, 253–258.
- Naldrett, A. J., 1994. The Sudbury-Noril'sk symposium, an overview. *Proceedings of the Sudbury-Noril'sk symposium*, Ontario Geol. Surv. Spec. Publ. v. 5, pp. 3-8.
- Naldrett A.J., 2004, *Magmatic sulfide deposits: Geology, Geochemistry and Exploration*: Heidelberg, Springer Verlag, 728 pp.
- Naldrett A.J., Wilson A., Kinnaird J., Yudovskaya M., Chunnett G., 2012. The origin of chromitites and related PGE mineralization in the Bushveld Complex: new mineralogical and petrological constraints. *Miner. Deposita* 47, 209–232.
- Nogueira, A.C.R., Truckenbrod, W., Costa, J.B.S., Pinheiro, R.V.L., 1994. Análise faciológica e estrutural da Formação Águas Claras, Pré-Cambriano da Serra dos Carajás. In: SBG-NNO (Eds.), *Simpósio de Geologia da Amazônia, Resumos Expandidos*. Belém, pp. 363–364.
- Nogueira, A.C.R., Truckenbrod, W., Pinheiro, R.V.L., 2000. Storm and tide-dominated siliciclastic deposits of the Archean Águas Claras Formation, Serra dos Carajás, Brazil. In: *31th International Geological Congress, Rio de Janeiro, Brazil, Extended Abstracts*, 1 CD-ROM.

- Olszewski, W.J., Wirth, K.R., Gibbs, A.K., Gaudette, H.E., 1989. The age, origin, and tectonics of the Grão Pará Group and associated rocks, Serra dos Carajás, Brazil: Archean continental volcanism and rifting. *Precam. Res.* 42, 229–254.
- Pidgeon, R.T., Macambira, M.J.B., Lafon, J.M., 2000. Th-U-Pb isotopic systems and internal structures of complex zircons from enderbite from the Pium Complex, Carajás Province, Brazil: evidence for the ages of granulite facies metamorphism and the protolith of the enderbite. *Chem. Geol.* 166, 159-171.
- Putnis, A. 2009. Mineral replacement reactions. *Reviews in Mineralogy and Geochemistry* 70 (1), 87-124.
- Requia K., Stein H., Fontboté L., Chiaradia M., 2003. Re–Os and Pb–Pb geochronology of the Archean Salobo iron oxide copper–gold deposit, Carajás Mineral Province, northern Brazil. *Miner. Deposita* 38, 727-738
- Rivalenti, G., Mazzucchelli, M., Girardi, V.A.V., Cavazzini, G., Finatti, C., Barbieri, M.A., Texeira, W., 1998. Petrogenesis of the Paleoproterozoic basalt–andesite–rhyolite dyke association on the Carajás region, Amazonian craton. *Lithos* 43, 235–265.
- Santos, J.O.S., Groves, D.I., Hartmann, L.A., Moura, M.A., Mc-Naughton, N.J., 2001. Gold deposits of the Tapajós and Alta Floresta domains, Tapajós-Parima orogenic belt, Amazon craton, Brazil. *Miner. Deposita* 36, 278–299.
- Soares, A.D.V., Santos, A.B., Vieira, E.A., Bella, V.M., Martins, L.P.B., 1994. Área Águas Claras: Contexto geológico e mineralizações. In: SBG-NNO (Eds.), *Simpósio de Geologia da Amazônia*, Belém, Anais, vol. 4, pp. 379–382.
- Souza, S.R.B., Macambira, M.J.B., Sheller, T., 1996. Novos dados geocronológicos para os granitos deformados do Rio Itacaiúnas (Serra dos Carajás, PA), implicações estratigráficas. In: SBG-NNO (Eds.), *Simpósio de Geologia da Amazônia*, Belém, Anais, vol. 5, pp. 380-383.
- Suita, M.T.F., 1988. Geologia da Área Luanga com Ênfase na Petrologia do Complexo Básico-Ultrabásico Luanga e Depósitos de Cromita Associados. Unpubl M.Sc thesis, n° 46, Universidade de Brasília, 322 pp.

- Sun S.S., McDonough W.F., 1989. Chemical and isotopic systematics of oceanic basalts: implications for mantle composition and processes. In: Saunders AD, Norry MJ (Eds.), *Magmatism in the Ocean Basins*. Geological Society Special Publication, pp. 313–345.
- Talkington, R.W.S., Lipin, B.R., 1986. Platinum-Group Minerals in Chromite Seams of the Stillwater Complex, Montana. *Econ. Geol.* 81, 1179-1186.
- Tallarico, F.H.B., Groves, D.I., Figueiredo, B.R., Grainger, C.J., Beadry, C., 2005. Neoproterozoic and Paleoproterozoic metallogeny of the Carajás copper-gold belt. In: SBG (Eds.), *I Simpósio Brasileiro de Metalogenia, Gramado. Extended Abstracts, CD-Rom*.
- Teixeira, A.S., 2013. *Geologia, Petrologia e Geocronologia do Complexo Acamadado Lago Grande: Evidencia para uma Suite Magmática Mineralizada a PGE na Província Carajás – Brasil*. Unpubl. M.Sc. thesis, Universidade de Brasília, Brazil, 108 pp.
- Teixeira, J.B.G., Eggler, D.H., 1994. Petrology, Geochemistry, and Tectonic Setting of Archaean Basaltic and Dioritic Rocks from the N4 Iron Deposit, Serra dos Carajás, Pará, Brazil. *Acta Geologica Leopoldensia*, pp. 71-114.
- Trendall, A.F., Basei, M.A.S., De Laeter, J.R., Nelson, D.R., 1998. SHRIMP zircon U-Pb constraints on the age of the Carajás Formation, Grão Pará Group, Amazon Craton. *J. South Am. Earth Sci.* 11, 265–277.
- Vasquez, M.L., Carvalho, J.M.A., Sousa, C.S., Ricci, P.S.F.; Macambira, E.M.B.; Costa, L.T.R., 2008. *Mapa Geológico do Pará em SIG*. CPRM.
- Villas, R.N., Santos, M.D., 2001. Gold deposits of the Carajás mineral province: Deposit types and metallogenesis. *Miner. Deposita* 36, 300–331.
- Wang, C.Y., Zhou, M.F., Qi L., 2010. Origin of extremely PGE-rich mafic magma system: An example from the Jinbaoshan ultramafic sill, Emeishan large igneous province, SW China. *Lithos* 119, 147–161.
- Wedepohl, K. H., 1995. The composition of the continental crust. *Geochim. Cosmochim. Acta* 59, 1217-1232.

Zaccarini, F., Garuti, G., Cawthorn, R.G., 2002. Platinum-group minerals in chromitite xenoliths from Onverwacht and Tweefontein ultramafic pipes, eastern Bushveld Complex, South Africa. *Can. Mineral.* 40, 481-497.

Zuchetti, M., 2007. Rochas máficas do Supergrupo Grão Pará e sua relação com a mineralização de ferro dos depósitos N4 e N5, Carajás, PA. Unpubl. Ph.D. thesis, Nº 7, Universidade Federal de Minas Gerais, 165pp.

## CONCLUSÕES

O estudo do Complexo Lago Grande possibilitou estabelecer as seguintes conclusões que são apresentadas abaixo:

a) O Complexo Lago Grande – CLG é uma intrusão acamadada de médio porte (12 km x 1,7 km), alongada no sentido nordeste/sudoeste. Compõe-se principalmente por rochas máficas cumuláticas, seguidas por cúmulos de natureza ultramáfica. Do ponto de vista estrutural o CLG está com a estratigrafia magmática invertida, sendo recoberto, na porção sudeste, por rochas metamórficas pertencentes ao Complexo Xingu

b) A composição dos cúmulos de olivina do CLG ( $Fo_{82.5-85.7}$ ) indica cristalização a partir de um magma parental relativamente primitivo (ou relativamente rico em MgO). A variação da composição das olivinas na Zona Ultramáfica indica uma reversão na sua composição sugerindo um sistema de cristalização aberto, com reequilíbrio pela entrada de novos pulsos magmáticos. Os minerais cúmulos presentes no CLG e suas relações texturais sugerem a seguinte sequência de cristalização: olivina + cromita; ortopiroxênio + cromita; ortopiroxênio, ortopiroxênio + plagioclásio e ortopiroxênio + plagioclásio + clinopiroxênio.

c) Há evidências de que o magma que originou o CLG foi contaminado com elementos da crosta continental antiga durante seu posicionamento tectônico. Estas evidências são: 1) O perfil dos elementos traços estáveis das rochas gabróicas do CLG, normalizados ao manto, indicam fracionamento destas rochas, com enriquecimento em LREE e Th e importante empobrecimento em Nb e Ta. 2) Dados isotópicos de Nd em rochas máficas e ultramáficas retornam idade modelo entre 2,94 e 3,56 Ga, com  $\epsilon_{Nd} (T=2.72 \text{ Ga})$  negativa entre (-0,32 to -4,25). Estes dados são coerentes com o posicionamento tectônico do CLG no Complexo Xingu, que tem ca 3 Ga.

d) A idade U-Pb em zircão para o Complexo Lago Grande foi determinada, neste estudo, em  $2722 \pm 53$  Ma. Essa idade é concordante com a idade de



cristalização do Complexo de Luanga ( $2763\pm 6$  Ma, Machado et al., 1991), fornecendo assim, o primeiro resultado analítico que confirma a interpretação de que as intrusões acamadadas da porção leste de Carajás são resultado de eventos comagmáticos (Machado et al., 1991, Ferreira Filho et al., 2007).

e) Análises isotópicas U-Pb em cristais de zircão de uma porção pegmatóide do gabro do Complexo Lago Grande mostram um conjunto de dados concordantes ou levemente discordantes em  $2553\pm 61$  Ma. Essa idade corresponde aos dados de zircões de minerais hidrotermais dos depósitos de Cu-Au Bahia e Salobo em Carajás. Parecem também corresponder a uma perturbação significativa do sistema U-Pb durante o evento hidrotermal regional associado à origem dos depósitos tipo IOCG.

f) Diferentes tipos de mineralizações de PGE ocorrem no Complexo Lago Grande, tais como: mineralização primária de PGE associada a cromitito pobre em sulfetos; harzburgito portador de sulfetos e mineralização hidrotermal de PGE associada a harzburgitos portadores de sulfetos alterados e venulados.

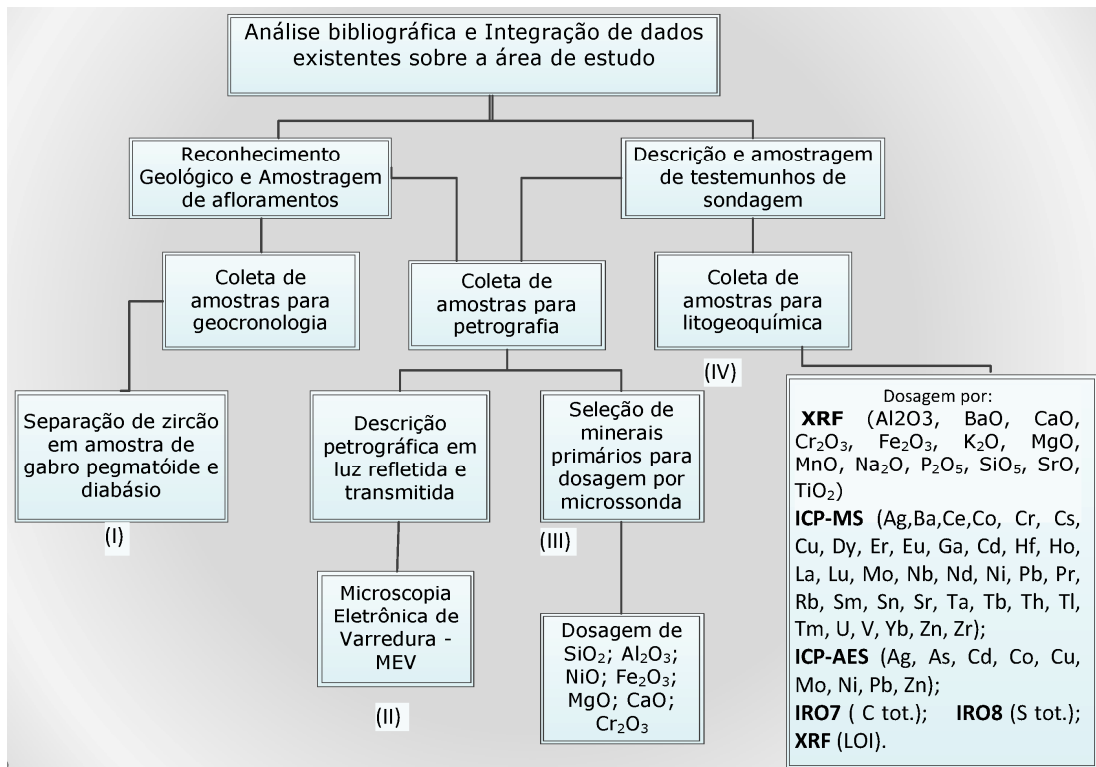
g) A distribuição de diferentes tipos de mineralização de PGE nos complexos de Lago Grande e Luanga, assim como em outras intrusões localizadas na porção leste da Província Mineral Carajás, sugerem que elas são provenientes de um tipo de magma mafico-ultramáfico enriquecido em PGE, designado por Ferreira Filho et al., (2007) como Suíte Magmática Serra Leste. Os resultados petrológicos indicam que a Suíte Magmática Serra Leste se originou a partir de um magma basáltico silicoso rico em magnésio, similar ao líquido parental dos principais depósitos mundiais de sulfetos-PGE.

h) Programas exploratórios para PGE na porção leste da Província Mineral de Carajás deverão considerar como possíveis controles os corpos intrusivos acamadados mineralizadas em PGE, assim como os depósitos hidrotermais de PGE.

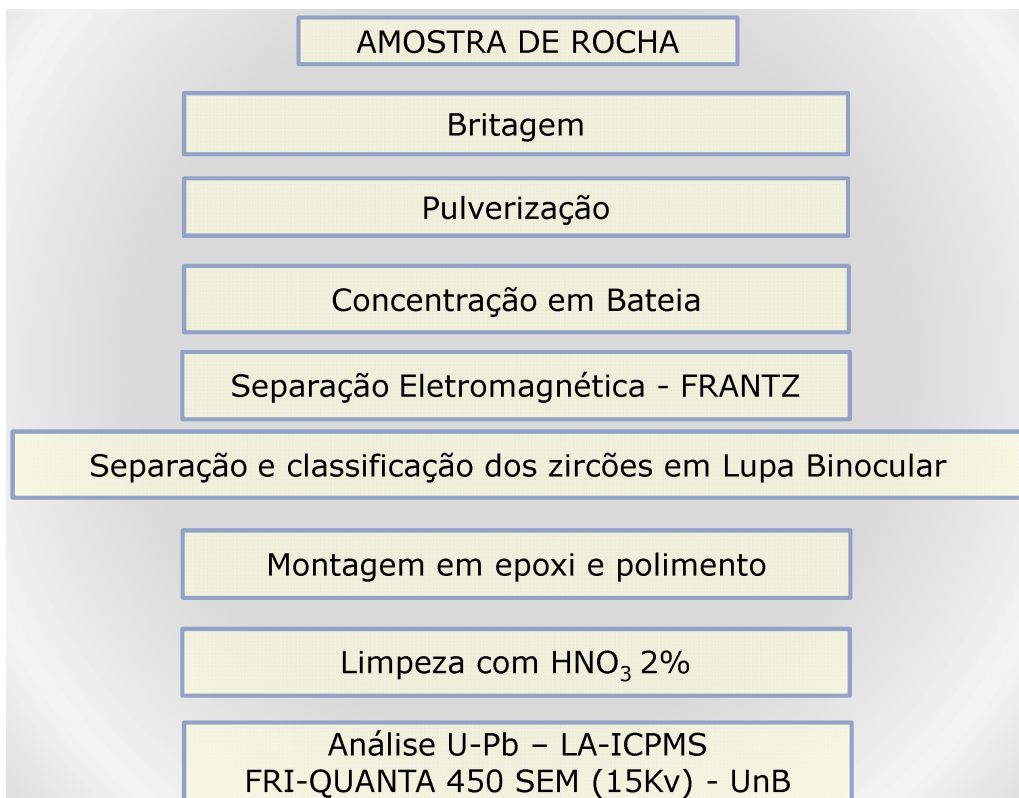
## **ANEXOS**

## Anexo I – Fluxogramas

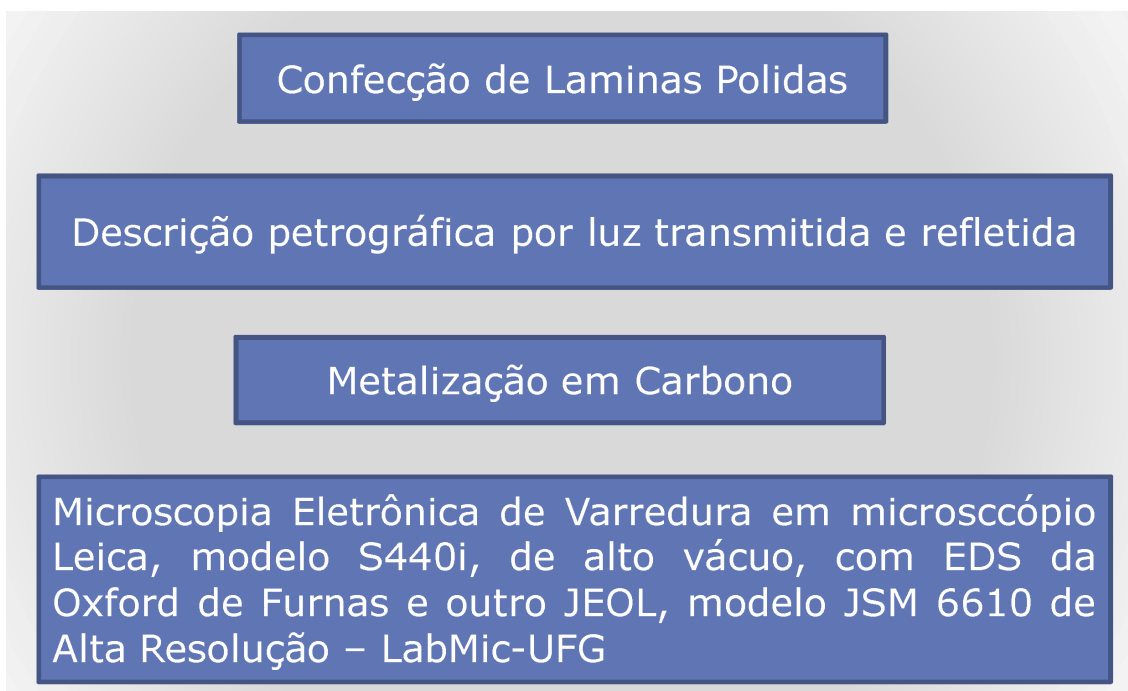
## Fluxograma 1 - Fluxograma da metodologia de trabalho



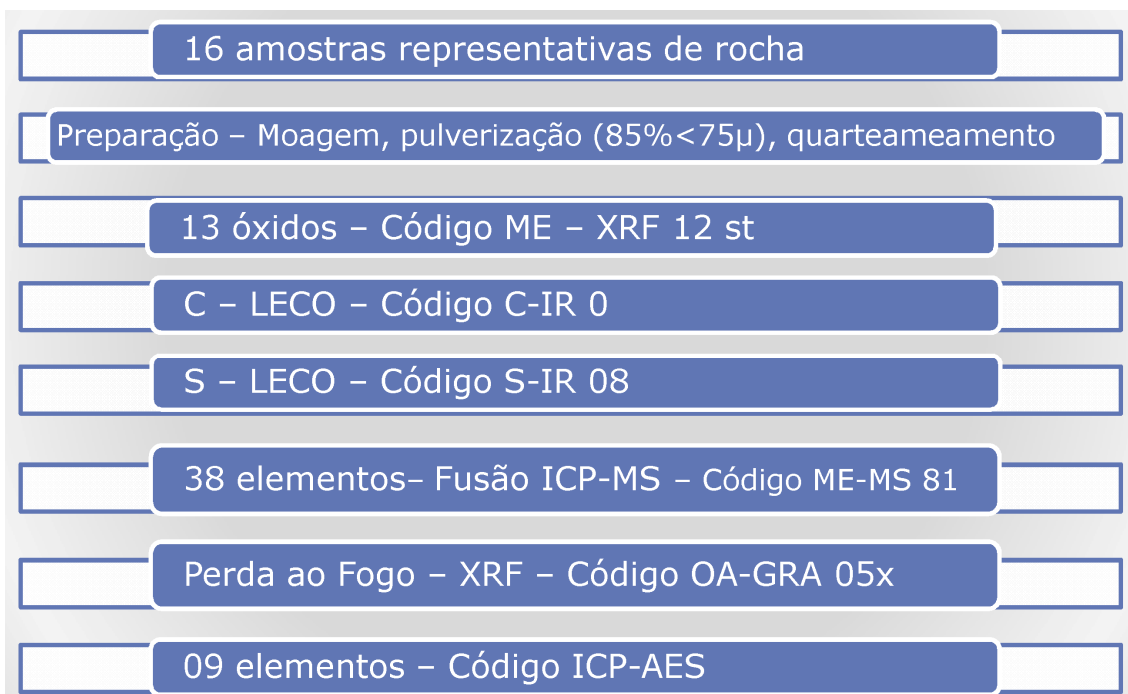
## Fluxograma 2 - Fluxograma de preparação de amostras para geocronologia



Fluxograma 3 - Fluxograma de preparação de amostras para petrografia e microscopia eletrônica de varredura - MEV



Fluxograma 4 - Fluxograma de preparação de amostras para litogeoquímica



Anexo II - Análise de Química Mineral

BH11210260 - Finalized  
 CLIENT : CAFON - Cesar Fonseca Ferreira Filho  
 # of Samples : 8  
 DATE RECEIVED : 2011-10-31 DATE FINALIZED : 2011-12-06  
 PROJECT : LUANGA SUL  
 CERTIFICATE COMMENTS :  
 PO NUMBER :

	ME-XRF12st	ME-XRF12st	ME-XRF12st	ME-XRF12st	ME-XRF12st	ME-XRF12st	ME-XRF12st	ME-XRF12st	ME-XRF12st	ME-XRF12st
SAMPLE	Al2O3	BaO	CaO	Cr2O3	Fe2O3	K2O	MgO	MnO	Na2O	P2O5
DESCRIPTION	%	%	%	%	%	%	%	%	%	%
LUSL-08	18,300	0,037	9,490	0,006	7,130	1,050	7,290	0,127	3,230	0,007
LUSL-09	16,050	0,028	14,250	0,004	8,580	0,463	5,910	0,156	2,370	0,006
LUSL-11	22,200	0,048	11,400	<0.001	3,890	1,090	4,250	0,100	3,790	0,006
LUSL-19	13,850	0,049	9,990	0,044	14,050	2,100	7,370	0,302	1,650	0,079
LUSL-20b	19,000	0,069	9,000	0,075	7,160	1,695	6,060	0,194	3,450	0,008
LUSL-21b	13,650	0,019	9,830	0,021	15,300	0,481	6,730	0,204	2,910	0,258
LUSL-WO-A	2,720	0,040	46,400	<0.001	1,650	0,574	1,460	0,039	0,420	0,130
LUSL-WO-B	2,300	0,042	48,100	<0.001	1,400	0,482	1,400	0,034	0,279	0,119

	ME-XRF12st	ME-XRF12st	ME-XRF12st	ME-MS81	ME-MS81	ME-MS81	ME-MS81	ME-MS81	ME-MS81	ME-MS81
SAMPLE	SiO2	SrO	TiO2	Ag	Ba	Ce	Co	Cr	Cs	Cu
DESCRIPTION	%	%	%	ppm	ppm	ppm	ppm	ppm	ppm	ppm
LUSL-08	50,900	0,032	0,130	1,000	262,000	7,700	51,900	70,000	0,560	295,000
LUSL-09	50,100	0,051	1,020	<1	138,000	8,700	31,700	20,000	0,400	45,000
LUSL-11	51,800	0,054	0,110	<1	351,000	7,900	15,700	30,000	0,950	17,000
LUSL-19	49,000	0,019	1,040	<1	349,000	9,600	55,000	350,000	0,750	155,000
LUSL-20b	52,300	0,052	0,110	<1	586,000	9,100	34,700	40,000	0,780	12,000
LUSL-21b	47,700	0,045	2,690	<1	144,500	41,000	56,800	260,000	0,520	324,000
LUSL-WO-A	16,550	0,142	0,160	<1	209,000	25,600	7,500	70,000	0,310	24,000
LUSL-WO-B	15,750	0,128	0,160	<1	165,500	22,600	6,900	50,000	0,360	12,000

	ME-MS81	ME-MS81	ME-MS81	ME-MS81	ME-MS81	ME-MS81	ME-MS81	ME-MS81	ME-MS81	ME-MS81
SAMPLE	Dy	Er	Eu	Ga	Gd	Hf	Ho	La	Lu	Mo
DESCRIPTION	ppm	ppm	ppm	ppm	ppm	ppm	ppm	ppm	ppm	ppm
LUSL-08	0,820	0,540	0,420	15,800	0,730	<0.2	0,160	4,300	0,090	2,000
LUSL-09	1,090	0,620	0,570	18,600	0,900	1,000	0,200	4,900	0,100	2,000
LUSL-11	0,950	0,640	0,520	19,900	1,000	0,300	0,220	4,500	0,080	2,000
LUSL-19	4,200	2,510	0,930	17,100	3,360	1,400	0,840	3,500	0,370	2,000
LUSL-20b	1,010	0,530	0,510	18,400	1,100	<0.2	0,210	5,200	0,100	2,000
LUSL-21b	6,650	3,820	2,250	24,000	7,970	5,400	1,350	16,300	0,450	3,000
LUSL-WO-A	2,030	1,310	0,550	5,200	2,450	0,500	0,460	12,300	0,190	3,000
LUSL-WO-B	1,940	1,250	0,460	4,700	1,910	0,900	0,390	10,600	0,150	2,000

	ME-MS81	ME-MS81	ME-MS81	ME-MS81	ME-MS81	ME-MS81	ME-MS81	ME-MS81	ME-MS81	ME-MS81
SAMPLE	Nb	Nd	Ni	Pb	Pr	Rb	Sm	Sn	Sr	Ta
DESCRIPTION	ppm	ppm	ppm	ppm	ppm	ppm	ppm	ppm	ppm	ppm
LUSL-08	0,200	3,200	126,000	106,000	0,860	51,800	0,670	1,000	291,000	<0.1
LUSL-09	1,700	3,500	80,000	6,000	0,940	19,000	0,960	1,000	443,000	0,100
LUSL-11	<0.2	4,100	83,000	<5	1,070	48,700	1,170	1,000	497,000	0,100
LUSL-19	2,600	7,800	133,000	9,000	1,490	157,000	2,590	1,000	152,500	0,200
LUSL-20b	<0.2	3,800	105,000	6,000	1,040	72,100	0,910	1,000	476,000	<0.1
LUSL-21b	17,100	23,700	147,000	11,000	4,860	17,700	6,760	7,000	399,000	1,600
LUSL-WO-A	3,900	10,000	40,000	9,000	2,610	21,100	2,220	3,000	1,280,000	0,300
LUSL-WO-B	4,600	9,800	41,000	6,000	2,290	15,400	1,960	2,000	1,080,000	0,300

	ME-MS81	ME-MS81	ME-MS81	ME-MS81	ME-MS81	ME-MS81	ME-MS81	ME-MS81	ME-MS81	ME-MS81
SAMPLE	Tb	Th	Tl	Tm	U	V	W	Y	Yb	Zn
DESCRIPTION	ppm	ppm	ppm	ppm	ppm	ppm	ppm	ppm	ppm	ppm
LUSL-08	0,140	0,250	<0.5	0,070	0,200	187,000	4,000	4,600	0,500	445,000
LUSL-09	0,190	1,670	<0.5	0,090	1,180	679,000	6,000	6,000	0,610	73,000
LUSL-11	0,170	0,410	<0.5	0,080	0,260	99,000	3,000	5,600	0,500	55,000
LUSL-19	0,590	0,170	<0.5	0,350	0,220	340,000	3,000	23,500	2,440	355,000
LUSL-20b	0,170	0,350	<0.5	0,080	0,210	154,000	4,000	5,500	0,510	89,000
LUSL-21b	1,050	3,060	<0.5	0,510	0,510	526,000	2,000	38,700	2,970	122,000
LUSL-WO-A	0,300	1,740	<0.5	0,160	1,460	40,000	2,000	16,000	1,190	70,000
LUSL-WO-B	0,320	1,620	<0.5	0,120	1,430	29,000	5,000	14,300	1,060	39,000

	ME-MS81	ME-4ACD81	ME-4ACD81	ME-4ACD81	ME-4ACD81	ME-4ACD81	ME-4ACD81	ME-4ACD81	ME-4ACD81	ME-4ACD81
SAMPLE	Zr	Ag	As	Cd	Co	Cu	Mo	Ni	Pb	Zn
DESCRIPTION	ppm	ppm	ppm	ppm	ppm	ppm	ppm	ppm	ppm	ppm
LUSL-08	9,000	<0.5	<5	1,000	47,000	311,000	<1	113,000	118,000	481,000
LUSL-09	44,000	<0.5	<5	<0.5	27,000	44,000	<1	73,000	<2	59,000
LUSL-11	15,000	<0.5	5,000	<0.5	14,000	13,000	<1	76,000	<2	37,000
LUSL-19	57,000	<0.5	<5	0,600	44,000	164,000	<1	114,000	7,000	367,000
LUSL-20b	8,000	<0.5	<5	<0.5	31,000	6,000	<1	87,000	<2	80,000
LUSL-21b	179,000	<0.5	<5	<0.5	41,000	314,000	<1	110,000	<2	85,000
LUSL-WO-A	26,000	<0.5	<5	<0.5	6,000	10,000	<1	12,000	<2	38,000
LUSL-WO-B	30,000	0,600	<5	<0.5	5,000	3,000	<1	10,000	<2	20,000

	ME-MS42	ME-MS42	ME-MS42	ME-MS42	ME-MS42	ME-MS42	S-IR08	C-IR07	OA-GRA05x
SAMPLE	As	Bi	Hg	Sb	Se	Te	S	C	LOI 1000
DESCRIPTION	ppm	ppm	ppm	ppm	ppm	ppm	%	%	%
LUSL-08	1,400	0,560	0,023	<0.05	0,400	0,020	0,050	0,050	2,430
LUSL-09	0,200	0,020	0,012	<0.05	<0.2	0,010	0,020	0,070	1,610
LUSL-11	0,900	0,050	0,013	<0.05	<0.2	<0.01	0,010	0,060	2,230
LUSL-19	1,300	0,120	0,014	<0.05	0,400	0,010	0,060	0,050	1,730
LUSL-20b	0,200	0,060	0,009	<0.05	<0.2	0,010	0,010	0,060	1,680
LUSL-21b	0,200	0,120	0,016	<0.05	0,600	0,010	0,010	0,050	1,200
LUSL-WO-A	<0.1	0,060	0,017	<0.05	0,400	0,020	<0.01	8,350	29,880
LUSL-WO-B	<0.1	0,040	0,010	<0.05	0,400	0,020	<0.01	8,760	30,590



ALS Brasil Ltda.  
 Rua São Paulo, 685, Célia,  
 CEP:33.200-000 Vespasiano  
 Belo Horizonte MG  
 Phone: +55 (31) 3621 3907 Fax: +55 (31) 3621 8433  
 www.alsglobal.com

To: CESAR FONSECA FERREIRA FILHO  
 SQN 107, BLOCO I, APT 403, ASA NORTE,  
 BRASILIA DF 70.743-090

Page: 1  
 Finalized Date: 6-DEC-2011  
 Account: CAFON

**CERTIFICATE BH11210260**

Project: LUANGA SUL  
 P.O. No.:  
 This report is for 8 Rock samples submitted to our lab in Belo Horizonte, MG, Brazil on 31-OCT-2011.  
 The following have access to data associated with this certificate:  
 CESAR FONSECA

SAMPLE PREPARATION	
ALS CODE	DESCRIPTION
WEI-21	Received Sample Weight
LOG-22	Sample login - Rcd w/o BarCode
PUL-QC	Pulverizing QC Test
PUL-31	Pulverize split to 85% <75 um

ANALYTICAL PROCEDURES		
ALS CODE	DESCRIPTION	INSTRUMENT
ME-XRF12st	Whole rock by XRF-selected analytes	XRF
ME-MS81	38 element fusion ICP-MS	ICP-MS
ME-4ACD81	Base Metals by 4-acid dig.	ICP-AES
ME-MS42	Up to 34 elements by ICP-MS	ICP-MS
C-IR07	Total Carbon (Leco)	LECO
S-IR08	Total Sulphur (Leco)	LECO
OA-GRA05x	LOI for XRF	WST-SEQ

To: CESAR FONSECA FERREIRA FILHO  
 ATTN: CESAR FONSECA  
 SQN 107, BLOCO I, APT 403, ASA NORTE,  
 BRASILIA DF 70.743-090

This is the Final Report and supersedes any preliminary report with this certificate number. Results apply to samples as submitted. All pages of this report have been checked and approved for release.

Signature:

Rene Mamani, Laboratory Manager, Peru





ALS Brasil Ltda.  
 Rua São Paulo, 685, Célia,  
 CEP:33.200-000 Vespasiano  
 Belo Horizonte MG  
 Phone: +55 (31) 3621 3907 Fax: +55 (31) 3621 8433  
 www.alsglobal.com

To: CESAR FONSECA FERREIRA FILHO  
 SQN 107, BLOCO I, APT 403, ASA NORTE,  
 BRASÍLIA DF 70.743-090

Page: 2 - A  
 Total # Pages: 2 (A - E)  
 Finalized Date: 6-DEC-2011  
 Account: CAFON

Project: LUANGA SUL

**CERTIFICATE OF ANALYSIS BH11210260**

Sample Description	Method Analyte Units LOR	WEI-21	ME-XRF12st	ME-XRF12st	ME-XRF12st	ME-XRF12st	ME-XRF12st	ME-XRF12st	ME-XRF12st	ME-XRF12st	ME-XRF12st	ME-XRF12st	ME-XRF12st	ME-XRF12st	ME-XRF12st	ME-MS81
		Recvd Wt. kg	Al2O3 %	BaO %	CaO %	Cr2O3 %	Fe2O3 %	K2O %	MgO %	MnO %	Na2O %	P2O5 %	SiO2 %	SrO %	TiO2 %	Ag ppm
		0.02	0.01	0.001	0.01	0.001	0.01	0.001	0.01	0.001	0.001	0.001	0.01	0.001	0.01	1
LUSL-08		0.15	18.30	0.037	9.49	0.006	7.13	1.050	7.29	0.127	3.23	0.007	50.9	0.032	0.13	1
LUSL-09		0.24	16.05	0.028	14.25	0.004	8.58	0.463	5.91	0.156	2.37	0.006	50.1	0.051	1.02	<1
LUSL-11		0.25	22.2	0.048	11.40	<0.001	3.89	1.090	4.25	0.100	3.79	0.006	51.8	0.054	0.11	<1
LUSL-19		0.26	13.85	0.049	9.99	0.044	14.05	2.10	7.37	0.302	1.650	0.079	49.0	0.019	1.04	<1
LUSL-20b		0.14	19.00	0.069	9.00	0.075	7.16	1.695	6.06	0.194	3.45	0.008	52.3	0.052	0.11	<1
LUSL-21b		0.10	13.65	0.019	9.83	0.021	15.30	0.481	6.73	0.204	2.91	0.258	47.7	0.045	2.69	<1
LUSL-WO-A		0.08	2.72	0.040	46.4	<0.001	1.65	0.574	1.46	0.039	0.420	0.130	16.55	0.142	0.16	<1
LUSL-WO-B		0.13	2.30	0.042	48.1	<0.001	1.40	0.482	1.40	0.034	0.279	0.119	15.75	0.128	0.16	<1



ALS Brasil Ltda.  
 Rua São Paulo, 685, Célia,  
 CEP:33.200-000 Vespasiano  
 Belo Horizonte MG  
 Phone: +55 (31) 3621 3907 Fax: +55 (31) 3621 8433  
 www.alsglobal.com

To: CESAR FONSECA FERREIRA FILHO  
 SQN 107, BLOCO I, APT 403, ASA NORTE,  
 BRASÍLIA DF 70.743-090

Page: 2 - B  
 Total # Pages: 2 (A - E)  
 Finalized Date: 6-DEC-2011  
 Account: CAFON

Project: LUANGA SUL

**CERTIFICATE OF ANALYSIS BH11210260**

Sample Description	Method Analyte Units LOR	ME-MS81	ME-MS81	ME-MS81	ME-MS81	ME-MS81	ME-MS81	ME-MS81	ME-MS81	ME-MS81	ME-MS81	ME-MS81	ME-MS81	ME-MS81	ME-MS81	ME-MS81
		Ba ppm	Ce ppm	Co ppm	Cr ppm	Cs ppm	Cu ppm	Dy ppm	Er ppm	Eu ppm	Ga ppm	Gd ppm	Hf ppm	Ho ppm	La ppm	Lu ppm
		0.5	0.5	0.5	10	0.01	5	0.05	0.03	0.03	0.1	0.05	0.2	0.01	0.5	0.01
LUSL-08		262	7.7	51.9	70	0.56	295	0.82	0.54	0.42	15.8	0.73	<0.2	0.16	4.3	0.09
LUSL-09		138.0	8.7	31.7	20	0.40	45	1.09	0.62	0.57	18.6	0.90	1.0	0.20	4.9	0.10
LUSL-11		351	7.9	15.7	30	0.95	17	0.95	0.64	0.52	19.9	1.00	0.3	0.22	4.5	0.08
LUSL-19		349	9.6	55.0	350	0.75	155	4.20	2.51	0.93	17.1	3.36	1.4	0.84	3.5	0.37
LUSL-20b		586	9.1	34.7	40	0.78	12	1.01	0.53	0.51	18.4	1.10	<0.2	0.21	5.2	0.10
LUSL-21b		144.5	41.0	56.8	260	0.52	324	6.65	3.82	2.25	24.0	7.97	5.4	1.35	16.3	0.45
LUSL-WO-A		209	25.6	7.5	70	0.31	24	2.03	1.31	0.55	5.2	2.45	0.5	0.46	12.3	0.19
LUSL-WO-B		165.5	22.6	6.9	50	0.36	12	1.94	1.25	0.46	4.7	1.91	0.9	0.39	10.6	0.15



ALS Brasil Ltda.  
 Rua São Paulo, 685, Célia,  
 CEP:33.200-000 Vespasiano  
 Belo Horizonte MG  
 Phone: +55 (31) 3621 3907 Fax: +55 (31) 3621 8433  
 www.alsglobal.com

To: CESAR FONSECA FERREIRA FILHO  
 SQN 107, BLOCO I, APT 403, ASA NORTE,  
 BRASILIA DF 70.743-090

Page: 2 - C  
 Total # Pages: 2 (A - E)  
 Finalized Date: 6-DEC-2011  
 Account: CAFON

Project: LUANGA SUL

**CERTIFICATE OF ANALYSIS BH11210260**

Sample Description	Method Analyte Units LOR	ME-MS81	ME-MS81	ME-MS81	ME-MS81	ME-MS81	ME-MS81	ME-MS81	ME-MS81	ME-MS81	ME-MS81	ME-MS81	ME-MS81	ME-MS81	ME-MS81	ME-MS81
		Mo ppm	Nb ppm	Nd ppm	Ni ppm	Pb ppm	Pr ppm	Rb ppm	Sm ppm	Sr ppm	Sr ppm	Ta ppm	Tb ppm	Th ppm	Ti ppm	Tm ppm
		2	0.2	0.1	5	5	0.03	0.2	0.03	1	0.1	0.1	0.01	0.05	0.5	0.01
LUSL-08		2	0.2	3.2	126	106	0.86	51.8	0.67	1	291	<0.1	0.14	0.25	<0.5	0.07
LUSL-09		2	1.7	3.5	80	6	0.94	19.0	0.96	1	443	0.1	0.19	1.67	<0.5	0.09
LUSL-11		2	<0.2	4.1	83	<5	1.07	48.7	1.17	1	497	0.1	0.17	0.41	<0.5	0.08
LUSL-19		2	2.6	7.8	133	9	1.49	157.0	2.59	1	152.5	0.2	0.59	0.17	<0.5	0.35
LUSL-20b		2	<0.2	3.8	105	6	1.04	72.1	0.91	1	476	<0.1	0.17	0.35	<0.5	0.08
LUSL-21b		3	17.1	23.7	147	11	4.86	17.7	6.76	7	399	1.6	1.05	3.06	<0.5	0.51
LUSL-WO-A		3	3.9	10.0	40	9	2.61	21.1	2.22	3	1280	0.3	0.30	1.74	<0.5	0.16
LUSL-WO-B		2	4.6	9.8	41	6	2.29	15.4	1.96	2	1080	0.3	0.32	1.62	<0.5	0.12



ALS Brasil Ltda.  
 Rua São Paulo, 685, Célia,  
 CEP:33.200-000 Vespasiano  
 Belo Horizonte MG  
 Phone: +55 (31) 3621 3907 Fax: +55 (31) 3621 8433  
 www.alsglobal.com

To: CESAR FONSECA FERREIRA FILHO  
 SQN 107, BLOCO I, APT 403, ASA NORTE,  
 BRASILIA DF 70.743-090

Page: 2 - D  
 Total # Pages: 2 (A - E)  
 Finalized Date: 6-DEC-2011  
 Account: CAFON

Project: LUANGA SUL

**CERTIFICATE OF ANALYSIS BH11210260**

Sample Description	Method Analyte Units LOR	ME-MS81	ME-MS81	ME-MS81	ME-MS81	ME-MS81	ME-MS81	ME-MS81	ME-4ACD81	ME-4ACD81	ME-4ACD81	ME-4ACD81	ME-4ACD81	ME-4ACD81	ME-4ACD81	ME-4ACD81
		U ppm	V ppm	W ppm	Y ppm	Yb ppm	Zn ppm	Zr ppm	Ag ppm	As ppm	Cd ppm	Co ppm	Cu ppm	Mo ppm	Ni ppm	Pb ppm
		0.05	5	1	0.5	0.03	5	2	0.5	5	0.5	1	1	1	1	2
LUSL-08		0.20	187	4	4.6	0.50	445	9	<0.5	<5	1.0	47	311	<1	113	118
LUSL-09		1.18	679	6	6.0	0.61	73	44	<0.5	<5	<0.5	27	44	<1	73	<2
LUSL-11		0.26	99	3	5.6	0.50	55	15	<0.5	5	<0.5	14	13	<1	76	<2
LUSL-19		0.22	340	3	23.5	2.44	355	57	<0.5	<5	0.6	44	164	<1	114	7
LUSL-20b		0.21	154	4	5.5	0.51	89	8	<0.5	<5	<0.5	31	6	<1	87	<2
LUSL-21b		0.51	526	2	38.7	2.97	122	179	<0.5	<5	<0.5	41	314	<1	110	<2
LUSL-WO-A		1.46	40	2	16.0	1.19	70	26	<0.5	<5	<0.5	6	10	<1	12	<2
LUSL-WO-B		1.43	29	5	14.3	1.06	39	30	0.6	<5	<0.5	5	3	<1	10	<2



ALS Brasil Ltda.  
 Rua São Paulo, 685, Célia,  
 CEP:33.200-000 Vespasiano  
 Belo Horizonte MG  
 Phone: +55 (31) 3621 3907 Fax: +55 (31) 3621 8433  
 www.alsglobal.com

To: CESAR FONSECA FERREIRA FILHO  
 SQN 107, BLOCO I, APT 403, ASA NORTE,  
 BRASILIA DF 70.743-090

Page: 2 - E  
 Total # Pages: 2 (A - E)  
 Finalized Date: 6-DEC-2011  
 Account: CAFON

Project: LUANGA SUL

CERTIFICATE OF ANALYSIS BH11210260

Sample Description	Method Analyte Units LOR	ME-4ACD81	ME-MS42	ME-MS42	ME-MS42	ME-MS42	ME-MS42	ME-MS42	S-IR08	C-IR07	QA-GRA05x
		Zn ppm	As ppm	Bi ppm	Hg ppm	Sb ppm	Se ppm	Te ppm	S %	C %	LOI 1000 %
		2	0.1	0.01	0.005	0.05	0.2	0.01	0.01	0.01	0.01
LUSL-08		481	1.4	0.56	0.023	<-0.05	0.4	0.02	0.05	0.05	2.43
LUSL-09		59	0.2	0.02	0.012	<-0.05	<-0.2	0.01	0.02	0.07	1.61
LUSL-11		37	0.9	0.05	0.013	<-0.05	<-0.2	<-0.01	0.01	0.06	2.23
LUSL-19		367	1.3	0.12	0.014	<-0.05	0.4	0.01	0.06	0.05	1.73
LUSL-20b		80	0.2	0.06	0.009	<-0.05	<-0.2	0.01	0.01	0.06	1.68
LUSL-21b		85	0.2	0.12	0.016	<-0.05	0.6	0.01	0.01	0.05	1.20
LUSL-WO-A		38	<0.1	0.06	0.017	<-0.05	0.4	0.02	<-0.01	8.35	29.88
LUSL-WO-B		20	<0.1	0.04	0.010	<-0.05	0.4	0.02	<-0.01	8.76	30.59



ALS Brasil Ltda.  
 Rua São Paulo, 685, Célvia,  
 CEP:33.200-000 Vespasiano  
 Belo Horizonte MG  
 Phone: +55 (31) 3621 3907 Fax: +55 (31) 3621 8433  
 www.alsglobal.com

To: **CESAR FONSECA FERREIRA FILHO**  
**SQN 107, BLOCO I, APT 403, ASA NORTE,**  
**BRASILIA DF 70.743-090**

Page: 1  
 Finalized Date: 6-DEC-2011  
 Account: CAFON

**QC CERTIFICATE BH11210260**

Project: LUANGA SUL  
 P.O. No.:  
 This report is for 8 Rock samples submitted to our lab in Belo Horizonte, MG, Brazil on 31-OCT-2011.  
 The following have access to data associated with this certificate:  
 CESAR FONSECA

SAMPLE PREPARATION	
ALS CODE	DESCRIPTION
WEI-21	Received Sample Weight
LOG-22	Sample login - Rcd w/o BarCode
PUL-QC	Pulverizing QC Test
PUL-31	Pulverize split to 85% <75 um

ANALYTICAL PROCEDURES		
ALS CODE	DESCRIPTION	INSTRUMENT
ME-XRF12st	Whole rock by XRF-selected analytes	XRF
ME-MS81	38 element fusion ICP-MS	ICP-MS
ME-4ACD81	Base Metals by 4-acid dig.	ICP-AES
ME-MS42	Up to 34 elements by ICP-MS	ICP-MS
C-IR07	Total Carbon (Leco)	LECO
S-IR08	Total Sulphur (Leco)	LECO
OA-GRA05x	LOI for XRF	WST-SEQ

To: **CESAR FONSECA FERREIRA FILHO**  
**ATTN: CESAR FONSECA**  
**SQN 107, BLOCO I, APT 403, ASA NORTE,**  
**BRASILIA DF 70.743-090**

This is the Final Report and supersedes any preliminary report with this certificate number. Results apply to samples as submitted. All pages of this report have been checked and approved for release.

Signature:

Rene Mamani, Laboratory Manager, Peru





ALS Brasil Ltda.  
 Rua São Paulo, 685, Célia,  
 CEP:33.200-000 Vespasiano  
 Belo Horizonte MG  
 Phone: +55 (31) 3621 3907 Fax: +55 (31) 3621 8433  
 www.alsglobal.com

To: CESAR FONSECA FERREIRA FILHO  
 SQN 107, BLOCO I, APT 403, ASA NORTE,  
 BRASILIA DF 70.743-090

Page: 2 - A  
 Total # Pages: 6 (A - E)  
 Finalized Date: 6-DEC-2011  
 Account: CAFON

Project: LUANGA SUL

**QC CERTIFICATE OF ANALYSIS BH11210260**

Sample Description	Method Analyte Units LOR	ME-XRF12st	ME-XRF12st	ME-XRF12st	ME-XRF12st	ME-XRF12st	ME-XRF12st	ME-XRF12st	ME-XRF12st	ME-XRF12st	ME-XRF12st	ME-XRF12st	ME-XRF12st	ME-XRF12st	ME-MS81	ME-MS81
		Al2O3	BaO	CaO	Cr2O3	Fe2O3	K2O	MgO	MnO	Na2O	P2O5	SiO2	SrO	TiO2	Ag	Ba
		%	%	%	%	%	%	%	%	%	%	%	%	ppm	ppm	
		0.01	0.001	0.01	0.001	0.01	0.001	0.01	0.001	0.001	0.01	0.001	0.01	1	0.5	
<b>STANDARDS</b>																
GBM398-4c																
Target Range - Lower Bound																
Upper Bound																
GBM999-5																
Target Range - Lower Bound																
Upper Bound																
LT1000/372																
Target Range - Lower Bound																
Upper Bound																
LT1000/372																
Target Range - Lower Bound																
Upper Bound																
LT1000/372																
Target Range - Lower Bound																
Upper Bound																
LT1007/318																
Target Range - Lower Bound																
Upper Bound																
LT1012/319																
Target Range - Lower Bound																
Upper Bound																
LT1012/319																
Target Range - Lower Bound																
Upper Bound																
MRGeo08																
Target Range - Lower Bound																
Upper Bound																
OREAS 146														<1	>10000	
Target Range - Lower Bound														<1	>10000	
Upper Bound														3	>10000	



ALS Brasil Ltda.  
 Rua São Paulo, 685, Célia,  
 CEP:33.200-000 Vespasiano  
 Belo Horizonte MG  
 Phone: +55 (31) 3621 3907 Fax: +55 (31) 3621 8433  
 www.alsglobal.com

To: CESAR FONSECA FERREIRA FILHO  
 SQN 107, BLOCO I, APT 403, ASA NORTE,  
 BRASILIA DF 70.743-090

Page: 2 - B  
 Total # Pages: 6 (A - E)  
 Finalized Date: 6-DEC-2011  
 Account: CAFON

Project: LUANGA SUL

**QC CERTIFICATE OF ANALYSIS BH11210260**

Sample Description	Method Analyte Units LOR	ME-MS81	ME-MS81	ME-MS81	ME-MS81	ME-MS81	ME-MS81	ME-MS81	ME-MS81	ME-MS81	ME-MS81	ME-MS81	ME-MS81	ME-MS81	ME-MS81	ME-MS81
		Ce ppm 0.5	Co ppm 0.5	Cr ppm 10	Cs ppm 0.01	Cu ppm 5	Dy ppm 0.05	Er ppm 0.03	Eu ppm 0.03	Ga ppm 0.1	Gd ppm 0.05	Hf ppm 0.2	Ho ppm 0.01	La ppm 0.5	Lu ppm 0.01	Mo ppm 2
<b>STANDARDS</b>																
GBM398-4c																
Target Range - Lower Bound																
Upper Bound																
GBM999-5																
Target Range - Lower Bound																
Upper Bound																
LT1000/372																
Target Range - Lower Bound																
Upper Bound																
LT1000/372																
Target Range - Lower Bound																
Upper Bound																
LT1007/318																
Target Range - Lower Bound																
Upper Bound																
LT1012/319																
Target Range - Lower Bound																
Upper Bound																
LT1012/319																
Target Range - Lower Bound																
Upper Bound																
MRGeo08																
Target Range - Lower Bound																
Upper Bound																
OREAS 146		4710	33.7	190	0.50	36	237	85.8	130.0	25.3	340	5.0	37.4	2450	6.75	62
Target Range - Lower Bound		4220	33.5	220	0.56	39	237	89.7	137.5	24.8	349	6.0	37.4	2240	6.47	60
Upper Bound		5160	37.8	240	0.62	49	246	95.7	139.5	27.6	395	6.0	40.5	2760	6.94	68





ALS Brasil Ltda.  
 Rua São Paulo, 685, Célia,  
 CEP:33.200-000 Vespasiano  
 Belo Horizonte MG  
 Phone: +55 (31) 3621 3907 Fax: +55 (31) 3621 8433  
 www.alsglobal.com

To: CESAR FONSECA FERREIRA FILHO  
 SQN 107, BLOCO I, APT 403, ASA NORTE,  
 BRASÍLIA DF 70.743-090

Page: 2 - C  
 Total # Pages: 6 (A - E)  
 Finalized Date: 6-DEC-2011  
 Account: CAFON

Project: LUANGA SUL

**QC CERTIFICATE OF ANALYSIS BH1210260**

Sample Description	Method Analyte Units LOR	ME-MS81 Nb ppm	ME-MS81 Nd ppm	ME-MS81 Ni ppm	ME-MS81 Pb ppm	ME-MS81 Pr ppm	ME-MS81 Rb ppm	ME-MS81 Sm ppm	ME-MS81 Sn ppm	ME-MS81 Sr ppm	ME-MS81 Ta ppm	ME-MS81 Tb ppm	ME-MS81 Th ppm	ME-MS81 Tl ppm	ME-MS81 Tm ppm	ME-MS81 U ppm
<b>STANDARDS</b>																
GBM398-4c																
Target Range - Lower Bound																
Upper Bound																
GBM999-5																
Target Range - Lower Bound																
Upper Bound																
LT1000/372																
Target Range - Lower Bound																
Upper Bound																
LT1000/372																
Target Range - Lower Bound																
Upper Bound																
LT1007/318																
Target Range - Lower Bound																
Upper Bound																
LT1012/319																
Target Range - Lower Bound																
Upper Bound																
LT1012/319																
Target Range - Lower Bound																
Upper Bound																
MRCeo08																
Target Range - Lower Bound																
Upper Bound																
OREAS 146		408	2200	78	664	555	28.5	457	45	3200	4.4	48.4	959	<0.5	10.60	2.95
Target Range - Lower Bound		339	1965	68	607	493	24.6	397	40	2790	3.8	42.5	813	<0.5	8.90	2.37
Upper Bound		415	2400	96	753	603	30.6	485	52	3410	4.8	51.9	993	1.5	10.90	3.01



ALS Brasil Ltda.  
 Rua São Paulo, 685, Célia,  
 CEP:33.200-000 Vespasiano  
 Belo Horizonte MG  
 Phone: +55 (31) 3621 3907 Fax: +55 (31) 3621 8433  
 www.alsglobal.com

To: CESAR FONSECA FERREIRA FILHO  
 SQN 107, BLOCO I, APT 403, ASA NORTE,  
 BRASILIA DF 70.743-090

Page: 2 - D  
 Total # Pages: 6 (A - E)  
 Finalized Date: 6-DEC-2011  
 Account: CAFON

Project: LUANGA SUL

**QC CERTIFICATE OF ANALYSIS BH11210260**

Sample Description	Method Analyte Units LOR	ME-MS81	ME-MS81	ME-MS81	ME-MS81	ME-MS81	ME-MS81	ME-4ACD81	ME-4ACD81	ME-4ACD81	ME-4ACD81	ME-4ACD81	ME-4ACD81	ME-4ACD81	ME-4ACD81	
		V ppm	W ppm	Y ppm	Yb ppm	Zn ppm	Zr ppm	Ag ppm	As ppm	Cd ppm	Co ppm	Cu ppm	Zr ppm	Mo ppm	Ni ppm	Pb ppm
		5	1	0.5	0.03	5	2	0.5	5	0.5	1	1	1	1	2	2
<b>STANDARDS</b>																
GBM398-4c								50.2	8	7.6	2000	3960	912	4130	>10000	5110
Target Range - Lower Bound								43.6	<5	6.0	1775	3500	805	3660	10550	4610
Upper Bound								54.4	17	8.8	2170	4280	986	4480	>10000	5630
GBM999-5																
Target Range - Lower Bound																
Upper Bound																
LT1000/372																
Target Range - Lower Bound																
Upper Bound																
LT1000/372																
Target Range - Lower Bound																
Upper Bound																
LT1007/318																
Target Range - Lower Bound																
Upper Bound																
LT1012/319																
Target Range - Lower Bound																
Upper Bound																
LT1012/319																
Target Range - Lower Bound																
Upper Bound																
MGeo08																
Target Range - Lower Bound																
Upper Bound																
OREAS 146		161	31	956	53.5	1410	252									
Target Range - Lower Bound		163	30	979	50.5	1300	255									
Upper Bound		140	22	814	48.1	1230	204									
Target Range - Lower Bound		182	30	996	58.9	1510	254									
Upper Bound																



ALS Brasil Ltda.  
 Rua São Paulo, 685, Célia,  
 CEP:33.200-000 Vespasiano  
 Belo Horizonte MG  
 Phone: +55 (31) 3621 3907 Fax: +55 (31) 3621 8433  
 www.alsglobal.com

To: CESAR FONSECA FERREIRA FILHO  
 SQN 107, BLOCO 1, APT 403, ASA NORTE,  
 BRASILIA DF 70.743-090

Page: 2 - E  
 Total # Pages: 6 (A - E)  
 Finalized Date: 6-DEC-2011  
 Account: CAFON

Project: LUANGA SUL

QC CERTIFICATE OF ANALYSIS BH11210260

Sample Description	Method Analyte Units LOR	ME-MS42	ME-MS42	ME-MS42	ME-MS42	ME-MS42	ME-MS42	S-IR08	C-IR07	QA-GRA05x
		As ppm 0.1	Bi ppm 0.01	Hg ppm 0.005	Sb ppm 0.05	Se ppm 0.2	Te ppm 0.01	S % 0.01	C % 0.01	LOI 1000 % 0.01
<b>STANDARDS</b>										
GBM398-4c										
Target Range - Lower Bound										
Upper Bound										
GBM999-5		3.2	0.61	0.049	4.85	1.0	0.27			
Target Range - Lower Bound		2.7	0.50	0.025	4.14	0.7	0.23			
Upper Bound		3.5	0.64	0.053	5.72	1.7	0.31			
LT1000/372									7.25	
Target Range - Lower Bound									7.25	
Upper Bound									6.99	
LT1000/372								3.53		
Target Range - Lower Bound								3.51		
Upper Bound								3.42		
LT1007/318										0.37
Target Range - Lower Bound										0.34
Upper Bound										0.38
LT1012/319										1.67
Target Range - Lower Bound										1.90
Upper Bound										1.81
LT1012/319										1.97
Target Range - Lower Bound										1.81
Upper Bound										1.97
LT1012/319								1.20		
Target Range - Lower Bound								1.17		
Upper Bound								1.13		
MRCeo08		34.5	0.78	0.079	3.54	1.2	0.02			
Target Range - Lower Bound		28.9	0.65	0.053	2.50	0.7	<0.01			
Upper Bound		35.5	0.81	0.087	3.50	1.7	0.04			
OREAS 146										
Target Range - Lower Bound										
Upper Bound										



ALS Brasil Ltda.  
 Rua São Paulo, 685, Célvia,  
 CEP:33.200-000 Vespasiano  
 Belo Horizonte MG  
 Phone: +55 (31) 3621 3907 Fax: +55 (31) 3621 8433  
 www.alsglobal.com

To: CESAR FONSECA FERREIRA FILHO  
 SQN 107, BLOCO I, APT 403, ASA NORTE,  
 BRASILIA DF 70.743-090

Page: 3 - A  
 Total # Pages: 6 (A - E)  
 Finalized Date: 6-DEC-2011  
 Account: CAFON

Project: LUANGA SUL

**QC CERTIFICATE OF ANALYSIS BH11210260**

Sample Description	Method Analyte Units LOR	ME-XRF12st	ME-XRF12st	ME-XRF12st	ME-XRF12st	ME-XRF12st	ME-XRF12st	ME-XRF12st	ME-XRF12st	ME-XRF12st	ME-XRF12st	ME-XRF12st	ME-XRF12st	ME-MS81	ME-MS81	
		Al2O3 %	BaO %	CaO %	Cr2O3 %	Fe2O3 %	K2O %	MgO %	MnO %	Na2O %	P2O5 %	SiO2 %	SrO %	TiO2 %	Ag ppm	Ba ppm
<b>STANDARDS</b>																
OREAS-45P																
Target Range - Lower Bound																
Upper Bound																
OREAS-45P														<1	286	
OREAS-45P														1	290	
Target Range - Lower Bound														<1	252	
Upper Bound														3	310	
PD-1																
PD-1																
Target Range - Lower Bound																
Upper Bound																
SARM-11																
Target Range - Lower Bound																
Upper Bound																
SARM-12		0.78	0.005	1.11	0.004	95.2	0.013	2.88	0.224	0.012	0.108	0.34	0.016	0.73		
Target Range - Lower Bound		0.72	0.003	1.03	<-0.001	90.5	0.011	2.65	0.207	0.010	0.103	0.31	0.013	0.67		
Upper Bound		0.82	0.007	1.15	0.005	100.0	0.015	2.95	0.231	0.014	0.115	0.37	0.017	0.77		
SY-4															<1	360
Target Range - Lower Bound															<1	306
Upper Bound															3	375
<b>BLANKS</b>																
BLANK																
BLANK																
Target Range - Lower Bound																
Upper Bound																
BLANK																
Target Range - Lower Bound																
Upper Bound																
BLANK																
Target Range - Lower Bound																
Upper Bound																



ALS Brasil Ltda.  
 Rua São Paulo, 685, Célia,  
 CEP:33.200-000 Vespasiano  
 Belo Horizonte MG  
 Phone: +55 (31) 3621 3907 Fax: +55 (31) 3621 8433  
 www.alsglobal.com

To: CESAR FONSECA FERREIRA FILHO  
 SQN 107, BLOCO I, APT 403, ASA NORTE,  
 BRASILIA DF 70.743-090

Page: 3 - B  
 Total # Pages: 6 (A - E)  
 Finalized Date: 6-DEC-2011  
 Account: CAFON

Project: LUANGA SUL

**QC CERTIFICATE OF ANALYSIS BH11210260**

Sample Description	Method Analyte Units LOR	ME-MS81 Ce ppm 0.5	ME-MS81 Co ppm 0.5	ME-MS81 Cr ppm 10	ME-MS81 Cs ppm 0.01	ME-MS81 Cu ppm 5	ME-MS81 Dy ppm 0.05	ME-MS81 Er ppm 0.03	ME-MS81 Eu ppm 0.03	ME-MS81 Ga ppm 0.1	ME-MS81 Gd ppm 0.05	ME-MS81 Hf ppm 0.2	ME-MS81 Ho ppm 0.01	ME-MS81 La ppm 0.5	ME-MS81 Lu ppm 0.01	ME-MS81 Mo ppm 2
<b>STANDARDS</b>																
OREAS-45P																
Target Range - Lower Bound																
Upper Bound																
OREAS-45P		49.8	119.5	1130	1.93	703	4.33	2.21	1.22	21.7	4.06	6.2	0.81	25.3	0.35	4
OREAS-45P		56.1	116.5	1180	1.94	693	4.20	2.17	1.28	23.5	3.94	7.8	0.80	27.9	0.31	4
Target Range - Lower Bound		43.5	107.5	1020	1.66	621	3.64	1.95	1.03	20.2	3.55	6.1	0.69	21.8	0.27	<2
Upper Bound		54.3	132.5	1260	2.06	771	4.56	2.45	1.33	24.9	4.45	7.9	0.87	27.8	0.35	7
PD-1																
PD-1																
Target Range - Lower Bound																
Upper Bound																
SARM-11																
Target Range - Lower Bound																
Upper Bound																
SARM-12																
Target Range - Lower Bound																
Upper Bound																
SY-4		133.0	2.5	10	1.49	7	19.65	15.10	2.20	36.4	15.15	10.9	4.59	61.7	2.32	<2
Target Range - Lower Bound		109.5	1.7	<10	1.34	<5	16.35	12.75	1.77	31.4	12.55	9.3	3.86	51.7	1.88	<2
Upper Bound		134.5	3.9	30	1.66	17	20.1	15.65	2.23	38.6	15.45	11.9	4.74	64.3	2.32	6
<b>BLANKS</b>																
BLANK																
BLANK																
Target Range - Lower Bound																
Upper Bound																
BLANK																
Target Range - Lower Bound																
Upper Bound																
BLANK																
Target Range - Lower Bound																
Upper Bound																





ALS Brasil Ltda.  
 Rua São Paulo, 685, Célia,  
 CEP:33.200-000 Vespasiano  
 Belo Horizonte MG  
 Phone: +55 (31) 3621 3907 Fax: +55 (31) 3621 8433  
 www.alsglobal.com

To: CESAR FONSECA FERREIRA FILHO  
 SQN 107, BLOCO I, APT 403, ASA NORTE,  
 BRASILIA DF 70.743-090

Page: 3 - C  
 Total # Pages: 6 (A - E)  
 Finalized Date: 6-DEC-2011  
 Account: CAFON

Project: LUANGA SUL

**QC CERTIFICATE OF ANALYSIS BH11210260**

Sample Description	Method Analyte Units LOR	ME-MS81	ME-MS81	ME-MS81	ME-MS81	ME-MS81	ME-MS81	ME-MS81	ME-MS81	ME-MS81	ME-MS81	ME-MS81	ME-MS81	ME-MS81	ME-MS81	
		Nb ppm	Nd ppm	Ni ppm	Pb ppm	Pr ppm	Rb ppm	Sm ppm	Sr ppm	Sr ppm	Ta ppm	Tb ppm	Th ppm	Tl ppm	Tm ppm	U ppm
<b>STANDARDS</b>																
OREAS-45P																
Target Range - Lower Bound																
Upper Bound																
OREAS-45P		23.3	21.5	383	23	5.67	24.6	4.51	4	33.5	1.6	0.73	9.90	<0.5	0.33	2.42
OREAS-45P		24.1	21.5	384	25	5.70	24.4	4.40	5	33.9	1.7	0.63	9.46	<0.5	0.31	2.54
Target Range - Lower Bound		21.4	18.8	342	11	4.83	20.5	4.03	<1	29.2	1.3	0.61	8.77	<0.5	0.28	2.11
Upper Bound		26.6	23.2	429	33	5.97	25.5	4.99	5	36.0	1.9	0.77	10.85	1.5	0.36	2.69
PD-1																
PD-1																
Target Range - Lower Bound																
Upper Bound																
SARM-11																
Target Range - Lower Bound																
Upper Bound																
SARM-12																
Target Range - Lower Bound																
Upper Bound																
SY-4		14.1	59.9	8	10	15.95	58.4	13.40	8	1175	0.8	2.79	1.31	<0.5	2.46	0.84
Target Range - Lower Bound		11.5	51.2	<5	<5	13.45	49.3	11.40	6	1070	0.7	2.33	1.21	<0.5	2.06	0.66
Upper Bound		14.5	62.8	19	21	16.55	60.7	14.00	10	1310	1.1	2.87	1.59	1.5	2.54	0.94
<b>BLANKS</b>																
BLANK																
BLANK																
Target Range - Lower Bound																
Upper Bound																
BLANK																
Target Range - Lower Bound																
Upper Bound																
BLANK																
Target Range - Lower Bound																
Upper Bound																



ALS Brasil Ltda.  
 Rua São Paulo, 685, Célia,  
 CEP:33.200-000 Vespasiano  
 Belo Horizonte MG  
 Phone: +55 (31) 3621 3907 Fax: +55 (31) 3621 8433  
 www.alsglobal.com

To: CESAR FONSECA FERREIRA FILHO  
 SQN 107, BLOCO I, APT 403, ASA NORTE,  
 BRASILIA DF 70.743-090

Page: 3 - D  
 Total # Pages: 6 (A - E)  
 Finalized Date: 6-DEC-2011  
 Account: CAFON

Project: LUANGA SUL

**QC CERTIFICATE OF ANALYSIS BH11210260**

Sample Description	Method Analyte Units LOR	ME-MS81	ME-MS81	ME-MS81	ME-MS81	ME-MS81	ME-MS81	ME-4ACD81	ME-4ACD81	ME-4ACD81	ME-4ACD81	ME-4ACD81	ME-4ACD81	ME-4ACD81	ME-4ACD81	
		V	W	Y	Yb	Zn	Zr	Ag	As	Cd	Co	Cu	Mo	Ni	Pb	Zn
		ppm	ppm	ppm	ppm	ppm	ppm	ppm	ppm	ppm	ppm	ppm	ppm	ppm	ppm	
		5	1	0.5	0.03	5	2	0.5	5	0.5	1	1	1	1	2	
<b>STANDARDS</b>																
OREAS-45P								0.9	13	<0.5	115	772	<1	380	21	139
Target Range - Lower Bound								<0.5	<5	<0.5	107	673	<1	346	17	125
Upper Bound								1.5	24	1.5	133	825	3	425	27	157
OREAS-45P		276	4	18.8	2.09	157	260									
OREAS-45P		284	5	20.0	2.30	152	246									
Target Range - Lower Bound		225	3	15.7	1.66	122	249									
Upper Bound		287	7	20.3	2.34	160	309									
PD-1																
PD-1																
Target Range - Lower Bound																
Upper Bound																
SARM-11																
Target Range - Lower Bound																
Upper Bound																
SARM-12																
Target Range - Lower Bound																
Upper Bound																
SY-4		8	1	124.0	15.70	91	582									
Target Range - Lower Bound		<5	<1	106.5	13.30	78	481									
Upper Bound		18	4	131.5	16.30	108	593									
<b>BLANKS</b>																
BLANK																
BLANK																
Target Range - Lower Bound																
Upper Bound																
BLANK								<0.5	<5	<0.5	1	<1	<1	<1	<2	<2
Target Range - Lower Bound								<0.5	<5	<0.5	<1	<1	<1	<1	<2	<2
Upper Bound								1.0	10	1.0	2	2	2	2	4	4
BLANK																
Target Range - Lower Bound																
Upper Bound																



ALS Brasil Ltda.  
 Rua São Paulo, 685, Célvia,  
 CEP:33.200-000 Vespasiano  
 Belo Horizonte MG  
 Phone: +55 (31) 3621 3907 Fax: +55 (31) 3621 8433  
 www.alsglobal.com

To: CESAR FONSECA FERREIRA FILHO  
 SQN 107, BLOCO I, APT 403, ASA NORTE,  
 BRASILIA DF 70.743-090

Page: 3 - E  
 Total # Pages: 6 (A - E)  
 Finalized Date: 6-DEC-2011  
 Account: CAFON

Project: LUANGA SUL

**QC CERTIFICATE OF ANALYSIS BH11210260**

Sample Description	Method Analyte Units LOR	ME-MS42	ME-MS42	ME-MS42	ME-MS42	ME-MS42	ME-MS42	S-IR08	C-IR07	OA-GRA05x
		As ppm	Bi ppm	Hg ppm	Sb ppm	Se ppm	Te ppm	S %	C %	LOI 1000 %
<b>STANDARDS</b>										
OREAS-45P										
Target Range - Lower Bound										
Upper Bound										
OREAS-45P										
OREAS-45P										
Target Range - Lower Bound										
Upper Bound										
PD-1								8.27		
PD-1								8.29		
Target Range - Lower Bound								7.93		
Upper Bound								8.53		
SARM-11										0.55
Target Range - Lower Bound										0.49
Upper Bound										0.57
SARM-12										
Target Range - Lower Bound										
Upper Bound										
SY-4										
Target Range - Lower Bound										
Upper Bound										
<b>BLANKS</b>										
BLANK									<0.01	
BLANK									<0.01	
Target Range - Lower Bound									<0.01	
Upper Bound									0.02	
BLANK										
Target Range - Lower Bound										
Upper Bound										
BLANK		<0.1	<0.01	0.008	<0.05	<0.2	<0.01			
Target Range - Lower Bound		<0.1	<0.01	<0.005	<0.05	<0.2	<0.01			
Upper Bound		0.2	0.02	0.010	0.10	0.4	0.02			





ALS Brasil Ltda.  
 Rua São Paulo, 685, Célia,  
 CEP:33.200-000 Vespasiano  
 Belo Horizonte MG  
 Phone: +55 (31) 3621 3907 Fax: +55 (31) 3621 8433  
 www.alsglobal.com

To: CESAR FONSECA FERREIRA FILHO  
 SQN 107, BLOCO I, APT 403, ASA NORTE,  
 BRASILIA DF 70.743-090

Page: 4 - A  
 Total # Pages: 6 (A - E)  
 Finalized Date: 6-DEC-2011  
 Account: CAFON

Project: LUANGA SUL

**QC CERTIFICATE OF ANALYSIS BH11210260**

Sample Description	Method Analyte Units LOR	ME-XRF12st Al2O3 %	ME-XRF12st BaO %	ME-XRF12st CaO %	ME-XRF12st Cr2O3 %	ME-XRF12st Fe2O3 %	ME-XRF12st K2O %	ME-XRF12st MgO %	ME-XRF12st MnO %	ME-XRF12st Na2O %	ME-XRF12st P2O5 %	ME-XRF12st SiO2 %	ME-XRF12st SrO %	ME-XRF12st TiO2 %	ME-MS81 Ag ppm	ME-MS81 Ba ppm
		0.01	0.001	0.01	0.001	0.01	0.001	0.01	0.001	0.001	0.001	0.01	0.001	0.01	1	0.5
<b>BLANKS</b>																
BLANK															<1	<0.5
BLANK															<1	<0.5
BLANK															<1	0.5
Target Range - Lower Bound															<1	<0.5
Upper Bound															2	1.0
BLANK		<0.01	<0.001	<0.01	<0.001	<0.01	0.004	<0.01	0.002	<0.001	0.002	96.2	<0.001	<0.01		
Target Range - Lower Bound		<0.01	<0.001	<0.01	<0.001	<0.01	<0.001	<0.01	<0.001	<0.001	<0.001	95.0	<0.001	<0.01		
Upper Bound		0.02	0.002	0.02	0.002	0.02	0.002	0.02	0.002	0.002	0.002	100.0	0.002	0.02		
BLANK																
Target Range - Lower Bound																
Upper Bound																
BLANK																
Target Range - Lower Bound																
Upper Bound																
<b>DUPLICATES</b>																
A18																
DUP																
Target Range - Lower Bound																
Upper Bound																
A22a																
DUP																
Target Range - Lower Bound																
Upper Bound																
A22b																
DUP																
Target Range - Lower Bound																
Upper Bound																
A23																
DUP																
Target Range - Lower Bound																
Upper Bound																



ALS Brasil Ltda.  
 Rua São Paulo, 685, Célia,  
 CEP:33.200-000 Vespasiano  
 Belo Horizonte MG  
 Phone: +55 (31) 3621 3907 Fax: +55 (31) 3621 8433  
 www.alsglobal.com

To: CESAR FONSECA FERREIRA FILHO  
 SQN 107, BLOCO I, APT 403, ASA NORTE,  
 BRASÍLIA DF 70.743-090

Page: 4 - B  
 Total # Pages: 6 (A - E)  
 Finalized Date: 6-DEC-2011  
 Account: CAFON

Project: LUANGA SUL

**QC CERTIFICATE OF ANALYSIS BH11210260**

Sample Description	Method Analyte Units LOR	ME-MS81 Ce ppm 0.5	ME-MS81 Co ppm 0.5	ME-MS81 Cr ppm 10	ME-MS81 Cs ppm 0.01	ME-MS81 Cu ppm 5	ME-MS81 Dy ppm 0.05	ME-MS81 Er ppm 0.03	ME-MS81 Eu ppm 0.03	ME-MS81 Ga ppm 0.1	ME-MS81 Gd ppm 0.05	ME-MS81 Hf ppm 0.2	ME-MS81 Ho ppm 0.01	ME-MS81 La ppm 0.5	ME-MS81 Lu ppm 0.01	ME-MS81 Mo ppm 2
<b>BLANKS</b>																
BLANK		<0.5	<0.5	<10	0.02	<5	<0.05	<0.03	<0.03	<0.1	<0.05	<0.2	<0.01	<0.5	<0.01	<2
BLANK		<0.5	<0.5	<10	<0.01	<5	<0.05	<0.03	<0.03	<0.1	<0.05	<0.2	<0.01	<0.5	<0.01	<2
BLANK		<0.5	<0.5	10	<0.01	<5	<0.05	<0.03	<0.03	0.2	<0.05	<0.2	<0.01	<0.5	<0.01	<2
Target Range - Lower Bound		<0.5	<0.5	<10	<0.01	<5	<0.05	<0.03	<0.03	<0.1	<0.05	<0.2	<0.01	<0.5	<0.01	<2
Upper Bound		1.0	1.0	20	0.02	10	0.10	0.06	0.06	0.2	0.10	0.4	0.02	1.0	0.02	4
BLANK																
Target Range - Lower Bound																
Upper Bound																
BLANK																
Target Range - Lower Bound																
Upper Bound																
BLANK																
Target Range - Lower Bound																
Upper Bound																
<b>DUPLICATES</b>																
A18 DUP																
Target Range - Lower Bound																
Upper Bound																
A22a DUP																
Target Range - Lower Bound																
Upper Bound																
A22b DUP																
Target Range - Lower Bound																
Upper Bound																
A23 DUP																
Target Range - Lower Bound																
Upper Bound																



ALS Brasil Ltda.  
 Rua São Paulo, 685, Célia,  
 CEP:33.200-000 Vespasiano  
 Belo Horizonte MG  
 Phone: +55 (31) 3621 3907 Fax: +55 (31) 3621 8433  
 www.alsglobal.com

To: CESAR FONSECA FERREIRA FILHO  
 SQN 107, BLOCO I, APT 403, ASA NORTE,  
 BRASILIA DF 70.743-090

Page: 4 - C  
 Total # Pages: 6 (A - E)  
 Finalized Date: 6-DEC-2011  
 Account: CAFON

Project: LUANGA SUL

**QC CERTIFICATE OF ANALYSIS BH11210260**

Sample Description	Method Analyte Units LOR	ME-MS81 Nb ppm	ME-MS81 Nd ppm	ME-MS81 Ni ppm	ME-MS81 Pb ppm	ME-MS81 Pr ppm	ME-MS81 Rb ppm	ME-MS81 Sm ppm	ME-MS81 Sn ppm	ME-MS81 Sr ppm	ME-MS81 Ta ppm	ME-MS81 Tb ppm	ME-MS81 Th ppm	ME-MS81 Tl ppm	ME-MS81 Tm ppm	ME-MS81 U ppm
		0.2	0.1	5	5	0.03	0.2	0.03	1	0.1	0.1	0.01	0.05	0.5	0.01	0.05
<b>BLANKS</b>																
BLANK		<0.2	<0.1	<5	<5	<0.03	<0.2	<0.03	<1	<0.1	<0.1	<0.01	<0.05	<0.5	<0.01	<0.05
BLANK		<0.2	<0.1	<5	<5	<0.03	<0.2	<0.03	<1	<0.1	<0.1	<0.01	<0.05	<0.5	<0.01	<0.05
BLANK		<0.2	<0.1	5	<5	<0.03	<0.2	<0.03	<1	0.1	<0.1	<0.01	<0.05	<0.5	<0.01	<0.05
Target Range - Lower Bound		<0.2	<0.1	<5	<5	<0.03	<0.2	<0.03	<1	<0.1	<0.1	<0.01	<0.05	<0.5	<0.01	<0.05
Upper Bound		0.4	0.2	10	10	0.06	0.4	0.06	2	0.2	0.2	0.02	0.10	1.0	0.02	0.10
BLANK																
Target Range - Lower Bound																
Upper Bound																
BLANK																
Target Range - Lower Bound																
Upper Bound																
BLANK																
Target Range - Lower Bound																
Upper Bound																
<b>DUPLICATES</b>																
A18																
DUP																
Target Range - Lower Bound																
Upper Bound																
A22a																
DUP																
Target Range - Lower Bound																
Upper Bound																
A22b																
DUP																
Target Range - Lower Bound																
Upper Bound																
A23																
DUP																
Target Range - Lower Bound																
Upper Bound																



ALS Brasil Ltda.  
 Rua São Paulo, 685, Célia,  
 CEP:33.200-000 Vespasiano  
 Belo Horizonte MG  
 Phone: +55 (31) 3621 3907 Fax: +55 (31) 3621 8433  
 www.alsglobal.com

To: CESAR FONSECA FERREIRA FILHO  
 SQN 107, BLOCO I, APT 403, ASA NORTE,  
 BRASILIA DF 70.743-090

Page: 4 - D  
 Total # Pages: 6 (A - E)  
 Finalized Date: 6-DEC-2011  
 Account: CAFON

Project: LUANGA SUL

**QC CERTIFICATE OF ANALYSIS BH11210260**

Sample Description	Method Analyte Units LOR	ME-MS81	ME-MS81	ME-MS81	ME-MS81	ME-MS81	ME-MS81	ME-4ACD81	ME-4ACD81	ME-4ACD81	ME-4ACD81	ME-4ACD81	ME-4ACD81	ME-4ACD81	ME-4ACD81	ME-4ACD81
		V ppm 5	W ppm 1	Y ppm 0.5	Yb ppm 0.03	Zn ppm 5	Zr ppm 2	Ag ppm 0.5	As ppm 5	Cd ppm 0.5	Co ppm 1	Cu ppm 1	Mo ppm 1	Ni ppm 1	Pb ppm 2	Zn ppm 2
<b>BLANKS</b>																
BLANK		<5	<1	<0.5	<0.03	<5	<2									
BLANK		<5	<1	<0.5	<0.03	<5	<2									
BLANK		<5	<1	<0.5	<0.03	<5	<2									
Target Range - Lower Bound		<5	<1	<0.5	<0.03	<5	<2									
Upper Bound		10	2	1.0	0.05	10	4									
BLANK																
Target Range - Lower Bound																
Upper Bound																
BLANK																
Target Range - Lower Bound																
Upper Bound																
BLANK																
Target Range - Lower Bound																
Upper Bound																
<b>DUPLICATES</b>																
A18																
DUP																
Target Range - Lower Bound																
Upper Bound																
A22a																
DUP																
Target Range - Lower Bound																
Upper Bound																
A22b								<0.5	<5	<0.5	47	59	<1	234	<2	41
DUP								<0.5	<5	<0.5	46	57	<1	234	<2	43
Target Range - Lower Bound								<0.5	<5	<0.5	43	54	<1	221	<2	38
Upper Bound								1.0	10	1.0	50	62	2	247	4	46
A23																
DUP																
Target Range - Lower Bound																
Upper Bound																



ALS Brasil Ltda.  
 Rua São Paulo, 685, Célia,  
 CEP:33.200-000 Vespasiano  
 Belo Horizonte MG  
 Phone: +55 (31) 3621 3907 Fax: +55 (31) 3621 8433  
 www.alsglobal.com

To: CESAR FONSECA FERREIRA FILHO  
 SQN 107, BLOCO I, APT 403, ASA NORTE,  
 BRASILIA DF 70.743-090

Page: 4 - E  
 Total # Pages: 6 (A - E)  
 Finalized Date: 6-DEC-2011  
 Account: CAFON

Project: LUANGA SUL

**QC CERTIFICATE OF ANALYSIS BH11210260**

Sample Description	Method Analyte Units LOR	ME-MS42 As ppm	ME-MS42 BI ppm	ME-MS42 Hg ppm	ME-MS42 Sb ppm	ME-MS42 Se ppm	ME-MS42 Te ppm	S-IR08 S %	C-IR07 C %	OA-GRA05x LOI 1000 %
<b>BLANKS</b>										
BLANK										
BLANK										
BLANK										
Target Range - Lower Bound										
Target Range - Upper Bound										
BLANK										
Target Range - Lower Bound										
Target Range - Upper Bound										
BLANK										0.01000000
Target Range - Lower Bound										0.02000000
Target Range - Upper Bound										
BLANK								-0.01		
BLANK								-0.01		
Target Range - Lower Bound								-0.01		
Target Range - Upper Bound								0.02		
<b>DUPLICATES</b>										
A18								-0.01		
DUP								-0.01		
Target Range - Lower Bound								-0.01		
Target Range - Upper Bound								0.02		
A22a									0.17	
DUP									0.17	
Target Range - Lower Bound									0.16	
Target Range - Upper Bound									0.18	
A22b										1.39
DUP										1.24
Target Range - Lower Bound										1.27
Target Range - Upper Bound										1.36
A23		0.9	0.03	0.017	<0.05	<0.2	0.01			1.40
DUP		1.0	0.03	0.016	<0.05	<0.2	0.01			1.13
Target Range - Lower Bound		0.8	0.02	0.010	<0.05	<0.2	<0.01			1.22
Target Range - Upper Bound		1.1	0.04	0.023	0.10	0.4	0.02			1.31





ALS Brasil Ltda.  
 Rua São Paulo, 685, Célia,  
 CEP:33.200-000 Vespasiano  
 Belo Horizonte MG  
 Phone: +55 (31) 3621 3907 Fax: +55 (31) 3621 8433  
 www.alsglobal.com

To: CESAR FONSECA FERREIRA FILHO  
 SQN 107, BLOCO I, APT 403, ASA NORTE,  
 BRASILIA DF 70.743-090

Page: 5 - A  
 Total # Pages: 6 (A - E)  
 Finalized Date: 6-DEC-2011  
 Account: CAFON

Project: LUANGA SUL

**QC CERTIFICATE OF ANALYSIS BH11210260**

Sample Description	Method Analyte Units LOR	ME-XRF12st	ME-XRF12st	ME-XRF12st	ME-XRF12st	ME-XRF12st	ME-XRF12st	ME-XRF12st	ME-XRF12st	ME-XRF12st	ME-XRF12st	ME-XRF12st	ME-XRF12st	ME-XRF12st	ME-MS81	ME-MS81
		Al2O3 %	BaO %	CaO %	Cr2O3 %	Fe2O3 %	K2O %	MgO %	MnO %	Na2O %	P2O5 %	SiO2 %	SrO %	TiO2 %	Ag ppm	Ba ppm
		0.01	0.001	0.01	0.001	0.01	0.001	0.01	0.001	0.001	0.001	0.01	0.001	0.01	1	0.5
<b>DUPLICATES</b>																
EZ_01		19.35	0.049	8.21	-0.001	11.70	1.845	3.17	0.092	3.42	0.042	51.0	0.035	0.49		
DUP		19.35	0.052	8.26	-0.001	11.75	1.850	3.19	0.094	3.43	0.043	51.1	0.036	0.50		
Target Range - Lower Bound		18.85	0.048	8.02	-0.001	11.40	1.800	3.09	0.090	3.34	0.040	49.8	0.034	0.47		
Upper Bound		19.85	0.053	8.45	0.002	12.05	1.895	3.27	0.096	3.51	0.045	52.3	0.037	0.52		
LUSL-09																
DUP																
Target Range - Lower Bound																
Upper Bound																
LUSL-11																
DUP																
Target Range - Lower Bound																
Upper Bound																
LUSL-19																
DUP																
Target Range - Lower Bound																
Upper Bound																
LUSL-20b															<1	586
DUP															<1	579
Target Range - Lower Bound															<1	553
Upper Bound															2	612
LUSL-WO-A																
DUP																
Target Range - Lower Bound																
Upper Bound																
LUSL-WO-B																
DUP																
Target Range - Lower Bound																
Upper Bound																
FD25 - 198.40																
DUP																
Target Range - Lower Bound																
Upper Bound																



ALS Brasil Ltda.  
 Rua São Paulo, 685, Célvia,  
 CEP:33.200-000 Vespasiano  
 Belo Horizonte MG  
 Phone: +55 (31) 3621 3907 Fax: +55 (31) 3621 8433  
 www.alsglobal.com

To: CESAR FONSECA FERREIRA FILHO  
 SQN 107, BLOCO I, APT 403, ASA NORTE,  
 BRASILIA DF 70.743-090

Page: 5 - 8  
 Total # Pages: 6 (A - E)  
 Finalized Date: 6-DEC-2011  
 Account: CAFON

Project: LUANGA SUL

**QC CERTIFICATE OF ANALYSIS BH11210260**

Sample Description	Method Analyte Units LOR	ME-MS81	ME-MS81	ME-MS81	ME-MS81	ME-MS81	ME-MS81	ME-MS81	ME-MS81	ME-MS81	ME-MS81	ME-MS81	ME-MS81	ME-MS81	ME-MS81	ME-MS81
		Ce ppm	Co ppm	Cr ppm	Cs ppm	Cu ppm	Dy ppm	Er ppm	Eu ppm	Ga ppm	Gd ppm	Hf ppm	Ho ppm	La ppm	Lu ppm	Mo ppm
<b>DUPLICATES</b>																
EZ_01 DUP Target Range - Lower Bound Upper Bound		0.5	0.5	10	0.01	5	0.05	0.03	0.03	0.1	0.05	0.2	0.01	0.5	0.01	2
LUSL-09 DUP Target Range - Lower Bound Upper Bound																
LUSL-11 DUP Target Range - Lower Bound Upper Bound																
LUSL-19 DUP Target Range - Lower Bound Upper Bound																
LUSL-20b DUP Target Range - Lower Bound Upper Bound		9.1 9.3 8.2 10.2	34.7 34.6 32.4 36.9	40 40 30 50	0.78 0.84 0.76 0.86	12 10 5 17	1.01 1.03 0.92 1.12	0.53 0.60 0.51 0.62	0.51 0.46 0.43 0.54	18.4 18.5 17.4 19.5	1.10 1.04 0.97 1.17	-0.2 -0.2 -0.2 0.4	0.21 0.19 0.18 0.22	5.2 5.4 4.5 6.1	0.10 0.06 0.07 0.09	2 2 -2 4
LUSL-WO-A DUP Target Range - Lower Bound Upper Bound																
LUSL-WO-B DUP Target Range - Lower Bound Upper Bound																
FD25 - 198.40 DUP Target Range - Lower Bound Upper Bound																



ALS Brasil Ltda.  
 Rua São Paulo, 685, Célvia,  
 CEP:33.200-000 Vespasiano  
 Belo Horizonte MG  
 Phone: +55 (31) 3621 3907 Fax: +55 (31) 3621 8433  
 www.alsglobal.com

To: CESAR FONSECA FERREIRA FILHO  
 SQN 107, BLOCO I, APT 403, ASA NORTE,  
 BRASILIA DF 70.743-090

Page: 5 - C  
 Total # Pages: 6 (A - E)  
 Finalized Date: 6-DEC-2011  
 Account: CAFON

Project: LUANGA SUL

**QC CERTIFICATE OF ANALYSIS BH11210260**

Sample Description	Method Analyte Units LOR	ME-MS81	ME-MS81	ME-MS81	ME-MS81	ME-MS81	ME-MS81	ME-MS81	ME-MS81	ME-MS81	ME-MS81	ME-MS81	ME-MS81	ME-MS81	ME-MS81	ME-MS81
		Nb ppm	Nd ppm	Ni ppm	Pb ppm	Pr ppm	Rb ppm	Sm ppm	Sn ppm	Sr ppm	Ta ppm	Tb ppm	Th ppm	Tl ppm	Tm ppm	U ppm
<b>DUPLICATES</b>																
EZ_01 DUP Target Range - Lower Bound Upper Bound		0.2	0.1	5	5	0.03	0.2	0.03	1	0.1	0.1	0.01	0.05	0.5	0.01	0.05
LUSL-09 DUP Target Range - Lower Bound Upper Bound																
LUSL-11 DUP Target Range - Lower Bound Upper Bound																
LUSL-19 DUP Target Range - Lower Bound Upper Bound																
LUSL-20b DUP Target Range - Lower Bound Upper Bound		<0.2 <0.2 <0.2 0.4	3.8 3.9 3.6 4.1	105 99 92 112	6 6 <5 10	1.04 1.00 0.94 1.10	72.1 70.9 67.7 75.3	0.91 0.95 0.85 1.01	1 1 <1 2	476 466 447 495	<0.1 <0.1 <0.1 0.2	0.17 0.15 0.14 0.18	0.35 0.35 0.28 0.42	<0.5 <0.5 <0.5 1.0	0.08 0.08 0.07 0.09	0.21 0.22 0.15 0.28
LUSL-WO-A DUP Target Range - Lower Bound Upper Bound																
LUSL-WO-B DUP Target Range - Lower Bound Upper Bound																
FD25 - 198.40 DUP Target Range - Lower Bound Upper Bound																





ALS Brasil Ltda.  
 Rua São Paulo, 685, Célvia,  
 CEP:33.200-000 Vespasiano  
 Belo Horizonte MG  
 Phone: +55 (31) 3621 3907 Fax: +55 (31) 3621 8433  
 www.alsglobal.com

To: CESAR FONSECA FERREIRA FILHO  
 SQN 107, BLOCO I, APT 403, ASA NORTE,  
 BRASILIA DF 70.743-090

Page: 5 - D  
 Total # Pages: 6 (A - E)  
 Finalized Date: 6-DEC-2011  
 Account: CAFON

Project: LUANGA SUL

**QC CERTIFICATE OF ANALYSIS BH11210260**

Sample Description	Method Analyte Units LOR	ME-MS81	ME-MS81	ME-MS81	ME-MS81	ME-MS81	ME-MS81	ME-4ACD81	ME-4ACD81	ME-4ACD81	ME-4ACD81	ME-4ACD81	ME-4ACD81	ME-4ACD81	ME-4ACD81	
		V ppm	W ppm	Y ppm	Yb ppm	Zn ppm	Zr ppm	Ag ppm	As ppm	Cd ppm	Co ppm	Cu ppm	Mo ppm	Ni ppm	Pb ppm	Zn ppm
<b>DUPLICATES</b>																
EZ_01 DUP Target Range - Lower Bound Upper Bound		5	1	0.5	0.03	5	2	0.5	5	0.5	1	1	1	1	2	2
LUSL-09 DUP Target Range - Lower Bound Upper Bound																
LUSL-11 DUP Target Range - Lower Bound Upper Bound								<0.5	5	<0.5	14	13	<1	76	<2	37
								<0.5	<5	<0.5	14	12	<1	70	<2	37
								1.0	10	1.0	16	14	2	78	4	41
LUSL-19 DUP Target Range - Lower Bound Upper Bound																
LUSL-20b DUP Target Range - Lower Bound Upper Bound		154	4	5.5	0.51	89	8									
		147	3	5.2	0.52	89	9									
		138	2	4.6	0.46	80	6									
		163	5	6.1	0.57	98	11									
LUSL-WO-A DUP Target Range - Lower Bound Upper Bound																
LUSL-WO-B DUP Target Range - Lower Bound Upper Bound																
FD25 - 198.40 DUP Target Range - Lower Bound Upper Bound																



ALS Brasil Ltda.  
 Rua São Paulo, 685, Célia,  
 CEP:33.200-000 Vespasiano  
 Belo Horizonte MG  
 Phone: +55 (31) 3621 3907 Fax: +55 (31) 3621 8433  
 www.alsglobal.com

To: CESAR FONSECA FERREIRA FILHO  
 SQN 107, BLOCO I, APT 403, ASA NORTE,  
 BRASILIA DF 70.743-090

Page: 5 - E  
 Total # Pages: 6 (A - E)  
 Finalized Date: 6-DEC-2011  
 Account: CAFON

Project: LUANGA SUL

**QC CERTIFICATE OF ANALYSIS BH11210260**

Sample Description	Method Analyte Units LOR	ME-MS42 As ppm	ME-MS42 Bi ppm	ME-MS42 Hg ppm	ME-MS42 Sb ppm	ME-MS42 Se ppm	ME-MS42 Te ppm	S-IR08 S %	C-IR07 C %	QA-GRA05x LOI 1000 %
<b>DUPLICATES</b>										
EZ_01 DUP Target Range - Lower Bound Upper Bound		0.1	0.01	0.005	0.05	0.2	0.01	0.01	0.01	0.01
LUSL-09 DUP Target Range - Lower Bound Upper Bound									0.07 0.06 0.05 0.08	
LUSL-11 DUP Target Range - Lower Bound Upper Bound										
LUSL-19 DUP Target Range - Lower Bound Upper Bound		1.3 1.3 1.1 1.5	0.12 0.12 0.10 0.14	0.014 0.020 0.011 0.023	<-0.05 <-0.05 <-0.05 0.10	0.4 0.5 <-0.2 0.7	0.01 0.02 <-0.01 0.02			
LUSL-20b DUP Target Range - Lower Bound Upper Bound										
LUSL-WO-A DUP Target Range - Lower Bound Upper Bound									8.35 8.34 8.13 8.56	
LUSL-WO-B DUP Target Range - Lower Bound Upper Bound								<-0.01 <-0.01 <-0.01 0.02		
FD25 - 198.40 DUP Target Range - Lower Bound Upper Bound								3.13 3.22 3.09 3.26		



ALS Brasil Ltda.  
 Rua São Paulo, 685, Célia,  
 CEP:33.200-000 Vespasiano  
 Belo Horizonte MG  
 Phone: +55 (31) 3621 3907 Fax: +55 (31) 3621 8433  
 www.alsglobal.com

To: CESAR FONSECA FERREIRA FILHO  
 SQN 107, BLOCO I, APT 403, ASA NORTE,  
 BRASILIA DF 70.743-090

Page: 6 - A  
 Total # Pages: 6 (A - E)  
 Finalized Date: 6-DEC-2011  
 Account: CAFON

Project: LUANGA SUL

**QC CERTIFICATE OF ANALYSIS BH11210260**

Sample Description	Method Analyte Units LOR	ME-XRF12st	ME-XRF12st	ME-XRF12st	ME-XRF12st	ME-XRF12st	ME-XRF12st	ME-XRF12st	ME-XRF12st	ME-XRF12st	ME-XRF12st	ME-XRF12st	ME-XRF12st	ME-XRF12st	ME-MS81	ME-MS81
		Al2O3	BaO	CaO	Cr2O3	Fe2O3	K2O	MgO	MnO	Na2O	P2O5	SiO2	SrO	TiO2	Ag	Ba
		%	%	%	%	%	%	%	%	%	%	%	%	ppm	ppm	
		0.01	0.001	0.01	0.001	0.01	0.001	0.01	0.001	0.001	0.01	0.001	0.01	1	0.5	
<b>DUPLICATES</b>																
ORIGINAL															<1	157.0
DUP															<1	150.0
Target Range - Lower Bound															<1	145.5
Upper Bound															2	161.5
ORIGINAL															<1	3870
DUP															<1	3780
Target Range - Lower Bound															<1	3630
Upper Bound															2	4020



ALS Brasil Ltda.  
 Rua São Paulo, 685, Célvia,  
 CEP:33.200-000 Vespasiano  
 Belo Horizonte MG  
 Phone: +55 (31) 3621 3907 Fax: +55 (31) 3621 8433  
 www.alsglobal.com

To: CESAR FONSECA FERREIRA FILHO  
 SQN 107, BLOCO I, APT 403, ASA NORTE,  
 BRASILIA DF 70.743-090

Page: 6 - B  
 Total # Pages: 6 (A - E)  
 Finalized Date: 6-DEC-2011  
 Account: CAFON

Project: LUANGA SUL

**QC CERTIFICATE OF ANALYSIS BH11210260**

Sample Description	Method Analyte Units LOR	ME-MS81 Ce ppm 0.5	ME-MS81 Co ppm 0.5	ME-MS81 Cr ppm 10	ME-MS81 Cs ppm 0.01	ME-MS81 Cu ppm 5	ME-MS81 Dy ppm 0.05	ME-MS81 Er ppm 0.03	ME-MS81 Eu ppm 0.03	ME-MS81 Ga ppm 0.1	ME-MS81 Gd ppm 0.05	ME-MS81 Hf ppm 0.2	ME-MS81 Ho ppm 0.01	ME-MS81 La ppm 0.5	ME-MS81 Lu ppm 0.01	ME-MS81 Mo ppm 2
		<b>DUPLICATES</b>														
ORIGINAL		31.8	1.4	40	0.23	10	1.26	0.70	0.49	<0.1	1.76	2.0	0.25	16.5	0.09	2
DUP		30.3	1.1	40	0.25	8	1.20	0.83	0.51	<0.1	1.55	2.0	0.26	15.2	0.11	2
Target Range - Lower Bound		29.0	0.7	30	0.22	<5	1.12	0.70	0.45	<0.1	1.52	1.7	0.23	14.6	0.09	<2
Upper Bound		33.1	1.8	50	0.26	10	1.34	0.83	0.56	0.2	1.79	2.3	0.28	17.1	0.12	4
ORIGINAL		248	14.0	70	8.07	38	3.54	2.30	1.93	32.1	4.45	19.4	0.72	135.5	0.37	3
DUP		254	14.4	70	7.79	39	3.81	2.16	1.89	31.3	4.24	17.9	0.66	128.5	0.29	4
Target Range - Lower Bound		238	13.0	60	7.52	32	3.44	2.09	1.78	30.0	4.08	17.5	0.65	125.0	0.30	<2
Upper Bound		264	15.4	80	8.34	45	3.91	2.37	2.04	33.4	4.61	19.8	0.73	139.0	0.36	4



ALS Brasil Ltda.  
 Rua São Paulo, 685, Célia,  
 CEP:33.200-000 Vespasiano  
 Belo Horizonte MG  
 Phone: +55 (31) 3621 3907 Fax: +55 (31) 3621 8433  
 www.alsglobal.com

To: CESAR FONSECA FERREIRA FILHO  
 SQN 107, BLOCO I, APT 403, ASA NORTE,  
 BRASILIA DF 70.743-090

Page: 6 - C  
 Total # Pages: 6 (A - E)  
 Finalized Date: 6-DEC-2011  
 Account: CAFON

Project: LUANGA SUL

**QC CERTIFICATE OF ANALYSIS BH11210260**

Sample Description	Method Analyte Units LOR	ME-MS81 Nb ppm	ME-MS81 Nd ppm	ME-MS81 Ni ppm	ME-MS81 Pb ppm	ME-MS81 Pr ppm	ME-MS81 Rb ppm	ME-MS81 Sm ppm	ME-MS81 Sn ppm	ME-MS81 Sr ppm	ME-MS81 Ta ppm	ME-MS81 Tb ppm	ME-MS81 Th ppm	ME-MS81 Tl ppm	ME-MS81 Tm ppm	ME-MS81 U ppm
		0.2	0.1	5	5	0.03	0.2	0.03	1	0.1	0.1	0.01	0.05	0.5	0.01	0.05
		<b>DUPLICATES</b>														
ORIGINAL		6.0	12.6	22	7	3.25	7.1	2.58	2	24.7	0.3	0.21	4.31	<0.5	0.12	0.67
DUP		6.1	11.5	26	7	3.12	7.6	2.54	2	23.8	0.5	0.23	5.42	<0.5	0.10	0.62
Target Range - Lower Bound		5.5	11.3	18	<5	3.00	6.8	2.40	<1	22.9	0.3	0.20	4.57	<0.5	0.09	0.56
Upper Bound		6.6	12.8	30	10	3.37	7.9	2.72	3	25.6	0.5	0.24	5.16	1.0	0.13	0.73
ORIGINAL		107.0	65.7	37	40	20.4	145.0	8.09	6	403	4.3	0.59	24.4	<0.5	0.32	6.13
DUP		109.5	62.4	33	35	19.90	143.5	7.23	5	396	4.1	0.56	24.4	<0.5	0.28	5.73
Target Range - Lower Bound		102.5	60.7	28	31	19.10	137.0	7.25	4	379	3.9	0.54	23.1	<0.5	0.28	5.58
Upper Bound		114.0	67.4	42	44	21.2	151.5	8.07	7	420	4.5	0.61	25.7	1.0	0.33	6.28



ALS Brasil Ltda.  
 Rua São Paulo, 685, Célia,  
 CEP:33.200-000 Vespasiano  
 Belo Horizonte MG  
 Phone: +55 (31) 3621 3907 Fax: +55 (31) 3621 8433  
 www.alsglobal.com

To: CESAR FONSECA FERREIRA FILHO  
 SQN 107, BLOCO I, APT 403, ASA NORTE,  
 BRASILIA DF 70.743-090

Page: 6 - D  
 Total # Pages: 6 (A - E)  
 Finalized Date: 6-DEC-2011  
 Account: CAFON

Project: LUANGA SUL

**QC CERTIFICATE OF ANALYSIS BH11210260**

Sample Description	Method Analyte Units LOR	ME-MS81 V ppm 5	ME-MS81 W ppm 1	ME-MS81 Y ppm 0.5	ME-MS81 Yb ppm 0.03	ME-MS81 Zn ppm 5	ME-MS81 Zr ppm 2	ME-4ACD81 Ag ppm 0.5	ME-4ACD81 As ppm 5	ME-4ACD81 Cd ppm 0.5	ME-4ACD81 Co ppm 1	ME-4ACD81 Cu ppm 1	ME-4ACD81 Mo ppm 1	ME-4ACD81 Ni ppm 1	ME-4ACD81 Pb ppm 2	ME-4ACD81 Zn ppm 2
		<b>DUPLICATES</b>														
ORIGINAL		15	3	7.4	0.41	16	67									
DUP		19	4	7.3	0.45	17	73									
Target Range - Lower Bound		11	2	6.5	0.38	11	65									
Upper Bound		23	5	8.2	0.48	22	76									
ORIGINAL		319	4	24.5	1.98	101	836									
DUP		314	3	23.4	1.97	100	765									
Target Range - Lower Bound		296	2	22.3	1.85	90	758									
Upper Bound		337	5	25.6	2.10	111	843									





ALS Brasil Ltda.  
 Rua São Paulo, 685, Célia,  
 CEP:33.200-000 Vespasiano  
 Belo Horizonte MG  
 Phone: +55 (31) 3621 3907 Fax: +55 (31) 3621 8433  
 www.alsglobal.com

To: CESAR FONSECA FERREIRA FILHO  
 SQN 107, BLOCO I, APT 403, ASA NORTE,  
 BRASILIA DF 70.743-090

Page: 6 - E  
 Total # Pages: 6 (A - E)  
 Finalized Date: 6-DEC-2011  
 Account: CAFON

Project: LUANGA SUL

**QC CERTIFICATE OF ANALYSIS BH11210260**

Sample Description	Method Analyte Units LOR	ME-MS42 As ppm 0.1	ME-MS42 Bi ppm 0.01	ME-MS42 Hg ppm 0.005	ME-MS42 Sb ppm 0.05	ME-MS42 Se ppm 0.2	ME-MS42 Te ppm 0.01	S-IR08 S %	C-IR07 C %	OA-GRA05x LOI 1000 %
ORIGINAL DUP Target Range - Lower Bound Upper Bound	<b>DUPLICATES</b>									
ORIGINAL DUP Target Range - Lower Bound Upper Bound										



**WORKORDER  
CONFIRMATION FOR  
BH11210260**

Print date Oct 26, 2011  
Client Code **CAFON**  
Page 1 of 2

**To:**  
Cesar Fonseca  
Cesar Fonseca Ferreira Filho  
SQN 107, Bloco I, Apt 403, Asa Norte,  
Brasilia DF  
Brazil 70.743-090

**WO Billing address:**  
Cesar Fonseca  
Cesar Fonseca Ferreira Filho  
SQN 107, Bloco I, Apt 403, Asa  
Norte,  
Brasilia DF  
Brazil 70.743-090

**WORKORDER DISTRIBUTION**

<u>REPORT DESCRIPTION</u>	<u>DESTINATION PERSON</u>	<u>DELIVERY</u>
Certificate of analysis	Cesar Fonseca	Email
Invoice	Cesar Fonseca	Email
ALS Minerals Standard QC format	Cesar Fonseca	Email
QC Certificate	Cesar Fonseca	Email
Work Order	Cesar Fonseca	Email
Excel Format	Cesar Fonseca	Email

---

Samples submitted by:	CESAR FILHO	Total Samples Received:	8
Project:	LUANGA SUL	Pulp Disposition:	Paid Storage after 90 Days
P. O. #:		Reject Disposition:	Monthly Storage
Sample Type:	Rock	First Sample Description:	LUSL-08
Date Received:	October 24, 2011	Carrier and Waybill:	
Sample Origin:	Distrito Federal, Brazil		

**ANALYTICAL WORK REQUESTED:**

**PREP**

8	CRU-31	Fine crushing - 70% <2mm
8	LOG-22	Sample login - Rcd w/o BarCode
8	PUL-31	Pulverize split to 85% <75 um
8	SPL-21	Split sample - riffle splitter
8	WEI-21	Received Sample Weight

Analytes Requested: Recvd Wt.





**WORKORDER  
CONFIRMATION FOR  
BH11210260**

Print date Oct 26, 2011  
Client Code CAFON  
Page 2 of 2

**ANALYTICAL**

- 8 C-IR07 Total Carbon (Leco)  
Analytes Requested: C
- 8 ME-4ACD81 Base Metals by 4-acid dig.  
Analytes Requested: Ag,Cd,Co,Cu,Mo,Ni,Pb,Zn  
IF Ag >= 100 ppm THEN RUN METHOD Ag-OG62  
IF Co >= 10000 ppm THEN RUN METHOD Co-OG62  
IF Cu >= 10000 ppm THEN RUN METHOD Cu-OG62  
IF Mo >= 10000 ppm THEN RUN METHOD Mo-OG62  
IF Ni >= 10000 ppm THEN RUN METHOD Ni-OG62  
IF Pb >= 10000 ppm THEN RUN METHOD Pb-OG62  
IF Zn >= 10000 ppm THEN RUN METHOD Zn-OG62
- 8 ME-ICP06 Whole Rock Package - ICP-AES  
Analytes Requested: Al<sub>2</sub>O<sub>3</sub>,BaO,CaO,Cr<sub>2</sub>O<sub>3</sub>,Fe<sub>2</sub>O<sub>3</sub>,K<sub>2</sub>O,MgO,MnO,Na<sub>2</sub>O,P<sub>2</sub>O<sub>5</sub>,SiO<sub>2</sub>,SrO,TiO<sub>2</sub>
- 8 ME-MS42 Up to 34 elements by ICP-MS  
Analytes Requested: As,Bi,Hg,Sb,Se,Te
- 8 ME-MS81 38 element fusion ICP-MS  
Analytes Requested:  
Ba,Ce,Cr,Cs,Dy,Er,Eu,Ga,Gd,Hf,Ho,La,Lu,Nb,Nd,Pr,Rb,Sm,Sn,Sr,Ta,Tb,Th,Tl,Tm,U,V,W,Y,Yb,Zr
- 8 OA-GRA05 Loss on Ignition at 1000C  
Analytes Requested: LOI
- 8 S-IR08 Total Sulphur (Leco)  
Analytes Requested: S
- 8 TOT-ICP06 Total Calculation for ICP06  
Analytes Requested: Total

**MISCELLANEOUS ITEMS:**

- 8 SHP-21 Per Sample Shipping Charge



**WORKORDER  
CONFIRMATION FOR  
BH11213769**

Print date Oct 31, 2011  
Client Code **CAFON**  
Page 1 of 2

**To:**  
Cesar Fonseca  
Cesar Fonseca Ferreira Filho  
SQN 107, Bloco I, Apt 403, Asa Norte,  
Brasilia DF  
Brazil 70.743-090

**WO Billing address:**  
Cesar Fonseca  
Cesar Fonseca Ferreira Filho  
SQN 107, Bloco I, Apt 403, Asa  
Norte,  
Brasilia DF  
Brazil 70.743-090

**WORKORDER DISTRIBUTION**

<u>REPORT DESCRIPTION</u>	<u>DESTINATION PERSON</u>	<u>DELIVERY</u>
Certificate of analysis	Cesar Fonseca	Email
Invoice	Cesar Fonseca	Email
ALS Minerals Standard QC format	Cesar Fonseca	Email
QC Certificate	Cesar Fonseca	Email
Work Order	Cesar Fonseca	Email
Excel Format	Cesar Fonseca	Email

---

Samples submitted by:	CÉSAR FILHO	Total Samples Received:	18
Project:	LUANGA SUL	Pulp Disposition:	Return after 90 Days
P. O. #:		Reject Disposition:	Return
Sample Type:	Drill Core	First Sample Description:	LUSL 26-260,50
Date Received:	October 31, 2011	Carrier and Waybill:	SEDEX SZ081477141BR
Sample Origin:	Distrito Federal, Brazil		

**ANALYTICAL WORK REQUESTED:**

**PREP**  
18 LOG-22 Sample login - Rcd w/o BarCode  
18 PUL-31 Pulverize split to 85% <75 um  
18 WEI-21 Received Sample Weight  
Analytes Requested: Recvd Wt.



# WORKORDER CONFIRMATION FOR BH11213769

Print date Oct 31, 2011  
Client Code CAFON  
Page 2 of 2

## ANALYTICAL

- 13 C-IR07 Total Carbon (Leco)  
Analytes Requested: C
- 13 ME-4ACD81 Base Metals by 4-acid dig.  
Analytes Requested: Ag,As,Cd,Co,Cu,Mo,Ni,Pb,Zn  
IF Ag >= 100 ppm THEN RUN METHOD Ag-OG62  
IF Co >= 10000 ppm THEN RUN METHOD Co-OG62  
IF Cu >= 10000 ppm THEN RUN METHOD Cu-OG62  
IF Mo >= 10000 ppm THEN RUN METHOD Mo-OG62  
IF Ni >= 10000 ppm THEN RUN METHOD Ni-OG62  
IF Pb >= 10000 ppm THEN RUN METHOD Pb-OG62  
IF Zn >= 10000 ppm THEN RUN METHOD Zn-OG62
- 13 ME-MS42 Up to 34 elements by ICP-MS  
Analytes Requested: As,Bi,Hg,Sb,Se,Te
- 13 ME-MS81 38 element fusion ICP-MS  
Analytes Requested:  
Ag,Ba,Ce,Co,Cr,Cs,Cu,Dy,Er,Eu,Ga,Gd,Hf,Ho,La,Lu,Mo,Nb,Nd,Ni,Pb,Pr,Rb,Sm,Sn,Sr,Ta,Tb,Th,Tl,Tm,  
U,V,W,Y,Yb,Zn,Zr
- 13 ME-XRF12st Whole rock by XRF-selected ana  
Analytes Requested: Al2O3,BaO,CaO,Cr2O3,Fe2O3,K2O,MgO,MnO,Na2O,P2O5,SiO2,SrO,TiO2
- 13 OA-GRA05x LOI for XRF  
Analytes Requested: LOI 1000
- 7 PGM-NAA26 PGM NiS collection NAA finish  
Analytes Requested: Au,Ir,Os,Pd,Pt,Rh,Ru
- 13 S-IR08 Total Sulphur (Leco)  
Analytes Requested: S

## MISCELLANEOUS ITEMS:

- 18 SHP-21 Per Sample Shipping Charge

Anexo III – Petrografia

AMOSTRA: **LUSL-01** CLASSIFICAÇÃO DA ROCHA: **CLINOPIROXENITO**

COMPOSIÇÃO MINERALÓGICA

***Mineralogia principal***

Clinopiroxênio

Ortopiroxênio

Hornblenda

***Mineralogia acessória - < 1%***

Minerais opacos (Ilm, Hm, Py e Lm)

Biotita

DESCRIÇÃO MICROSCÓPICA

Rocha de granulação grossa (> 5 mm), onde antigos cristais de clinopiroxênio, e subordinadamente, ortopiroxênio, estão quase totalmente substituídos por anfibólio. Os resquícios de ortopiroxênio e clinopiroxênio são distinguidos pelas cores de interferência e ângulo de extinção, sendo o último predominante; os limites dos antigos cristais mostram-se retos a côncavo-convexos.

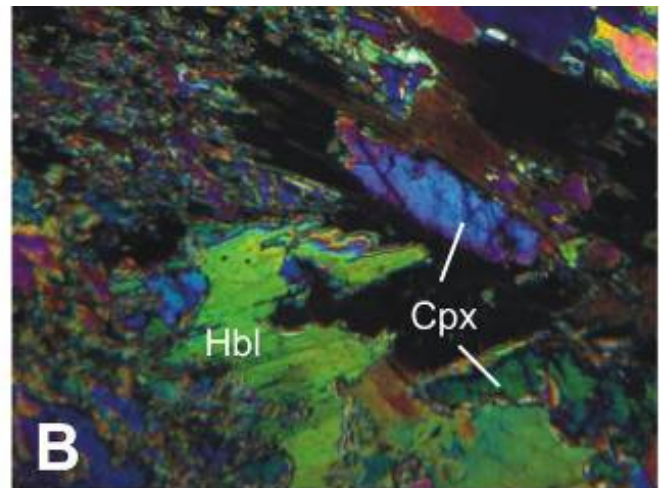
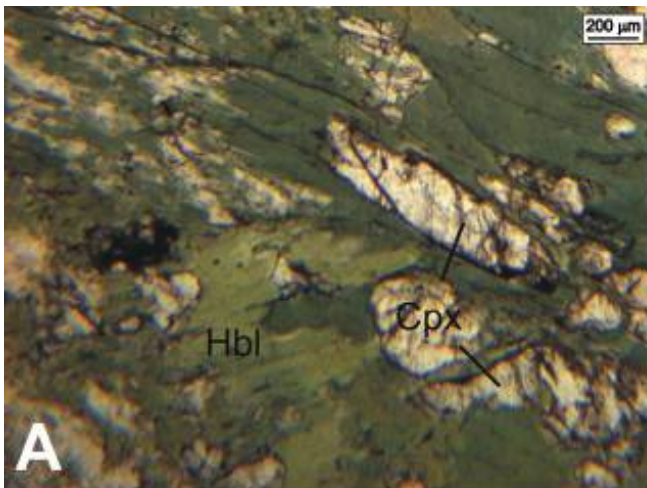
O anfibólio é verde, com forte pleocroísmo, variando de verde amarelado pálido a verde oliva, granulação fina (< 2 mm) a ultrafina, forma subédrica predominantemente, hábito tabular, por vezes prismático ou em mosaicos poligonizados de cristais, sendo classificado como hornblenda. Alguns cristais apresentam extinção ondulante.

Os minerais opacos possuem granulação fina a ultrafina, forma anédrica a subédrica, ocorrendo geralmente nos espaços intergranulares ou como finas inclusões nos cristais de piroxênio. O principal opaco identificado foi a ilmenita algumas vezes com halo de alteração para titanita.

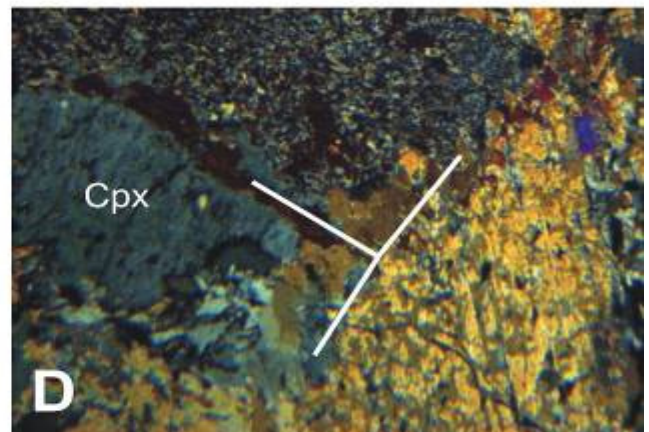
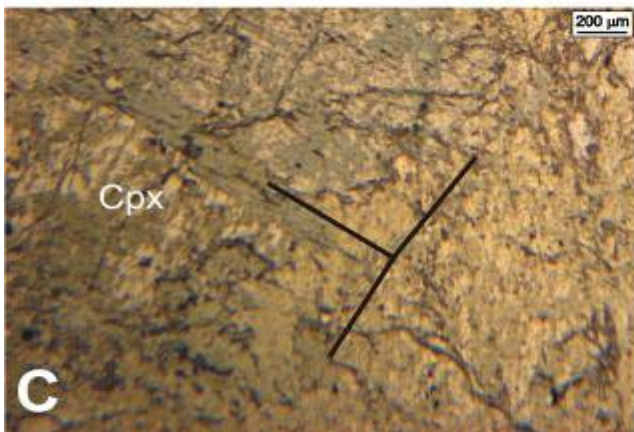
Finas vênulas com preenchimento por anfibólio ocorrem nos limites intergranulares ou cortando cristais de minerais.

A reconstituição dos minerais originais da rocha aponta uma proporção relativa de 95 % de clinopiroxênio e < 5% de ortopiroxênio, classificando o protólito da rocha como clinopiroxenito, cujas relações texturais apontam para uma rocha cumulática do tipo adcumulática. Devido a transformação quase que total destes para anfibólio a classificação final é de metaclinopiroxenito, metamorfisado em fácies anfibolito.

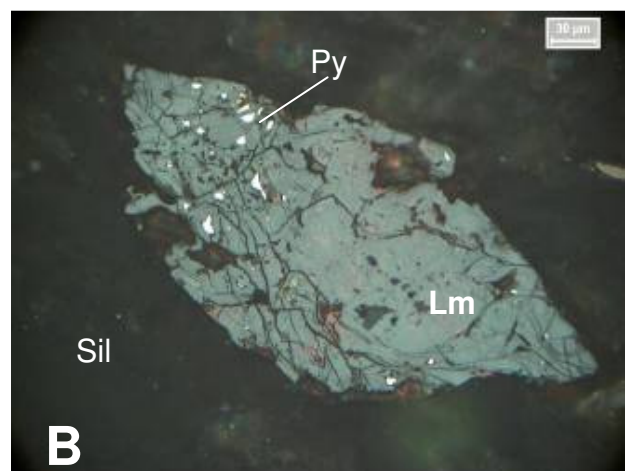




Prancha LUSL-01 – A e B) Fotomicrografia em luz natural e luz polarizada, respectivamente, apresentando resquícios do clinopiroxênio em processo de transformação para hornblenda.



Prancha LUSL-01 – C e D) Fotomicrografia em luz natural e luz polarizada, respectivamente, mostrando a junção de três antigos cristais de clinopiroxênio, cujo contato entre eles é marcado pela presença de pequenos cristais de hornblenda.



Prancha LUSL-01 – Opacos – A) cristal de pirita (Py) com início de oxidação para limonita (cinza); B) limonita (Lm) substituindo pirita (Py). Obj. a óleo. Luz natural.

AMOSTRA: **LUSL-03**

CLASSIFICAÇÃO DA ROCHA:

**Wehrlito**

COMPOSIÇÃO MINERALÓGICA

***Mineralogia principal***

**1%**

Clinopiroxênio: 75%

Olivina: 15%

Minerais opacos: 10%

***Mineralogia acessória - <***

Serpentina

DESCRIÇÃO MICROSCÓPICA

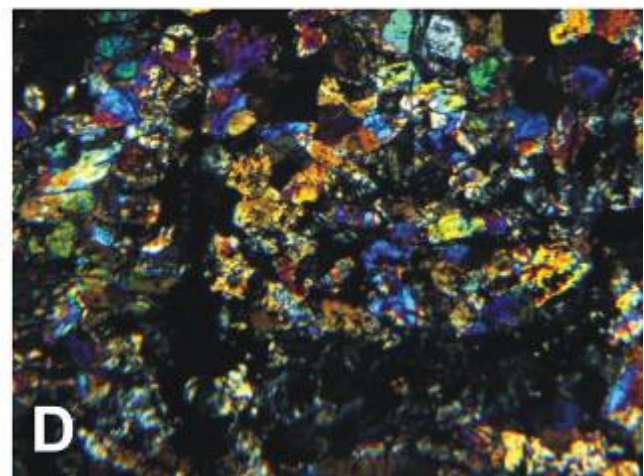
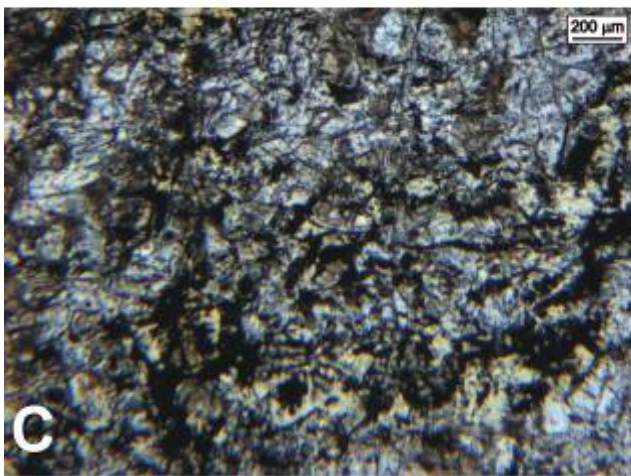
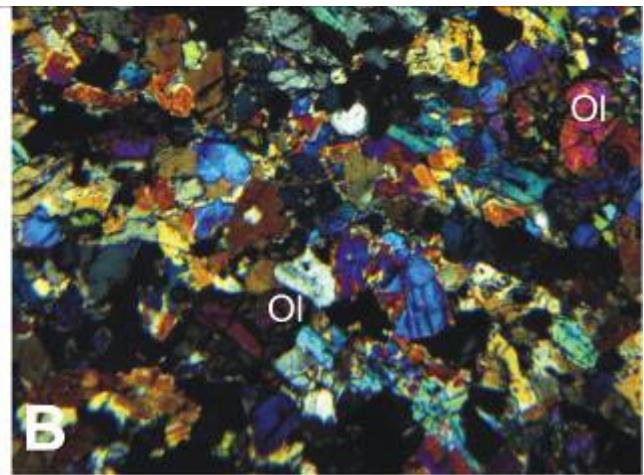
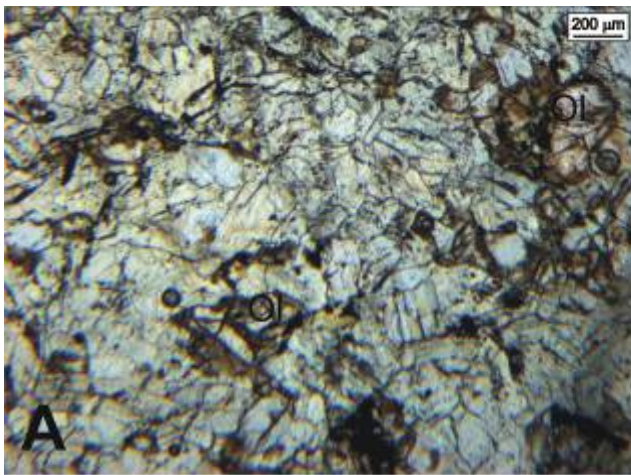
Rocha de granulação muito fina, onde os cristais não ultrapassam 1 mm em dimensão, composta predominantemente por clinopiroxênio, e subordinadamente, por olivina. O clinopiroxênio apresenta-se em cristais incolores, forma anédrica a subédrica, constituindo um mosaico de cristais poligonizados, onde alguns apresentam hábito tabular, extinção ondulante, além da presença de diminutos minerais opacos acompanhando as linhas de clivagem.

Os cristais de olivina são anédricos, incolores, porém alguns exibem um tingimento marrom pálido (brucita?), provavelmente devido ao processo de serpentinização, que se mostra presente nas bordas e nas fraturas internas dos cristais.

Os minerais opacos estão dispersos por toda a rocha, apresentando granulação ultrafina, forma anédrica a subédrica, hábito acicular, e comumente formam aglomerados irregulares ou vênulas milimétricas (até 2 mm), onde estão associados com serpentina *mesh*.

A classificação da rocha, baseada no conteúdo mineralógico é de um wehrlito, e sua textura com efeitos de recristalização classifica-se como do tipo sacaroidal ou granoblástica, caracterizando assim um metawehlito.





Prancha LUSL-03 – A e B) Fotomicrografia em luz natural e luz polarizada, respectivamente, apresentando a textura poligonal granoblástica, marcada pelo predomínio de cristais de clinopiroxênio sobre cristais de olivina; C e D) Fotomicrografia em luz natural e luz polarizada, respectivamente, mostrando faixa mais enriquecida em minerais opacos e serpentina (cor de interferência cinza).



AMOSTRA: **LUSL-04**

CLASSIFICAÇÃO DA ROCHA: **LHERZOLITO**

COMPOSIÇÃO MINERALÓGICA

**Mineralogia principal**

**1%**

Clinopiroxênio

Ortopiroxênio

Olivina

**Mineralogia acessória - <**

Minerais opacos (Py, Ptl)

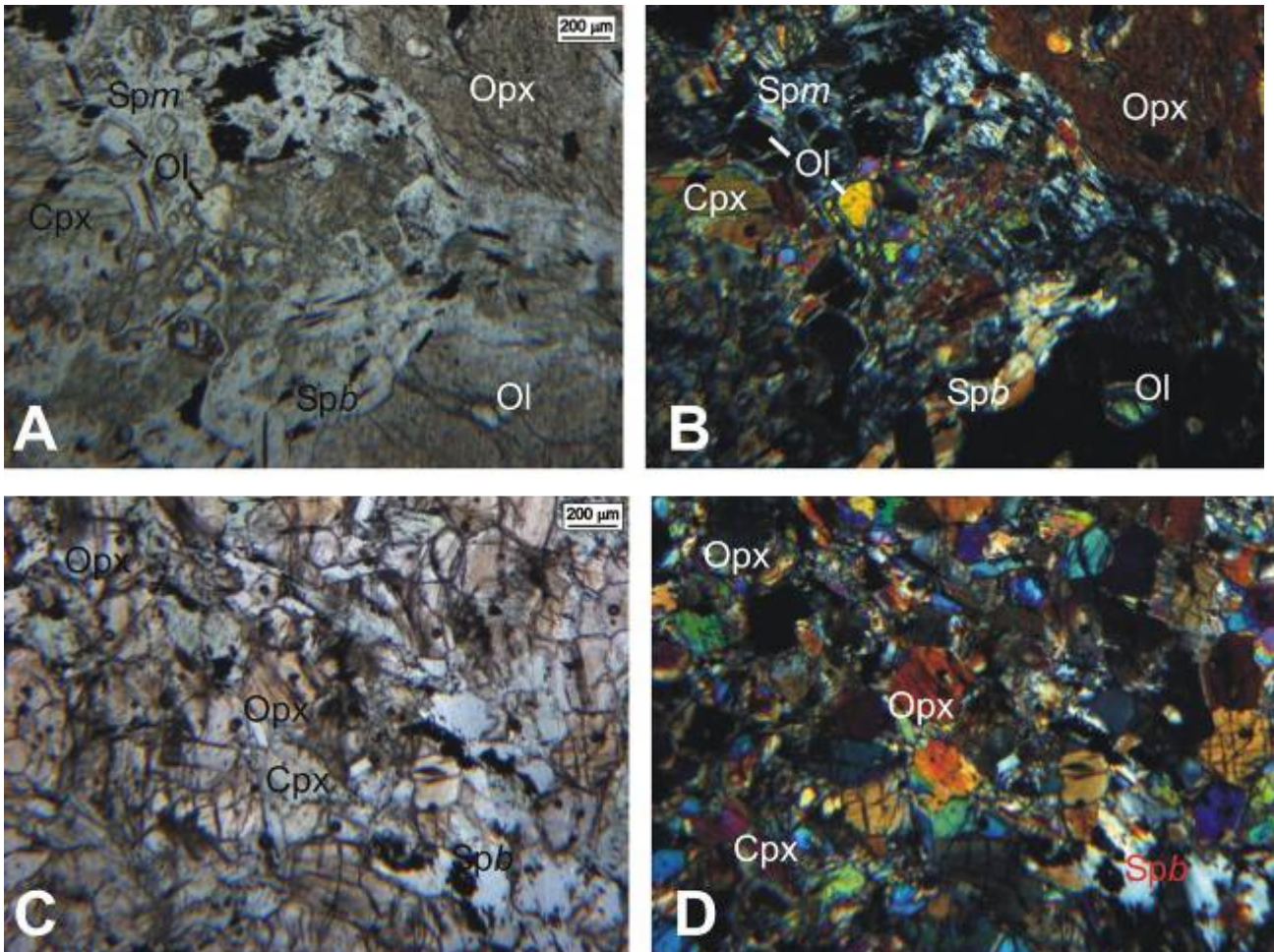
Serpentina

DESCRIÇÃO MICROSCÓPICA

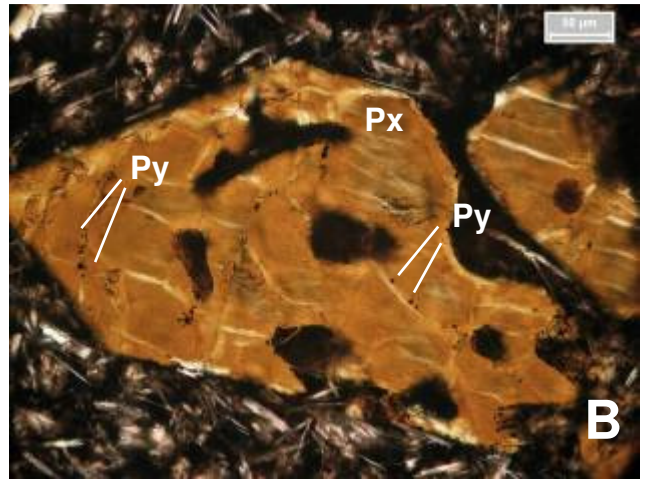
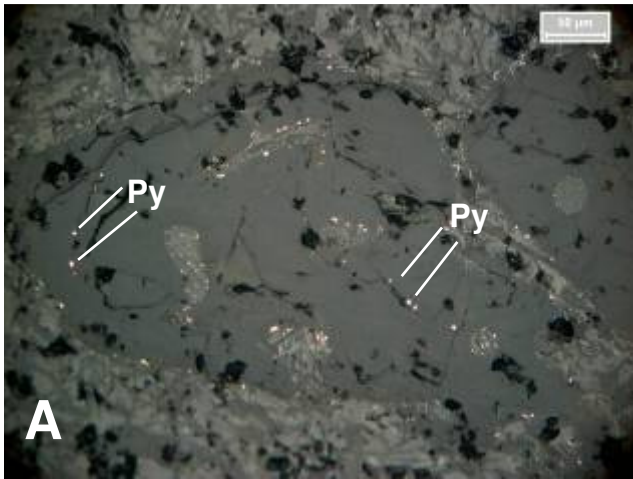
A lâmina apresenta dois domínios distintos, sendo o de menor expressão caracterizado por um mosaico de cristais poligonizados, granulação ultrafina, formado predominantemente por clinopiroxênio, e subordinadamente por ortopiroxênio e bastita. O ortopiroxênio por vezes apresenta lamelas de clinopiroxênio. A bastita forma cristais tabulares a aciculares, granulação muito fina, possuindo minerais opacos nas linhas de clivagem, com cores de interferência alta, além de extinção reta e ondulante. Tal porção pode ser caracterizada como websterito.

A porção predominante da lâmina apresenta composição mineralógica dada por clinopiroxênio, ortopiroxênio e olivina como fases primárias e tendo como fases secundárias de alteração/metamorfismo serpentina mesh, bastita e minerais opacos. Os cristais de piroxênio têm granulação média (2 a 5 mm; máxima de até 3,5 mm) a fina (< 2 mm), forma subédrica a anédrica, hábito quadrático a arredondado. Alguns cristais de piroxênio possuem caráter poiquilítico, com inclusões arredondadas de olivina e, secundariamente, de minerais opacos (pirita) e minerais translúcidos marrons (espinélio). Cristais de clinopiroxênio apresentam-se por vezes geminados, granulação fina, forma subédrica a anédrica, e também com caráter poiquilítico. A serpentina apresenta caracteristicamente textura mesh (lizardita), sendo produto de transformação da olivina e estando comumente associada com bastita. A bastita é incolor, apresentando relevo mais elevado do que a serpentina mesh, granulação muito fina a ultrafina, forma subédrica, hábito lamelar, e comumente com lamelas deformadas ou com kinks. Minerais opacos estão comumente associados a estes dois minerais, porém na serpentina estão salpicados em cristais ultrafinos de pirita com hábito quadrático a arredondado, enquanto que na bastita ocupam comumente as linhas de clivagem.

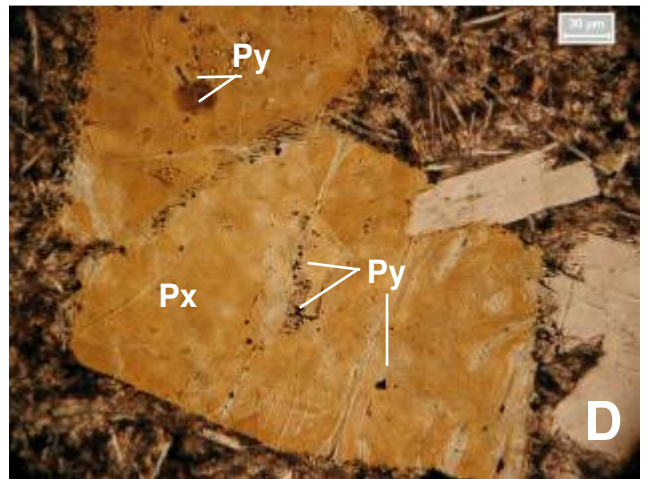
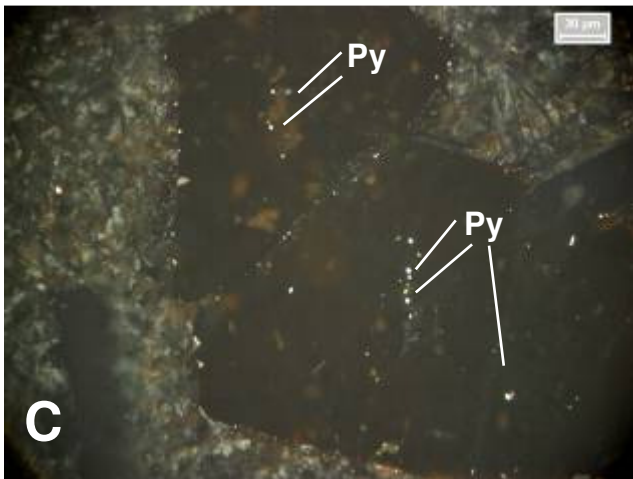
Considerando-se a bastita um pseudomorfo de cristais de piroxênios, tanto ortopiroxênio como clinopiroxênio, aliado a resquícios destes minerais mais olivina, podemos considerar que tal rocha trata-se de um lherzolito, onde as relações texturais apontam que olivina corresponde a material cumulus e intercumulus, enquanto orto e clinopiroxênio a cristais cumulus.



Prancha LUSL-04 – A e B) Fotomicrografia em luz natural e luz polarizada, respectivamente, da porção lherzolítica mostrando diferentes tipo de serpentina (Spm-mesh e Spb- bastita) e cristais poiquilíticos de ortopiroxênio com cadacristais de olivina, além de cristal de clinopiroxênio; C e D) Fotomicrografia em luz natural e luz polarizada, respectivamente, da porção websterítica, mostrando mosaico de cristais de clinopiroxênio e ortopiroxênio, além de placas de bastita.



Prancha LUSL-04 – Opacos – A) Piroxênio com diminutas inclusões de sulfetos (claros). Epi iluminação; B) luz transmitida. Ambas as imagens em luz natural.



Prancha LUSL-04 – Opacos – C) Piroxênio com diminutas inclusões de sulfetos (claros). Epi iluminação; D) cristal geminado de piroxênio, com inclusões de opacos segundo planos de clivagem. Luz transmitida. Ambas as imagens em luz natural.

AMOSTRA: **LUSL-08**

CLASSIFICAÇÃO DA ROCHA: **GABRO**

## COMPOSIÇÃO MINERALÓGICA

### ***Mineralogia principal***

**1%**

Plagioclásio: 80%

Anfibólio: 20%

### ***Mineralogia acessória - <***

Clorita

Minerais opacos

## DESCRIÇÃO MICROSCÓPICA

Rocha composta predominantemente por plagioclásio tendo ainda anfibólio e minerais opacos. Os cristais de plagioclásio encontram-se francamente saussuritizados, porém ainda é possível o reconhecimento de feições primárias como geminação polissintética e hábito tabular (prismas longos e curtos), indicando tratar-se de minerais cumulus. A forma é predominantemente subédrica e a granulação média, não ultrapassando 5 mm.

O anfibólio é verde, pleocroísmo médio (hornblenda e/ou actinolita) e apresenta-se numa massa interconectada de cristais subédricos, de granulação fina a muito fina, envolvendo cristais de plagioclásio; alguns cristais apresentam-se geminados, como prismas alongados (actinolita) e outros exibem extinção ondulante. Um tingimento marrom pálido ocorre de maneira superficial em cristais e anfibólio.

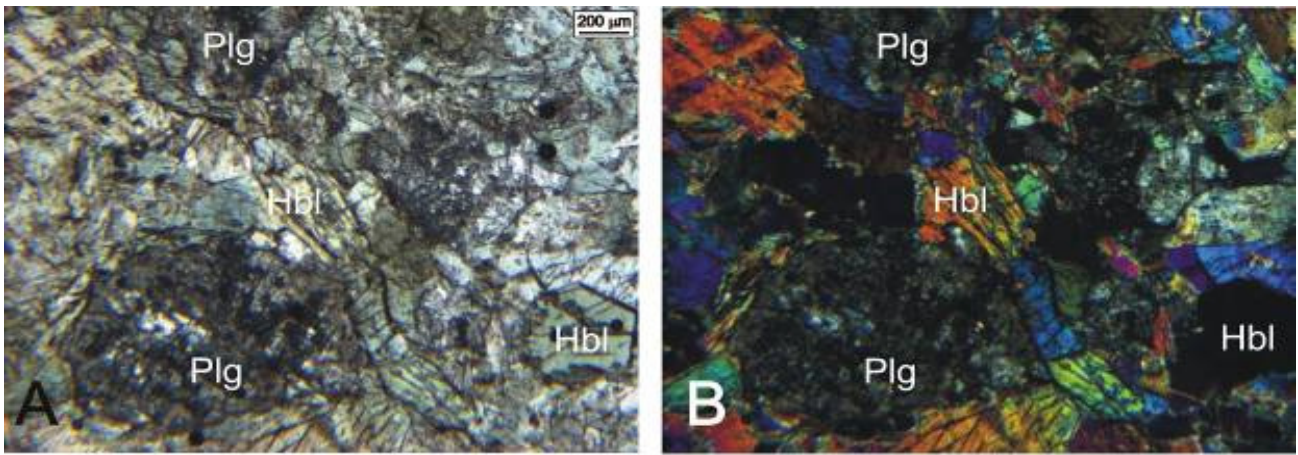
Minerais opacos são ultrafinos, forma acicular e ocorrem nas linhas de clivagem de anfibólio, ou formando grão isolado de hábito quadrático de ocorrência local.

Cristais de clorita, incolor a verde muito pálido, de granulação fina ocorrem localmente, associados a cristais de anfibólio, formando feixes de aspecto radial.

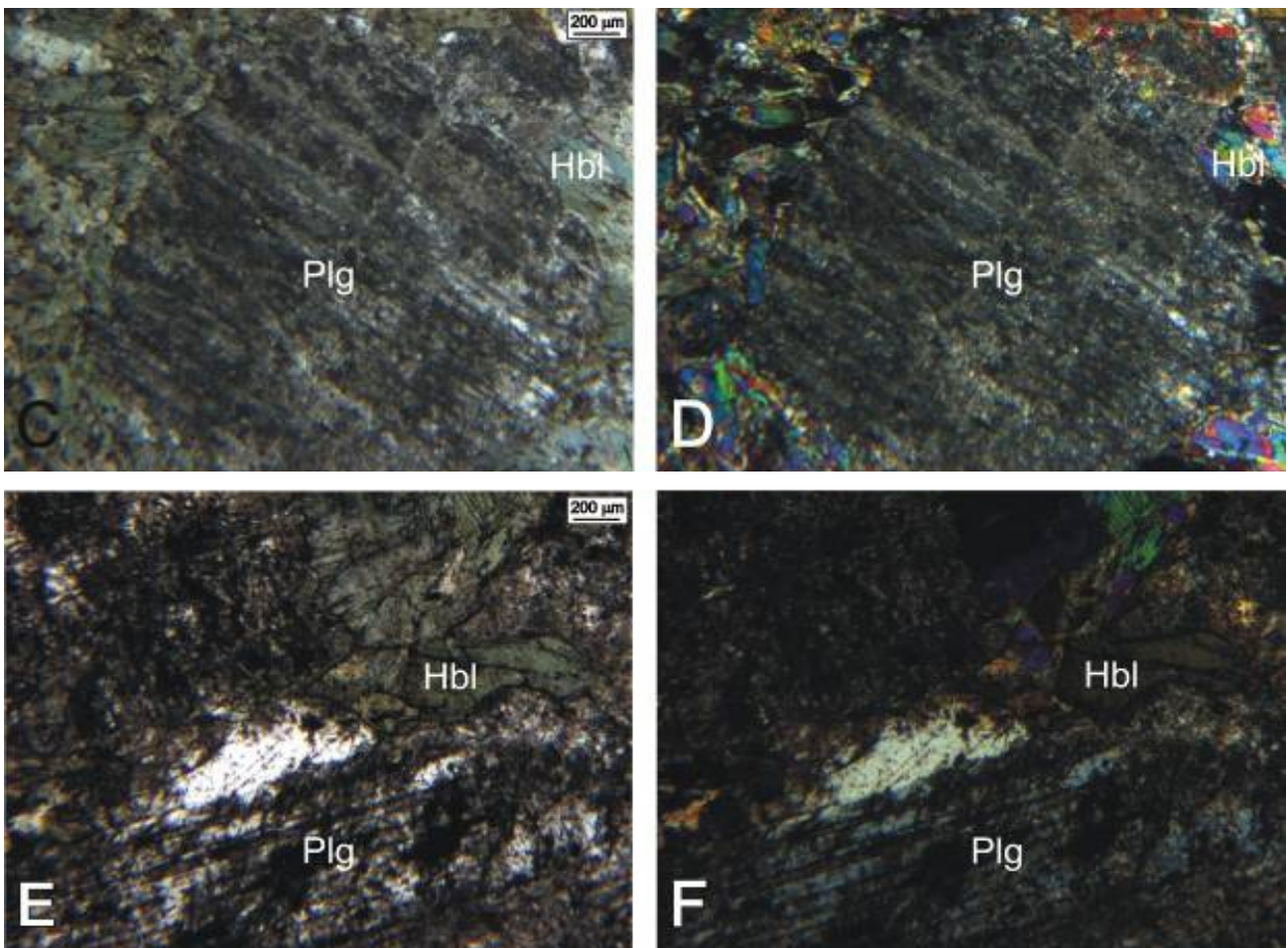
A quantidade relativa dos principais minerais e as relações texturais marcadas por resquícios de cristais cumulus aponta que a rocha é de um metagabro. A paragênese mineral caracterizada por plagioclásio, anfibólio e  $\pm$  clorita, indica a fácies anfibolito.

A textura é nematoblástica nos domínios de anfibólio, porém a forma de cristais de plagioclásio e orientação caótica dos eixos maiores dos mesmos aponta resquícios de feições cumuláticas.





Prancha LUSL-08 – A e B) Fotomicrografia em luz natural e luz polarizada, respectivamente, mostrando cristais de plagioclásio saussuritizados e hornblenda;



Prancha LUSL-08 – C e D) Fotomicrografia em luz natural e luz polarizada, respectivamente, com grão de plagioclásio de hábito quadrático mostrando forte saussuritização; E e F) Fotomicrografia em luz natural e luz polarizada, respectivamente, exibindo cristais de plagioclásio cuja forma tabular mais alongada indica herança da textura cumulática.

AMOSTRA: LUSL- 09  
QUARTZO

CLASSIFICAÇÃO DA ROCHA: GABRO COM

#### COMPOSIÇÃO MINERALÓGICA

##### **Mineralogia principal**

1%

Anfibólio e clinopiroxênio: 70%

Plagioclásio: 27

Quartzo: 3%

##### **Mineralogia acessória - <**

Minerais opacos

Carbonato

#### DESCRIÇÃO MICROSCÓPICA

A rocha apresenta uma intercalação de bandas milimétricas brancas e verdes, representadas respectivamente por plagioclásio e clinopiroxênio mais anfibólio. Nas bandas máficas, clinopiroxênio ocorre como resquílios de cristais grossos a médios, de forma anédrica, onde antigos limites de cristais são marcados pela presença de cristais poligonais de anfibólio, de granulação fina a muito fina. Internamente os cristais de clinopiroxênio são pervasivamente transformados para anfibólio. Tal anfibólio é verde oliva a marrom pálido e fortemente pleocróico, caracterizado como hornblenda.

As bandas brancas, compostas predominantemente por plagioclásio, possuem espessura milimétrica, sendo contínuas ou segmentadas, de aspecto escurecido (provavelmente pela presença de óxido de Fe-Ti), estando fortemente alteradas (saussuritia), com sobrecrecimento principalmente de epidoto, e mais raramente zoisita. Localmente, alguns resquílios de cristais muito finos, subédricos apreentam geminação polissintética.

O quartzo apresenta-se em cristais subédricos a anédricos (ameboidais), de aspecto límpido, com extinção em bandas, granulação muito fina, ocorrendo de forma dispersa na rocha nos dois tipos de bandas, cuja estimativa visual não ultrapassa de 3% da moda.

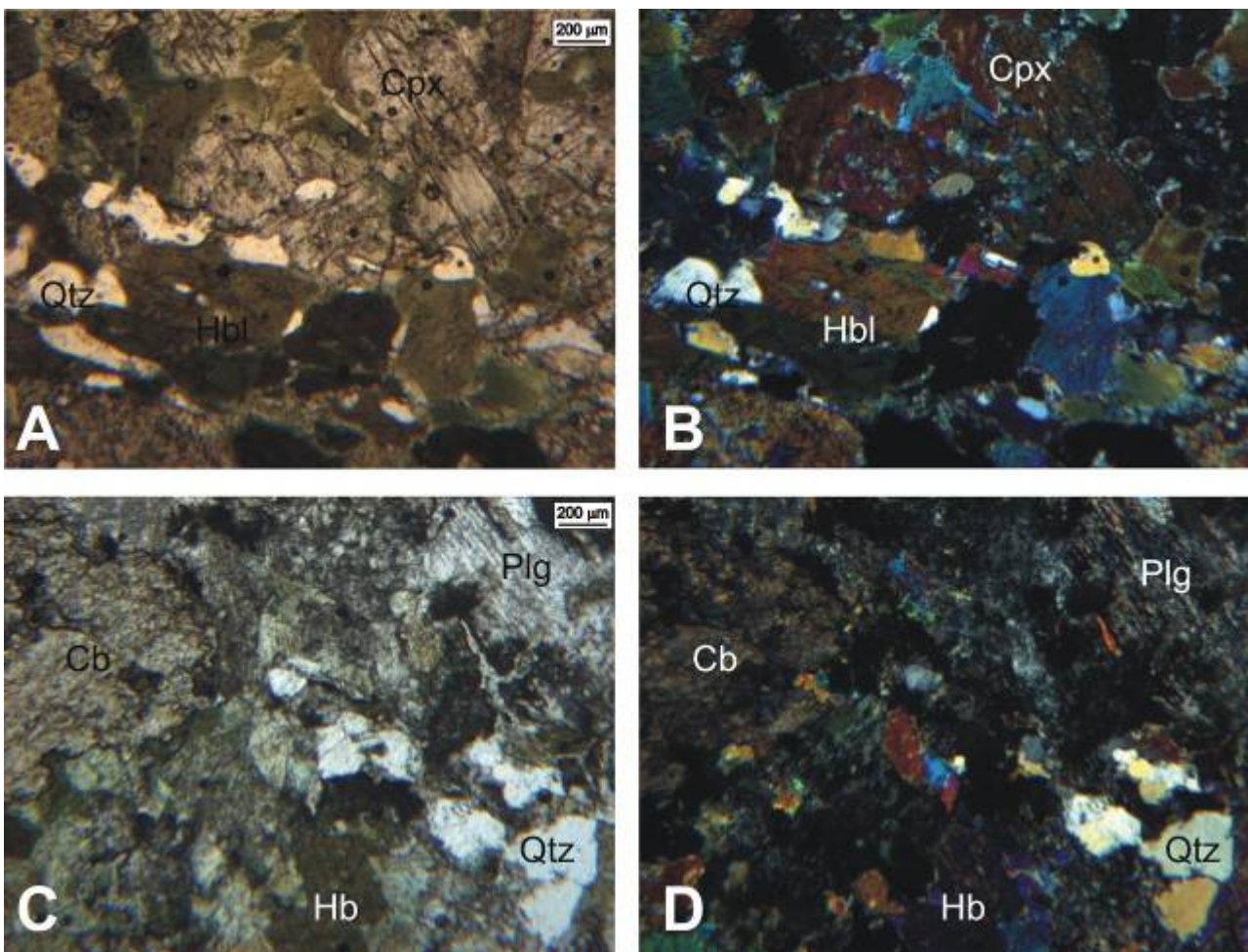
O carbonato ocorre como massas irregulares, geralmente nos contatos entre cristais de plagioclásio e anfibólio, possuindo granulação média a ultrafina, coloração marrom pálida, pleocróicos, onde os maiores cristais apresentam-se segmentados em cristais menores e com extinção ondulante.



Minerais opacos formam aglomerado local, com cristais anédricos, de granulação fina a ultrafina, apresentando íntima associação com epidoto.

Finas fraturas (<< 1 mm) com preenchimento de minerais do grupo do epidoto cortam transversalmente o bandamento da rocha.

O protólito corresponde a rocha gabróica, cuja assembléia metamórfica de hornblenda, plagioclásio, condiciona a fácies anfibolito e classifica a rocha como metagabro. A presença de quartzo sugere que este gabro corresponda a um produto mais tardio de diferenciação magmática, enquanto que a presença de carbonato mostra efeitos de alteração hidrotermal, do tipo carbonatação, responsável provavelmente pela forte saussuritização dos cristais de plagioclásio.



Prancha LUSL-09 – A e B) Fotomicrografia em luz natural e luz polarizada, respectivamente, exibindo cristais de clinopiroxênio e hornblenda, esta última produto de transformação metamórfica do primeiro; C e D) Fotomicrografia em luz natural e luz polarizada, respectivamente, com cristais de plagioclásio e quartzo, o primeiro fortemente saussuritizado e o quartzo com aspecto límpido. Grão de carbonato de forma irregular provavelmente marca processo de carbonatização da rocha.

AMOSTRA: LUSL- 10

CLASSIFICAÇÃO DA ROCHA:

## **ANFIBOLITO**

### COMPOSIÇÃO MINERALÓGICA

#### ***Mineralogia principal***

1%

Anfibólio: 70%

Plagioclásio: 28%

Minerais opacos: 2%

#### ***Mineralogia acessória - <***

Titanita, Zircão

Epidoto

### DESCRIÇÃO MICROSCÓPICA

Rocha composta predominantemente por anfibólio e plagioclásio, numa textura granonematoblástica. O anfibólio é verde oliva a marrom pálido, forma comumente subédrica e hábito tabular, por vezes mostrando seções basais típicas, e mais comumente, cristais com orientação preferencial de seu eixo maior, definindo a foliação principal da rocha; alguns se apresentam geminados.

Minerais opacos formam pequenos aglomerados ou ocorrem de maneira isolada e apresentam forma anédrica a subédrica, granulação ultrafina, por vezes com corona de epidoto ou titanita, hábito tabular, cuja elongação do cristal é paralela ao plano de foliação principal.

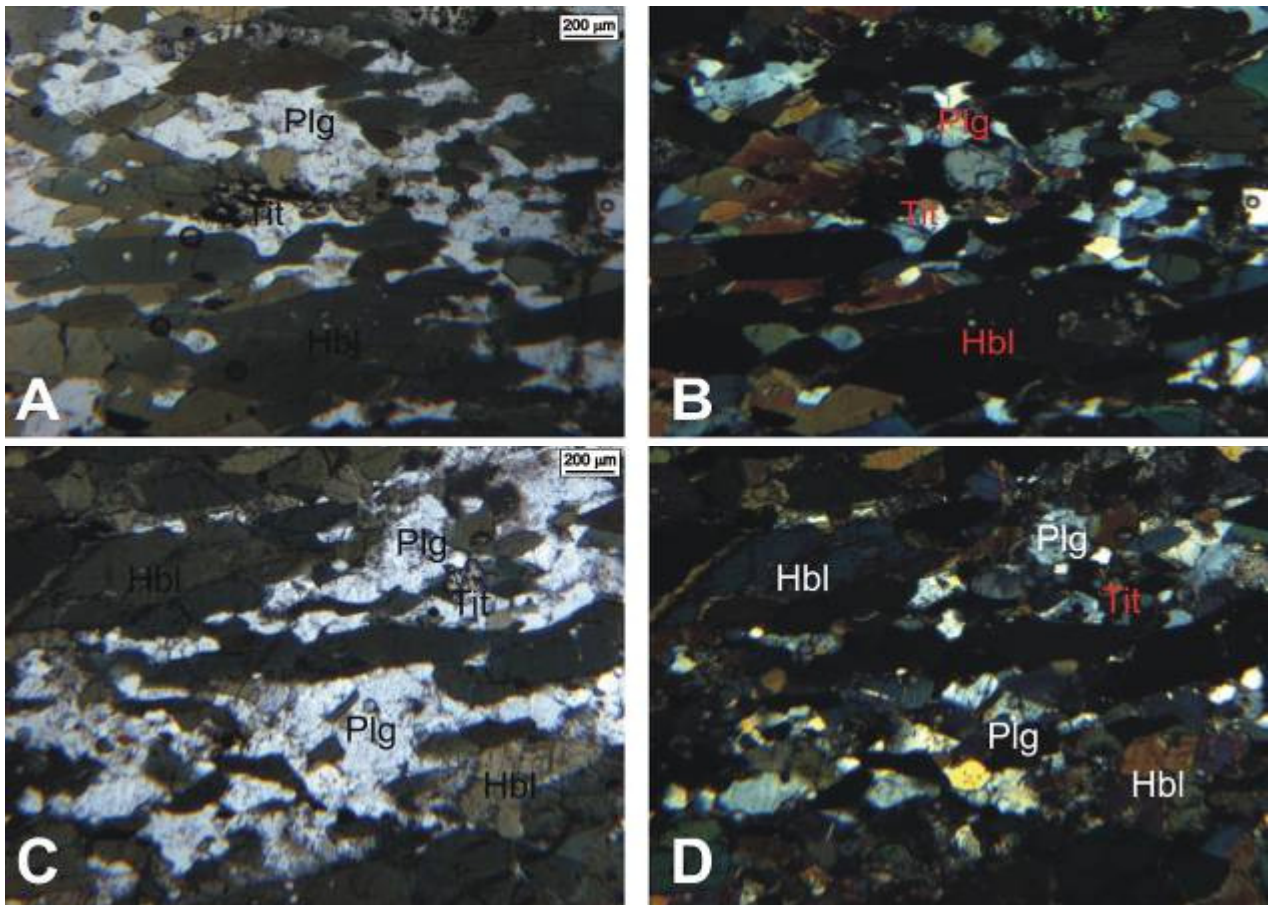
Titanita aparece por vezes associada com minerais opacos ou em meio de cristais de anfibólio e plagioclásio, apresentando grã ultrafina e forma anédrica. Zircão ocorre como cristal acicular, ultrafino em meio a cristais de plagioclásio. Epidoto por vezes forma corona em minerais opacos.

Os cristais de plagioclásio apresentam duas formas distintas de ocorrência, sendo a primeira representada por cristais muito finos (< 1 mm), forma anédrica, por vezes com geminação Carlsbad e/ou polissintética, extinção ondulante e inclusões diminutas de anfibólio, enquanto a segunda mostra cristais ultrafinos, hábito sacaroidal poligonizado, apresentando ou não geminação polissintética; saussurita é comumente vista nos dois tipos de ocorrência, tendo epidoto como produto mais aparente.

Fina vênula corta subparalelamente a foliação da rocha sendo preenchida por clorita.



A assembléia metamórfica caracterizada por hornblenda, plagioclásio,  $\pm$  titanita, condiciona a fácies anfibolito.



Prancha LUSL-10 – A e B) Fotomicrografia em luz natural e luz polarizada, respectivamente, com a mineralogia principal da rocha, dada por plagioclásio e hornblenda, e como acessórios titanita e minerais opacos; C e D) Fotomicrografia em luz natural e luz polarizada, respectivamente, exibindo a textura granonematoblástica.

AMOSTRA: **LUSL-12**

CLASSIFICAÇÃO DA ROCHA: **LEUCOGABRO**

## COMPOSIÇÃO MINERALÓGICA

### ***Mineralogia principal***

**1%**

Plagioclásio: 85%

Anfibólio: 15%

### ***Mineralogia acessória - <***

Minerais opacos

Clorita, Apatita

## DESCRIÇÃO MICROSCÓPICA

Rocha composta principalmente por plagioclásio e actinolita/tremolita, onde os cristais apresentam orientação preferencial de seus eixos maiores, caracterizando a foliação principal da rocha. Resquícios de clinopiroxênio apresentam granulação ultrafina, forma anédrica e bordas escurecidas, estando comumente associados com anfibólio.

Os cristais de plagioclásio apresentam comumente geminação polissintética, e por vezes Carlsbad, forma subédrica, estando fortemente saussuritizados/propilitizados, denotada por uma pátina amarronzada. Variam em granulação de média a muito fina, onde os cristais maiores alcançam até 4 mm de dimensão, enquanto os menores apresentam-se como mosaico poligonizado, alguns com extinção odulante.

A actinolita forma cristais subédricos, hábito tabular a acicular, granulação média (até 3,5 mm) a fina (< 2 mm), contendo comumente minerais opacos nas linhas de clivagem e orientação preferencial do eixo maior dos cristais, definindo assim um plano de foliação na rocha.

Clorita comumente ocorre no contato entre cristais de anfibólio e plagioclásio, ou também internamente nos primeiros.

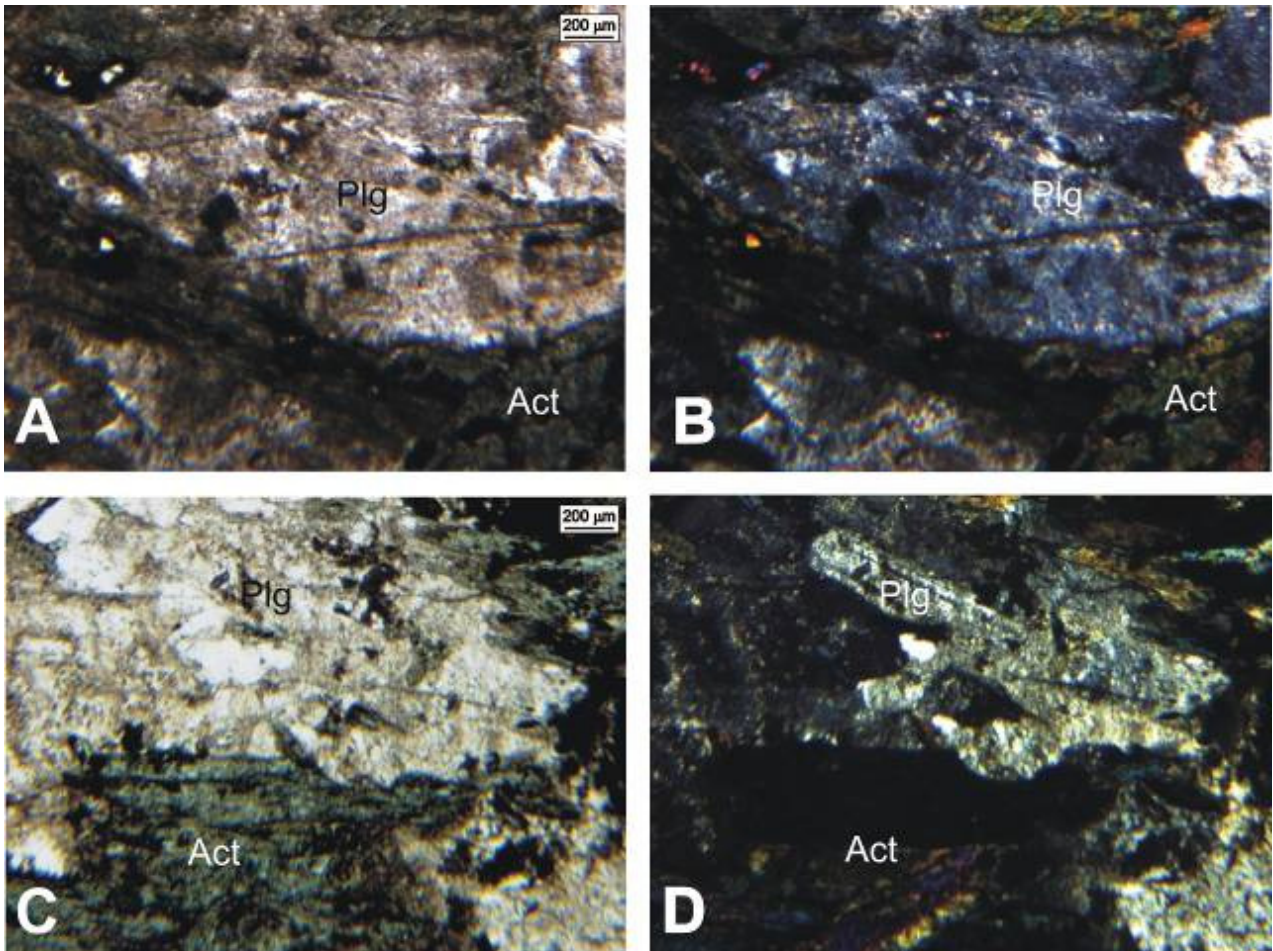
Os minerais opacos ocorrem de duas formas distintas, a primeira como raros cristais isolados, granulação ultrafina, forma subédrica, e a segunda correspondendo a um produto de alteração/metamorfismo, ocorrendo ao longo das linhas de clivagem de cristais de anfibólio ou acompanhando a geminação polissintética do plagioclásio.

De ocorrência local e restrita aparecem cristais ultrafinos de apatita, com forma subédrica e hábito arredondado a hexagonal.

A textura é marcada pela orientação preferencial dos cristais minerais, muito embora alguns se coloquem obliquamente a esta tendência. Tal orientação pode denotar um bandamento ígneo justamente pela não homogeneidade da orientação dos minerais, sugerindo uma feição cumulática; o paralelismo com uma foliação metamórfica não pode

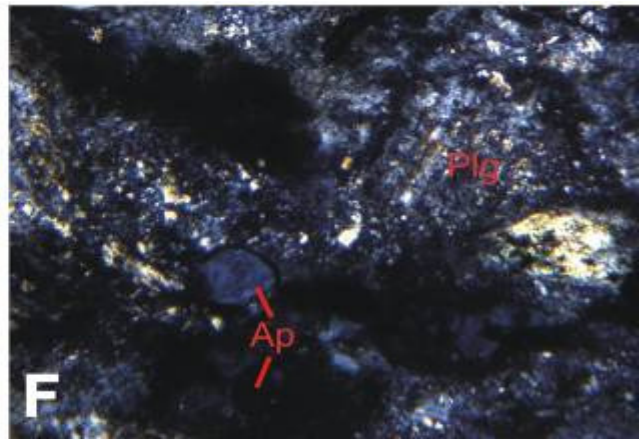
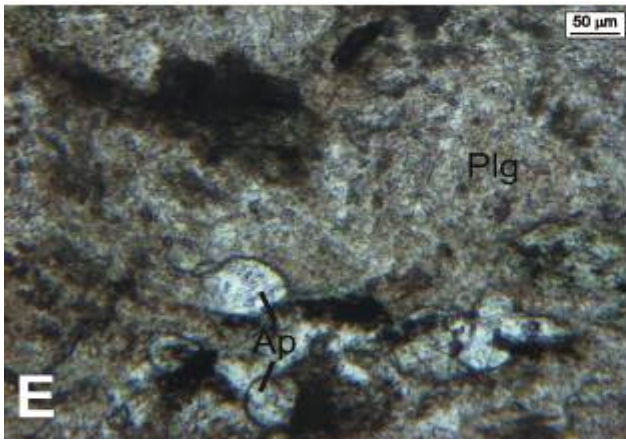
ser descartado. Finíssimas vênulas cortam a rocha e são preenchidas por epidoto e minerais opacos.

A assembléia metamórfica denotada por actinolita, plagioclásio e  $\pm$  clorita caracteriza a fácies xisto verde, e a composição mineralógica e proporção modal dos minerais principais, onde o plagioclásio aparece com mais de 65% na moda, classifica a rocha como metaleucogabro.



Prancha LUSL-12 – A e B) Fotomicrografia em luz natural e luz polarizada, respectivamente, com a mineralogia principal da rocha, dada por plagioclásio e actinolita, e resquícios diminutos de clinopiroxênio (cor de interferência mais alta); C e D) Fotomicrografia em luz natural e luz polarizada, respectivamente, exibindo grão subeuédrico de plagioclásio, de hábito tabular (ripa), indicando um resquício da textura ígnea original;





Prancha LUSL-12 – E e F) Fotomicrografia em luz natural e luz polarizada, respectivamente, mostrando cristais de apatita.

AMOSTRA: LUSL-13

CLASSIFICAÇÃO DA ROCHA: **ANFIBOLITO**

COMPOSIÇÃO MINERALÓGICA

**Mineralogia principal**

**Mineralogia acessória - <**

**1%**

Anfibólio: 70%

Minerais opacos

Plagioclásio: 30%

## DESCRIÇÃO MICROSCÓPICA

Rocha composta por anfibólio e plagioclásio numa textura granonematoblástica, de granulação média a fina, que define o plano de foliação principal da rocha.

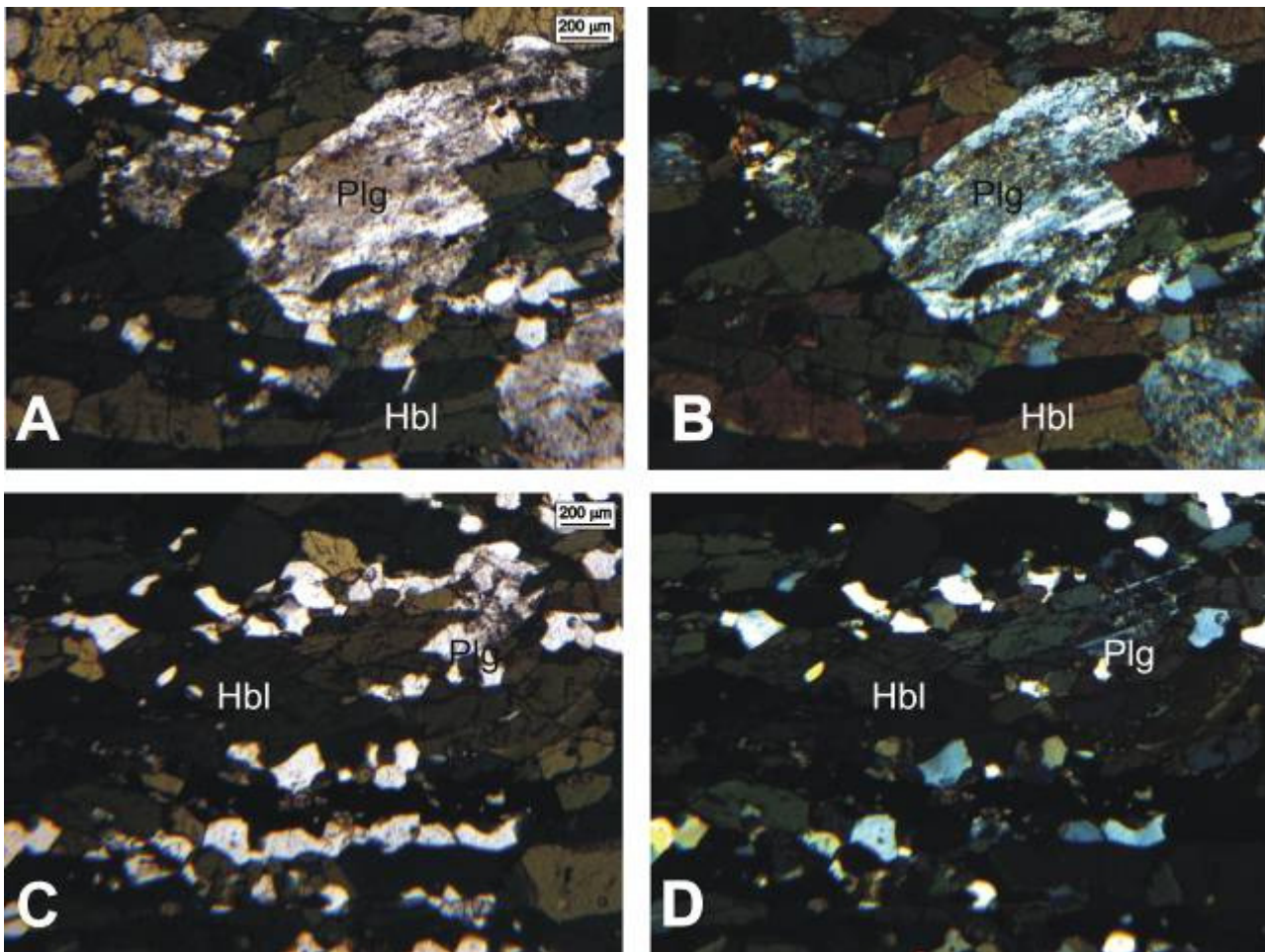
O plagioclásio ocorre de duas formas distintas. A primeira representada por cristais médios a finos, subédricos, fortemente saussuritizados, com orientação do eixo maior discordante a subparalela à direção de foliação principal, exibindo resquícios de geminação polissintética. O outro modo de ocorrência mostra cristais muito finos a ultrafinos, sem geminação, subédricos com limites retos a suturados, localmente em mosaicos poligonizados, evidenciando efeitos de recristalização, onde alguns exibem extinção em bandas ou ondulante.

Os cristais de anfibólio são verdes escuros a claros e com forte pleocroísmo, o que os caracteriza como hornblenda. Apresentam forma subédrica e hábito tabular e granulação fina a muito fina, com eixo maior orientado preferencialmente, definindo o plano de foliação principal da rocha.

Os minerais opacos são representados quase que exclusivamente por magnetita, que possui granulação fina a muito fina, forma anédrica a subédrica e com os cristais orientados em conformidade com os de anfibólio. A magnetita apresenta alteração incipiente para hematita. Hematita pulverulenta ocorre como fina poeira avermelhada em meio a cristais de anfibólio e plagioclásio.

Em termos estruturais a rocha apresenta apenas foliação definida principalmente pela orientação preferencial dos cristais de hornblenda, numa textura granonematoblástica. Localmente, finas vênulas de epidoto cortam obliquamente a foliação da rocha.

A fácies metamórfica é anfibolito, devido a presença de hornblenda e plagioclásio, que se caracterizam como fases minerais principais, classificando a rocha como anfibolito, de protólito ígneo de composição gabrótica.



Prancha LUSL-13 – A e B) Fotomicrografia em luz natural e luz polarizada, respectivamente, com a mineralogia principal da rocha, dada por plagioclásio e hornblenda, onde o primeiro apresenta cristais subédricos a euédricos, indicando resquícios da textura ígneas original; C e D) Fotomicrografia em luz natural e luz polarizada, respectivamente, exibindo a textura granonematoblástica da rocha, onde os cristais de plagioclásio apresentam-se poligonizados e com granulação mais fina.

AMOSTRA: **LUSL-15**  
**ANFIBOLITO**

CLASSIFICAÇÃO DA ROCHA:

#### COMPOSIÇÃO MINERALÓGICA

##### ***Mineralogia principal***

**1%**

Anfibólio: 80%

Plagioclásio: 20%

##### ***Mineralogia acessória - <***

Minerais opacos

Titanita

#### DESCRIÇÃO MICROSCÓPICA

Rocha fortemente foliada mostrando bandamento incipiente dado pela intercalação de bandas ricas em anfibólio e ricas em plagioclásio.

O anfibólio apresenta-se em cristais verdes, pleocróicos, forma subédrica, granulação predominantemente fina (< 2 mm), possuindo comumente hábito tabular com eixo maior orientado preferencialmente, o que define o plano de foliação principal.

Os cristais de plagioclásio apresentam granulação fina a muito fina, forma subédrica a anédrica, comumente saussuritizados e tendo como produtos principais desta transformação sericita e carbonato.

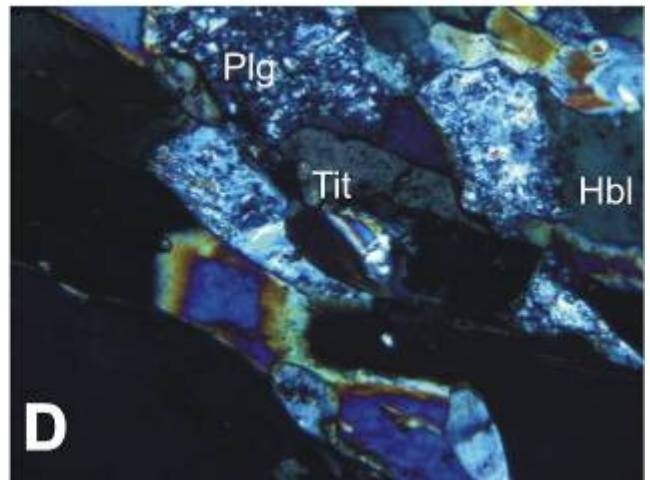
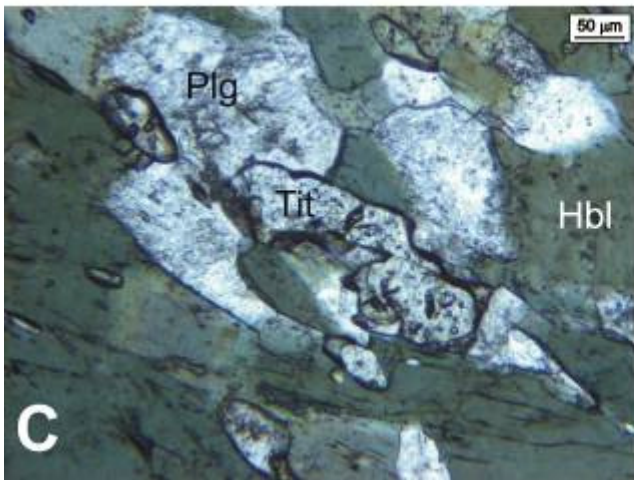
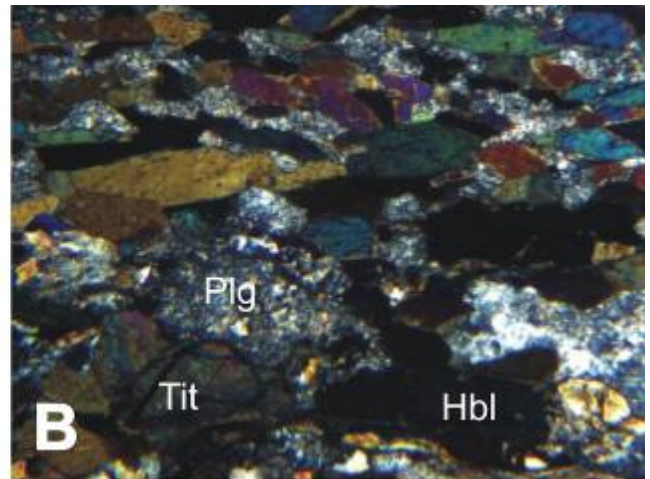
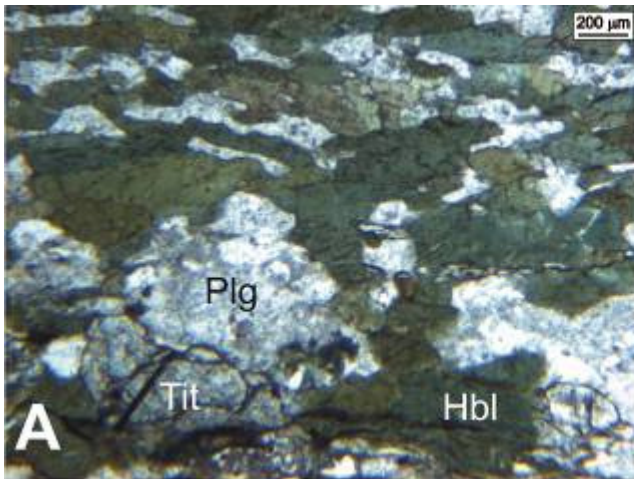
A titanita ocorre em cristais incolores a marrons pálidos, por vezes geminados, fracamente pleocróicos, subédricos a anédricos, granulação fina (< 2 mm) a ultrafina (<< 1 mm),. Tem distribuição esparsa por toda a rocha, ocorrendo de forma isolada ou em aglomerados de cristais, os mais finos condicionados à foliação da rocha, enquanto os mais grossos associados à banda mais rica em plagioclásio.

Os minerais opacos são raros e ocorrem nos planos de clivagem de cristais de anfibólio. São representados por magnetita e pirrotita oxidando-se para limonita.

Em termos estruturais apresenta foliação caracterizada pela orientação preferencial dos cristais de hornblenda, que juntamente com o mosaico de cristais de plagioclásio definem uma textura granonematoblástica. Fino e localizado bandamento composicional é observado.

A fácies metamórfica é anfibolito, caracterizada pela presença de hornblenda, plagioclásio e  $\pm$  titanita, e sua classificação petrográfica é anfibolito, de provável protólito gabróico (metamelagabro).





Prancha LUSL-15 – A e B) Fotomicrografia em luz natural e luz polarizada, respectivamente, com a mineralogia principal da rocha, dada por plagioclásio e hornblenda, e como acessório titanita, além da textura granonematoblástica; C e D) Fotomicrografia em luz natural e luz polarizada, respectivamente, mostrando cristais de titanita em meio a plagioclásio e hornblenda.



## COMPOSIÇÃO MINERALÓGICA

**Mineralogia principal****1%**

Hornblenda

Plagioclásio

**Mineralogia acessória - <**

Minerais do grupo do epidoto

Minerais opacos

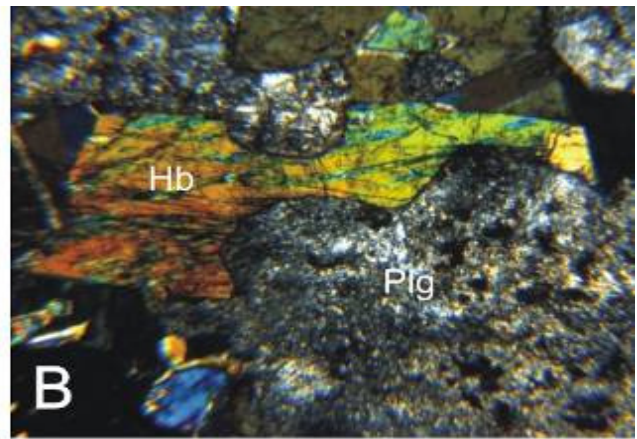
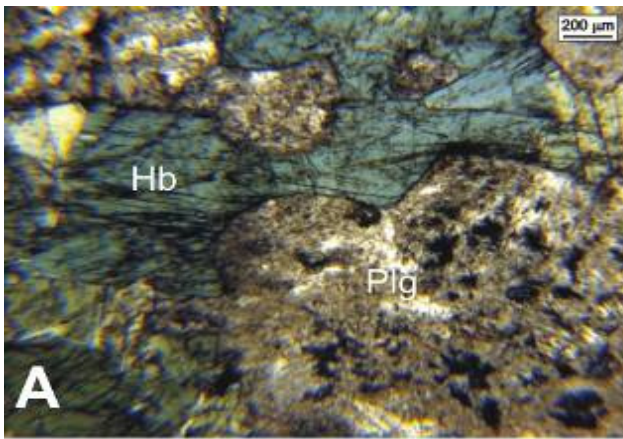
## DESCRIÇÃO MICROSCÓPICA

Anfibólio: cristais incolores, verde pálido a verde azulados, pleocroísmo médio a forte, granulação média (< 3mm) predominantemente, forma subédrica a anédrica, com hábito que varia de tabular a prismático. As diferentes cores e hábitos apresentados apontam para hornblenda, porém indo para uma composição de ferroactinolita. Alguns cristais são geminados, enquanto outros possuem inclusões de plagioclásio e de diminutos cristais de epidoto.

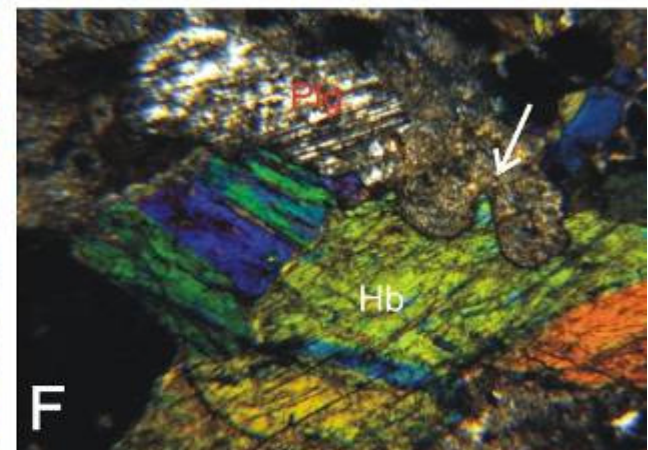
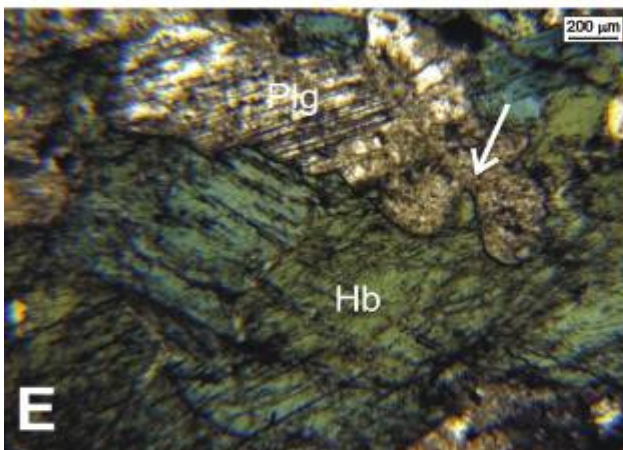
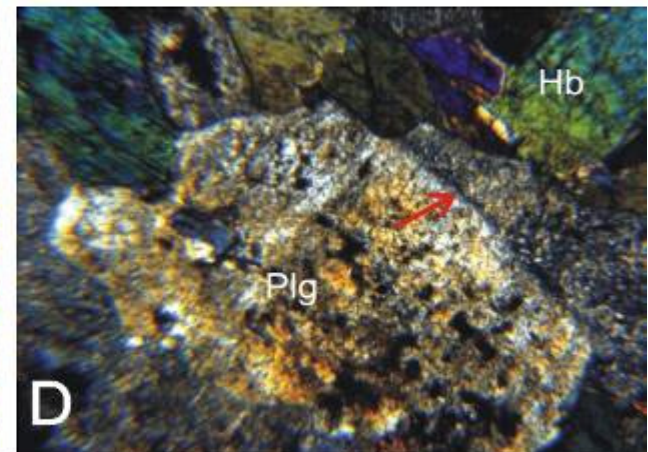
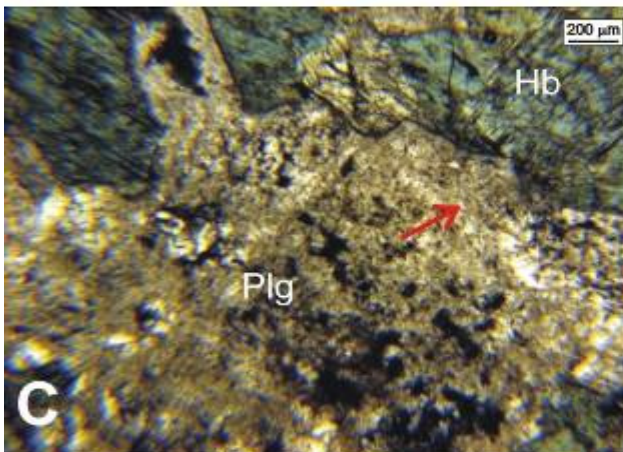
Plagioclásio: cristais subédricos a anédricos, granulação média, tipicamente com geminação polissintética, porém fortemente saussuritizados. Interpenetração com anfibólio (parecidas com golfo de corrosão) foi vista localmente. Alguns cristais apresentam zonamento concêntrico.

Os minerais opacos ocorrem de maneira localizada sobre cristais de plagioclásio, granulação ultrafina, forma anédrica a subédrica.

A textura da rocha é do tipo granoblástica isogranular. Em termos deformacionais a extinção ondulante está ausente em cristais de anfibólio e presente nos cristais de plagioclásio. Vênula de epidoto (?) corta obliquamente o acamamento da rocha. Em termos modais apresenta cerca de 20% de anfibólio e 80% de plagioclásio. A rocha classifica-se como metaleucogabro.



Prancha LUSL-20B – A e B) Fotomicrografias em luz natural e luz polarizada, respectivamente, mostrando a mineralogia principal da rocha dada por hornblenda e plagioclásio, este fortemente saussuritizado;



Prancha LUSL-20B – C e D) Fotomicrografias em luz natural e luz polarizada, respectivamente, onde grão de plagioclásio apresenta zonamento concêntrico (indicado pela seta); E e F) Fotomicrografias em luz natural e luz polarizada, respectivamente, exibindo grão de hornblenda em contato com plagioclásio, cujo limite mostra feição tipo golfo de corrosão (indicado pela seta).

## COMPOSIÇÃO MINERALÓGICA

**Mineralogia principal**

Clinopiroxênio: 60%

Plagioclásio: 40%

**Mineralogia acessória - < 1%**

Minerais opacos

Titanita

## DESCRIÇÃO MICROSCÓPICA

Rocha formada por micrólitos e ripas (fenocristais) de plagioclásio, entremeados com cristais anédricos a subédricos de augita, além de massa opaca que constitui a mesostase (solidificação da última fração magmática nos espaços entre os primeiros minerais já solidificados, podendo ser vítrea ou microgranular), formando uma textura do tipo ofítica. As ripas (cristais tabulares/fenocristais) de plagioclásio estão fortemente saussuritizados, enquanto os micrólitos encontram-se um pouco mais preservados de tal alteração.

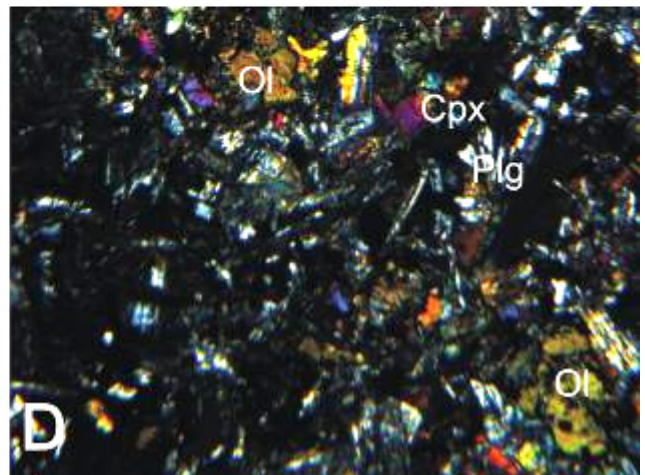
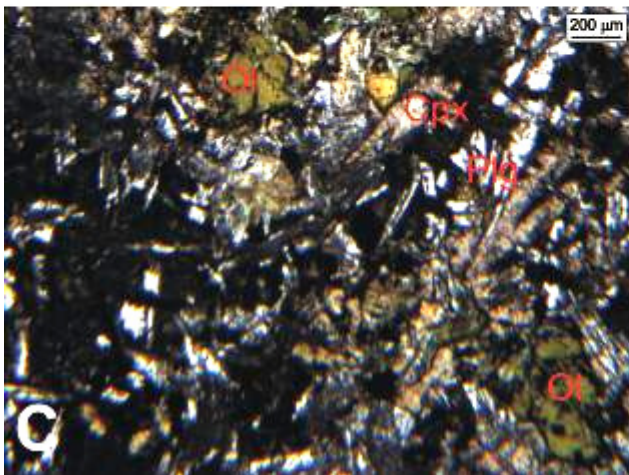
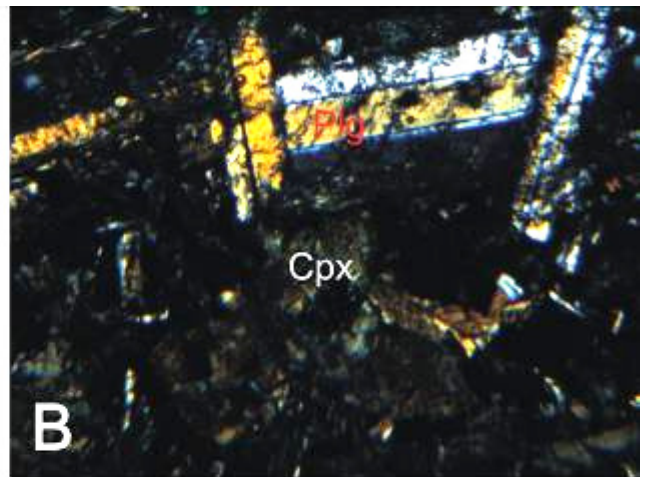
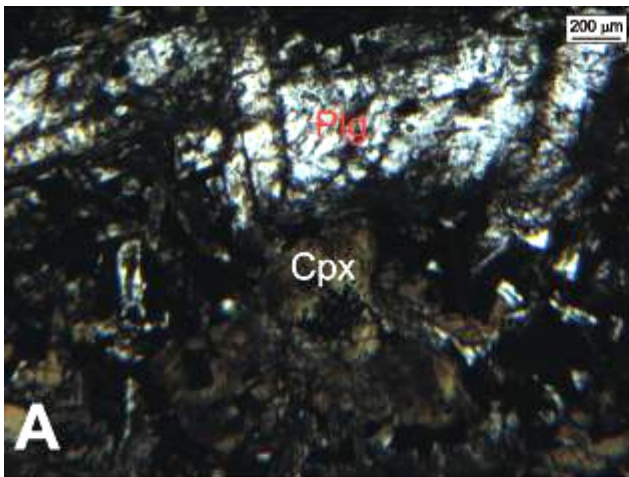
Os cristais de clinopiroxênio são rosa pálido, fracamente pleocróicos, apresentando forma subédrica e granulação muito fina a ultrafina, por vezes com extinção ondulante, classificados como augita. Comumente associa-se com mineral verde, pleocróico por vezes, com hábito plumoso ou fibroso, tratando-se provavelmente de clorita, porém muitas cores de interferência são altas (dúvida uralita/anfibólio= transformação de clinopiroxênio). Se esses minerais forem clorita representam então antigos cristais de olivina.

Fenocristais de plagioclásio, variando de 1 a 3,5 mm ocorrem de maneira dispersa na rocha, exibindo geminação polissintética e/ou Carlsbad, além de zonamento de borda e efeitos de saussuritização.

Minerais opacos estão dispersos por toda a rocha, mostrando forma euédrica a subédrica, hábito tabular a acicular e grã ultrafina (<< 1 mm).

A rocha não apresenta efeitos de deformação tectônica.





Prancha LUSL-21.B – A e B) Fotomicrografia em luz natural e luz polarizada, respectivamente, mostrando fenocristais de plagioclásio com geminação Carlsbad; C e D) Fotomicrografia em luz natural e luz polarizada, respectivamente, exibindo textura ofítica marcada por micrólitos de plagioclásio em meio a mesostáse (massa opaca), mostrando cristais de olivina em meio a textura ofítica.

AMOSTRA: **FD 02 – 44,00 m** CLASSIFICAÇÃO DA ROCHA: **OLIVINA ORTOPIROXENITO**

#### COMPOSIÇÃO MINERALÓGICA

##### **Mineralogia principal**

Ortopiroxênio: 95%

Cp)

Olivina: 5%

##### **Mineralogia acessória - < 1%**

Minerais opacos (Ptl, Po, Mg, Lm e

Serpentina

#### DESCRIÇÃO MICROSCÓPICA

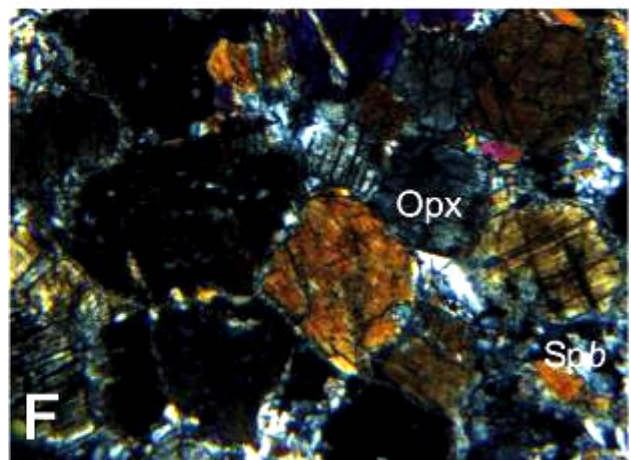
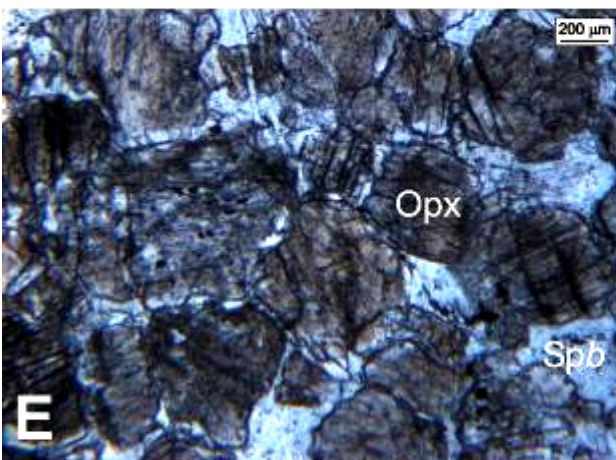
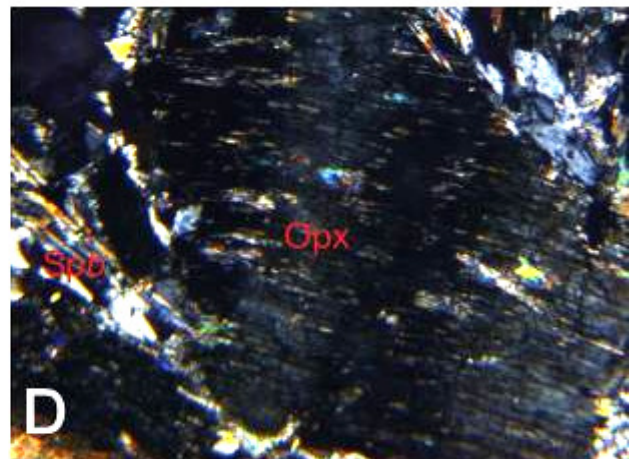
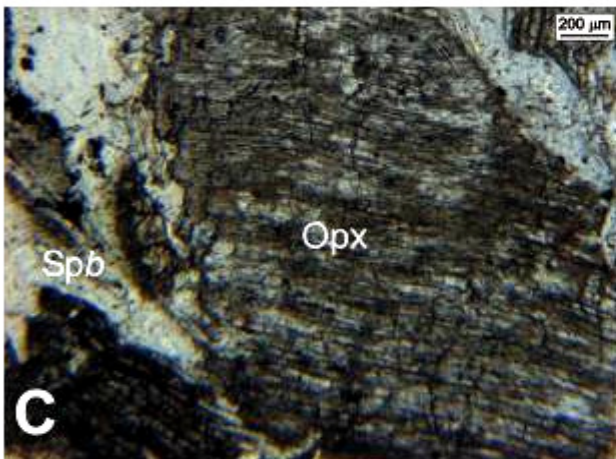
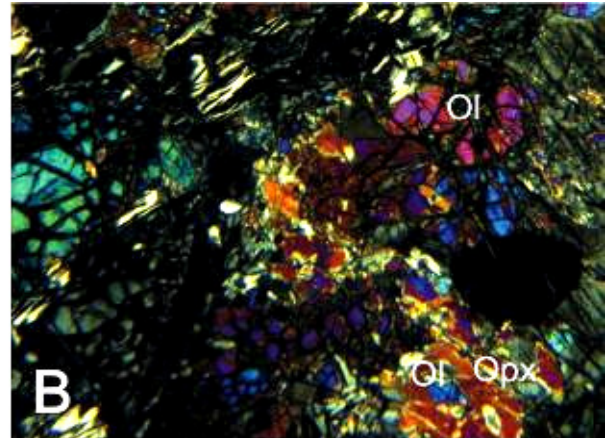
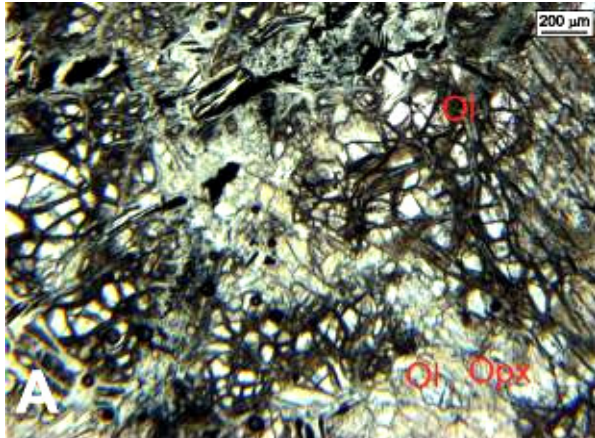
Rocha composta predominantemente por ortopiroxênio, e subordinadamente por olivina, onde os primeiros variam em granulação de muito fina a muito grossa (1 a 6 mm), com forma principalmente subédrica, alguns apresentando extinção ondulante e *kink bands*, enquanto outros possuem caráter poiquilítico (cadacristais de olivina), representando assim um heteroadcumulato. Os limites de cristais de ortopiroxênio possuem o desenvolvimento de uma mineralogia secundária/metamórfica de hidratação, caracterizada por talco, serpentina lamelar (bastita), e anfibólio, variando de hábito tabular a acicular, este com alta birrefringência e extinção reta, caracterizado como cumingtonita. A cumingtonita também aparece internamente nos cristais de ortopiroxênio, em cristais aciculares bem desenvolvidos, ou cortando vários pequenos cristais de ortopiroxênio. As lamelas de serpentina (bastita) chegam a atingir 1 mm de dimensão, onde as linhas de clivagem são realçadas pela presença de minerais opacos; a maioria das vezes mostram extinção em bandas e por vezes *kink bands*. Duas gerações de vênulas de serpentina são identificadas e pela disposição dos cristais parece tratar-se de crisotila, onde a última geração de vênula corta cristais de anfibólio.

A olivina se mostra fortemente fraturada e alterada para serpentina, onde a reconstituição dos limites de cristais mostra granulação fina a ultrafina e forma subédrica, ocorrendo em aglomerados de cristais ou como cadacristais em oikocristais de ortopiroxênio. Estima-se cerca de 5% de cristais de olivina e de acordo com isso a rocha classifica-se como olivina ortopiroxenito.

Os opacos são representados predominantemente por sulfetos, sendo que foram identificados pentlandita, pirrotita, e calcopirita. A pentlandita é o sulfeto mais frequente e ocorre preferencialmente em grandes agregados de cristais de forma intersticial aos silicatos ou preenchendo microfraturas. A pirrotita e a pentlandita se apresentam,

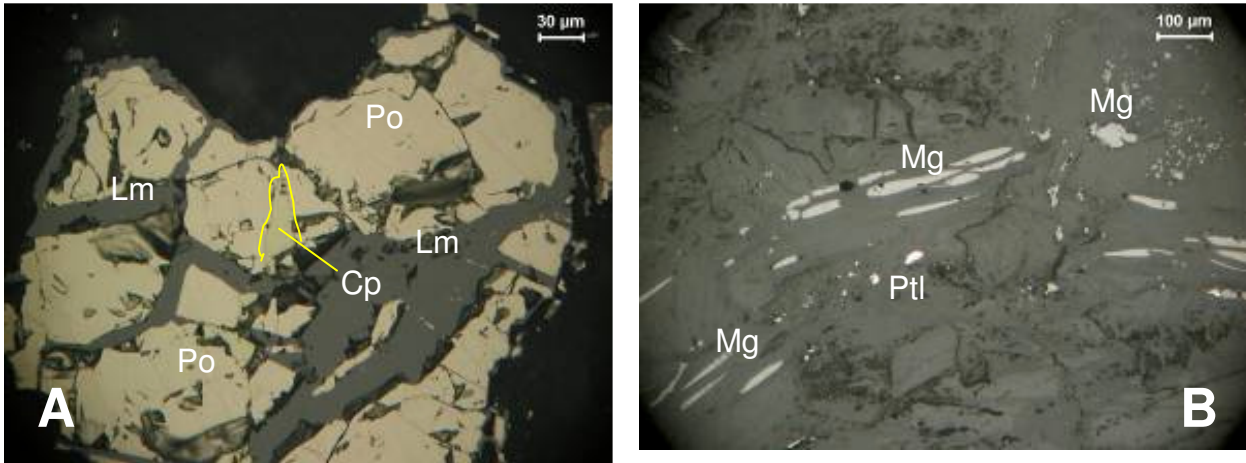


frequentemente, em processo de alteração para hidróxido de ferro. A calcopirita, sempre inalterada, ocorre inclusa na pentlandita e na pirrotita. Identificou-se também a magnetita, que ocorre como finos cristais alongados substituindo os ortopiroxênios e bastita, segundo as linhas de clivagem ou como cristais finos a ultrafinos com tamanhos de 1 a 2  $\mu\text{m}$  e forma subédrica a anédrica, disseminados na lâmina em meio a porções alteradas/serpentinizadas de ortopiroxênio e olivina.

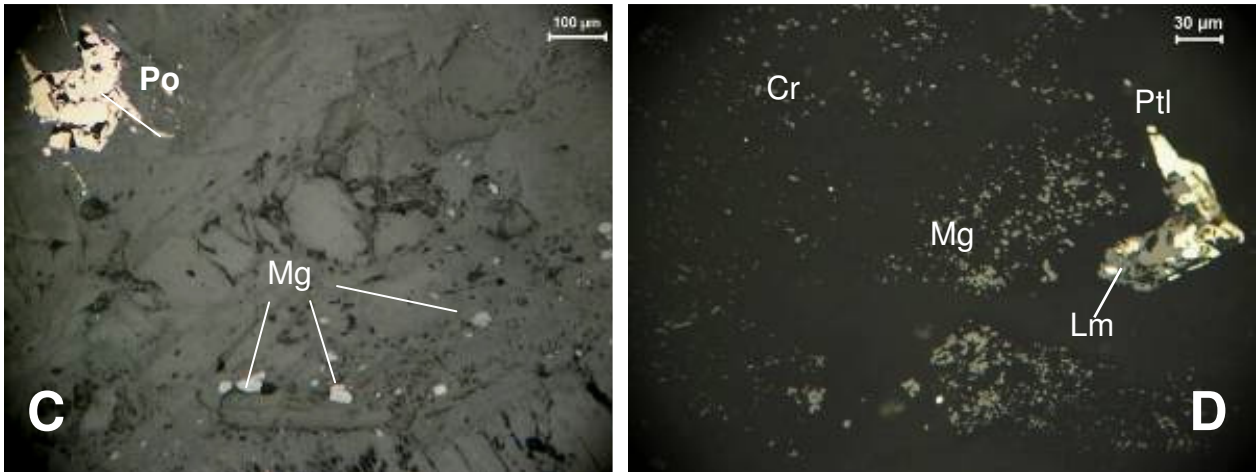


Prancha FD 02 – 44,00m – A e B) Fotomicrografia em luz natural e luz polarizada, respectivamente, mostrando cristais de olivina e ortopiroxênio com efeitos de

serpentinização; C e D) Fotomicrografia em luz natural e luz polarizada, respectivamente, exibindo cristal de ortopiroxênio com kink band, marcada por extinção ondulante; E e F) Fotomicrografia em luz natural e luz polarizada, respectivamente, mostrando textura cumulática.



Prancha FD 02 – 44,00m – Opacos – A) cristal de pirrotita (Po) alterando-se para hidróxido de ferro (Lm) e com inclusão de calcopirita (Cp). Obj. a óleo. Luz natural; B) Alinhamento dos cristais de magnetita (Mg) e outros pequenos disseminados e pentlandita (Ptl), sob luz natural;



Prancha FD 02 – 44,00m – Opacos – C) Grande cristal de pirrotita (Po) e pequenos cristais de cromita. Luz natural. D) Cristal de pentlandita (Ptl) alterando-se para hidróxido de ferro (Lm) e diminutos cristais de magnetita (Mg) disseminados. Obj. a óleo, sob luz natural.



AMOSTRA: **FD 02 – 110,00 m**  
**(PERIDOTITO)**

CLASSIFICAÇÃO DA ROCHA: **SERPENTINITO**

#### COMPOSIÇÃO MINERALÓGICA

##### ***Mineralogia principal***

**1%**

Serpentina  
Cp)

##### ***Mineralogia acessória - <***

Minerais opacos (Mg, Ptl e

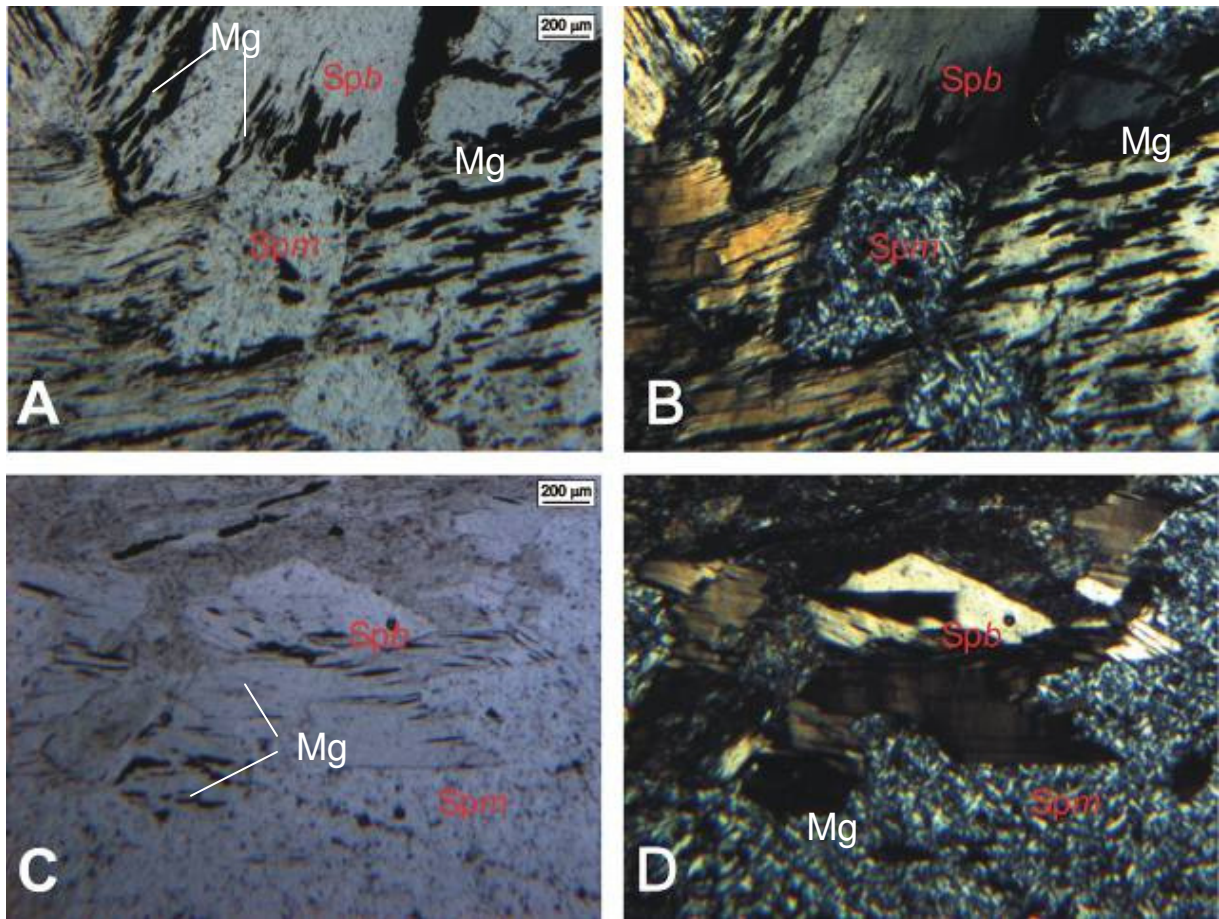
#### DESCRIÇÃO MICROSCÓPICA

Rocha composta predominantemente por serpentina, ocorrendo de duas formas distintas, sendo a primeira como uma massa microgranular, granulação ultrafina, por vezes com arranjos de cristais radiados, semelhante a bastita microgranular descrita por Viti & Mellini (1998). A outra forma corresponde a cristais incolores, sem plecoróismo, forma subédrica, granulação média (até 3mm) a muito fina (< 1 mm), hábito tabular, onde por vezes ocorrem minerais magnetita de hábito acicular nas linhas de clivagem. Ocorrem como cristais isolados ou formam aglomerados de cristais, onde a maioria deles apresenta extinção em bandas, e alguns com presença de *kinks*, características típicas de bastita. Finas vênulas subparalelas de crisotila cortam a rocha de maneira descontínua.

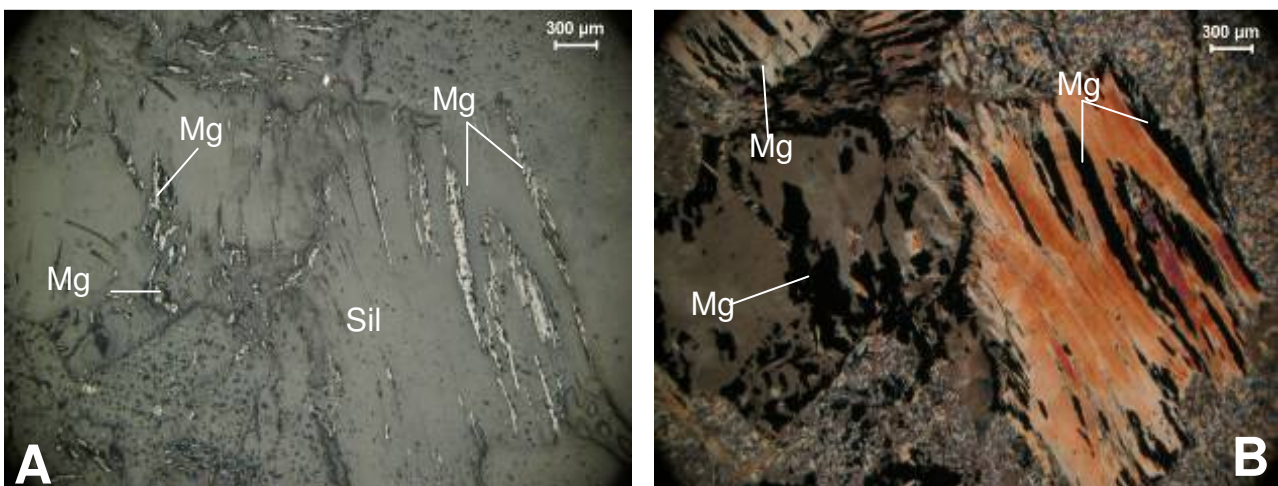
Localmente, relictos fortemente transformados de olivina, caracterizados por porções amarronzadas escuras com textura tipo quebra-cabeça em meio à massa microgranular de serpentina, aliado a presença de bastita em dois tipos texturais distintos sugere que o protólito trata-se de um peridotito.

Os minerais opacos possuem granulação ultrafina, forma subédrica, ocorrendo com mais frequência associado com bastita, e subordinadamente, na massa microgranular de serpentina. O principal opaco presente é a magnetita, que ocorre como agregados alongados segundo as linhas de clivagem da serpentina. Outros opacos identificados foram a pentlandita e a calcopirita, de pouca expressão e que ocorrem finamente disseminados na amostra.





Prancha FD 02 – 110,00 m - A e B) Fotomicrografia em luz natural e luz polarizada, respectivamente, mostrando dois tipos de serpentina, microgranular e bastita, onde algumas destas apresentam extinção ondulante e com magnetita nas linhas de clivagem; C e D) Fotomicrografia em luz natural e luz polarizada, respectivamente, com as mesmas feições anteriores.



Prancha FD 02 – 110,00 m – Opacos – A) magnetita (Mg) em agregados preenchendo fraturas e nas linhas de clivagem de silicatos, sob luz refletida, sem polarização; B) mesma imagem anterior (girada um pouco para a esquerda) com luz transmitida sob polarização.

## COMPOSIÇÃO MINERALÓGICA

**Mineralogia principal**

Serpentina

**Mineralogia acessória - < 1%**

Minerais opacos (Mg, Ptl, Cp e Cr)

## DESCRIÇÃO MICROSCÓPICA

Rocha composta predominantemente por serpentina que ocorre de duas formas distintas, sendo a predominante do tipo *mesh* e a segunda como bastita. A primeira comumente caracteriza a substituição de cristais de olivina, onde apenas fantasmas de limites de cristais são identificados, enquanto a segunda corresponde a pseudomorfos sobre cristais de piroxênio.

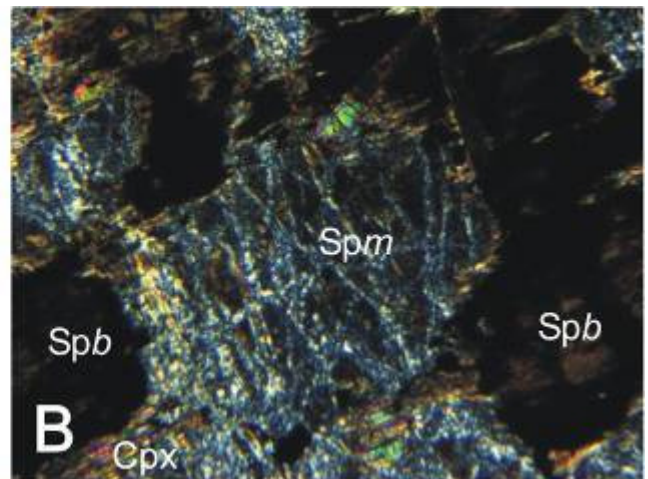
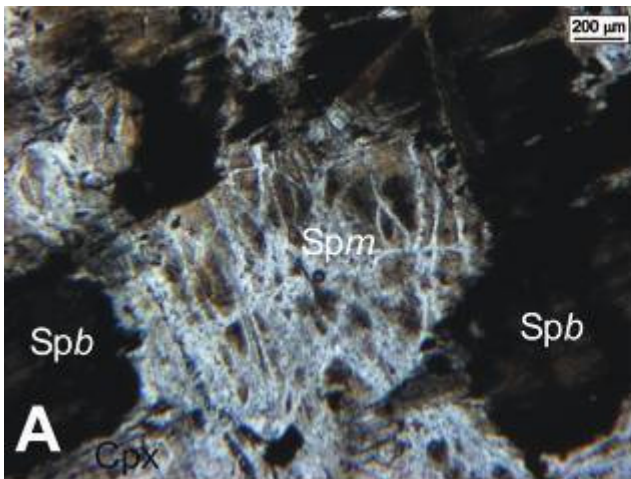
O piroxênio, classificado como clinopiroxênio devido altas cores de interferência e extinção oblíqua, apresenta-se em cristais tabulares, subédricos, por vezes com hábito ameboidal, granulação média, com tonalidades marrons a pretas, estas denotando a presença de fina poeira de minerais opacos e a progressiva transformação para bastita.

A bastita além de pseudomorfisar cristais de clinopiroxênio ocorre como cristais isolados em meio a textura *mesh*, e comumente possui minerais opacos, de forma acicular que se colocam no meio das linhas de clivagem. Alguns cristais exibem extinção ondulante e presença de *kinks*.

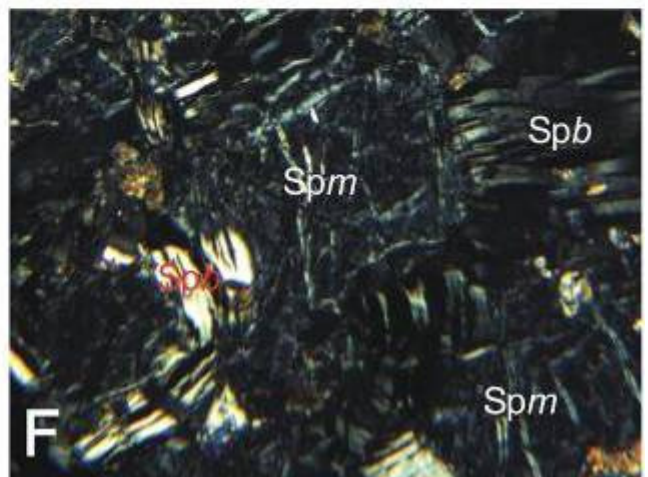
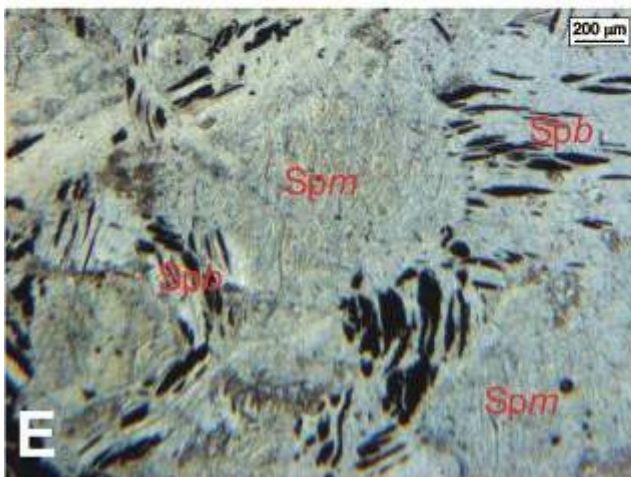
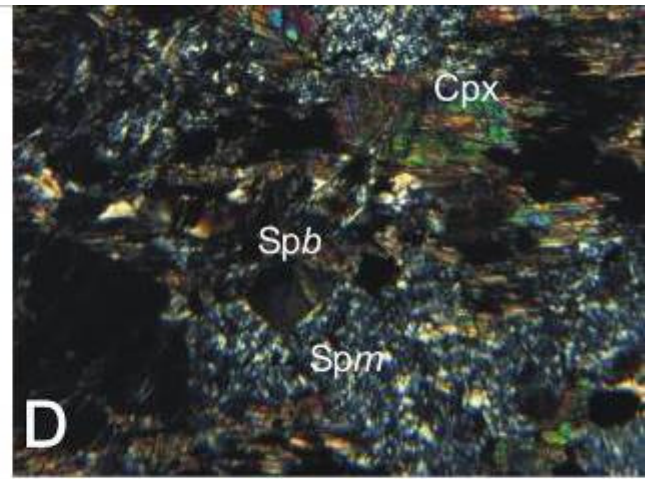
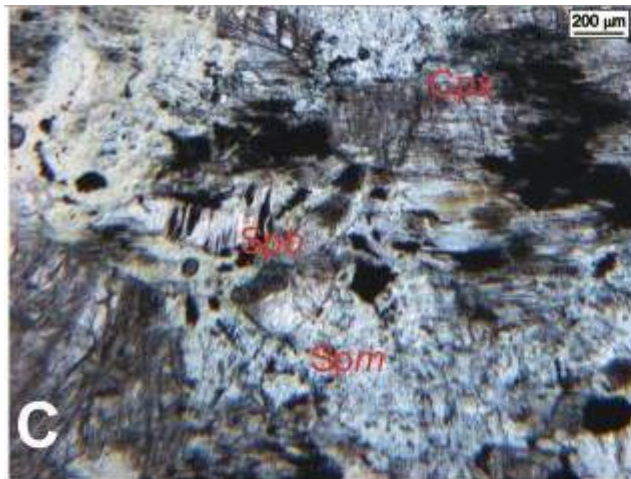
Os minerais opacos são ultrafinos, variando de subédricos a anédricos, com hábito acicular a tabular, quando associados à bastita, e com hábito quadrático quando disperso em meio à textura *mesh*. O principal opaco é a de magnetita, com os sulfetos (pentlandita e calcopirita) e cromita raros. A principal forma de ocorrência da cromita foi como finos cristais de cerca de 1 a 3  $\mu\text{m}$ , também foi observado cristal maior de intercrescido com dois de pentlandita e ambos alterando-se para hidróxido de ferro. A calcopirita ocorre sã e finamente disseminada na amostra.

A reconstituição do protólito, baseada na presença de serpentina *mesh* e bastita sobre clinopiroxênio, sugere que a mesma trata-se de um wehrlito.



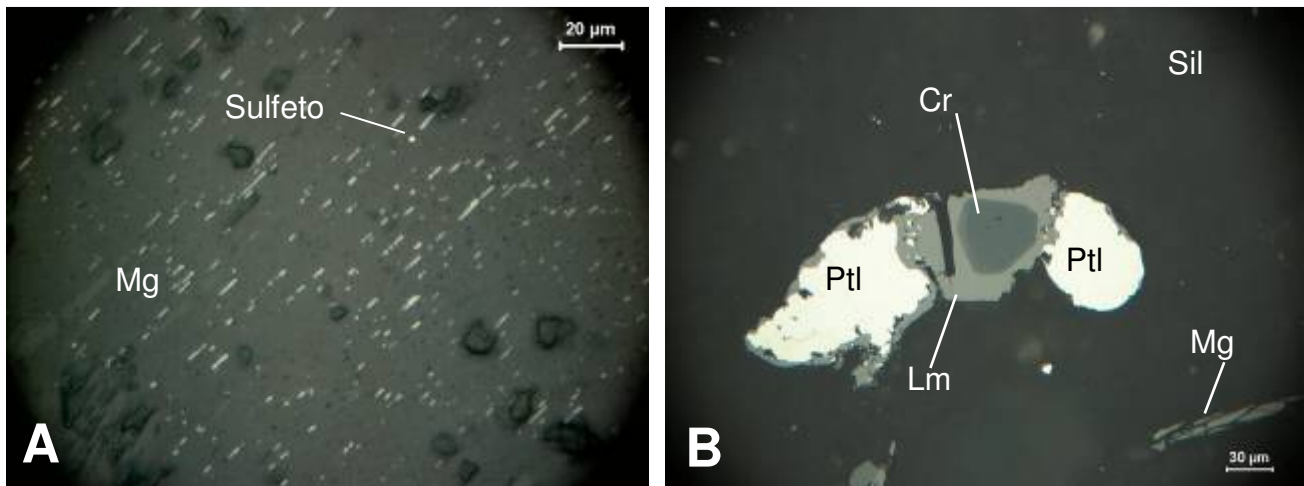


Prancha FD 02 – 110,75 m - (A e B) Fotomicrografia em luz natural e luz polarizada, respectivamente, mostrando forma ameboidal de antigos cristais de clinopiroxênio, que aparecem como resquícios nas bordas de cristais de bastita (Spb), marcados por fina poeira de minerais opacos. A serpentina mesh substitui antigos cristais de olivina.



Prancha FD 02 – 110,75 m - C e D) Fotomicrografia em luz natural e luz polarizada, respectivamente, mostrando resquícios de cristais de clinopiroxênio em meio a massa de serpentina mesh e bastita; E e F) Fotomicrografia em luz natural e luz polarizada,

respectivamente, exibindo porção totalmente serpentinizada, onde resquícios da mineralogia original são raros, predominando a massa de serpentina mesh e bastita.



Prancha FD 02 – 110,75 m – Opacos – A) Cristais ultrafinos de magnetita (Mg) alinhados e raro sulfeto . Obj. 50 X. Luz polarizada. B) Cristais de pentlandita (Ptl) e de cromita (Cr) intercrescidos e alterando para hidróxido de ferro (Lm). Obj. a óleo. Luz natural.

## COMPOSIÇÃO MINERALÓGICA

**Mineralogia principal**

1%

Olivina

**Mineralogia acessória - <**

Minerais opacos

## DESCRIÇÃO MICROSCÓPICA

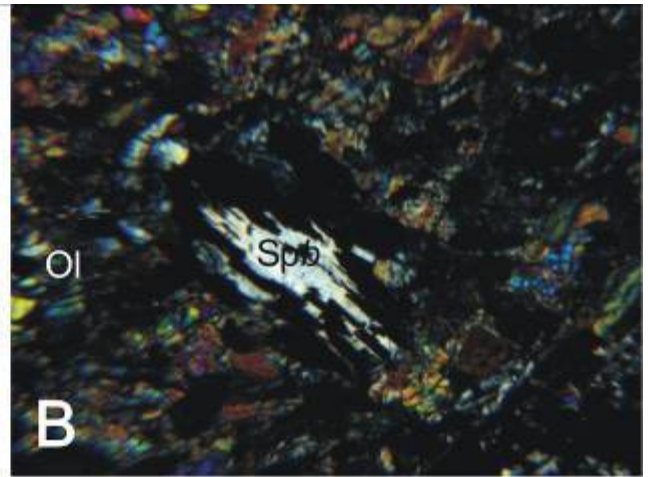
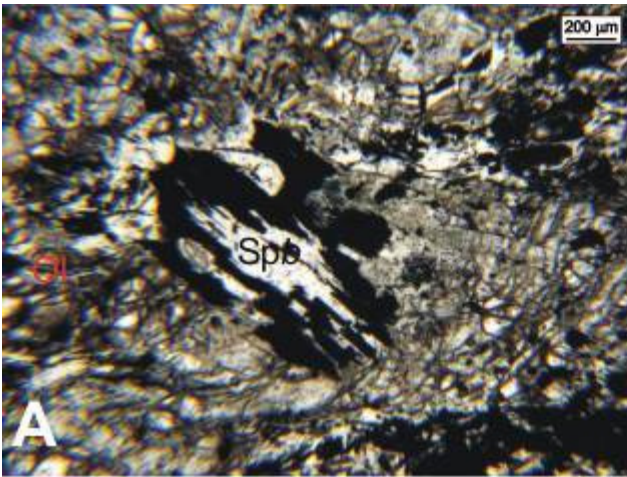
Rocha com anisotropia estrutural definida pelo arranjo orientado de filmes de minerais opacos que estão associados preferencialmente com lizardita e crisotila (mesh deformada), sendo ainda acompanhados por cristais prismáticos de anfibólio, como também por resquícios de cristais de clinopiroxênio, ortopiroxênio e olivinas; localmente, envolvem cristais de bastita.

A maioria dos cristais apresenta granulação muito fina, com forma subédrica num mosaico de cristais de arranjo granoblástico. Por vezes a foliação apresenta aspecto anastomosado, marcado pelo crescimento sincinemático de cristais de anfibólio (tremolita/cummingtonita) envolvendo olhos de piroxênio e olivina.

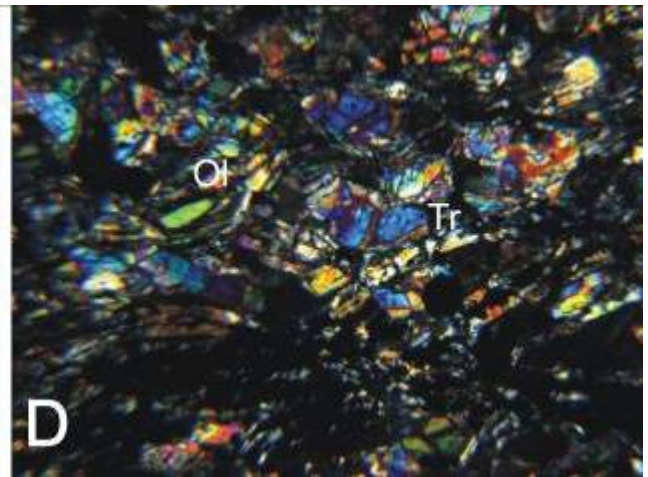
Vênulas de serpentina se colocam paralelas à foliação e a textura de modo geral é do tipo nematoblástica. Os cristais originais se encontram francamente fraturados enquanto os cristais de anfibólio crescidos orientados com eixo maior paralelo a foliação. Alguns deste encontram-se transformados para bastita.

Os opacos são representados principalmente pela magnetita, que ocorre como produto de alteração dos piroxênios, segundo as linhas de clivagem ou preenchendo microfraturas. Os sulfetos identificados foram a pirita e a calcopirita em finos cristais disseminados. A cromita ocorre como raros cristais subédricos de cerca de 10 µm.

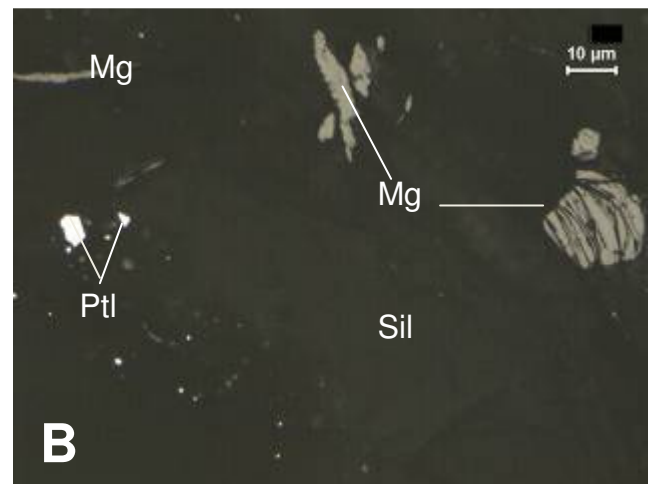
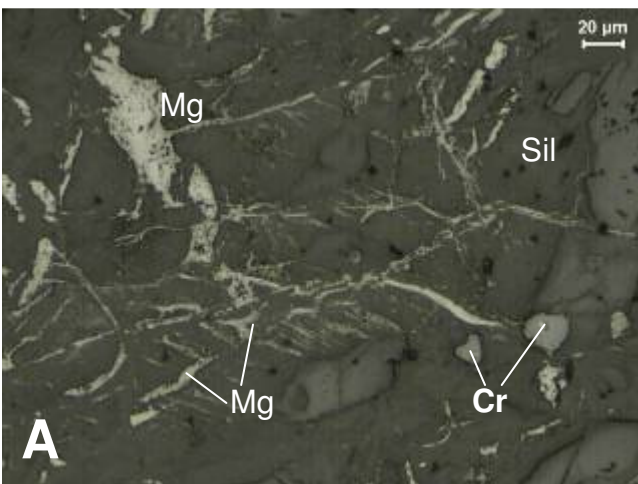




Prancha FD26 – 79,85 m - A e B) Placa de bastita em meio a cristais de anfibólio e resquícios de cristais de olivina;



Prancha FD26 – 79,85 m – C e D) mostrando a anisotropia estrutural da rocha, marcada pelo anastomosamento da foliação, marcada por cristais de tremolita e antigos cristais de olivina. Luz natural e luz polarizada, respectivamente.



Prancha FD26 – 79,85 m – Opacos – A) Magnetita (Mg) substituindo silicatos e raras cromitas (Cr); B) magnetita (Mg) substituindo silicatos e raros cristais de Pentlandita (Ptl). Obj. a óleo. Luz natural.

## COMPOSIÇÃO MINERALÓGICA

### ***Mineralogia principal***

**1%**

Ortopiroxênio

Po, Bv)

Clinopiroxênio

Olivina

### ***Mineralogia acessória - <***

Opacos (Cr, Mg, Ptl,

## DESCRIÇÃO MICROSCÓPICA

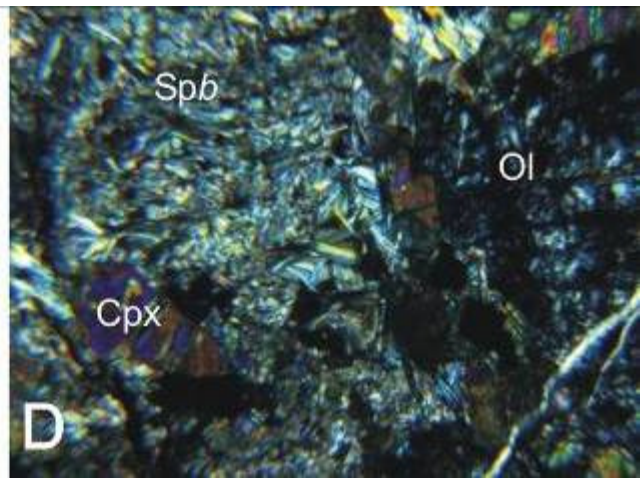
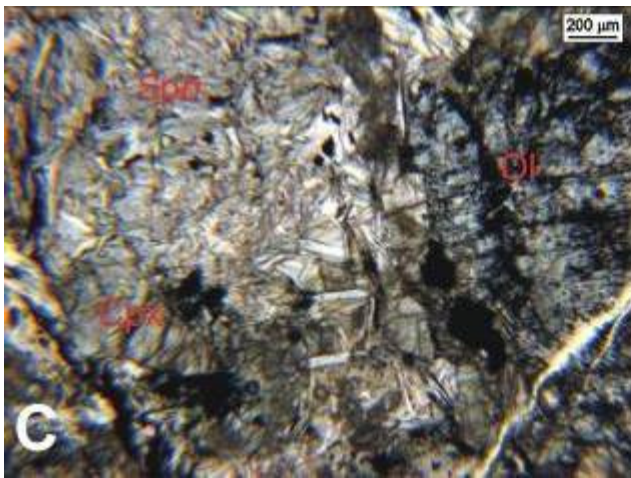
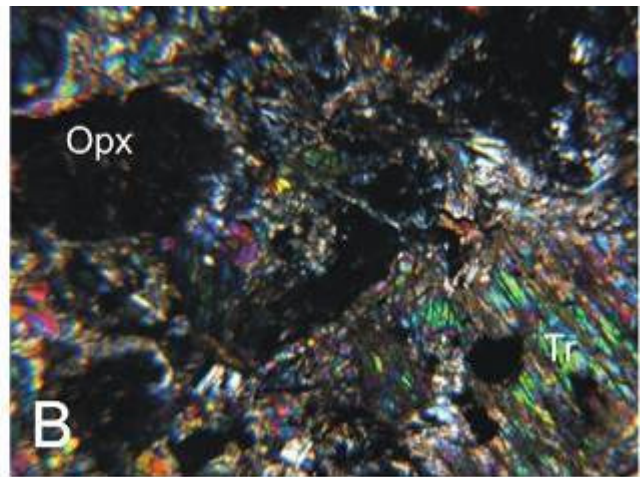
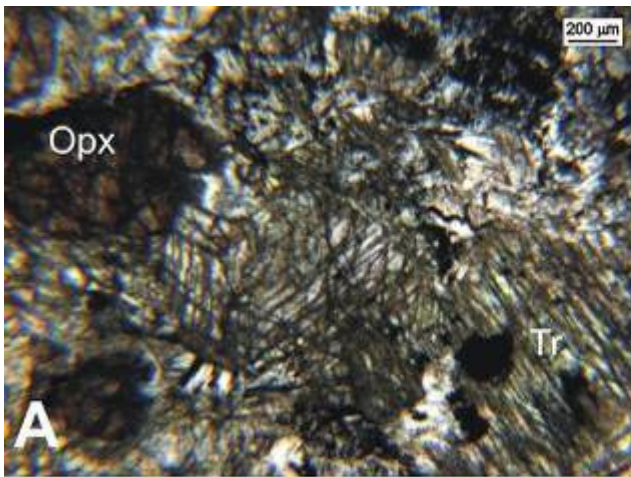
A rocha apresenta forte processo de serpentinização, mostrando restos da mineralogia original caracterizada por ortopiroxênio, clinopiroxênio e rara olivina. A reconstituição de limites de cristais mostra no geral uma granulação média (2 a 5 mm). Os cristais de ortopiroxênio são incolores a verde/rosa pálidos ou possuem pátina amarronzada, extinção reta, forma subédrica e granulação média a muito fina, enquanto os cristais de clinopiroxênio mostram-se incolores a verde/rosa pálidos, extinção oblíqua.

A bastita ocorre por vezes microgranular.

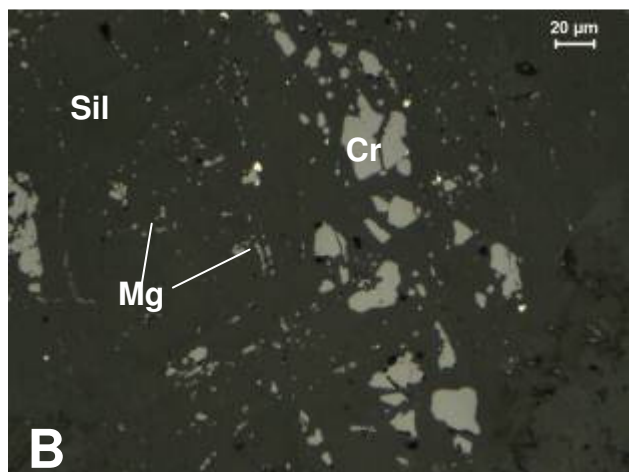
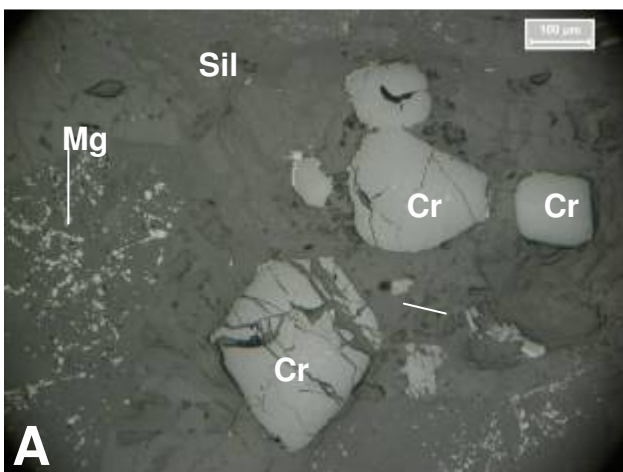
Os minerais opacos são representados por cromita, magnetita, pentlandita, pirrotita e bravoíta. A magnetita ocorre preenchendo as linhas de clivagem dos piroxênios, em aglomerados de cristais, ou ainda como uma fina poeira de cristais ou cristais aciculares a prismáticos com limites irregulares. A principal forma de ocorrência da cromita foi como cristais subédricos de tamanhos de poucos micrometros a cerca de 200 micrometros. A bravoíta (Fe, Ni) $S_2$  ocorre provavelmente como alteração da pentlandita (Fe,Ni) $S_8$  presente como exsoluções na pirrotita (FeS).

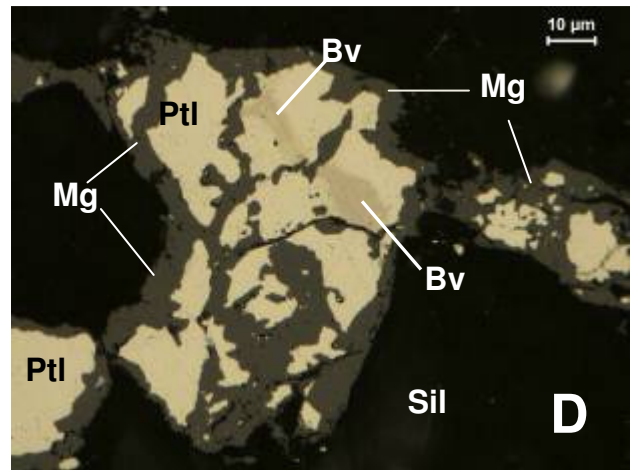
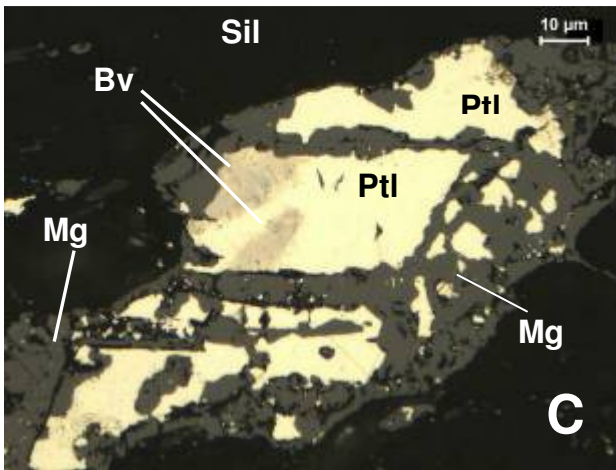
Cristais de anfibólio ocorrem bordejando cristais de ortopiroxênio, granulação fina (< 2 mm) a muito fina, forma subédrica e hábito prismático; são incolores a rosa pálido, possuindo extinção reta e alta birrefringência. Os cristais de olivina estão quase que totalmente transformados para serpentina mesh restando algumas ilhas de resquícios de cristais originais.





Prancha FD 26 – 99,85 m - A e B) Fotomicrografias em luz natural e luz polarizada, com presença de cristais de ortopiroxênio e tremolita; C e D) Fotomicrografias em luz natural e luz polarizada, respectivamente, exibindo cristal de olivina totalmente serpentizado, resquício de clinopiroxênio e domínio de microplacas de bastita.





Prancha FD 26 – 99,85 m – Opacos – A) Magnetita (Mg) como cristais ultrafinos sobre silicatos e grandes cristais de cromitas (Cr); B) Magnetita (Mg) muito fina alinhada, substituindo silicatos, alguns sulfetos ultrafinos disseminados e cromitas (Cr); C) Cristais de pentlandita (Ptl) alterando-se para magnetita (Mg) e com exsoluções de bravoíta (Bv). Obj. a óleo; D) Pentlandita (Ptl) alterando-se para magnetita (Mg) e com exsoluções de bravoíta. Obj. a óleo. N //.

## COMPOSIÇÃO MINERALÓGICA

### **Mineralogia principal**

**1%**

Ortopiroxênio

Clinopiroxênio

Olivina

### **Mineralogia acessória - <**

Opacos (Mg, Ptl, Cr)

## DESCRIÇÃO MICROSCÓPICA

Rocha composta predominantemente por (35%), mostrando forte processo de serpentinização. Os cristais de piroxênio são marrons pálidos, apresentando forma subédrica, hábito quadrático com vértices arredondados e granulação média (2 a 5 mm), distinguindo-se principalmente pela posição de extinção dos cristais (oblíqua para os clinopiroxênio), porém a predominância é de cristais de ortopiroxênio. Ambos possuem caráter poiquilítico, englobando pequenos cristais de olivina. Localmente formam aglomerados de cristais subédricos de tamanhos distintos.

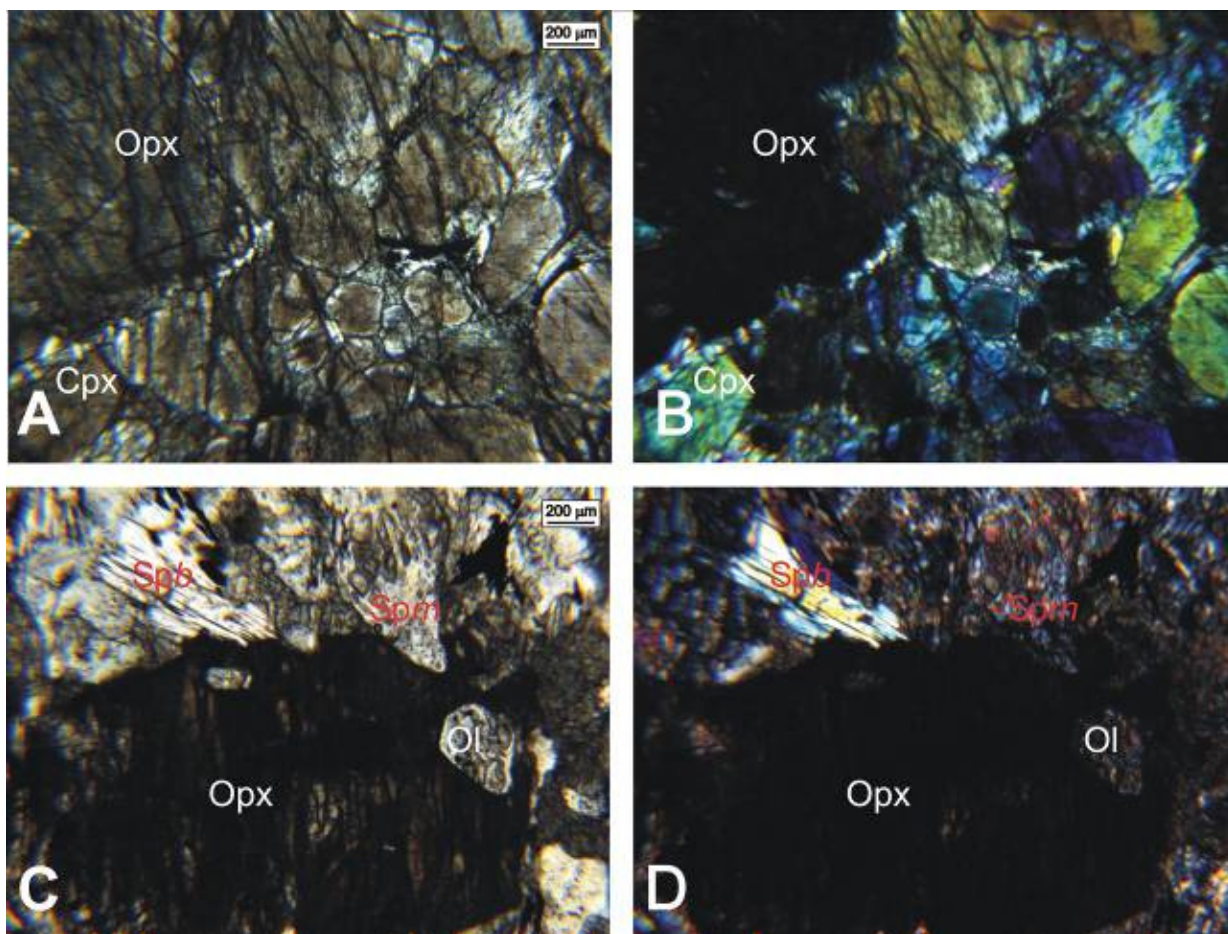
A olivina é quase que totalmente transformada para serpentina *mesh* e a reconstituição de antigos limites de cristais denota hábito arredondado, granulação fina (< 2 mm) a muito fina (< 1 mm).

Placas de bastita com franco desenvolvimento de minerais opacos nos planos de clivagem são comuns em meio a massa de serpentina *mesh*.

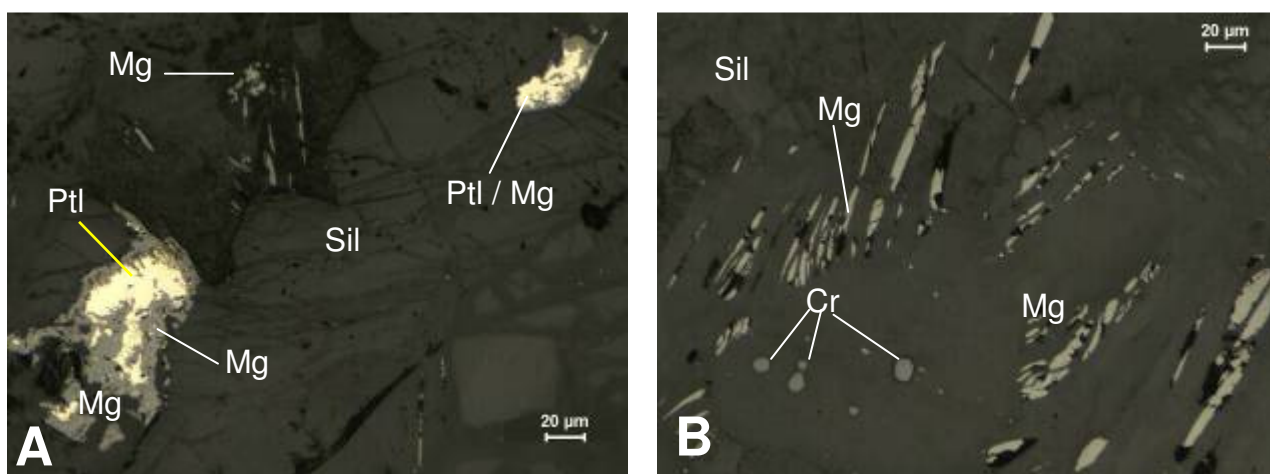
Amostra com predomínio da magnetita como mineral opaco, que ocorre como finíssima poeira sobre cristais de ortopiroxênio, massas irregulares ou aciculares de granulação muito fina em meio à massa serpentinizada, tipo *mesh* ou bastita. Ocorre ainda cromita como raros cristais subédricos menores do que 10 µm. O único sulfeto identificado foi a pentlandita que se apresenta alterando-se para magnetita.

Vênulas de crisotila cortam a rocha obliquamente a provável bandamento de acumulação. Textura adcumulática.





Prancha FD 26 – 117,45 m - A e B) Na sequencia, fotomicrografias em luz natural e luz polarizada, mostrando aglomerado de cristais de ortopiroxênio, e mais raramente, clinopiroxênio; C e D) Fotomicrografias em luz natural e luz polarizada, respectivamente, exibindo cristais poiquilíticos de ortopiroxênio com inclusões de olivina. Serpentina mesh (Spm) ocorre em meio a ilhas de resquícios de cristais de olivina, enquanto bastita (Spb) corresponde a antigos cristais de piroxênio.



Prancha FD 26 – 117,45 m – Opacos – A) Magnetita (Mg) alinhada segundo as linhas de clivagem dos silicatos e cristais de pentlandita(Ptl) alterando-se para magnetita (Mg); B) Magnetita (Mg) substituindo silicatos e raras cromitas arredondadas (Cr).

AMOSTRA: **FD 26 – 134,05 m**  
**HARZBURGITO**

CLASSIFICAÇÃO DA ROCHA:

#### COMPOSIÇÃO MINERALÓGICA

##### ***Mineralogia principal***

**1%**

Olivina

Ortopiroxênio

Antofilita/Cummingtonita

##### ***Mineralogia acessória - <***

Minerais opacos

Serpentina

#### DESCRIÇÃO MICROSCÓPICA

Rocha fortemente serpentizada, onde as ilhas de olivina estão preservadas em meio à textura mesh. Outra forma de ocorrência deste mineral é como inclusões em cristais de ortopiroxênio, onde está mais preservada da serpentização. A granulação da olivina é fina a muito fina (Foto In2) e sua forma predominante é subédrica com vértices arredondados.

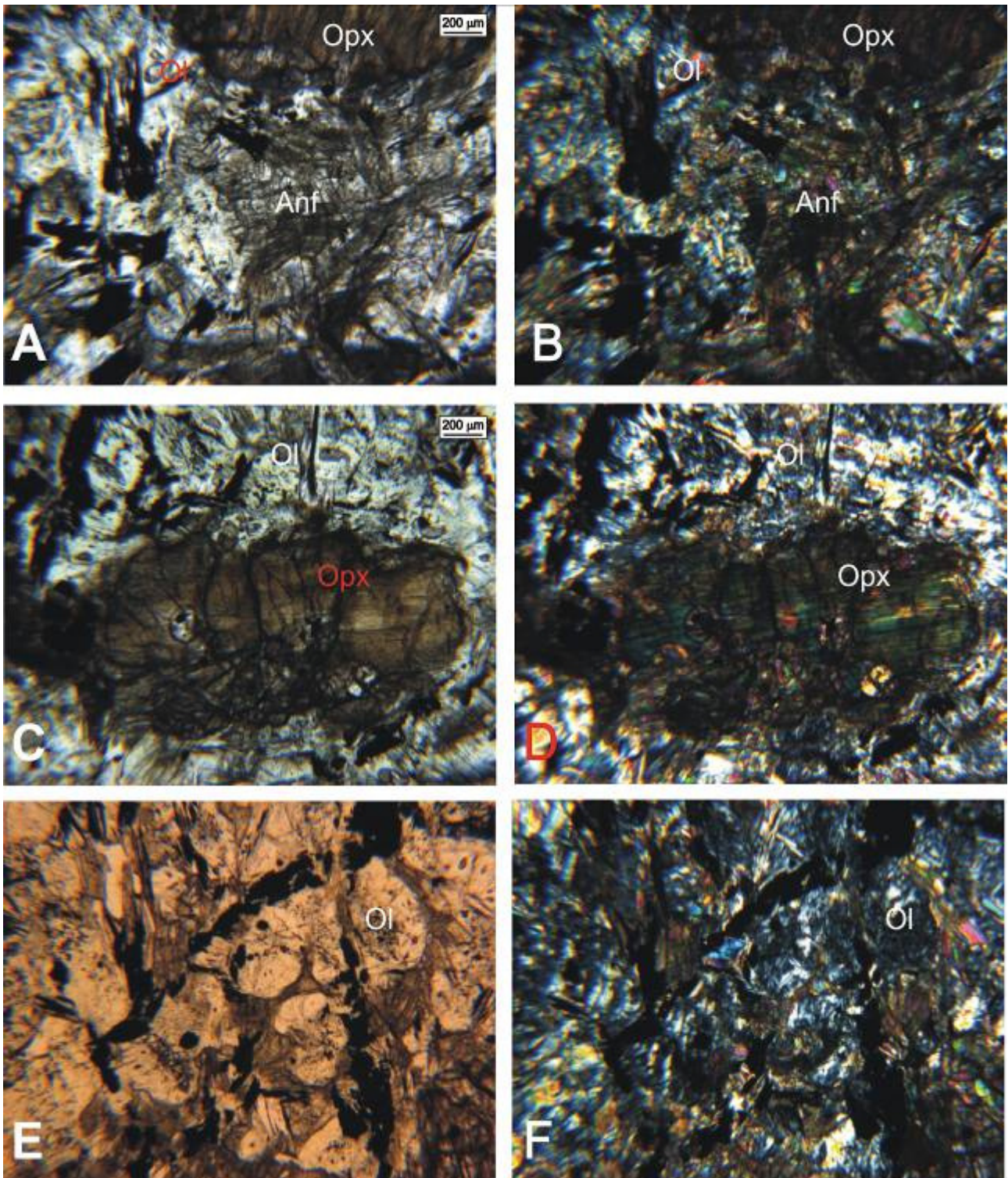
Os cristais de ortopiroxênio estão mais preservados, sendo incolores a rosa/verde pálidos, fraco pleocroísmo, forma subédrica e granulação média (até 4 mm) a fina (< 2 mm); alguns são poiquilíticos.

Nas bordas de cristais de ortopiroxênio ocorrem cristais incolores, forma subédrica de hábito prismático, granulação muito fina, e extinção reta, o que os caracteriza como antofilita; por vezes formam aglomerados de aspecto radiado. Tais cristais também ocorrem dispersos por toda a rocha e onde apresentam extinção oblíqua foram classificados como tremolita (ou cummingtonita).

Os minerais opacos formam pequenos aglomerados aciculares nos planos de clivagem de cristais de bastita, ou são massas de hábito quadrático a arredondados, sendo produto do processo de serpentização.

A lâmina possui 1/4 de área formada predominantemente por olivina (dunito), e os outros 3/4 corresponde a uma mistura ortopiroxênio, olivina e antofilita/cummingtonita de acordo com a ordem de abundância relativa do maior para o menor, traduzindo um cumulado harzburgítico.





Prancha FD 26 – 134,05 m - A e B) Fotomicrografias em luz natural e luz polarizada, respectivamente, mostrando grão de ortopiroxênio em meio a provável material intercumulus formado originalmente por clinopiroxênio, porém transformado para anfibólio e bastita; C e D) Fotomicrografias em luz natural e luz polarizada, respectivamente, exibindo grão poiquilítico de ortopiroxênio em meio a massa de serpentina mesh e bastita; E e F) ) Fotomicrografias em luz natural e luz polarizada, respectivamente, apresentando porção dominada por cristais de olivina fortemente serpentinizados.

## COMPOSIÇÃO MINERALÓGICA

**Mineralogia principal****1%**

Olivina

Ortopiroxênio

Brucita

**Mineralogia acessória - <**

Minerais opacos (Mg e Ptl)

Serpentina

## DESCRIÇÃO MICROSCÓPICA

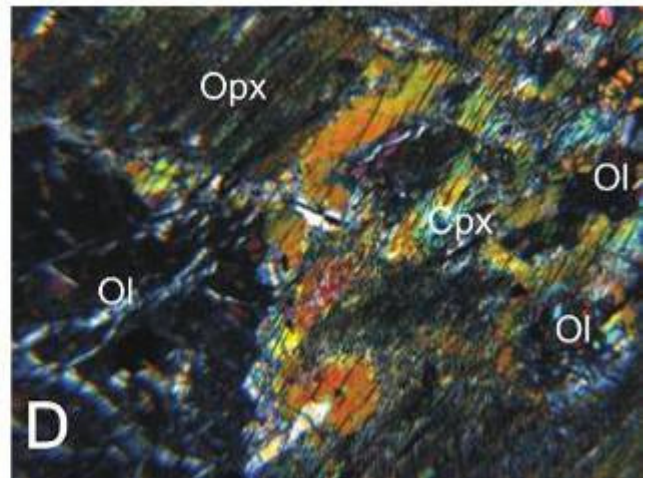
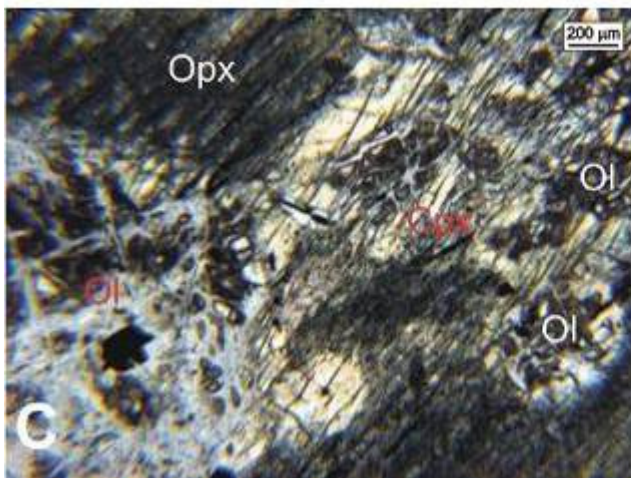
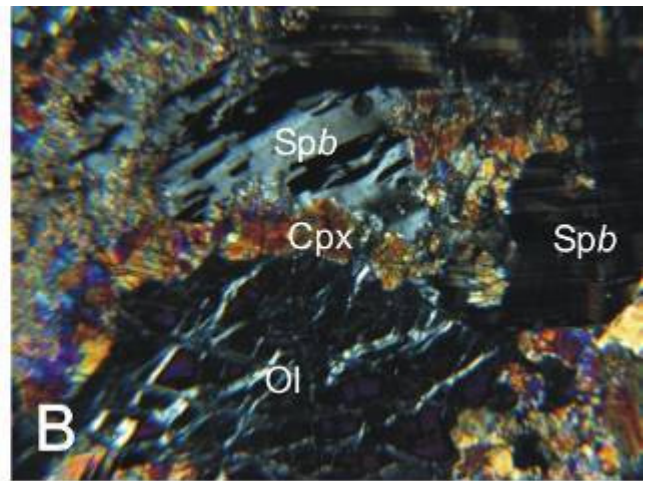
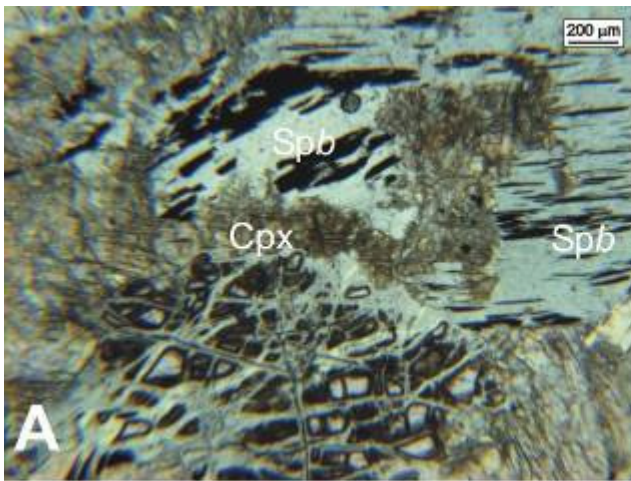
Rocha serpentizada (aprox. 90%), possuindo dois tipos predominantes de serpentina. A primeira corresponde a arranjos com textura mesh (lizardita-crisotila), onde resquícios de cristais de olivina estão presentes. A outra é caracterizada por placas de bastita bem desenvolvidas, alcançando até 4 mm em dimensão, possuindo cores de interferência de 1ª e 2ª ordem, possuindo frequentemente minerais opacos nas linhas de clivagem, e por vezes presença de kinks; extinção ondulante é comum. A forma das bastitas varia de subédrica a anédrica, onde esta última possui hábito ameboidal, caracterizando um material intercumulus e correspondente a antigos cristais de orto e/ou clinopiroxênio. Resquícios de cristais de clino e ortopiroxênio estão presentes, onde o primeiro apresenta as maiores dimensões (4 mm) e por vezes possuem inclusões de cristais de olivina (poiquilíticos).

Alguns cristais de olivina apresentam bordas com clinopiroxênio, este caracterizando um material intercumulus, inclusive para cristais de ortopiroxênio (bastita).

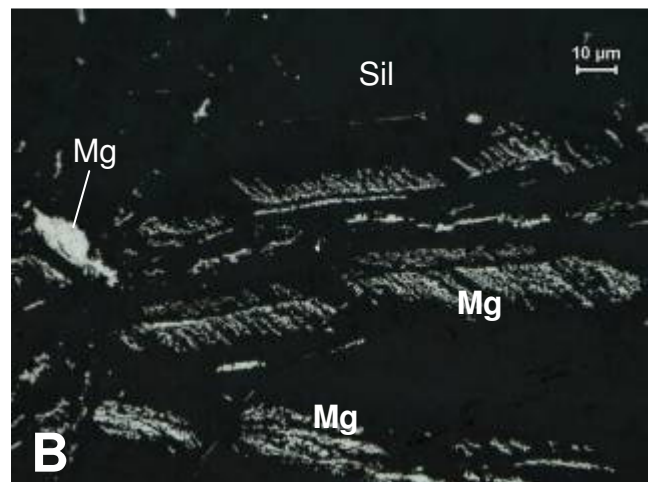
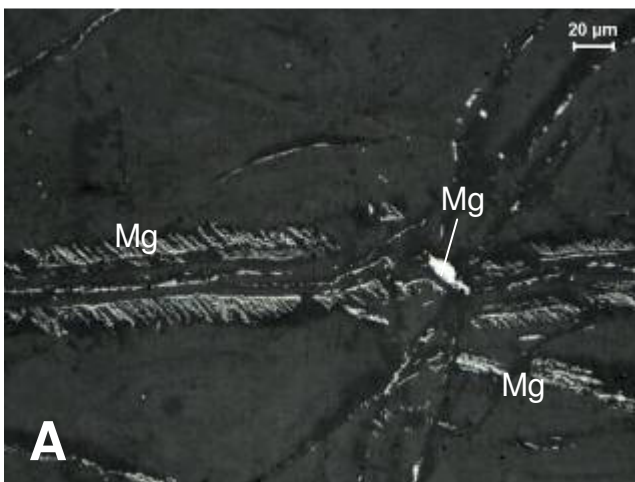
Os minerais opacos são frequentes e representados principalmente por magnetita, que ocorre comumente nas linhas de clivagem dos cristais de bastita, com hábito esquelético predominante.

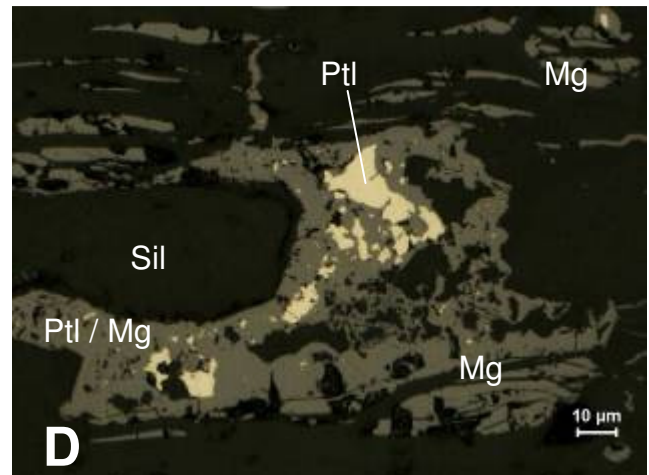
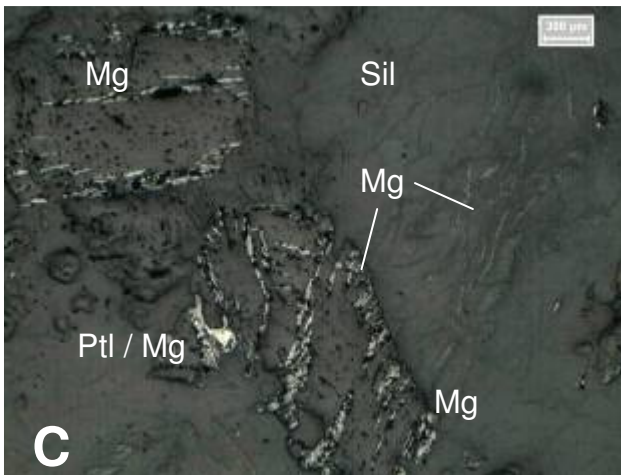
A granulação geral é média e o arranjo textural dos cristais mostra que a rocha trata-se de um cumulado de olivina e ortopiroxênio, tendo ainda clinopiroxênio como material intercumulus, caracterizando assim um harzburgito-lherzolito.





Prancha FD 26 – 152,90 m - A e B) Fotomicrografias em luz natural e luz polarizada, respectivamente, mostrando a mineralogia principal da rocha transformada para minerais do grupo da serpentina (serpentina mesh e bastita); C e D) Fotomicrografias em luz natural e luz polarizada, respectivamente, apresentando cristais de olivina, ortopiroxênio e clinopiroxênio, este último de caráter poiquilítico (cadacristais- inclusões- de olivina).





Prancha FD 26 – 152,90 m – Opacos – A) Magnetita (Mg) esquelética muito fina alinhada segundo as linhas de clivagem das bastitas; B) Detalhe da imagem anterior; C) Magnetita (Mg) mais bem desenvolvida alinhada segundo as linhas de clivagem de silicatos e cristal de pentlandita (Ptl) alterando-se para magnetita; D) Detalhe do cristal de pentlandita (Ptl) alterando-se para magnetita (Mg).

AMOSTRA: **FD 26 – 167,65 m**  
**HARZBURGITO**

CLASSIFICAÇÃO DA ROCHA:

#### COMPOSIÇÃO MINERALÓGICA

##### ***Mineralogia principal***

Olivina

##### ***Mineralogia acessória - < 1%***

Brucita, Ortopiroxênio,

Anfibólios, Serpentina

Minerais opacos (Mg, Po, Cr, Lm)

#### DESCRIÇÃO MICROSCÓPICA

Rocha composta por olivina, ortopiroxênio e clinopiroxênio num arranjo textural tipo cumulático. A fase cumulus é representada por olivina, que apresentam cristais de granulação média (2 a 5 mm), subédricos a euédricos, a maioria com vértices arredondados, e quase totalmente transformados para serpentina e magnetita. Internamente em alguns cristais de olivina ocorre faixas de coloração amarelo acastanhado pálido a esverdeado, caracterizada como brucita ( $Mg(OH)_2$ ).

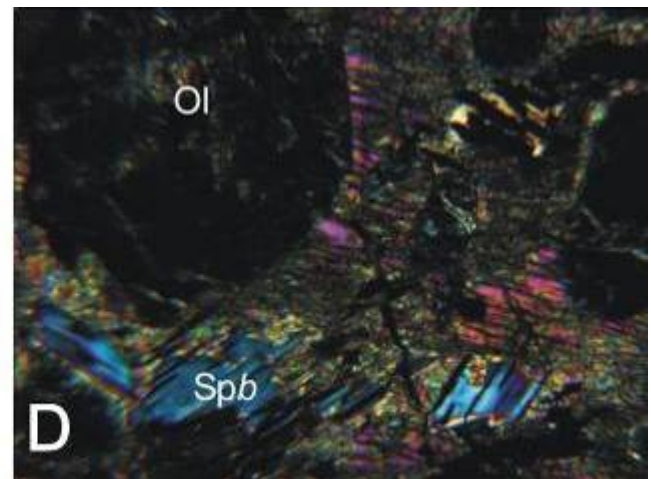
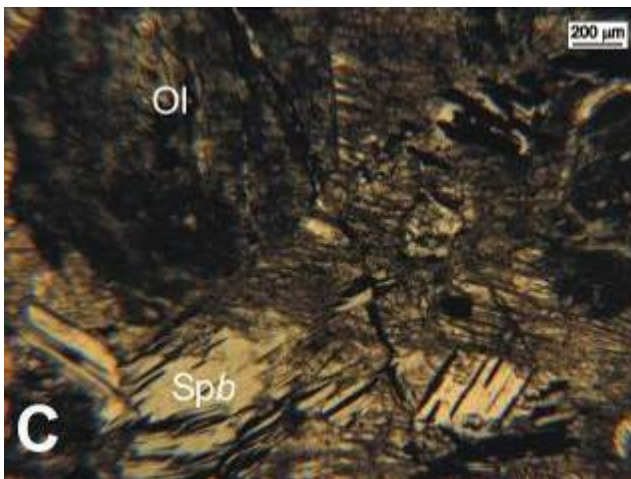
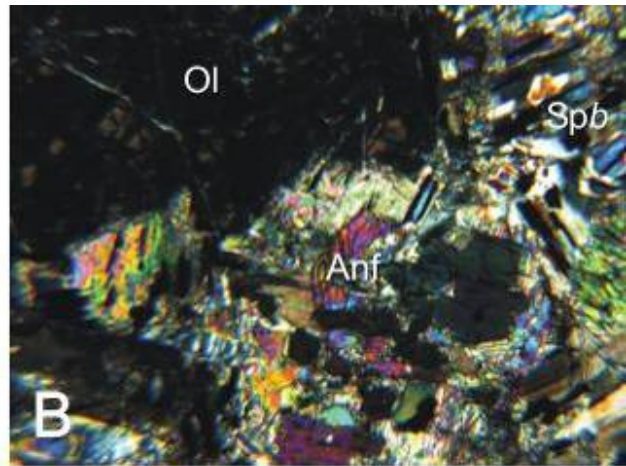
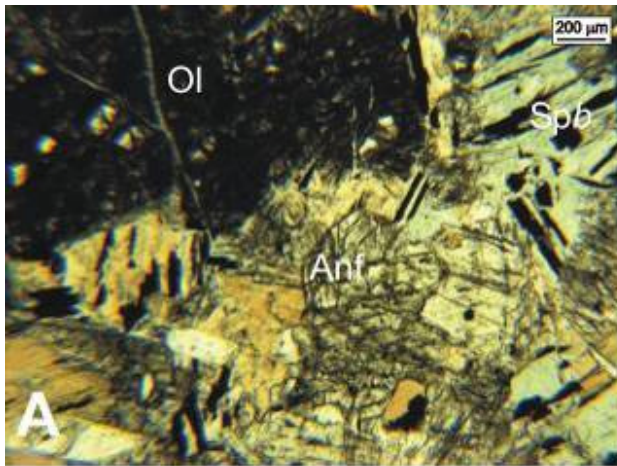
O material intercumulus é representado por cristais de ortopiroxênio e bastita. O primeiro apresenta forma ameboidal, salpicado por diminutos minerais opacos, além de conter inclusões ultrafinas ( $\ll 1$  mm) de olivina fortemente serpentinizada. Tal mineral por vezes é transformado para bastita, que corresponde a um mineral lamelar, incolor a castanho pálido, granulação fina a muito fina, possuindo em suas linhas de clivagem minerais opacos aciculares – magnetita. Comumente apresentam extinção em bandas e *kinks*, em cores de interferência variadas (desde baixa até alta).

O principal opaco observado é a magnetita, que ocorre como produto de alteração dos silicatos, segundo suas linhas de clivagem, algumas vezes já oxidada para hidróxidos de ferro. A cromita ocorre de forma restrita, principalmente como cristais subédricos arredondados de cerca de 10 micrometros. Como sulfeto identificou-se a pirrotita com tamanho variando de 01 micrometro a 40 micrometros. A pirrotita se apresenta com alteração para magnetita a partir das bordas e fraturas.

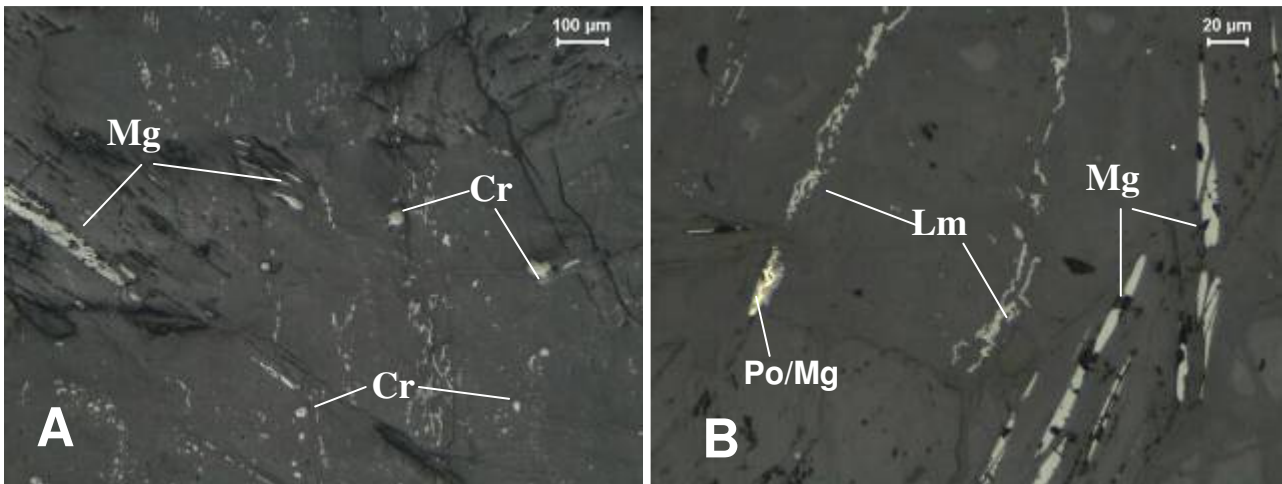
Localmente, em meio ao material intercumulus, ocorrem cristais de anfibólio, incolor, granulação fina ( $< 2$  mm) a muito fina ( $< 1$  mm), hábito tabular a prismático, associado com bastitas, que podem representar biotita, pois apresentam altas cores de interferência e *bird eyes*.



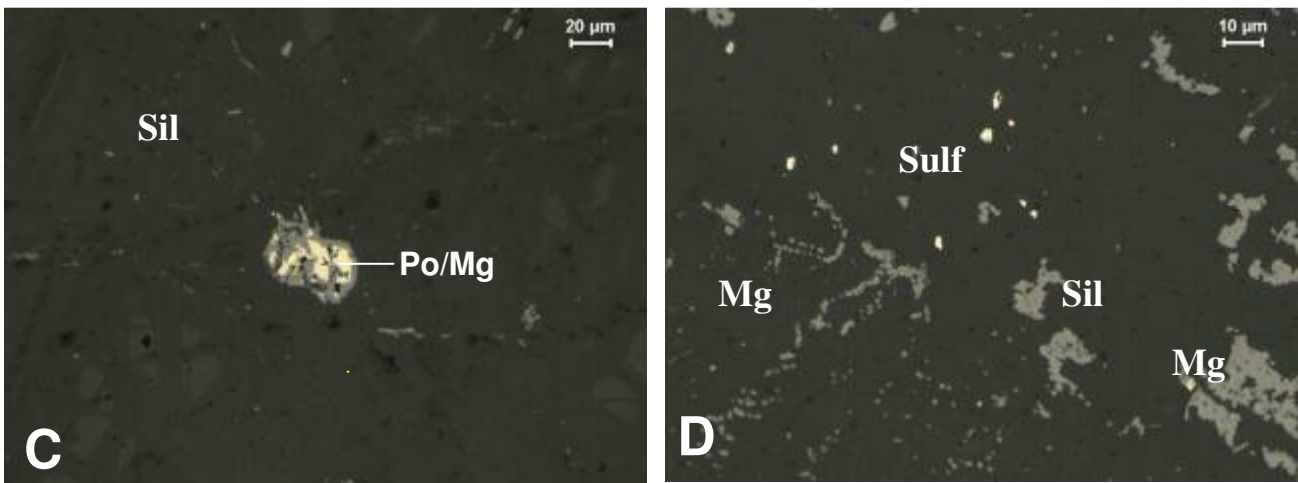
O arranjo textural e a composição modal, estimada na ordem de 70% de olivina e 30% de ortopiroxênio, caracterizam a rocha como olivina cumulado, de composição harzburgítica a olivina ortopiroxenito.



Prancha FD 26 – 167,65 m- A e B) Fotomicrografia mostrando cristais de olivina, bastita e anfibólio, em luz natural e luz polarizada, respectivamente; C e D) Fotomicrografias em luz natural e luz polarizada, respectivamente, exibindo cristais arredondados de olivina em meio a cristais de bastita (Spb), provavelmente representando antigos cristais de ortopiroxênio.



Prancha FD 26 – 167,65 m – Opacos – A) vista geral da forma de ocorrência da cromita (cinza claro arredondada) e da magnetita estirada (Mg); B) vista geral da forma de ocorrência da magnetita (Mg) substituindo silicatos, além de hidóxidos de ferro (cinza claro).



Prancha FD 26 – 167,65 m – Opacos – C) outro local da seção polida, com um dos raros cristais de pirrotita (Po) alterando-se para magnetita; D) Finos cristais de sulfetos associados à magnetita.

## COMPOSIÇÃO MINERALÓGICA

**Mineralogia principal**

Olivina

Serpentina

Piroxênio

Anfibólios (cummingtonita)

**Mineralogia acessória - < 1%**

Clorita

Talco

Minerais opacos (Mg, Ilm, Po, Ptl e Cp)

Carbonato

## DESCRIÇÃO MICROSCÓPICA

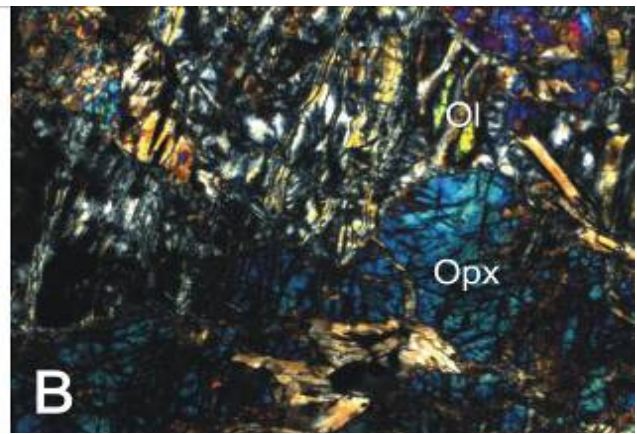
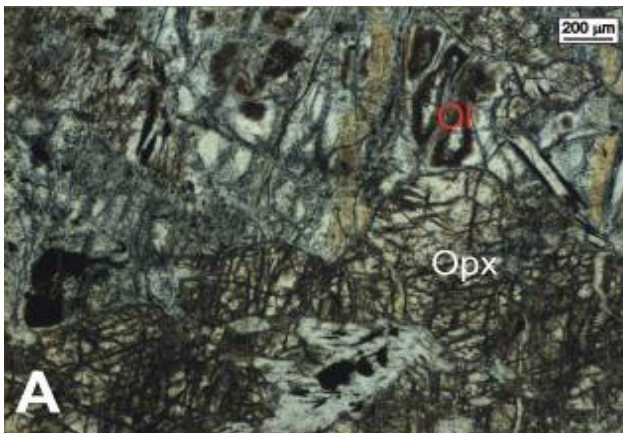
Rocha fortemente serpentizada, cuja mineralogia original retrata olivina de forma predominante e, subordinadamente, piroxênio. A serpentina corta a rocha sob a forma de finas vênulas de até 2 mm de largura, apresentando internamente dois tipos de arranjo, um do tipo radiado de fibras de serpentina e outro lembrando *comb texture*.

Cristais prismáticos de cummingtonita, com até 2 mm em dimensão. Os minerais opacos ocorrem finamente salpicados internamente no grão de anfibólio (Foto In1 e Ip1).

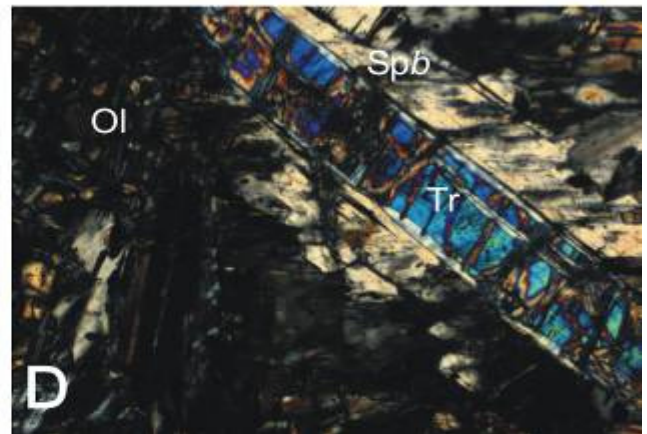
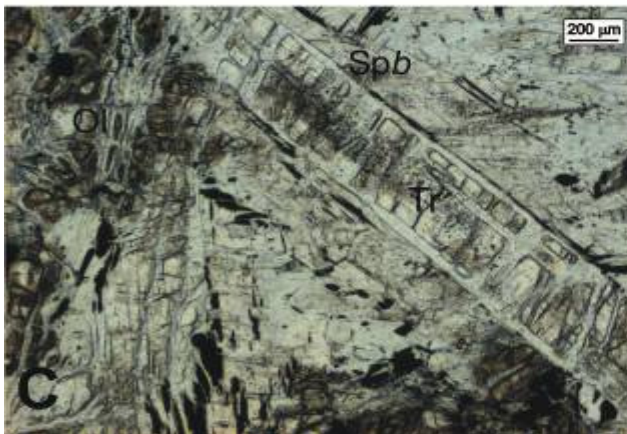
Os restos de anfibólio, determinados pelas linhas de clivagem a 60 e 120 e/ou pela forma mais prismática dos cristais, são predominantes. Por vezes formam aglomerados irregulares de cristais, lembrando um material intercumulus, no entanto, as terminações de algumas dessas massas são retas, indicando crescimento metamórfico.

Os minerais opacos possuem duas formas distintas de ocorrência: a primeira corresponde a cristais de ilmenita, com limites regulares, lisos, de hábito quadrático a arredondado, por vezes inclusos em cristais de olivina, e a segunda caracterizam cristais aciculares a prismáticos, com limites irregulares, traduzindo a magnetita oriunda da serpentização. Foram identificados, ainda, pirrotita, pentlantida e calcopirita. Os primeiros sulfetos alteram-se para magnetita a partir das bordas e fraturas. A calcopirita foi observada apenas como inclusões na pirrotita.

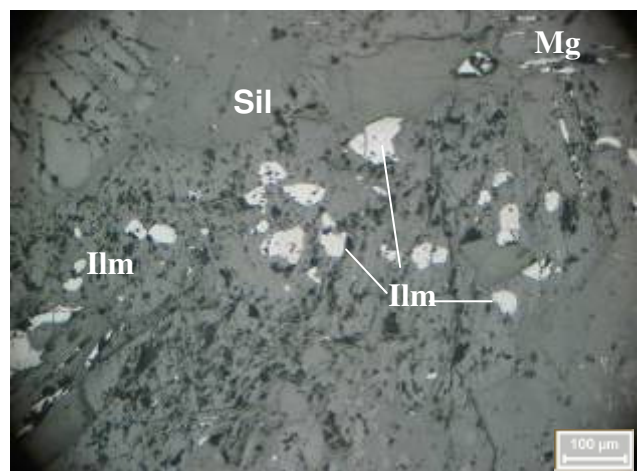
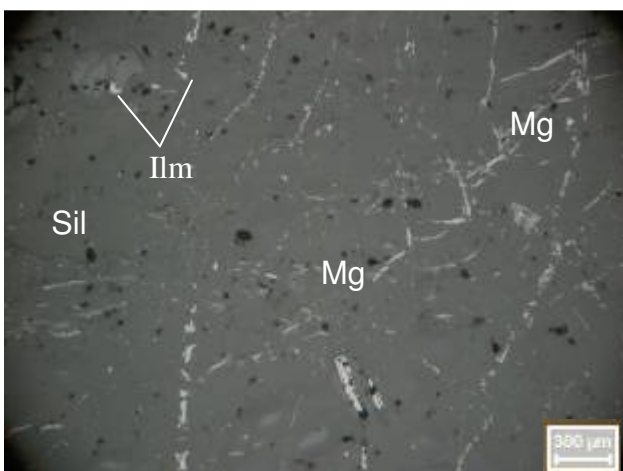




Prancha FD 26 – 179,60m – A e B) Fotomicrografia exibindo, em luz natural e luz polarizada, respectivamente cristais de olivina e ortopiroxênio, a primeira alterada para serpentina;

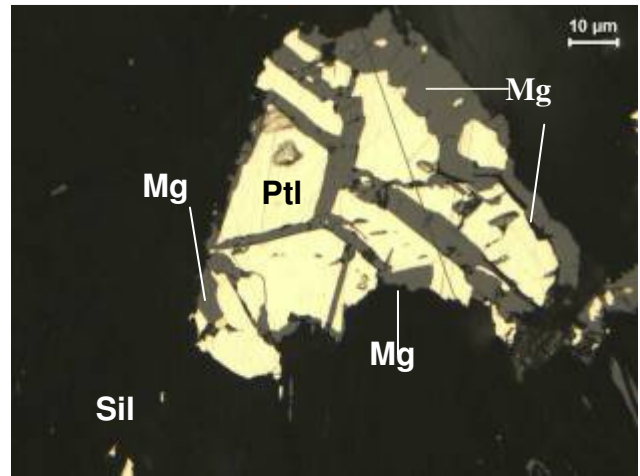
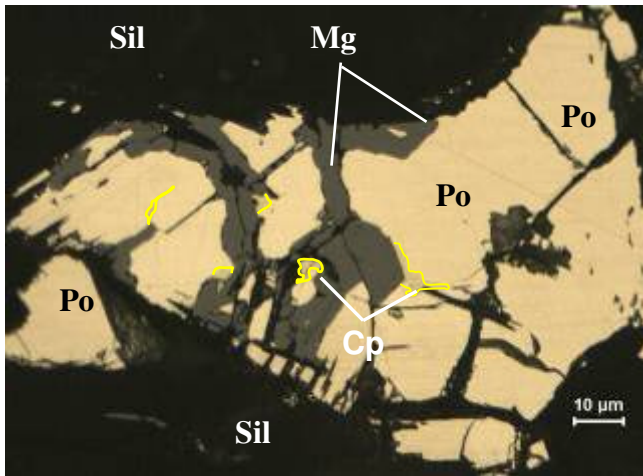


Prancha FD 26 – 179,60m – C e D) Fotomicrografias em luz natural e luz polarizada, respectivamente, exibindo grão prismático de tremolita em meio a placas de bastita; resquício de olivina pode ser visto na porção superior esquerda da imagem.



Prancha FD 26 – 179,60m – A) Visão geral, com magnetita (Mg) substituindo silicatos e

rara ilmenita (Ilm); B) Cristais de ilmenita (Ilm) próximos a cristais alongados de magnetita;



Prancha FD 26 – 179,60m – C) Grande cristal de pirrotita (Po) alterando-se para magnetita (Mg) e com exsoluções de calcopirita (áreas em amarelo). Imagem a óleo e sem polarização; D) pentlandita (Ptl) alterando-se magnetita (Mg). Imagem a óleo e sem polarização.

AMOSTRA: **FD 26 – 205,00 m** CLASSIFICAÇÃO DA ROCHA: **ANFIBOLITO** (olivina melagabro cisalhado)

## COMPOSIÇÃO MINERALÓGICA

### **Mineralogia principal**

Actinolita/Tremolita: 65%

Plagioclásio: 35%

### **Mineralogia acessória - < 1%**

Olivina + talco + clorita

Opacos (Mg)

## DESCRIÇÃO MICROSCÓPICA

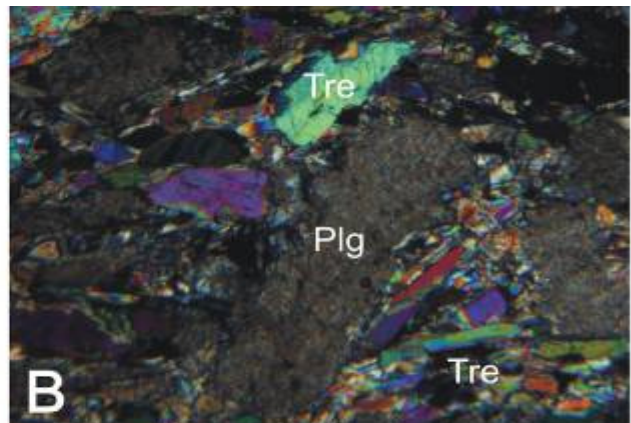
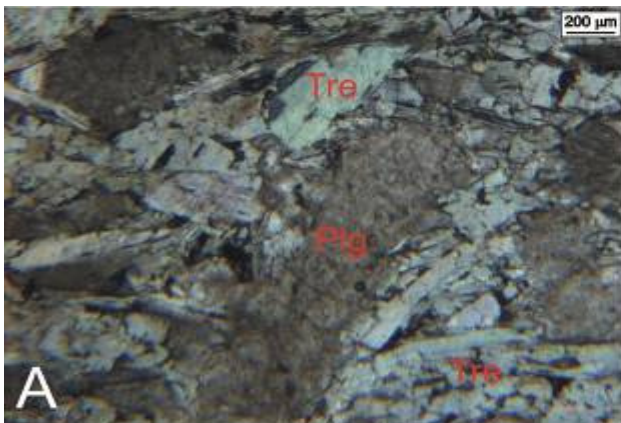
Rocha foliada, composta predominantemente por tremolita/actinolita e plagioclásio, tendo como acessórios: talco, olivina e minerais opacos. A foliação é definida pela orientação preferencial dos eixos maiores dos cristais de tremolita, enquanto os cristais de plagioclásio ocorrem como porfiroclastos em meio aos planos de foliação. A tremolita tem forma subédrica, granulação fina a ultrafina, em cristais tabulares e aciculares.

O plagioclásio corresponde a cristais fortemente saussuritizados, com forma anédrica a subédrica, granulação fina (1 a 2 mm) a muito fina (< 1 mm), onde pode se identificar os restos de geminação polissintética do mineral primário. Localmente são vistos alguns cristais de olivina, de granulação fina, forma subédrica de aspecto sigmoidal, aspecto zonado. A clorita ocorre em meio a cristais de tremolita, com hábito lamelar a acicular, granulação ultrafina. O talco de ocorrência local está associado a cristais de tremolita, parecendo ser um produto de transformação da tremolita.

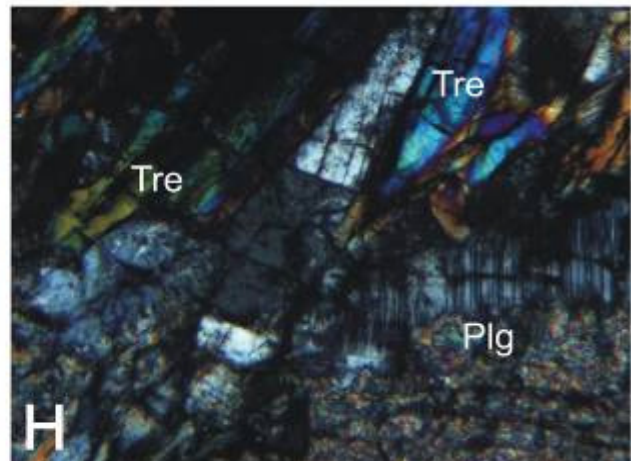
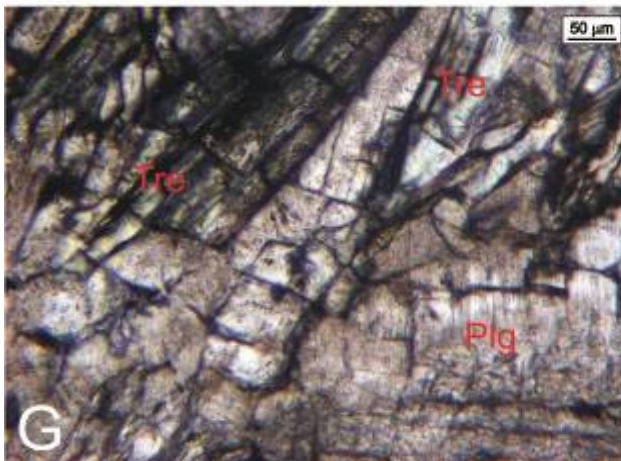
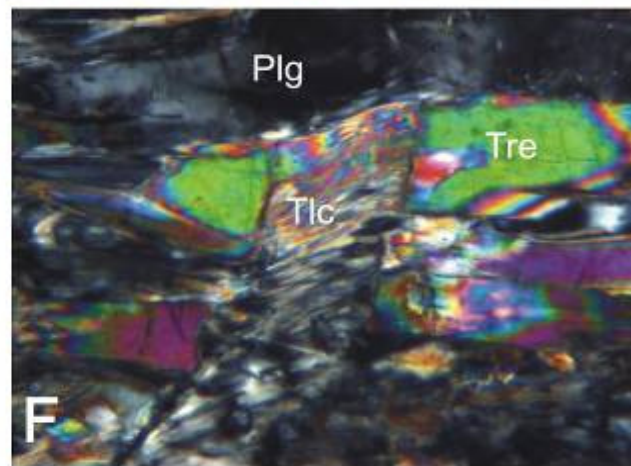
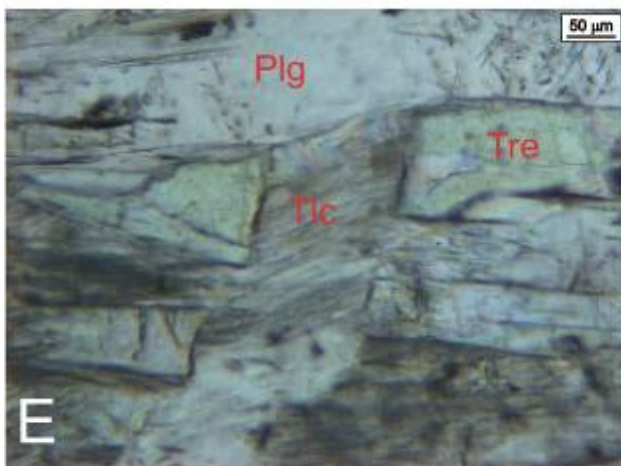
Os minerais opacos correspondem à fina poeira sobre cristais de plagioclásio saussuritizado ou nas linhas de clivagem da tremolita, tratando-se de magnetita como mineral secundário. Não foi identificado nenhum mineral opaco de caráter primário (magmático).

As presenças de plagioclásio e tremolita como minerais principais e olivina como acessório caracterizam a natureza da rocha como olivina metagabro foliado. Possui textura granonematoblástica, cuja assimetria de alguns *augens* de plagioclásio aliado ao crescimento sin-cinemático de alguns cristais de anfibólio, demonstram que a foliação metamórfica se formou sob condições de cisalhamento, em fácies xisto-verde a anfibolito.





Prancha FD 26 – 205,00 m - A e B) Fotomicrografia em luz natural e luz polarizada, respectivamente, onde grão subédrico de plagioclásio encontra-se totalmente saussuritizado e com orientação oblíqua a foliação/bandamento da rocha.



Prancha FD 26 – 205,00 m C e D) Fotomicrografia em luz natural e luz polarizada, respectivamente, exibindo grão de ortopiroxênio com kink band, marcada por extinção ondulante; E e F) Fotomicrografia em luz natural e luz polarizada, respectivamente, mostrando grão de plagioclásio saussuritizado com resquício de geminação polissintética na borda.

AMOSTRA: **FD 26 - 260,50 m**  
**LEUCOGABRO**

CLASSIFICAÇÃO DA ROCHA:

#### COMPOSIÇÃO MINERALÓGICA

##### ***Mineralogia acessória - < 1%***

##### ***Mineralogia principal***

Actinolita+Tremolita+Hornblenda

Clorita

Plagioclásio

Biotita

#### DESCRIÇÃO MICROSCÓPICA

Rocha composta predominantemente por plagioclásio, com moderada saussuritização e geminação polissintética (herança do mineral primário). Compõe-se por anfibólio, tendo como acessório clorita/biotita e minerais opacos. O anfibólio ocorre tanto como hornblenda como tremolita/actinolita. A hornblenda se caracteriza por cristais subédricos de granulação fina (< 2 mm), ocorrendo de forma isolada ou em aglomerados tipo mosaico. Está comumente transformada em suas bordas ou centros para anfibólio acicular. Os cristais de plagioclásio estão parcialmente saussuritizados e frequentemente exibem geminação polissintética e extinção ondulante, além de granulação fina a ultrafina e forma predominantemente subédrica.

AMOSTRA: **FD 26 – 220,00 m**

CLASSIFICAÇÃO DA ROCHA: **TREMOLITITO (PIROXENITO)**

#### COMPOSIÇÃO MINERALÓGICA

##### ***Mineralogia principal***

Actinolita/Tremolita

Ortoanfíbólio (antofilita ou gedrita?)

##### ***Mineralogia acessória - < 1%***

Clorita+ biotita

Opacos (Mg)

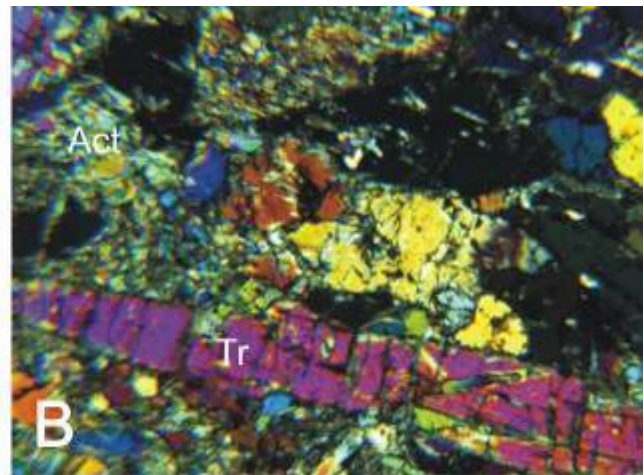
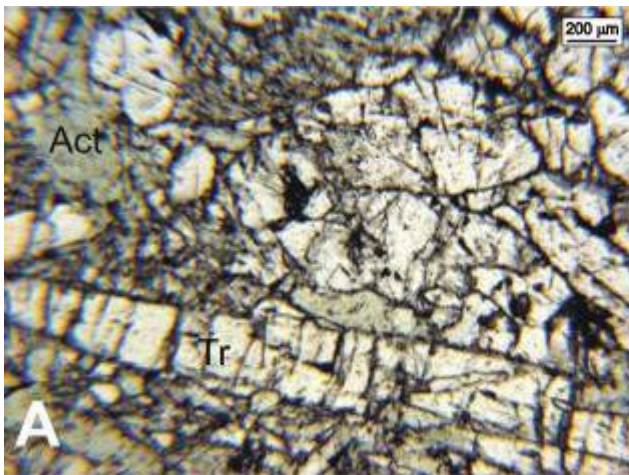
#### DESCRIÇÃO MICROSCÓPICA

Rocha composta predominantemente por cristais de anfíbólio de forma subédrica a euédrica, granulação média, onde alguns cristais alcançam até 4 mm em dimensão, sendo caracterizados como tremolita (cummingtonita) e actinolita muito fina e forma euédrica a anédrica. Tais minerais estão em contato mútuo e também imersos numa massa de cristais muito finos de anfíbólio mostrando uma orientação preferencial incipiente, que define uma foliação principal e textura diablástica. Alguns cristais euédricos de anfíbólio formam porfiroblastos envoltos pela massa muito fina definindo uma foliação do tipo anastomosada. Tais cristais possuem bordas transformadas para biotita. Textura diablástica.

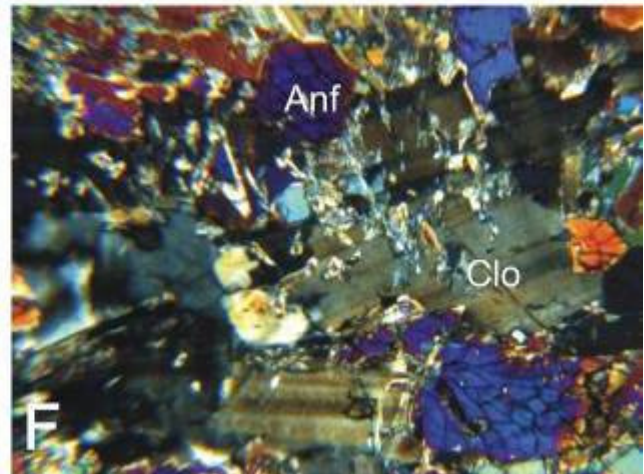
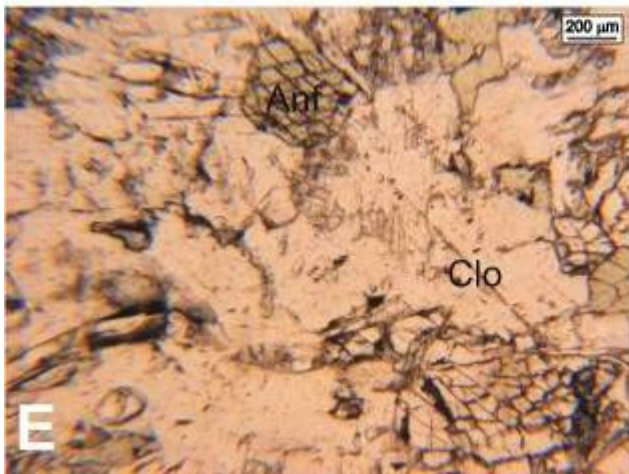
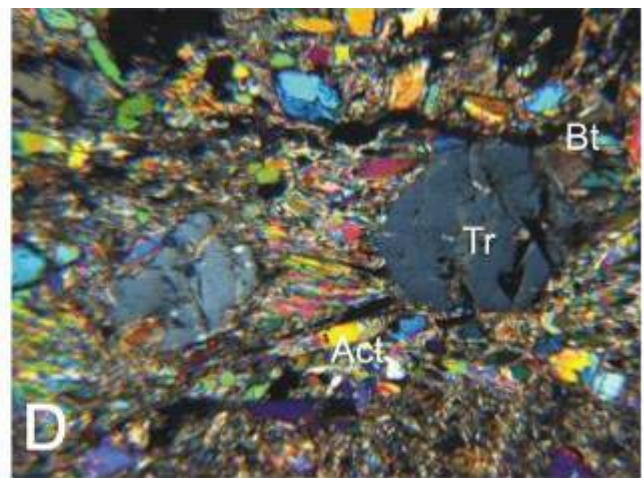
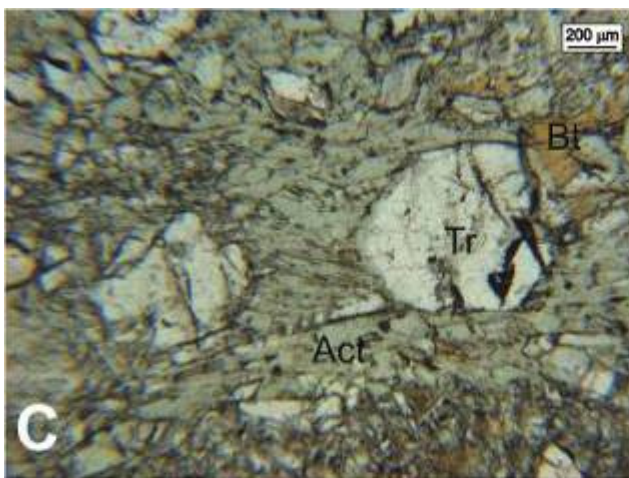
Minerais opacos são ultrafinos, hábito prismático, forma predominantemente subédrica, ocorrendo de forma rara e esparsa na rocha. Os opacos ocorrem também como fina poeira em linhas de clivagem de cristais de anfíbólio.

A rocha trata-se de um tremolitito, cuja paragênese mineral dada por tremolita-actinolita-clorita posiciona a rocha em fácies xisto verde, onde a presença de biotita aponta para mais altas condições desta fácies (Best, 2003).





Prancha FD 26 – 220,00 m – A e B) Fotomicrografias em luz natural e luz polarizada, respectivamente, exibindo cristais prismáticos de tremolita e tabulares de actinolita;



Prancha FD 26 – 220,00 m – C e D) Fotomicrografias em luz natural e luz polarizada, respectivamente, mostrando cristais subédricos de tremolita envoltos por cristais de actinolita, e mais raramente biotita, que definem o plano de foliação principal da rocha; E e F) Fotomicrografias em luz natural e luz polarizada, respectivamente, com presença de cristais de clorita em meio a cristais de anfibólio.

Anexo IV – Microscopia Eletrônica de Varredura - MEV

**1. AMOSTRA FD-02 44,00m**

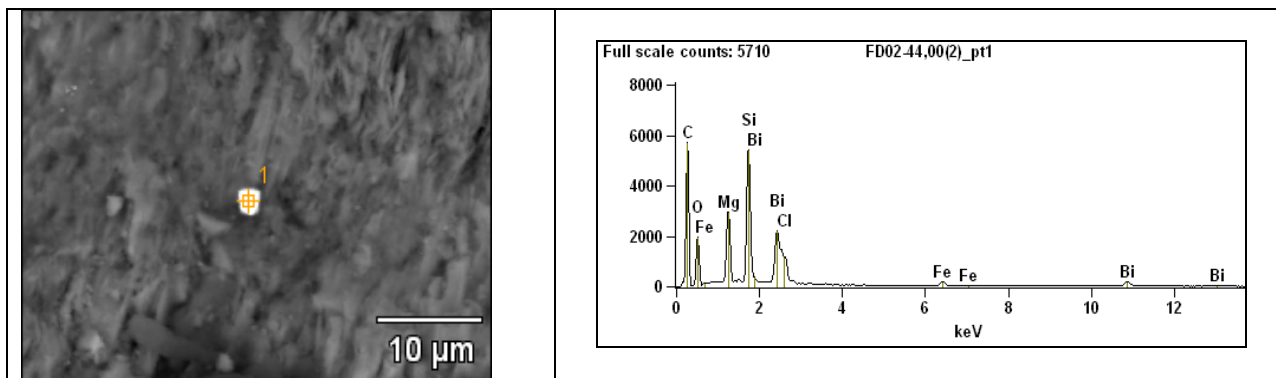


Figura 1.1: Detalhe da inclusão de cloreto de bismuto - Bismoclita (?) na serpentina. Ampliação 2.700x.

Weight %

	<i>Cl-K</i>	<i>Bi-M</i>
<b>FD02-44,00(2)_pt1</b>	15.44	84.56

Figura 1.1-A: Microanálises referentes ao cloreto de Bi - Bismoclita (?) da figura 1.1.

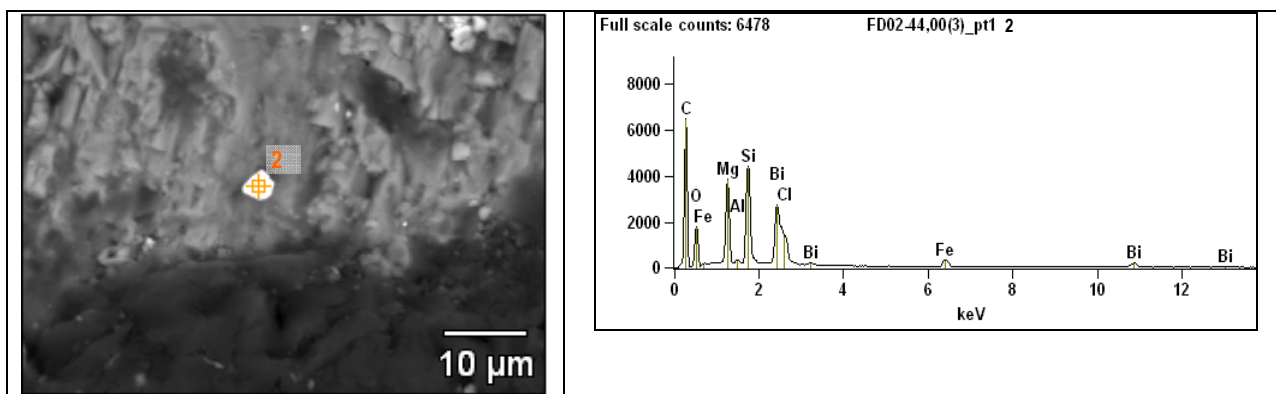


Figura 1.2: Detalhe da inclusão de cloreto de bismuto - Bismoclita (?) na serpentina. Ampliação 1.900x.

Weight %

	<i>Cl-K</i>	<i>Bi-M</i>
<b>FD02-44,00(3)_pt2</b>	15.80	84.20

Figura 1.2-A: Microanálises referentes ao cloreto de Bi - Bismoclita (?) da figura 1.2.

Resumo dos minerais de interesse encontrados na Amostra FD02 - 44,00m



MINERAL PROVÁVEL	COMPOSIÇÃO PROVÁVEL	COMPOSIÇÃO QUÍMICA analisada EDS			Arquivo
		O	Cl	Bi	
Bismoclita (?)	BiOCl	8,91	14,28	76,81	01
		8,91	13,95	77,14	02

## 2. AMOSTRA FD-02 44,50m

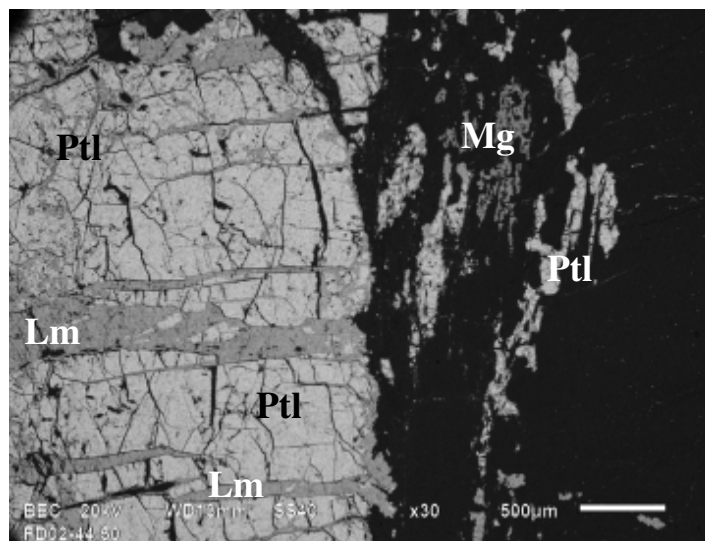


Figura 2.1: Aspecto geral da pentlandita (Ptl) com alteração para limonita (Lm). Ampliação 30x.

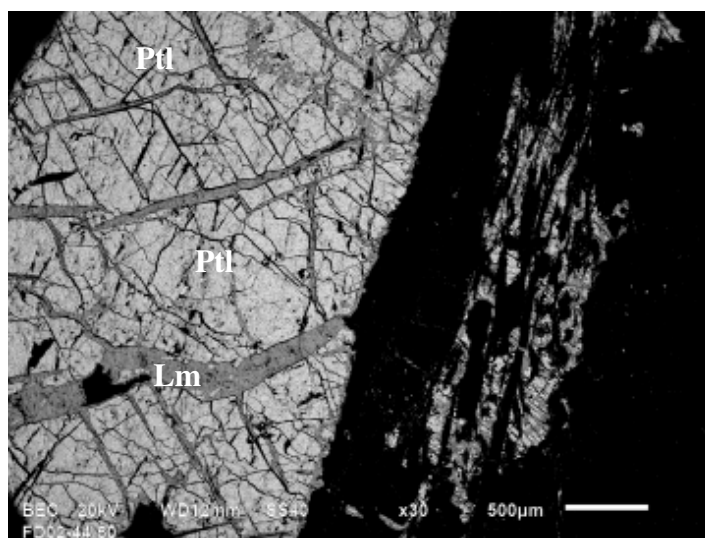


Figura 2.2: Outro local da lâmina com pentlandita alterando-se para limonita. Ampliação 30x.

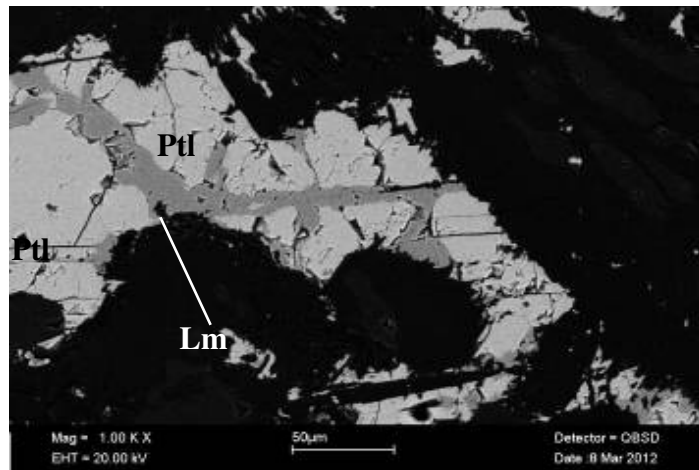


Figura 2.3: Outro local com pentlandita alterando-se para limonita. Ampliação 1.000x.

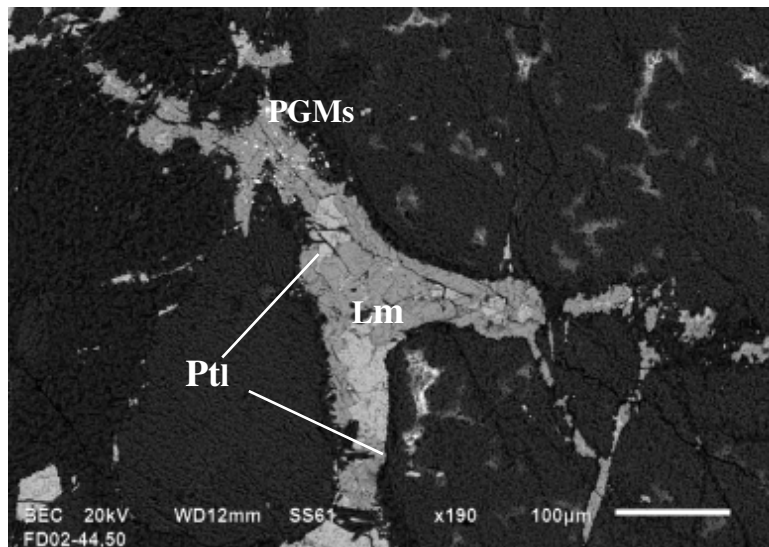


Figura 2.3: Pentlandita alterando para limonita, com inclusões de vários teluretos e PGMs. Ampliação 190x.

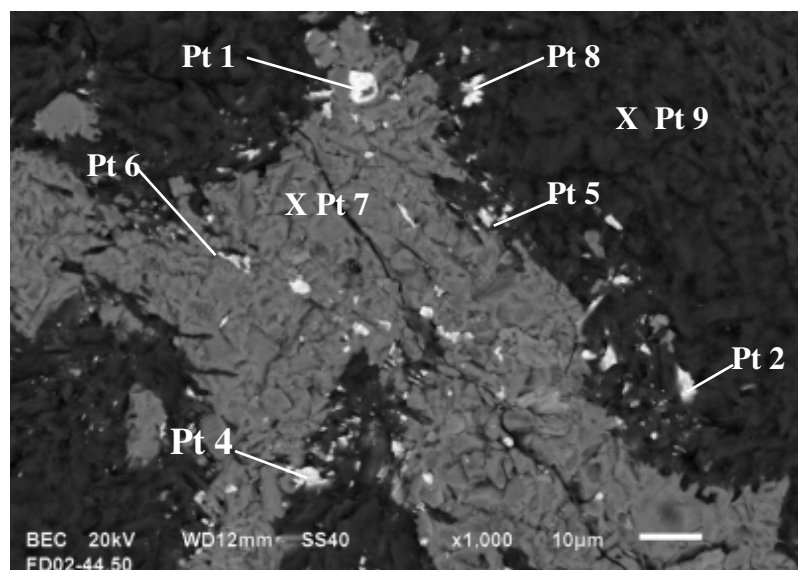
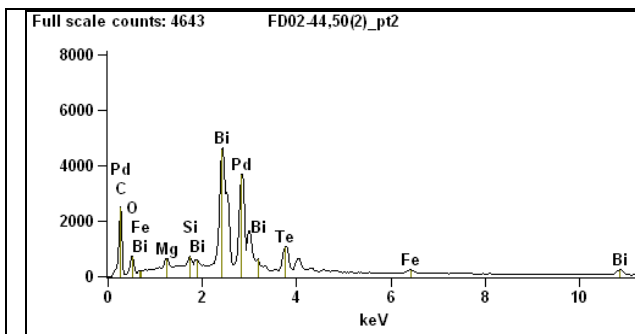
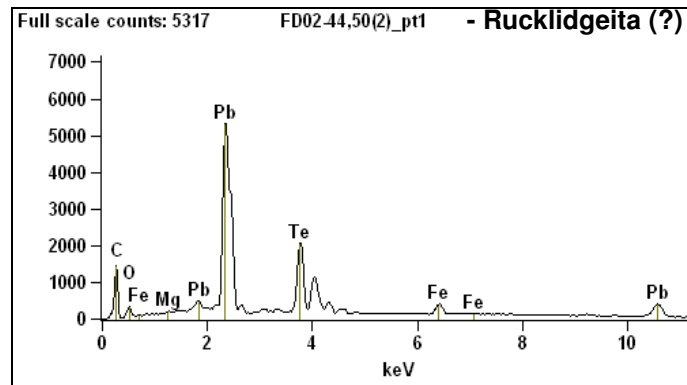
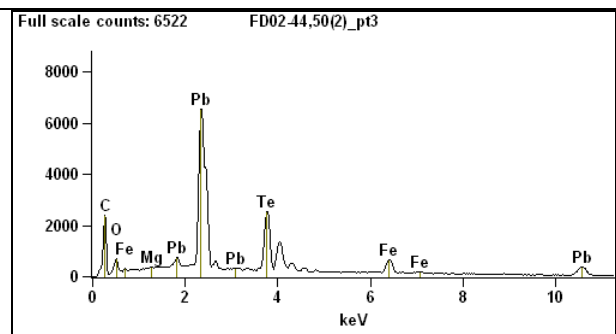


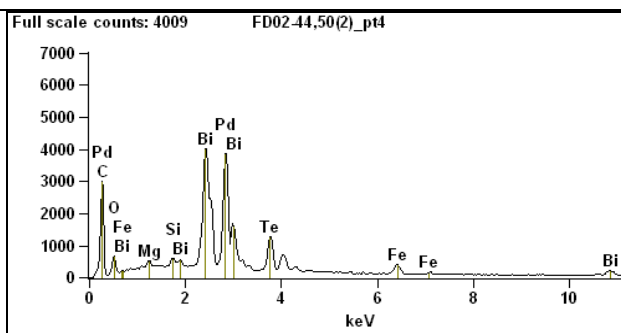
Figura 2.4: Inclusões de vários teluretos e PGMs na limonita da imagem 03. Ampliação 1.000x.



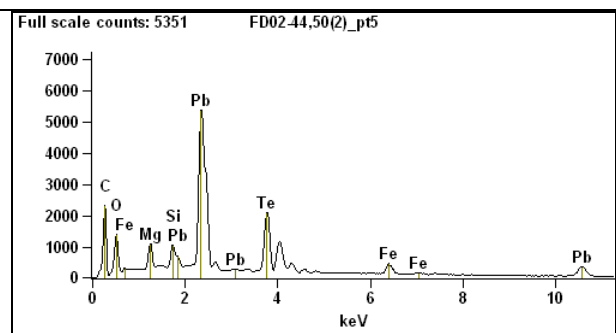
- Kotulskita(?)



- Altaíta (?)

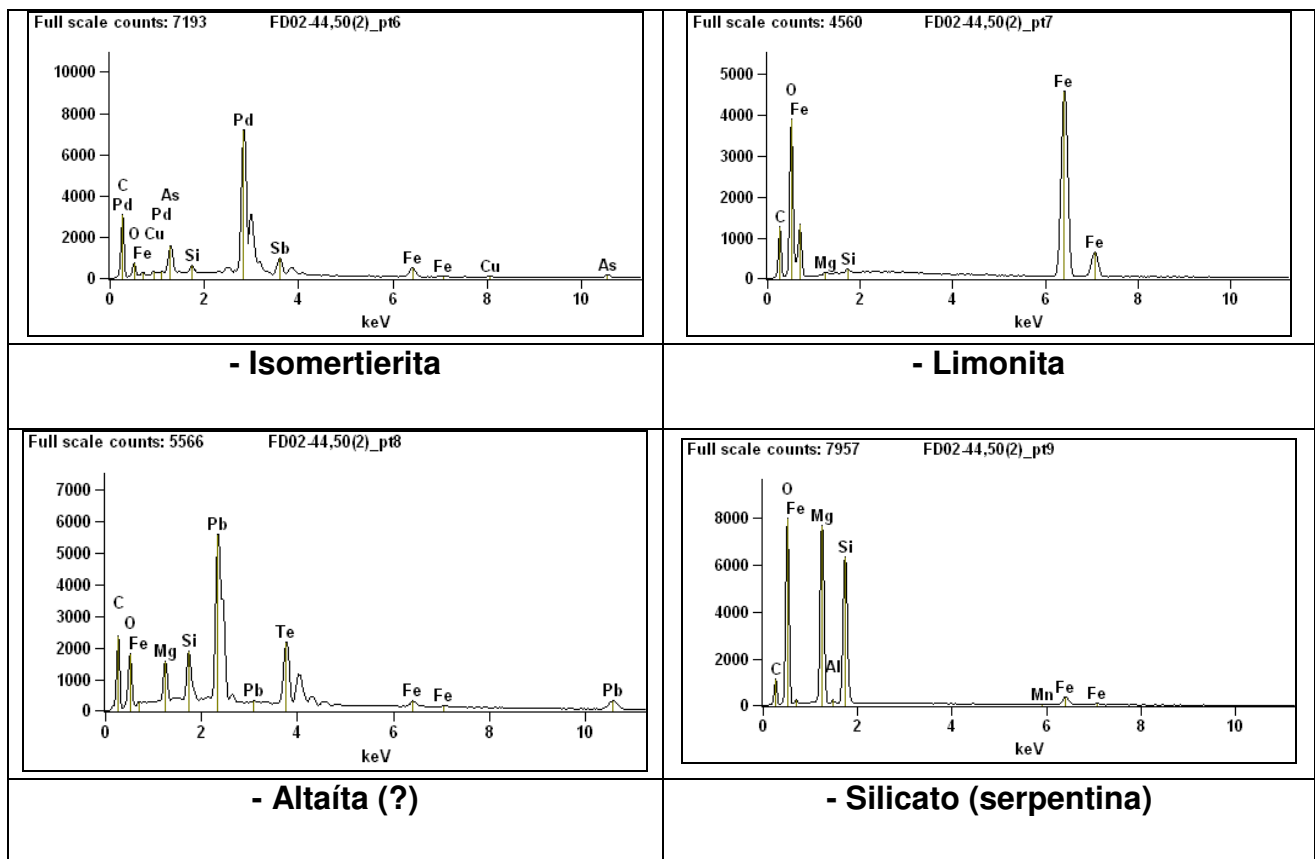


- Kotulskita (?)



- Altaíta (?)





	Weight %						
	As	Pd	Sb	Te	Re	Pb	Bi
FD02-44,50(2)_pt1				39.67	0.00	59.53	0.80
FD02-44,50(2)_pt2		38.98		19.14			41.88
FD02-44,50(2)_pt3				45.55		54.45	
FD02-44,50(2)_pt4		40.86		22.50			36.64
FD02-44,50(2)_pt5				44.67		55.33	
FD02-44,50(2)_pt6	7.99	74.56	17.45				
FD02-44,50(2)_pt8				45.77		54.23	

Figura 2.4-A: Microanálises referentes aos PGMs e teluretos da figura 2.4.

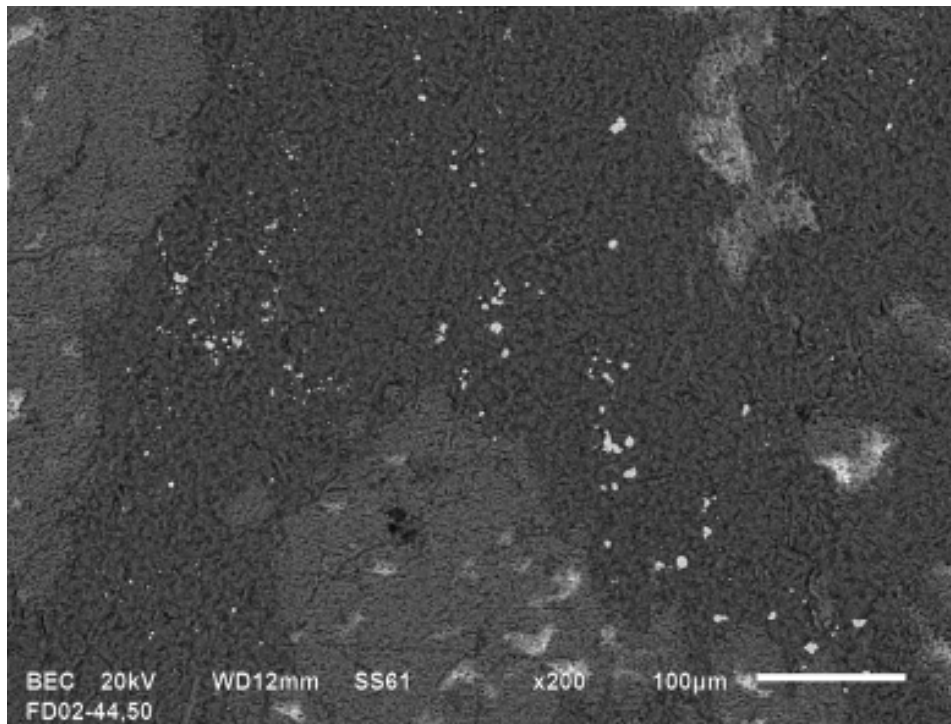


Figura 2.5: Vários cristais de magnetita disseminados na serpentina. Ampliação 200x.

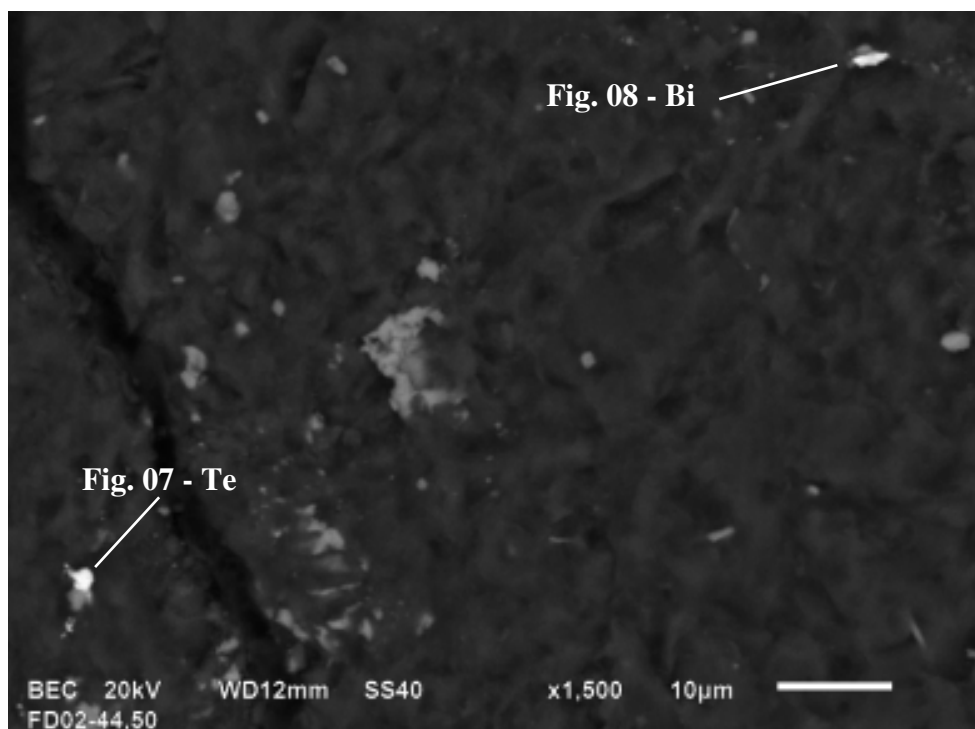


Figura 2.6: Inclusões de bismuteto e telureto na serpentina. Ampliação 1.500x.

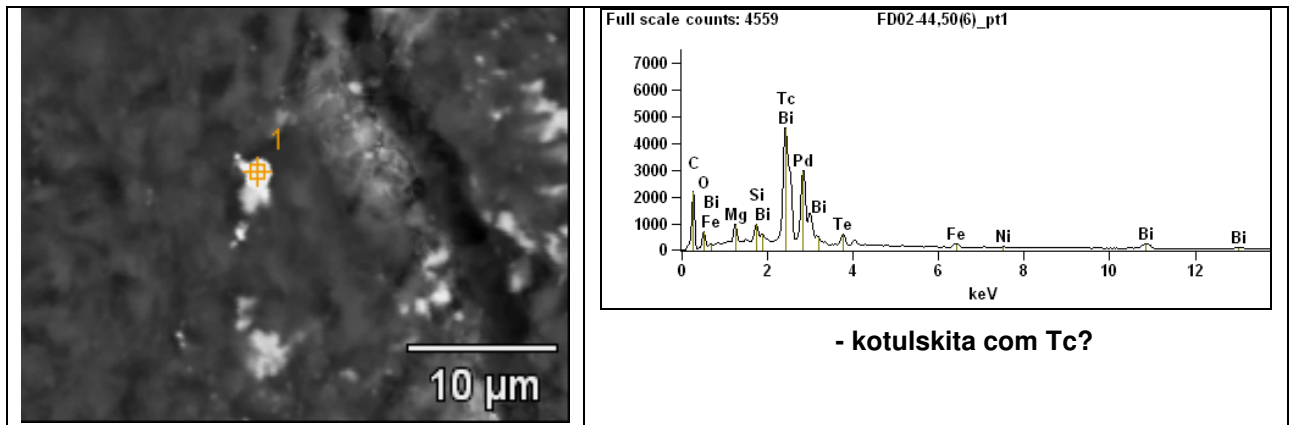


Figura 2.7: Detalhe da Inclusão de Kotulskita (?) na serpentina. Ampliação 3.000x.

	Weight %			
	<i>Tc-L</i>	<i>Pd-L</i>	<i>Te-L</i>	<i>Bi-M</i>
<b>FD02-44,50(6)_pt1</b>	7.77	39.65	9.76	42.82

Figura 2.7-A: Microanálises referentes ao telureto da figura 2.7.

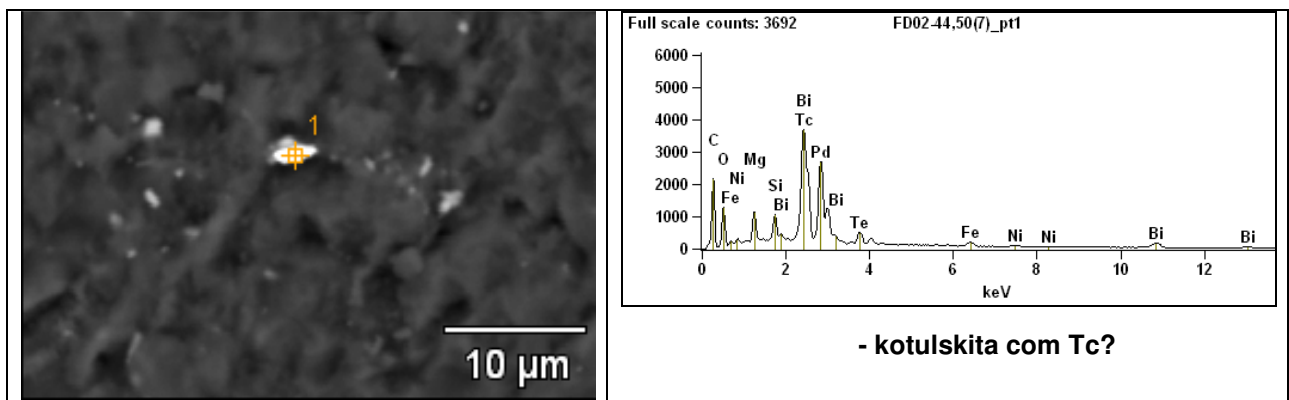


Figura 2.8: Detalhe da Inclusão de Kotulskita (?) na serpentina. Ampliação 3.000x.

	Weight %			
	<i>Tc-L</i>	<i>Pd-L</i>	<i>Te-L</i>	<i>Bi-M</i>
<b>FD02-44,50(7)_pt1</b>	9.13	43.03	9.58	38.26

Figura 2.8-A: Microanálises referentes ao telureto da figura 2.8.

Resumo dos PGMs encontrados na Amostra FD02-44,50m

CLASSE	MINERAL PROVÁVEL	COMPOSIÇÃO PROVÁVEL						Abund*	
			Pd	Te	Pb	Tc	Ag		
Pd dominante	PGE-Bi-Te-Pb	Polarite ?	(Pd,Te)PbBi	40,07	28,36	21,88			MA
	PGE-Bi-Te	kotulskita ?	(Pd,Te)Bi	38,98	19,14				A
	PGE-Bi-Te-Tc	kotulskita com Tc?	(Pd,Te,Tc)Bi	39,11	18,25		7,44		MA
	PGE-Ni-Pd	???	(Pd,Te, Tc)As	37,55	24,79		31,38		R
	PGE-Bi-Te-Pd	Majakite ?	PdNiAs (?)	45,45					R
	Sulfoarsenietos	Majakita c Ag e S?	(Ag,Ni,Pd)SAs	42,23				0,66	F
		???	(Pd)SAs	12,84					R
	Arsenietos	Majakita c Ag? ou Menshikovita?	(Ag, Ni,Pd)As	46,25				0,62	O
		Gersdoffita	(Ni)SAs						O
		Isomertierita	(Pd,Sb)As	74,56					R

\* Abundância relativa entre os PGM na amostra: MA - Muito abundante (>40%); A - Abundante (>10%); F - Frequente (>2%); O - Ocasional (>0,5%); R - raro (<0,5%)

Resumo dos teluretos encontrados na Amostra FD02-44,50m

MINERAL PROVÁVEL	COMPOSIÇÃO PROVÁVEL	COMPOSIÇÃO QUÍMICA analisada EDS			
		Te	Pb	Bi	ARQUIVO
Rucklidgeita?	(Bi,Pb) <sub>3</sub> Te <sub>4</sub>	39,67	59,53	0,80	02 - Pt 01
Kochkarita?	PbBi <sub>4</sub> Te <sub>7</sub>	47,56	50,65	1,79	08 - Pt 09
Altaíta ou Fairbankita/Plumbotellurita ou os dois?	PbTe ou Pb(TeO <sub>3</sub> ) (?)	32,05	67,95		08 - Pt 12
		35,58	64,42		08 - Pt 14
		38,89	61,11		09 - Pt 19
		39,10	60,90		08 - Pt 08
		39,66	60,34		09 - Pt 09
		39,68	60,32		09 - Pt 06
		39,89	60,11		09 - Pt 16
		39,92	60,08		09 - Pt 21
		40,49	59,51		08 - Pt 10
		41,13	58,87		08 - Pt 05
		41,16	58,84		09 - Pt 22
		41,19	58,81		09 - Pt 23
		41,20	58,80		09 - Pt14
		41,80	58,20		08 - Pt 13
		42,04	57,96		09 - Pt 05
		42,09	57,91		09 - Pt 18
		42,62	57,38		09 - Pt 08
		42,94	57,06		09 - Pt 10
		44,04	55,96		09 - Pt 11
		44,67	55,33		02 - Pt 05
44,81	55,19		09 - Pt 12		
44,97	55,03		09 - Pt 15		
45,55	54,45		02 - Pt 03		
45,77	54,23		02 - Pt 08		

### 3. Amostra 110,00 m

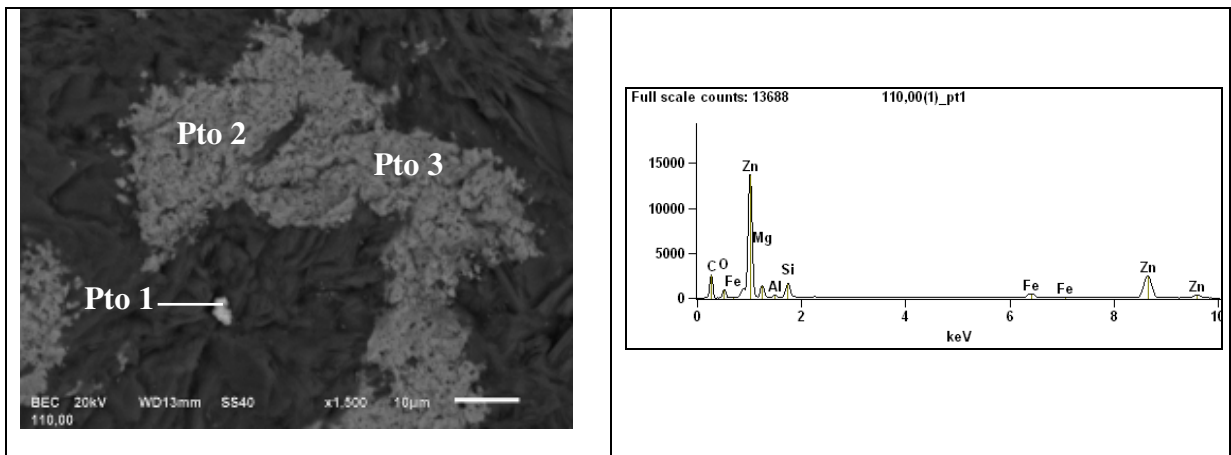


Figura 3.1: Detalhe da inclusão de zinco metálico na serpentina. Ampliação 1.500x.

Weight %	
<b>Zn-K</b>	
<b>110,00(1)_pt1</b>	100.00

Figura 3.1-A: Microanálises referentes ao zinco da figura 3.1.

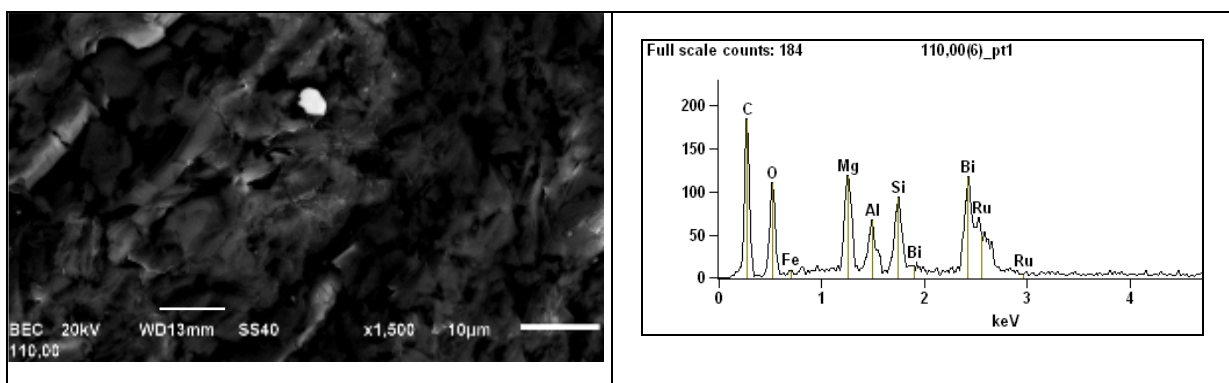
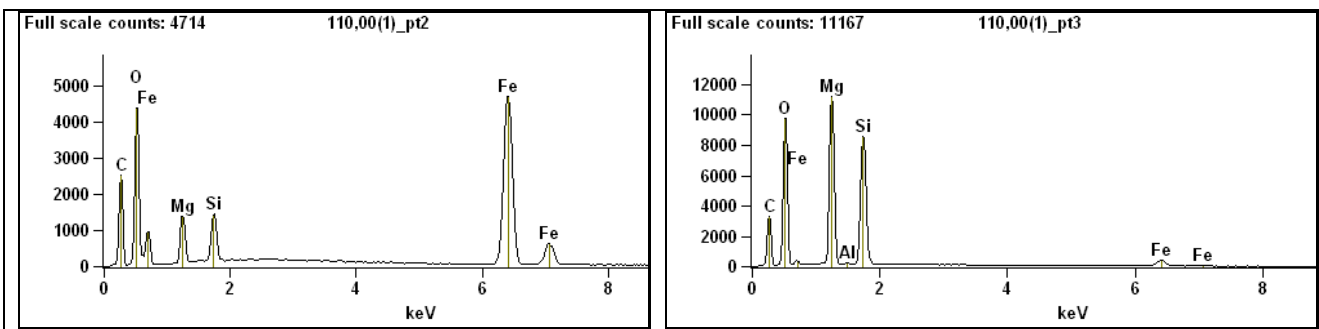




Figura 3.2: Detalhe da inclusão de Bismuteto de Ru na serpentina. Ampliação 1.500x.

Weight %	<i>Ru-L</i>	<i>Bi-M</i>
<b>110,00(6)_pt1</b>	10.48	89.52

Figura 3.2-A: Microanálises referentes ao Bismuteto de Ru da figura 3.2.

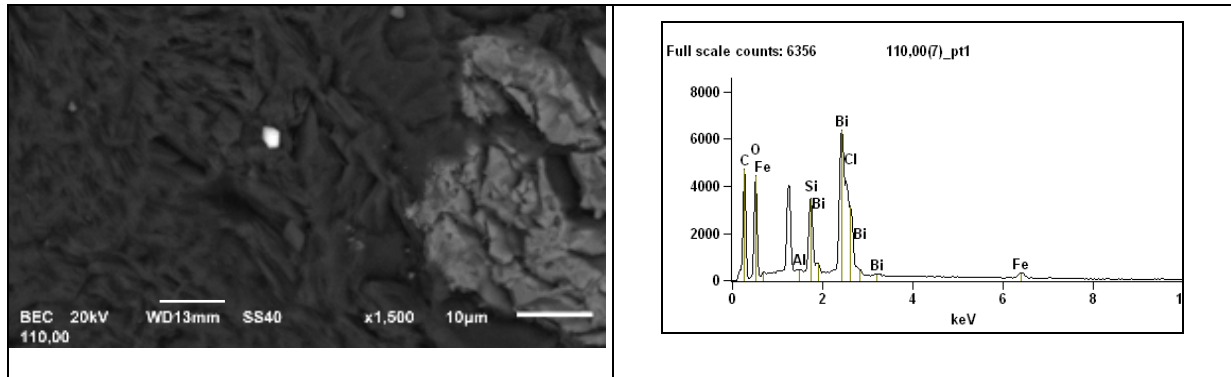


Figura 3.3: Detalhe da inclusão de cloreto de Bi - Bismocrita (?) na serpentina. Ampliação 1.500x.

Weight %	<i>O</i>	<i>Cl</i>	<i>Bi</i>
<b>110,00(7)_pt1</b>	8.90	13.59	77.50

Figura 3.3-A: Microanálises referentes ao cloreto de Bi - Bismocrita (?) da figura 3.3.

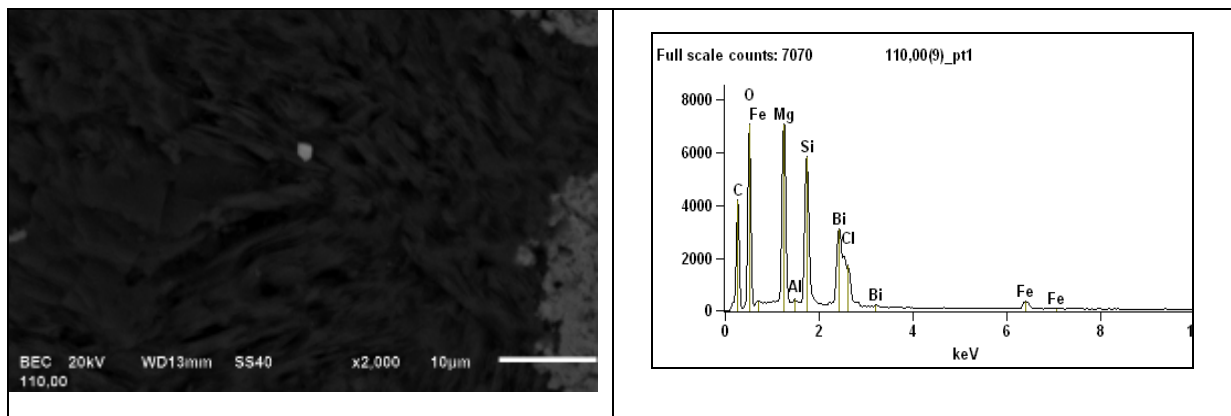


Figura 3.4: Detalhe da inclusão de cloreto de Bi na serpentina - Bismocrita (?). Ampliação 2.000x.

Weight %	<i>O</i>	<i>Cl</i>	<i>Bi</i>
<b>110,00(9)_pt1</b>	8.84	14.19	76.97

Figura 3.4-A: Microanálises referentes ao cloreto de Bi - Bismocrita (?) da figura 3.4.

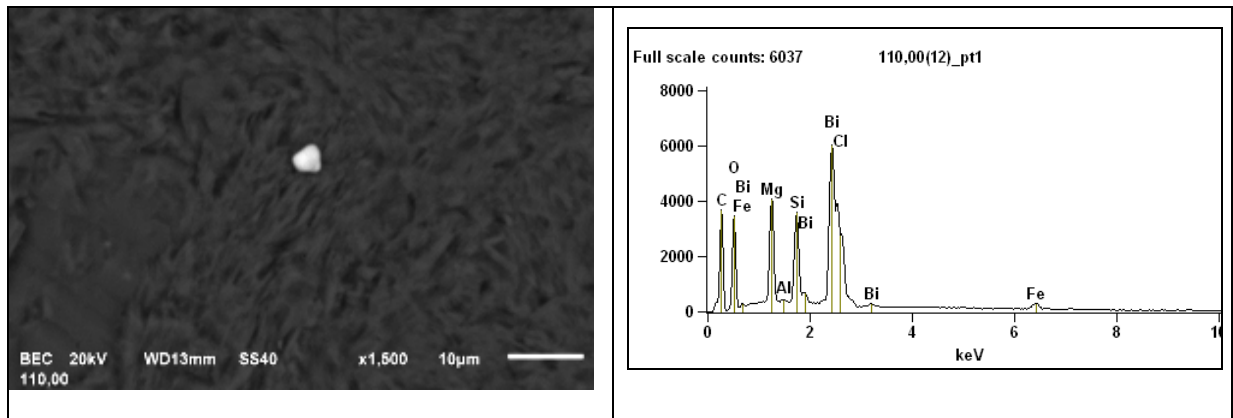


Figura 3.5: Detalhe da inclusão de outro cloreto de Bi - Bismoclita (?) na serpentina. Ampliação 1.500x.

Weight %

	<i>O</i>	<i>Cl</i>	<i>Bi</i>
<b>110,00(12)_pt1</b>	8.96	13.05	77.99

Figura 3.5-A: Microanálises referentes ao cloreto de Bi - Bismoclita (?) da figura 3.5.

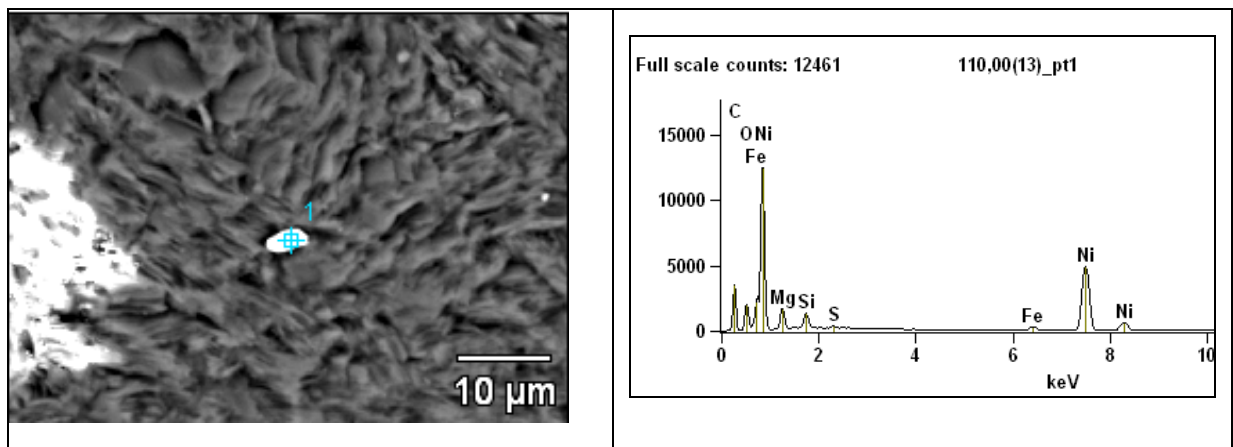


Figura 3.6: Detalhe da inclusão de níquel metálico na serpentina. Ampliação 1.500x.

Weight %

	<i>S</i>	<i>Ni</i>
<b>110,00(13)_pt1</b>	0.32	99.68

Figura 3.6-A: Microanálises referentes ao níquel metálico da figura 3.6.

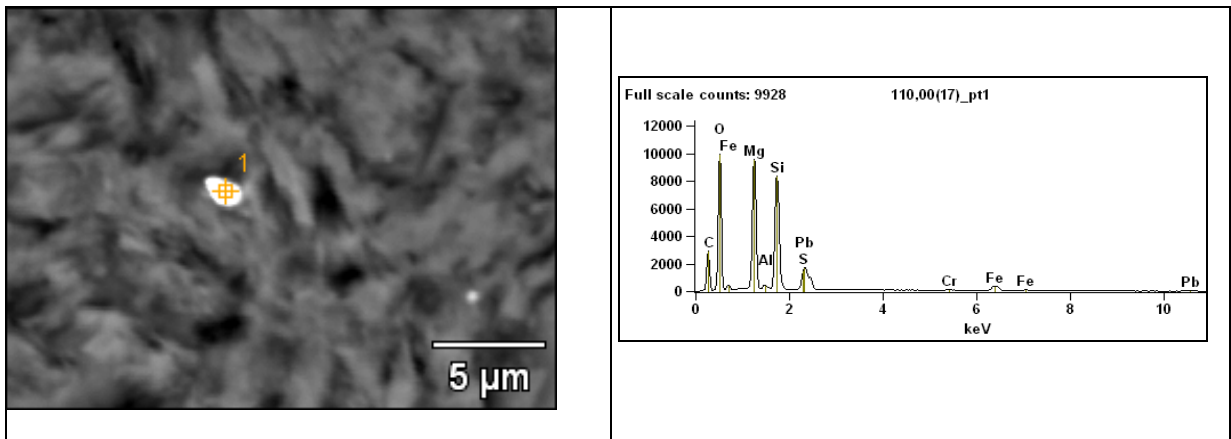


Figura 3.7: Detalhe da inclusão de associação Pb, Cr e S. Ampliação 5.000x.  
 Weight %

	<b>S</b>	<b>Cr</b>	<b>Pb</b>
<b>110,00(17)_pt1</b>	17.01	3.59	79.40

Figura 3.7-A: Microanálises referentes à associação Pb, Cr e S da figura 3.7.

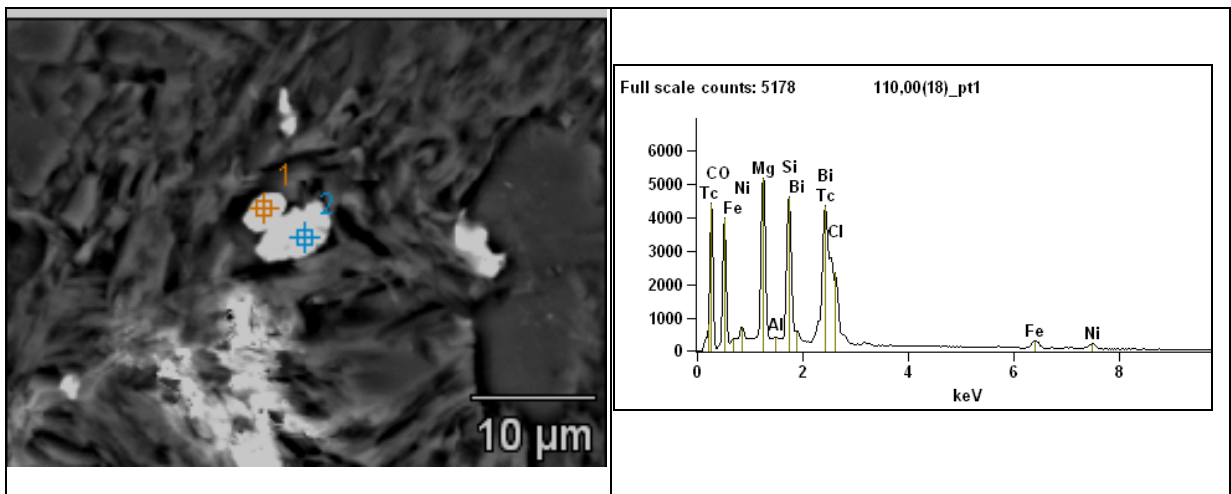


Figura 3.8: Detalhe da inclusão de associação Bi, Cl e Tc. Ampliação 2.500x.

Weight %

	<b>O</b>	<b>Cl</b>	<b>Tc</b>	<b>Bi</b>
<b>110,00(18)_pt1</b>	14.69	10.58	29.25	45.49

Figura 3.8-A: Microanálises referentes à associação Bi, Cl e Tc do ponto 1 da figura 3.8.

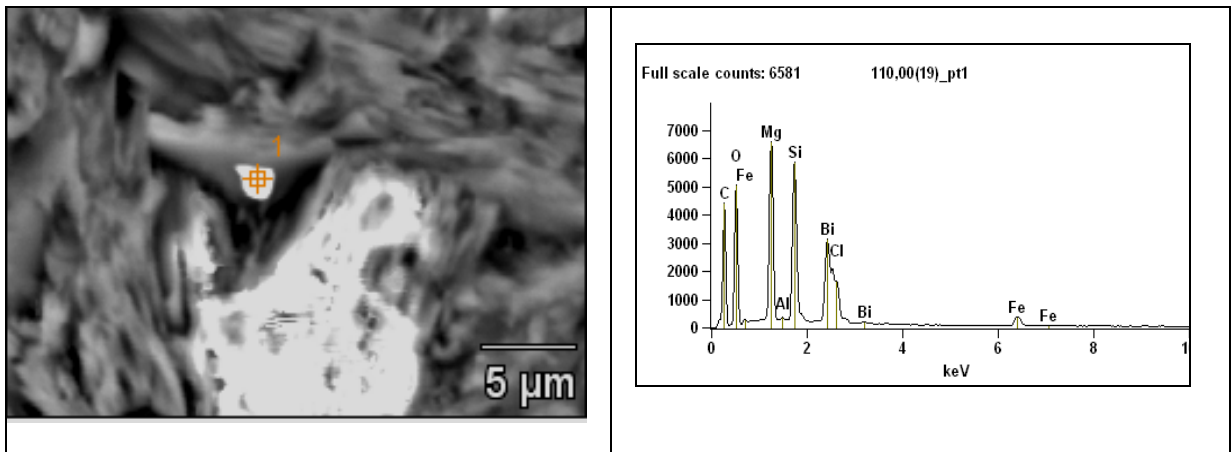


Figura 3.9: Detalhe da inclusão de cloreto de bismuto - Bismoclita (?). Ampliação 4.000x.

	Weight %		
	<i>O</i>	<i>Cl</i>	<i>Bi</i>
<b>110,00(19)_pt1</b>	8.84	14.15	77.00

Figura 3.9-A: Microanálises referentes ao cloreto de bismuto - Bismoclita (?) da figura 3.9.

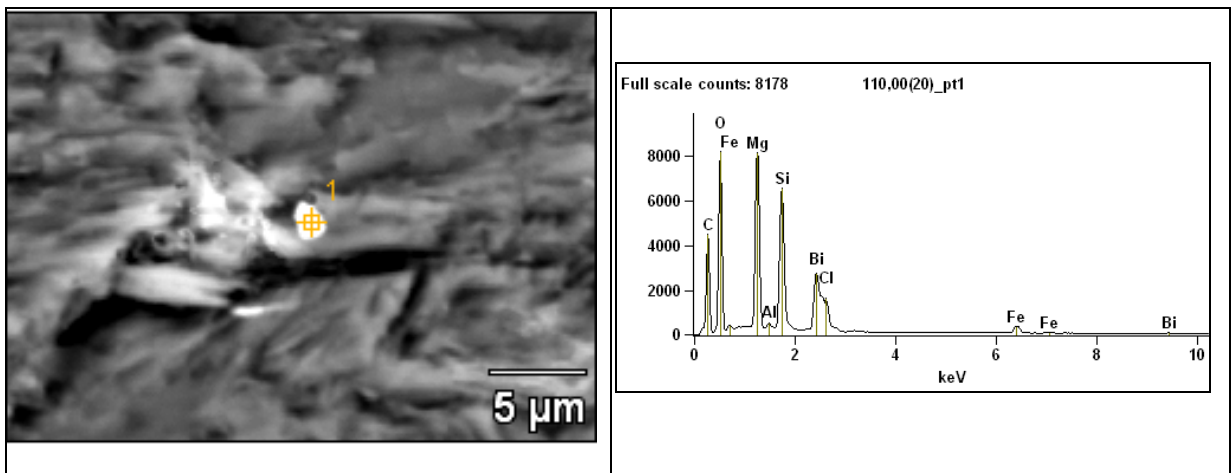


Figura 3.10: Detalhe da inclusão de cloreto de bismuto - Bismoclita (?). Ampliação 4.000x.

	Weight %		
	<i>O</i>	<i>Cl</i>	<i>Bi</i>
<b>110,00(20)_pt1</b>	8.77S	14.91	76.33

Figura 3.10-A: Microanálises referentes ao cloreto de bismuto - Bismoclita (?) da figura 3.10.

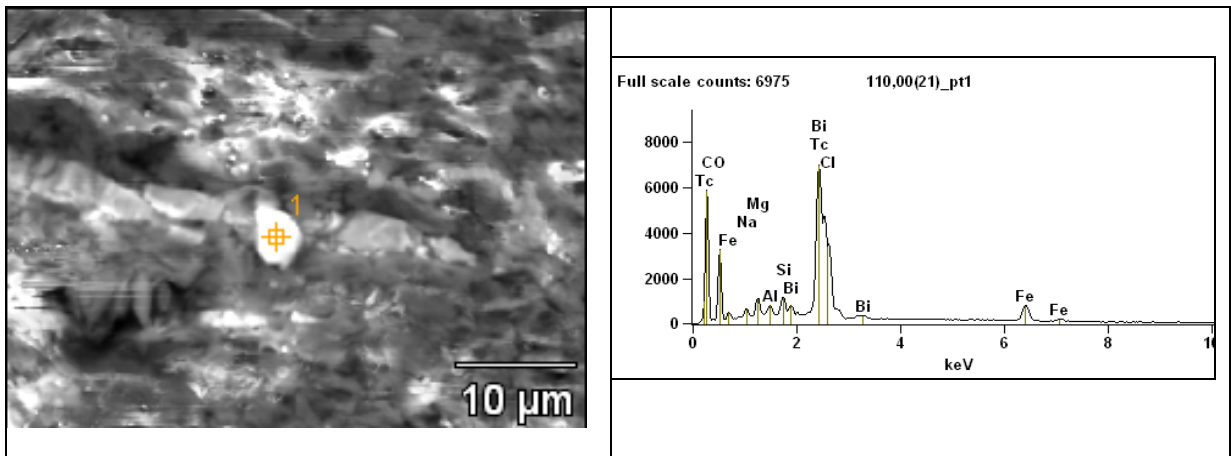


Figura 3.11: Detalhe da inclusão de cloreto de bismuto - Bismoclita (?). Ampliação 2.500x.

	Weight %			
	<i>O</i>	<i>Cl</i>	<i>Tc</i>	<i>Bi</i>
<b>110,00(21)_pt1</b>	10.88	12.32	9.86	66.94

Figura 3.11-A: Microanálises referentes à associação Bi, Cl e Tc da figura 3.11.

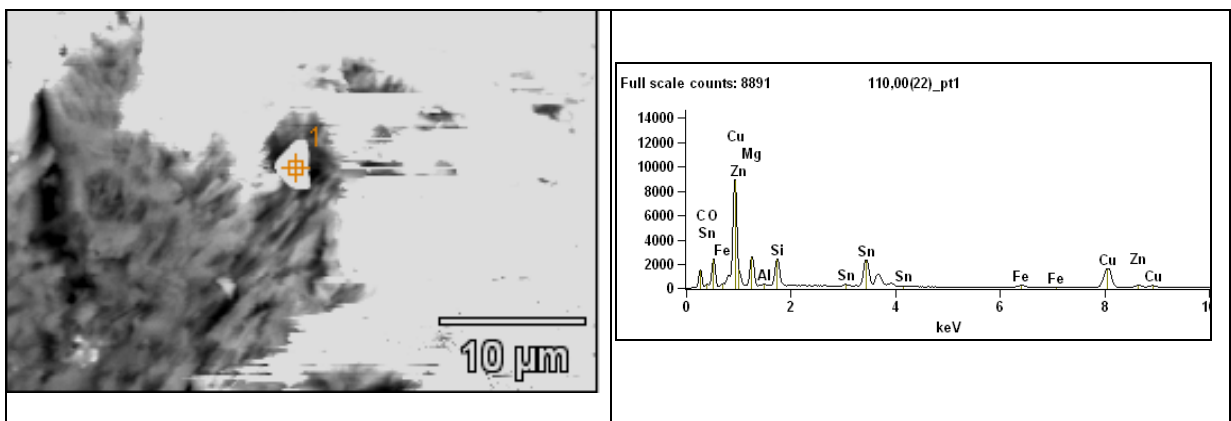


Figura 3.12: Detalhe da inclusão de liga metálica Cu/Zn/Sn. Ampliação 3.000x.

	Weight %		
	<i>Cu</i>	<i>Zn</i>	<i>Sn</i>
<b>110,00(22)_pt1</b>	55.05	8.18	36.77

Figura 3.12-A: Microanálises referentes à de liga metálica Cu/Zn/Sn da figura 3.12.

Resumo dos PGE, Haloides e Ligas Metálicas da Amostra FD02-110,00 m.

Mineral Provável	Composição Provável	Composição Química Analisada EDS (%)						Abundância Relativa	
		Bi	Cl	Ru	Tc	Zn	Cu		Sn
Desconhecido	RuBi	89,52		10,48					R
Daubreeita ou Bismoclita	BiO(OH,Cl) ou BiOCl	77,50	14,00						MA
???	???	53,26	12,53		34,20				R
Ligas metálicas	Zn					100,00			R
	Zn, Cu, Sn					8,18	55,05	36,77	

Legenda: MA-Muito abundante (>40%); A-Abundante (>10%); F-Frequente (>2%); O-Ocasional (>0,5%); R- Raro.

4. Amostra 110,75 m

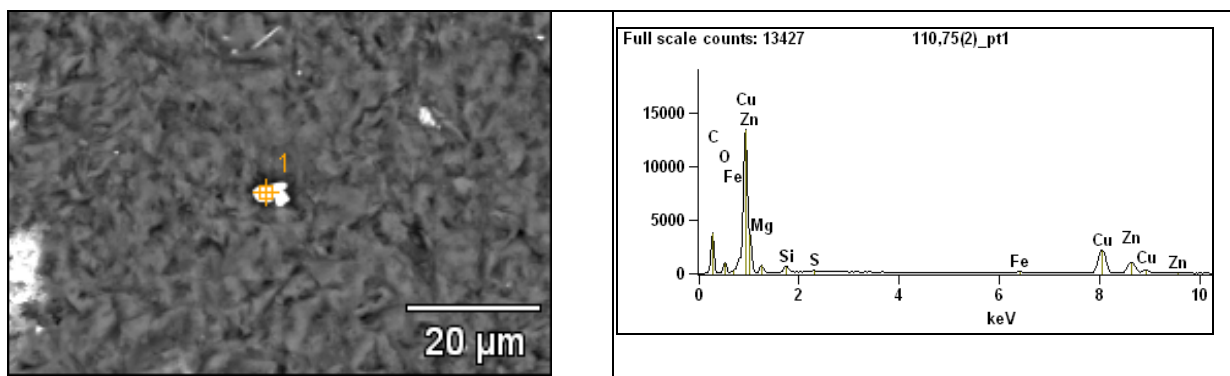


Figura 4.1: Detalhe da inclusão de liga metálica Cu/Zn/Sn. Ampliação 1.500x.

Weight %

	<b>O</b>	<b>S</b>	<b>Cu</b>	<b>Zn</b>
<b>110,75(2)_pt1</b>	8.07	0.15	58.81	32.97

Figura 4.1-A: Microanálises referentes à associação Cu/Zn/S da figura 4.1.



## 5. Amostra 163,25m – Cromitito

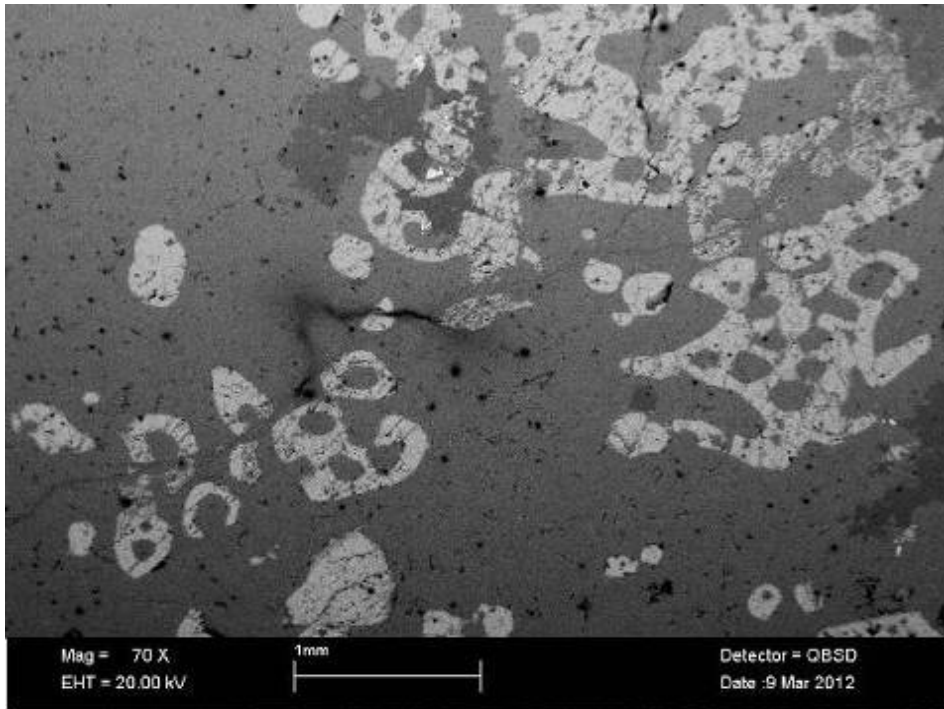


Figura 5.1: Aspecto geral da cromita – textura em atol. Ampliação 70x.

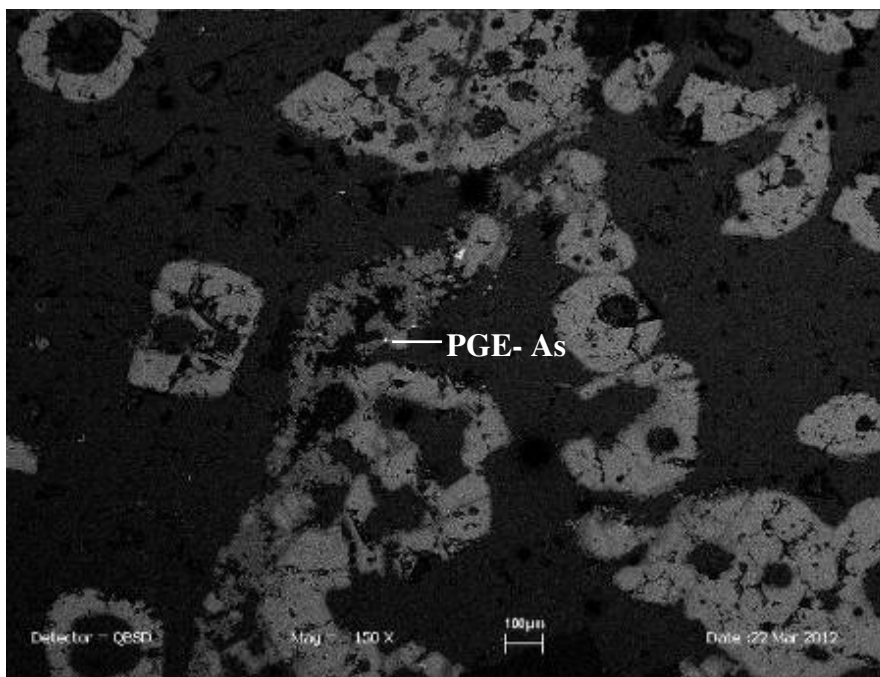


Figura 5.2: Local da Lâmina com cromita – textura em atol e inclusão de PGE-As. Ampliação 150x.

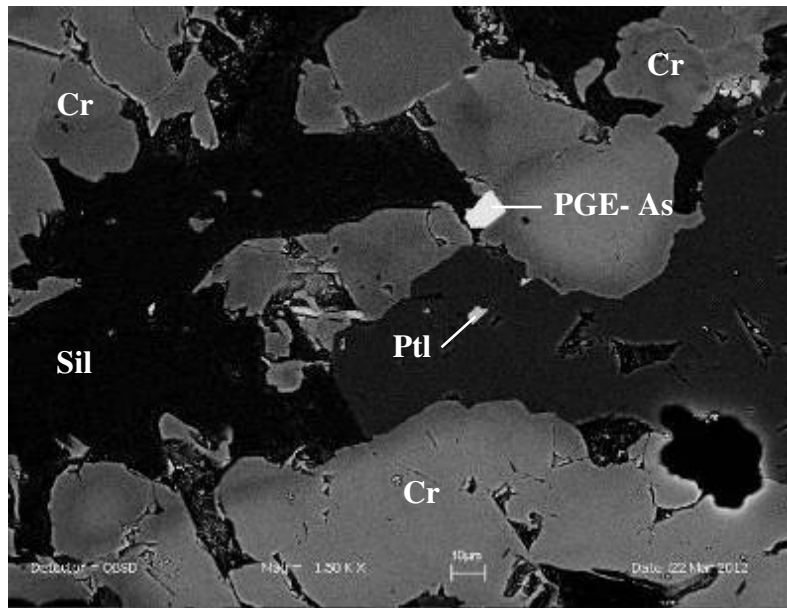


Figura 5.3: Detalhe da imagem anterior da cromita com inclusão de PGE-As. Ampliação 1.500x.

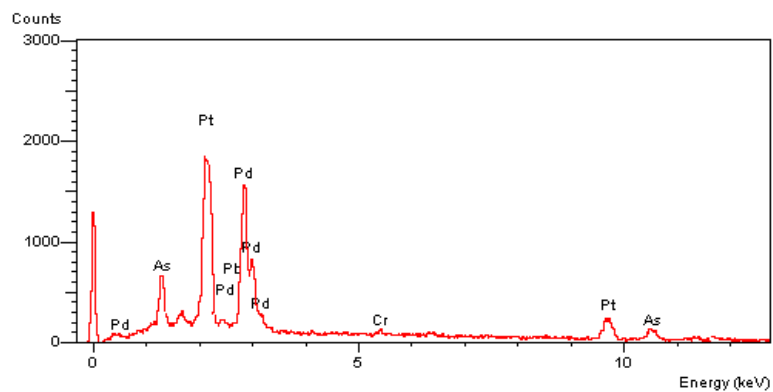


Figura 5.3-A: Microanálise do arsenieto de Pd e Pt da figura 5.3.

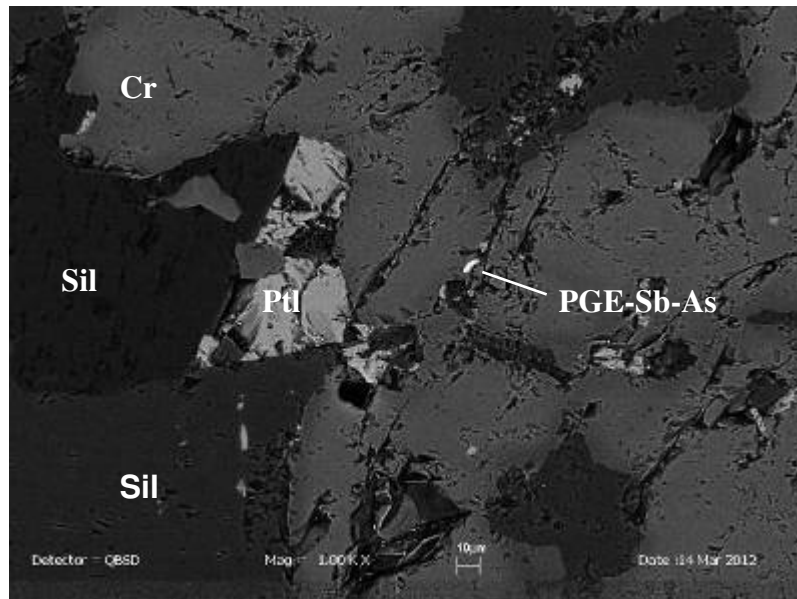


Figura 5.4: Cromita com inclusão de PGE-Sb-As. Ampliação 1.000x.

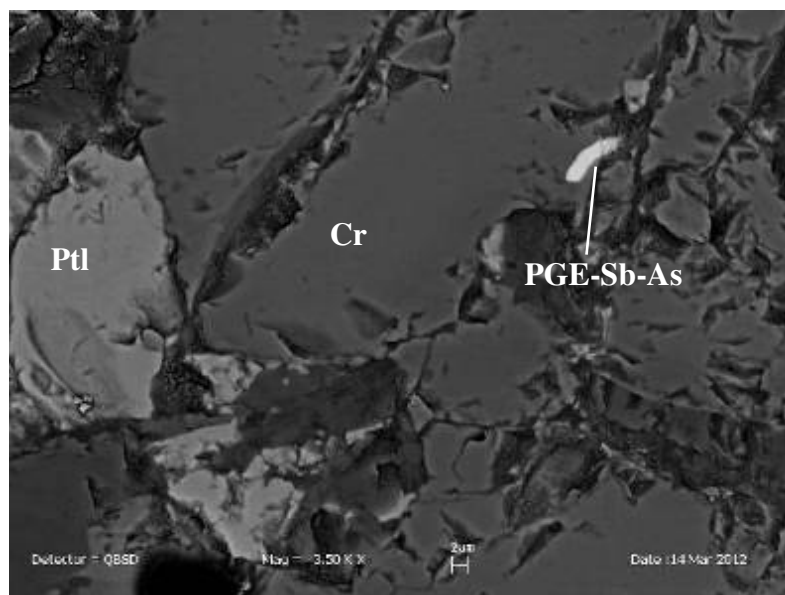


Figura 5.5: Detalhe da imagem anterior da cromita com inclusão de PGE-Sb-As. Ampliação 3500x.

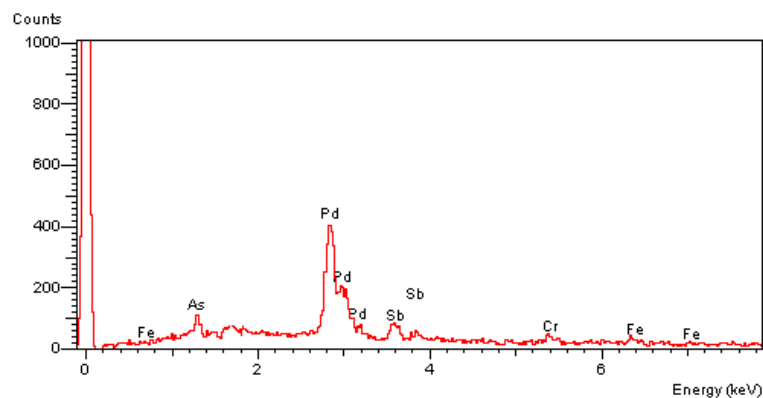


Figura 5.5-A: Microanálise do PGE-Sb-As – Mertierita (?) da figura 5.5.

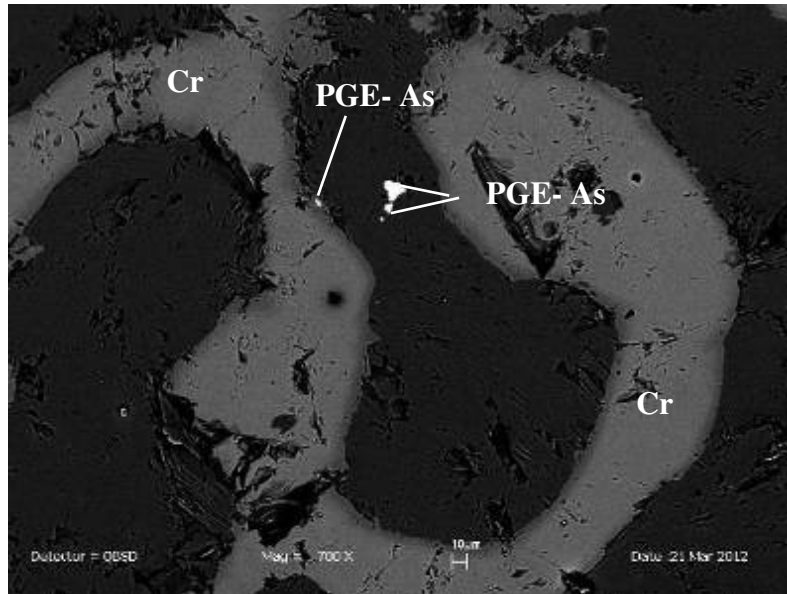


Figura 5.6: Silicato com inclusão de PGE-As: Sperrylita. Ampliação 700x.

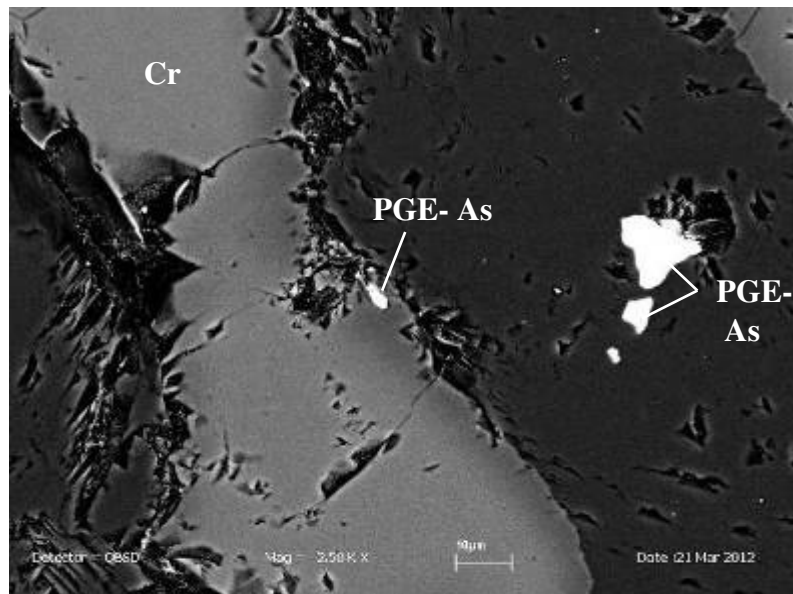


Figura 5.7: Detalhe da imagem anterior de silicato com inclusão de PGEs-As. Ampliação 2500x.



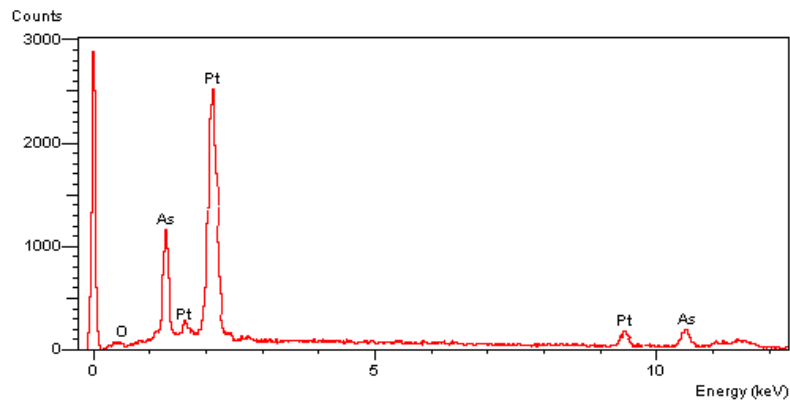


Figura 5.7-A: Microanálise do arsenieto de Pt - Sperrylita.

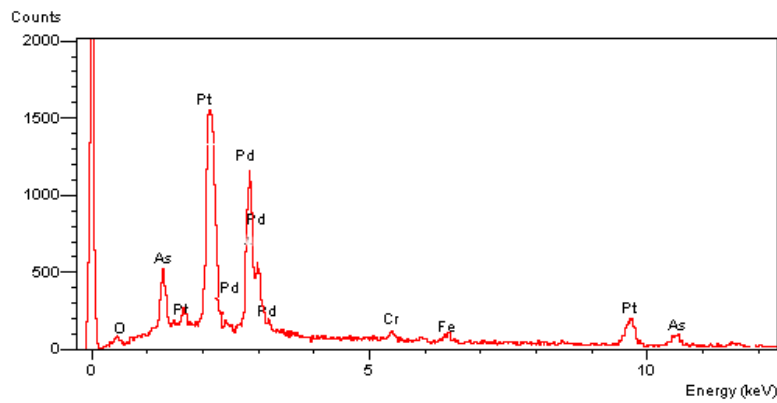


Figura 5.7-B: Microanálise do arsenieto de Pt e Pd.

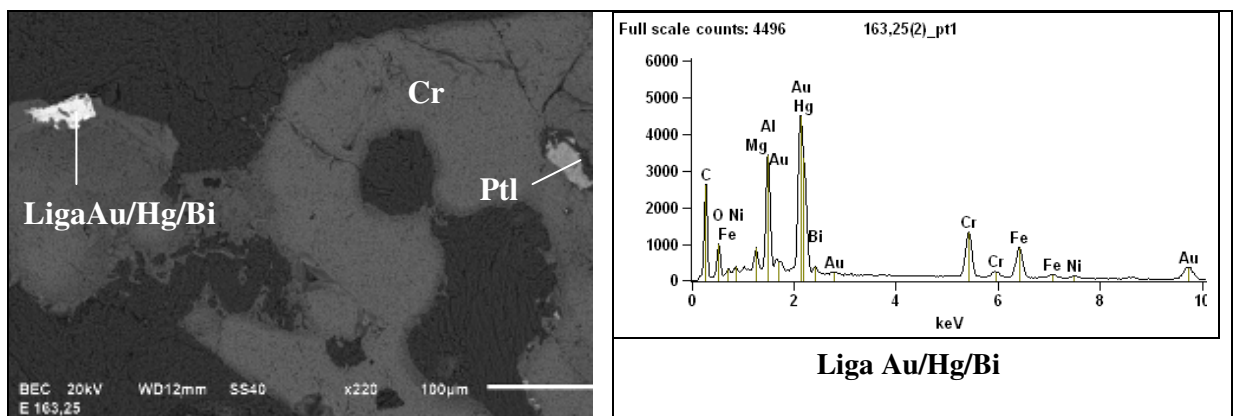


Figura 5.8: Cromita com liga de Au/Hg/Bi na borda. Ampliação 220x.

Weight %

	<i>Au</i>	<i>Hg</i>	<i>Bi</i>
<b>163,25(2)_pt1</b>	97.61	1.25	1.14

Figura 5.8-A: Microanálise do da liga de Au/Hg/Bi da figura 5.8.

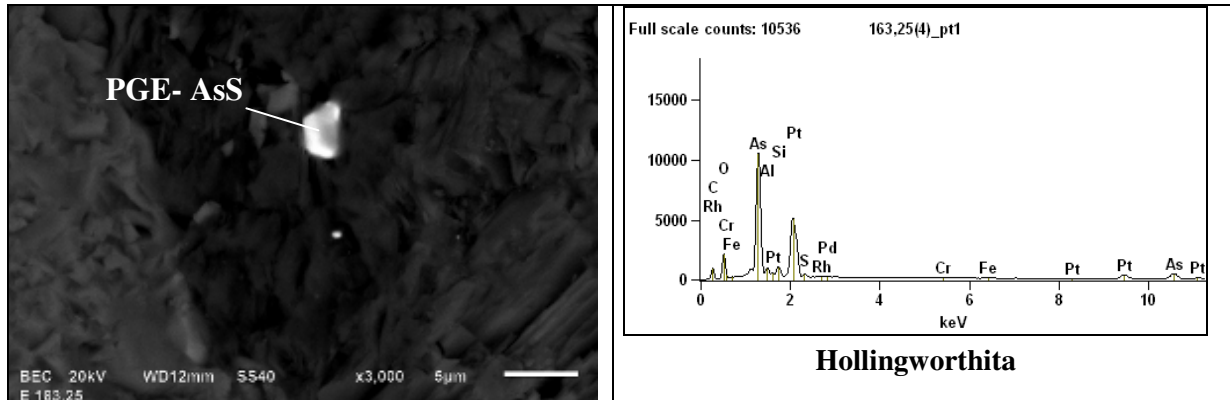


Figura 5.9: PGMs inclusos em silicato. Ampliação 3.000x.

Weight %

	<i>S</i>	<i>As</i>	<i>Rh</i>	<i>Pd</i>	<i>Pt</i>
<b>163,25(4)_pt1</b>	0.72	43.90	0.40	2.20	52.77

Figura 5.9-A: Microanálise indicando ser uma Hollingworthita da figura 5.9.

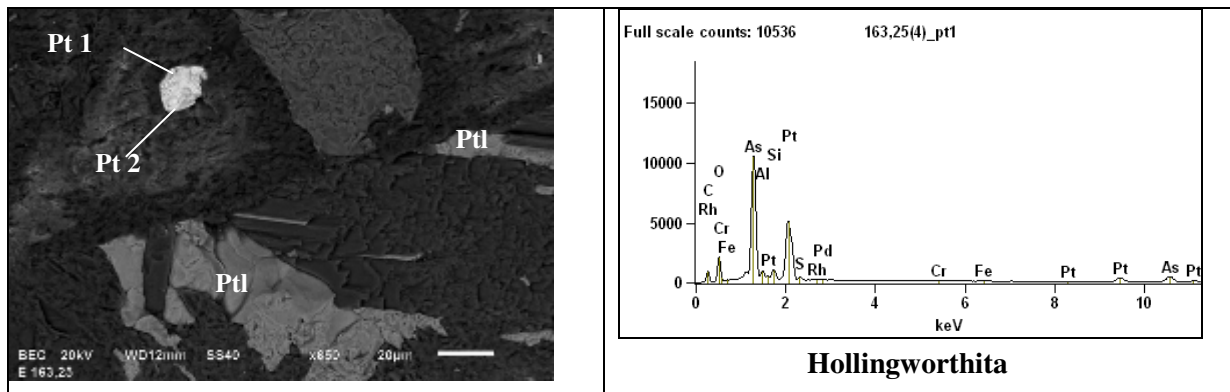
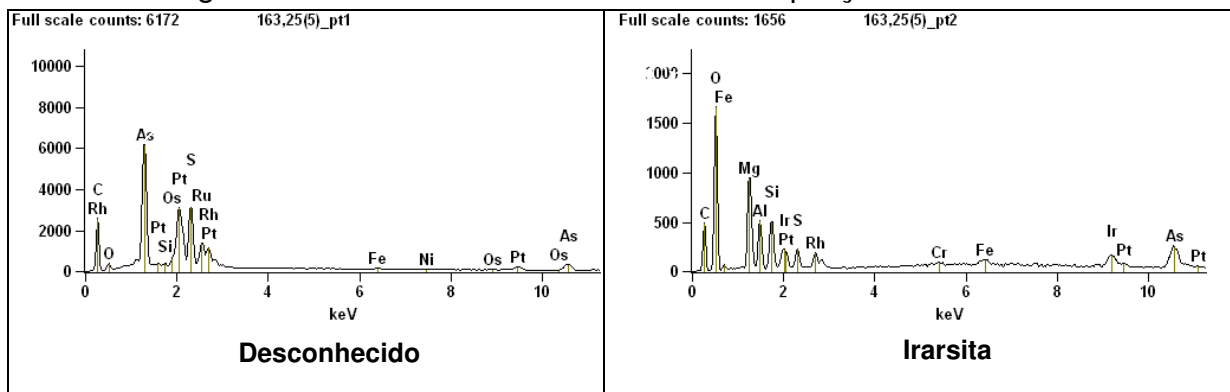


Figura 5.10: PGMs inclusos em silicato. Ampliação 650x.





Weight %

	<b>S</b>	<b>As</b>	<b>Ru</b>	<b>Rh</b>	<b>Os</b>	<b>Ir</b>	<b>Pt</b>
<b>163,25(5)_pt1</b>	17.80	29.92	19.69	6.20	4.14		22.26
<b>163,25(5)_pt2</b>	3.09	46.55		5.52		35.24	9.60

Figura 5.10-A: Microanálises referentes aos pontos 01 (desconhecido) e 02 (Irsarsita) da figura 5.10.

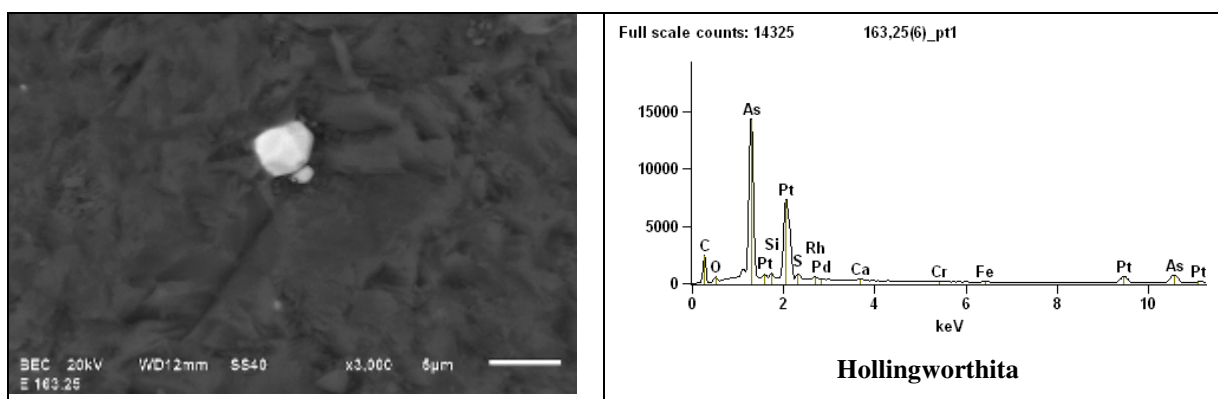


Figura 5.11: PGM incluso em silicato (serpentina). Ampliação 3.000x.

Weight %

	<b>S</b>	<b>As</b>	<b>Rh</b>	<b>Pd</b>	<b>Pt</b>
<b>163,25(6)_pt1</b>	1.16	41.67	3.16	1.24	52.77

Figura 5.11-A: Microanálise referente ao ponto 01 da figura 5.11 – Hollingworthita.

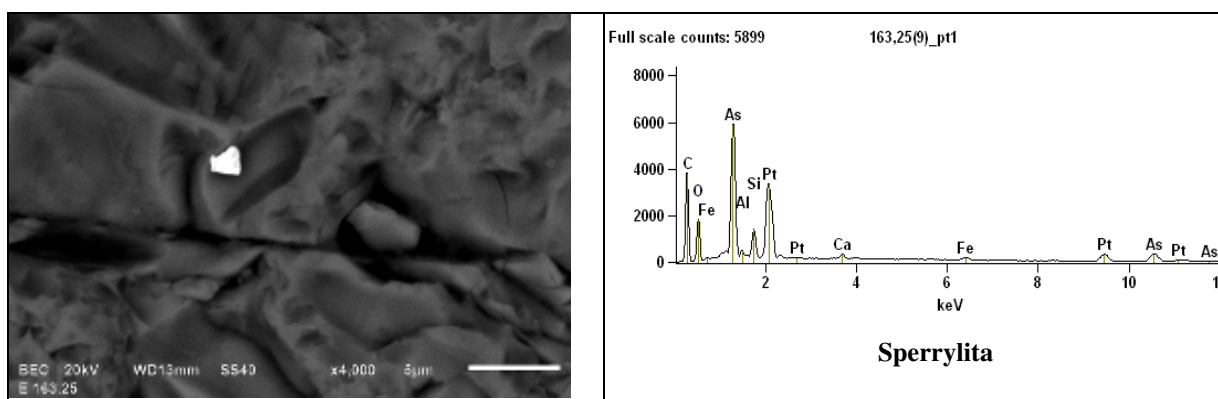


Figura 5.11: PGM incluso em silicato (serpentina). Ampliação 4.000x.

Weight %

	<b>As</b>	<b>Pt</b>
<b>163,25(9)_pt1</b>	42.49	57.51

Figura 5.11-A: Microanálise referente ao ponto 01 da figura 5.11 – Sperrylita.

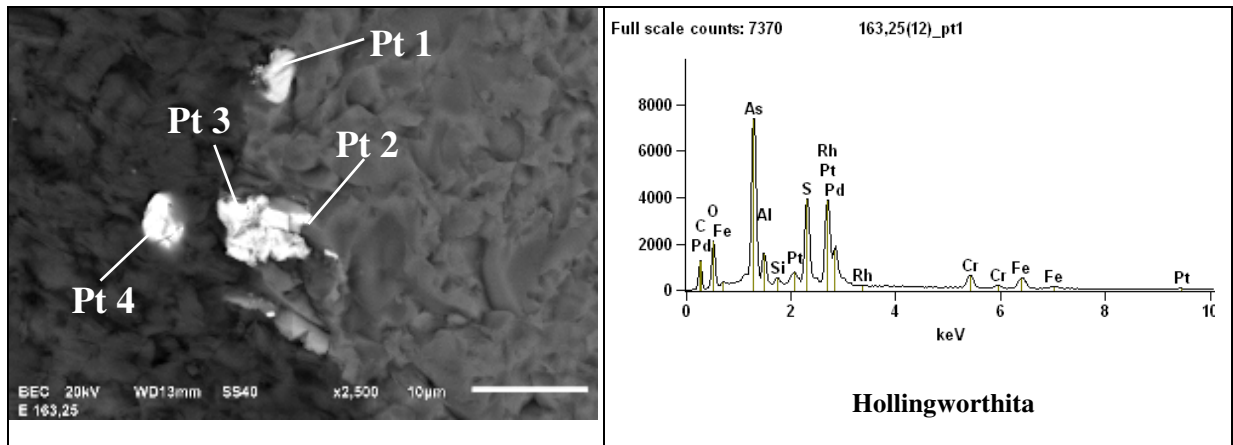
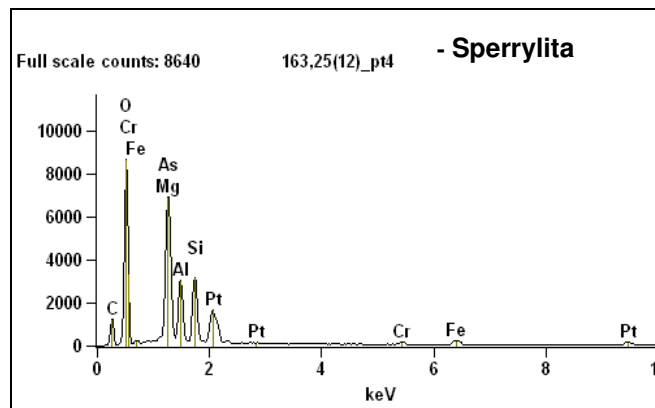
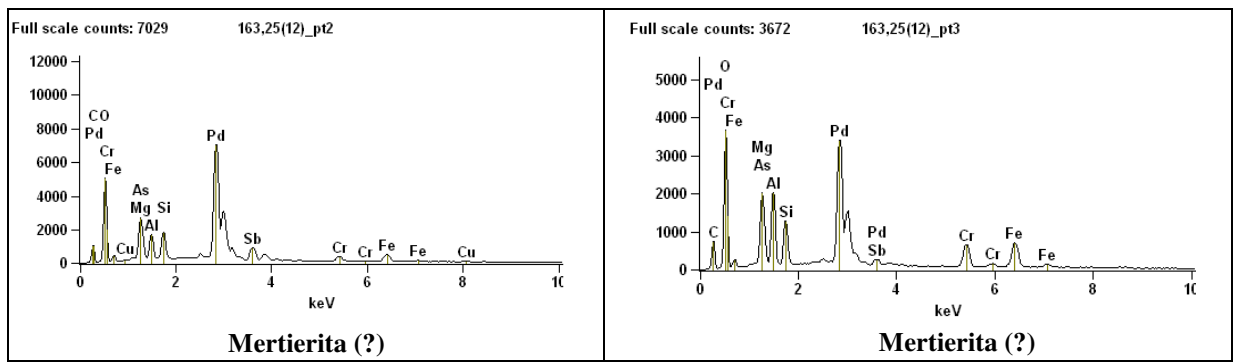


Figura 5.12: PGMs inclusos em silicato (serpentina). Ampliação 2.500x.



Weight %

	<b>S</b>	<b>As</b>	<b>Rh</b>	<b>Pd</b>	<b>Sb</b>	<b>Pt</b>
<b>163,25(12) pt1</b>	14.27	32.98	45.77	2.02		4.95
<b>163,25(12)_pt2</b>		7.97		73.91	18.12	
<b>163,25(12)_pt3</b>		18.00		74.29	7.71	
<b>163,25(12)_pt4</b>		43.51				56.49

Figura 5.12-A: Microanálises referentes aos PGMs da figura 5.12.

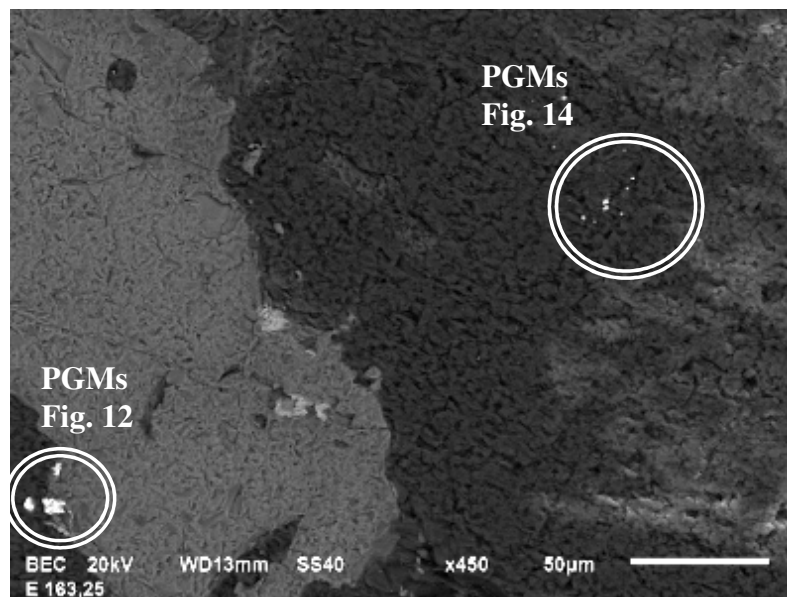


Figura 5.13: imagem panorâmica mostrando os PGMs da figura 12, na borda de uma cromita e os da próxima figura (14) disseminados na serpentina. Ampliação 450x.

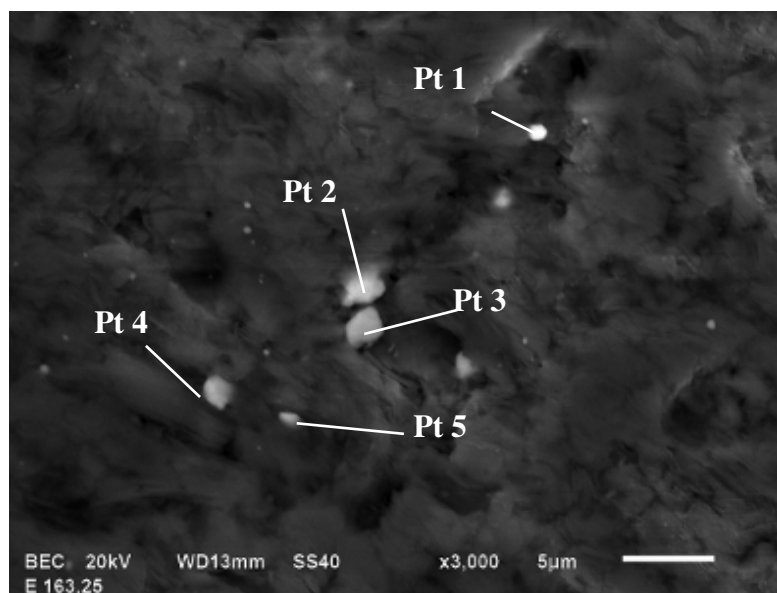
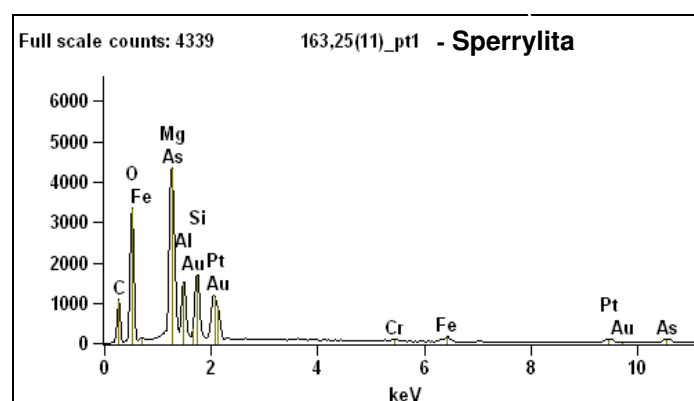
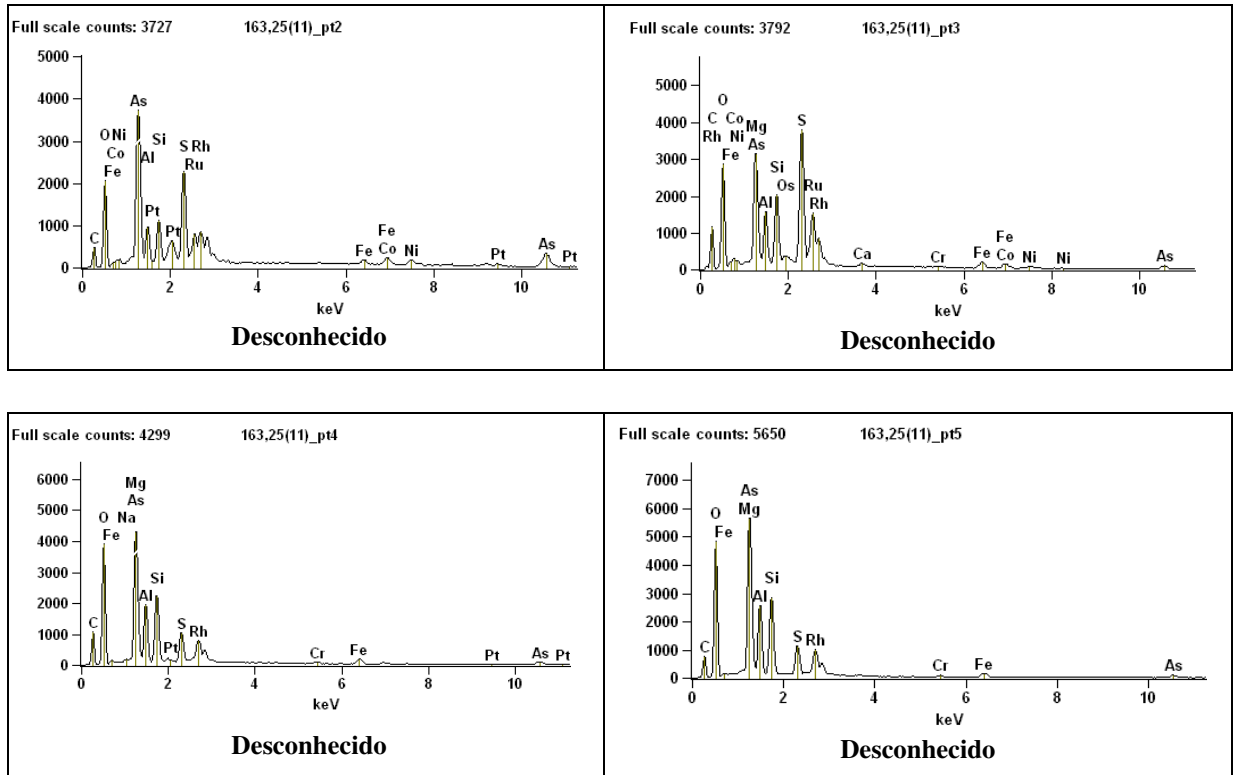


Figura 5.14: PGMs inclusos em silicato (serpentina). Ampliação 3.000x.





Weight %

	S	As	Ru	Rh	Os	Pt	Au
<b>163,25(11)_pt1</b>		39.40				56.24	4.37
<b>163,25(11)_pt2</b>	20.80	54.63	11.60	7.36		5.61	
<b>163,25(11)_pt3</b>	33.03	16.63	43.60	4.51	2.22		
<b>163,25(11)_pt4</b>	20.44	40.09		36.31		3.17	
<b>163,25(11)_pt5</b>	18.98	34.60		46.41			

Figura 5.14-A: Microanálises referentes aos PGMs da figura 5.14.

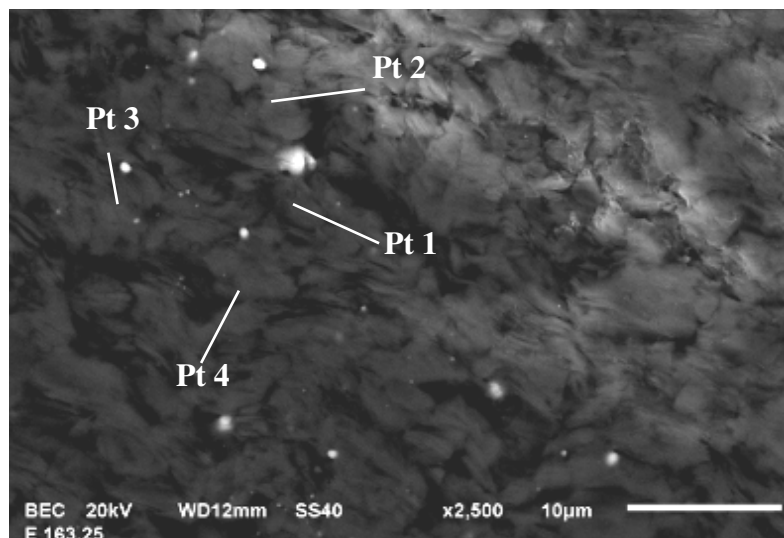
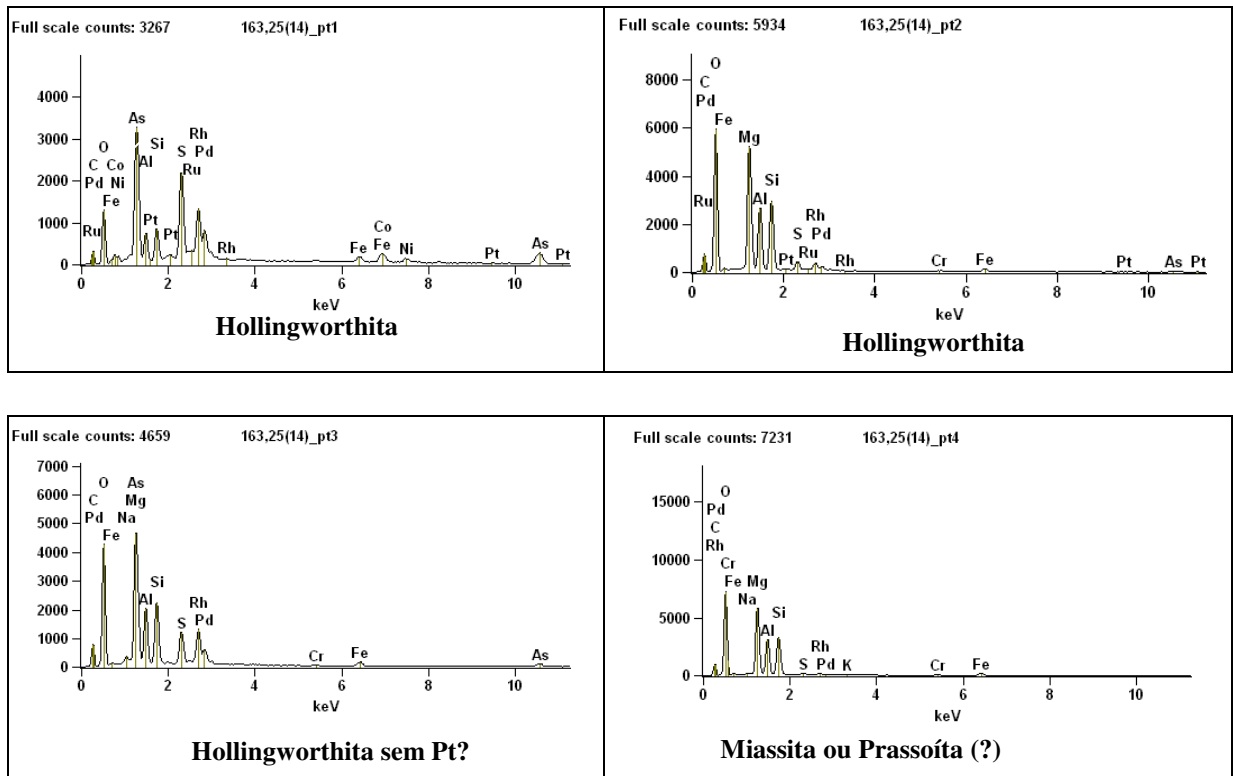


Figura 15: PGMs inclusos em silicato (serpentina). Ampliação 2.500x.



Weight %

	<b>S</b>	<b>As</b>	<b>Ru</b>	<b>Rh</b>	<b>Pd</b>	<b>Pt</b>
<b>163,25(14)_pt1</b>	18.22	40.83	3.90	29.22	5.91	1.93
<b>163,25(14)_pt2</b>	18.10	26.10	5.52	44.93	5.34	0.00
<b>163,25(14)_pt3</b>	16.68	31.90		48.98	2.43	
<b>163,25(14)_pt4</b>	29.42			64.92	5.66	

Figura 15-A: Microanálises referentes aos PGMs da figura 5.15.

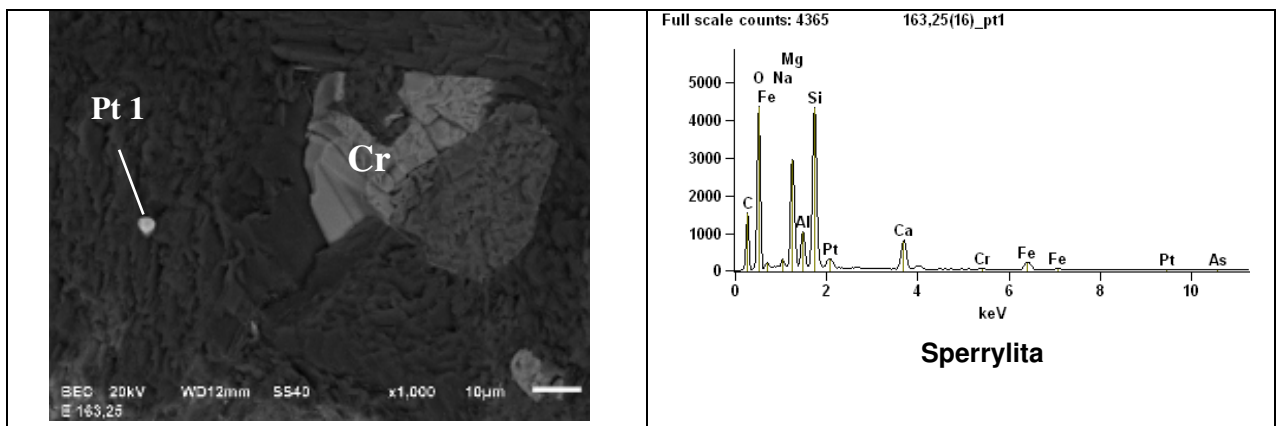


Figura 5.16: PGM ( sperrylita) incluído em silicato (serpentina). Ampliação 1.000x.

Weight %

	<i>As</i>	<i>Pt</i>
<b>163,25(16)_pt1</b>	34.47	65.53

Figura 5.16-A: Microanálise referente ao PGM Sperrylita da figura 5.16.

Resumo dos PGE e outros minerais de interesse na Amostra FD02-163,25m

CLASSE	MINERAL PROVÁVEL	COMPOSIÇÃO PROVÁVEL								Abund**	
			Pt	Pd	Rh	Ru	Ir	Os	Sb		Au
Pt dominante	Hollingworthita	(Rh, Pt, Pd)AsS	52,77	2,20	0,40						A
	Cherepanovite ou Polkanovite (?)	RhAs ou Rh <sub>12</sub> As <sub>7</sub>			>57,80*						F
	???	RhAsS			46,41						R
	Desconhecido	(Ru, Rh,Pt,Os)AsS	22,26		6,20	19,69		4,14			F
	Irarsita	(Ir, Ru, Rh, Pt)AsS	9,60		5,52		35,24				R
	Osarsita	(Os,Ru)AsS				9,19*		51,89*			R
	????	(Rh, Pt)AsS	3,17		36,31						R
	Sulfoarsenieto	Glaucodot	(Co,Fe)AsS		Tr						
Pt-AS	Sperrylita	PtAs <sub>2</sub>	57,51								A
Pd dominante	PGE-Sb-As	Mertierita, arsenopalladinita ou isomertierita		73,91					18,12		O
	PGE-As	Paladoarsenieto ou Stillwaterita		>73,94*							R
	PGE-AS-S	Hollingworthita (SEM Pt?)		2,43	48,98						R
	PGE-S	Miassita ou Prassoita (?)	Rh <sub>17</sub> S <sub>15</sub> com Pd		5,66	64,92					R
Au	Liga Au-Bi-Hg	Liga Au-Bi-Hg								97,61	R

\* fórmula teórica (sem análise quantitativa por EDS); \*\*\* Hollingworthita SEM Pt

\*\* Abundância relativa entre os PGM - MA - Muito abundante (>40%); A - Abundante (>10%); F - Frequente (>2%); O - Ocasional (>0,5%); R – raro (<0,5%).

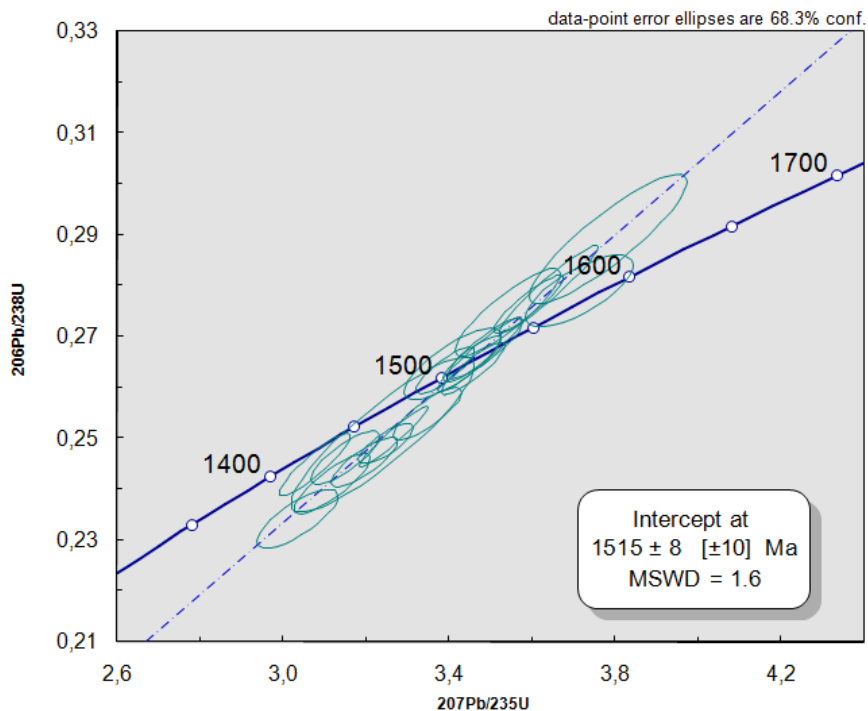


## Anexo V – Geocronologia

Análises U-Pb LA-MC-ICPMS em zircão de dique de diabásio – Amostra LUSL 21

1s(%)	6/8 ratio	1s(%)	7/6 age	1s(%)	7/5 age	1s(%)	6/8 age	1s(%)	Rho	Conc (%)
1,8	0,24488	1,7	1449,0	15,2	1426,8	14,1	1412,0	21,0	0,91	97,45
1,4	0,26336	1,1	1495,2	14,3	1502,1	10,7	1507,0	15,3	0,85	100,79
2,3	0,26464	1,7	1496,0	27,1	1506,2	17,8	1513,6	23,6	0,79	101,18
2,1	0,23421	1,6	1507,6	25,5	1416,4	16,1	1356,5	19,9	0,77	89,98
1,7	0,26769	1,5	1517,5	15,8	1524,2	13,3	1529,1	19,9	0,88	100,76
1,9	0,26651	1,8	1518,7	13,2	1521,3	15,2	1523,1	24,4	0,94	100,29
2,4	0,27477	2,1	1496,9	21,5	1536,2	18,7	1565,0	28,7	0,87	104,54
1,3	0,26569	1,1	1514,5	13,3	1517,1	10,5	1518,9	15,2	0,86	100,29
1,5	0,27643	1,4	1512,5	13,4	1547,5	12,1	1573,4	18,9	0,90	104,03
1,5	0,26369	1,3	1529,6	13,2	1517,4	11,5	1508,7	17,2	0,89	98,63
3,3	0,28921	2,9	1525,0	29,8	1589,0	26,6	1637,6	42,1	0,89	107,38
1,7	0,25039	1,6	1520,1	10,1	1473,0	13,0	1440,5	20,4	0,96	94,76
2,3	0,27897	1,7	1558,0	29,6	1574,1	18,3	1586,2	23,4	0,73	101,81
2,1	0,27933	2,0	1517,7	13,2	1558,0	17,1	1588,0	28,5	0,95	104,63
4,5	0,25075	4,0	1502,3	38,8	1466,8	34,9	1442,4	51,7	0,89	96,01
1,6	0,25482	1,3	1533,4	17,6	1492,1	12,6	1463,3	17,3	0,83	95,42
1,7	0,24625	1,4	1482,8	19,5	1444,8	13,4	1419,1	17,8	0,81	95,70
1,3	0,24897	1,0	1519,9	15,9	1468,5	10,4	1433,2	13,3	0,78	94,29
1,9	0,24113	1,6	1503,6	20,0	1437,1	14,9	1392,6	20,4	0,85	92,62
1,6	0,24533	1,3	1517,1	18,6	1455,9	12,7	1414,4	16,6	0,82	93,22

Plotagem intercepto superior de análise U-Pb - LA-MC-ICPMS em zircão do diabásio - Amostra LUSL 21



## Anexo VI - Litogeoquímica

BH11210260 - Finalized

CLIENT : CAFON - Cesar Fonseca Ferreira Filho

# of Samples : 8

DATE RECEIVED : 2011-10-31 DATE FINALIZED : 2011-12-06

PROJECT : LUANGA SUL

CERTIFICATE COMMENTS :

PO NUMBER :

SAMPLE	ME-XRF12	ME-XRF12	ME-XRF12	ME-XRF12	ME-XRF12	ME-XRF12	ME-XRF12	ME-XRF12	ME-XRF12	ME-XRF12	ME-XRF12	ME-XRF12	ME-XRF12	ME-XRF12	ME-MS81
DESCRIPTIO	Al2O3	BaO	CaO	Cr2O3	Fe2O3	K2O	MgO	MnO	Na2O	P2O5	SiO2	SrO	TiO2	Ag	
%	%	%	%	%	%	%	%	%	%	%	%	%	%	ppm	
LUSL-08	18,300	0,037	9,490	0,006	7,130	1,050	7,290	0,127	3,230	0,007	50,900	0,032	0,130	1,000	
LUSL-09	16,050	0,028	14,250	0,004	8,580	0,463	5,910	0,156	2,370	0,006	50,100	0,051	1,020	<1	
LUSL-11	22,200	0,048	11,400	<0.001	3,890	1,090	4,250	0,100	3,790	0,006	51,800	0,054	0,110	<1	
LUSL-19	13,850	0,049	9,990	0,044	14,050	2,100	7,370	0,302	1,650	0,079	49,000	0,019	1,040	<1	
LUSL-20b	19,000	0,069	9,000	0,075	7,160	1,695	6,060	0,194	3,450	0,008	52,300	0,052	0,110	<1	
LUSL-21b	13,650	0,019	9,830	0,021	15,300	0,481	6,730	0,204	2,910	0,258	47,700	0,045	2,690	<1	
LUSL-WO-A	2,720	0,040	46,400	<0.001	1,650	0,574	1,460	0,039	0,420	0,130	16,550	0,142	0,160	<1	
LUSL-WO-B	2,300	0,042	48,100	<0.001	1,400	0,482	1,400	0,034	0,279	0,119	15,750	0,128	0,160	<1	